# M dwarfs from the SDSS, 2MASS and WISE surveys: identification, characterisation and unresolved ultracool companionship

— **Neil James Cook** —

Centre for Astrophysics Research
— University of Hertfordshire —

Submitted to the University of Hertfordshire in partial fulfilment of the requirements of the degree of Ph.D.

**Principal Supervisor:** Prof. David J. Pinfield

— March 2016 —

# Acknowledgements

I would like to thank my principle supervisor Prof. David Pinfield, for all his invaluable guidance, for endless suggestions and new ways of seeing the problems at hand and for his faith in this work. I would like to thank Dr. Ben Burningham for all the conversations, comments on work and for reassuring me on how challenging this work could be and to Prof. Hugh Jones and Dr. Avril C. Day-Jones for all the discussions and comments on my work. I am infinitely grateful to Dr. Federico Marocco (my unofficial supervisor), whom has suffered my constant questioning (without ever telling me to go away!) and has been a unending source of help and knowledge from day one. I would like to thank Dr. Richard L. Smart and the IPERCOOL collaboration for the staff exchange program that has benefited my work greatly (especially my Chinese collaborators Youfen Wang, Kevin Zhaoxiang, Jing Zhong and A Li Lou).

I'd like to give a big thank you to Nancy Hine for putting up with me in the office and for being my partner in crime in all forms of procrastination. I would like to thank Mike Smith for countless PYTHON and statistical conversations the likes of which have improved every aspect of my work and to Geert (the Lord of PYTHON) for all those gems of knowledge. I would like to thank my present and past office mates (in alphabetical order), Beatriz Mingo, Carla Natário, Gaius Manser, Giulio Vestialbuio, Graham Thompson, Gülay Gürkan Uygun and Jonathan Westcott. To those I have lived with, the Horsa gardens crew over the years (again in alphabetical order) Andrés Burgos, Andy Gallagher, Emma Lofthouse (and Spectra), Hugo Ledo, Hywel Farnhill, Julie Djordjevic, living with you, the parties the boardgames has been a great experience. To Jess Schonhut, Alex Hocking, Mel Nadarajan, Carlos Contreras, Noemi Muzgo Correa, Ian and Liz Greenslade, David Campbell, Mark Gallaway, James Frith, Leigh Smith, Nick Wright, and all the others I have met at the University of Hertfordshire, I thank you for spending your precious time with me and making this an experience I will never forget.

To one of the best friends I have ever had Ben Hewitt, you have been a constant source of friendship, support and entertainment, every time I see you is like a day has never passed since we last met (and to Sam Hewitt for putting up with Ben and me!). To my Dunstable friends, Krystyann Jordan, Ashleigh Cunningham, Katherine Young, Daniel Metcalfe, Christina Harris, Victoria Allan, Dan Chilcott, Diane White, Kieran Ray, Daniel Slack, Tricia O'Toole and Andrew Abrahams; to my friends from the University of Manchester, to Flora Roth, Vicky Park, Simon Ray-Jones, Helen Ray-Jones, Carl-Johan Haster, Hazel Martindale, Sam Cusworth, Sandra Seljeset, Liam Crossley, Jeremy Tabick, Winnie Lam, Adam Fletcher, Vicky Chapman and Tom Fenton; and to my friends from further afield Steven Blair, Jonathan Gagné, Bethan Spinks, and Laura Howlett thank you for your constant support, understanding and for still being there for more despite my PhD slowly taking over my life.

To all my science and mathematics teachers over the years thank you for sticking in there and believing in me, having the experience of teaching classes myself has given me a renewed respect for what you do, and you are all not thanked nearly enough, without you I would have never been able to do the work I do today.

To my family, my mum and dad, Brigette and Terry, your love, kindness and support have never wavered. To my brothers Ian, Gary and Kevin, thank you for all the games and fun we had and the support you gave me. To my Aunts, Uncles and Cousins, thank you for your support and all the times you guys have made me laugh. To my Nan, Thelma your love and strength has always guided me. To my grandparents, Maureen and Derrick, without your inspirations as a child and your support through my studies I would not be where I am today.

And finally to Céline Arnouk, you came in to my life rather unexpectedly but I could not imagine my life now without you. You have been a constant source of strength, support and love, and I really wouldn't have been able to do this PhD without you, or have had nearly as many of the adventures that I have been lucky enough to have. You have travelled further than anyone and been there when I needed you most and I am very lucky to have you in my life. I wish also to thank the Arnouk and Haddad family for accepting me in to their family with such kindness.

**I dedicate this thesis and my work to my friends, my family, and most importantly to my parents and to Céline, without whom this work would never have been possible.**

# Abstract

The aim of this thesis is to use a cross-match between WISE, 2MASS and SDSS to identify a large sample of M dwarfs. Through the careful characterisation and quality control of these M dwarfs I aim to identify rare systems (i.e. unresolved UCD companions, young M dwarfs, late M dwarfs and M dwarfs with common proper motion companions).

Locating ultracool companions to M dwarfs is important for constraining low-mass formation models, the measurement of substellar dynamical masses and radii, and for testing ultracool evolutionary models. This is done by using an optimised method for identifying M dwarfs which may have unresolved ultracool companions. To do this I construct a catalogue of 440 694 M dwarf candidates, from WISE, 2MASS and SDSS, based on optical- and near-infrared colours and reduced proper motion. With strict reddening, photometric and quality constraints I isolate a sub-sample of 36 898 M dwarfs and search for possible mid-infrared M dwarf + ultracool dwarf candidates by comparing M dwarfs which have similar optical/near-infrared colours (chosen for their sensitivity to effective temperature and metallicity). I present 1 082 M dwarf + ultracool dwarf candidates for follow-up. Using simulated ultracool dwarf companions to M dwarfs, I estimate that the occurrence of unresolved ultracool companions amongst my M dwarf + ultracool dwarf candidates should be at least four times the average for my full M dwarf catalogue. I discuss yields of candidates based on my simulations.

The possible contamination and bias from misidentified M dwarfs is then discussed, from chance alignments with other M dwarfs and UCDs, from chance alignments with giant stars, from chance alignments with galaxies, and from blended systems (via visual inspection). I then use optical spectra from LAMOST to spectral type a subset of my M dwarf + ultracool dwarf candidates. These candidates need confirming as true M dwarf + ultracool dwarf systems thus I present a new method I developed to use low resolution near-infrared spectra which relies on two colour similar objects (one an excess candidate, one not) having very similar spectra. A spectral difference of these two colour similar objects should leave the signature of a UCD in the residual of their differences, which I look for using the difference in two spectral bands designed to identify UCD spectral features.

I then present the methods used to identify other rare systems from my full M dwarf catalogue. Young M dwarfs were identified by measuring equivalent widths of H$\alpha$ from the LAMOST spectra, and by measuring rotation periods from Kepler 2 light curves. I identify late M dwarfs photometrically (using reduced proper motion and colour cuts) and spectroscopically (using the LAMOST spectra with spectral indices from the literature). Also I present common proper motion analysis aimed at finding Tycho-2 primaries for my M dwarfs and look for physically separated M dwarf + M dwarf pairs (internally within my full M dwarf catalogue).

# Contents

# List of Figures

# List of Tables

# List of Equations

# List of Symbols

| | |
|---|---|
| Å | Angstrom (1.0 $\times 10^{-10}$ m) |
| $\alpha$,$\delta$ | Right Ascension and declination on the sky, measured in degrees |
| $A_\lambda$ | Extinction at wavelength, $\lambda$ |
| AU | Astronomical Unit (1.496 $\times 10^{11}$ m) |
| $A_\mathrm{v}$ | Visual Extinction |
| $\beta$ | The binary fraction |
| $c$ | Speed of Light (3.0 x $10^8$ m $\mathrm{s}^{-1}$) |
| $E(B-V)$ | Colour Excess |
| $g$,$r$,$i$,$z$ | SDSS photometric bands (centred at 0.46, 0.62, 0.66 and 0.89$\mu$m ) |
| Gyr | $10^9$ yr |
| $h$ | Planck Constant (6.62606896(33) $\times 10^{-34}$ $\mathrm{m}^2$ kg $\mathrm{s}^{-1}$) |
| $H_0$ | Hubble constant (72 km $\mathrm{s}^{-1}\mathrm{Mpc}^{-1}$) |
| $H_X$ | The reduced proper motion using photometric band X (i.e. $X = V$, $X = J$) |
| $J$,$H$,$K_S$ | 2MASS photometric bands (centred at 1.25, 1.65 and 2.16$\mu$m ) |
| $k_B$ | Boltzmann constant (1.3806504(24) $\times 10^{-23}$ J $\mathrm{K}^{-1}$) |
| $\lambda$ | Wavelength |
| $log\, g$ | A objects surface gravity, where g is measured in cgs units |
| $\mu$m | $10^{-6}$ m |
| $M_{jup}$ | Jupiter Mass (1.898 $\times 10^{27}$ kg) |
| Mpc | $10^6$ pc |
| $M_\odot$ | Solar Mass (1.989 $\times 10^{30}$ kg) |
| $\mu$,$\mu_\alpha$,$\mu_\delta$ | The total proper motion and the proper motion components in $\alpha$ and $\delta$, masured in arcsec $\mathrm{yr}^{-1}$ |
| $M_X$ | The absolute magnitude (apparent magnitude at 10 pc) in photometric band X (i.e. $X = V$, $X = J$) |

| | |
|---|---|
| Myr | $10^6$ yr |
| pc | parsec ($3.086 \times 10^{16}$ m) |
| $R_{jup}$ | Jupiter Radius ($6.991 \times 10^7$ m) |
| $R_\odot$ | Solar Radius ($6.963 \times 10^8$ m) |
| $\sigma$ | The uncertainty on a measurement (unless otherwise stated) |
| $T_{eff}$ | A objects effective surface temperature in Kelvin, K |
| $V$ | V band taken from the SDSS transformation |
| $V_J$ | Johnson V magnitude derived from $B_T$ and $V_T$ |
| $V_T$, $B_T$ | V band taken from the Tycho-2 catalogue. |
| $W1$,$W2$ | WISE photometric bands (centred at 3.4 and 4.6$\mu$m ) |

# Chapter 1: Introduction

M dwarfs are the very low mass end of the stellar sequence and thus, unlike the Sun, are so cool they glow red and emit most of their flux in the red optical and near infrared. As the lowest mass stars their properties overlap with the substellar regime of brown dwarfs and giant planets with their cool nature leading to a variety of complex physics. This thesis deals with the characterisation of these M dwarf with the intent to identify rare systems using some of the extremely large data sets currently available. In this chapter I will briefly introduce the concepts of ultracool dwarfs, the substellar regime of brown dwarfs and giant planets, and then introduce the key characteristics which define M dwarfs. One of the main aims of the thesis is the search for ultracool companions to M dwarfs and as such I summarise the work done previously in this rather uncertain field. I introduce the large catalogues I use, defining their basic properties especially those important for this work.

## 1.1 Ultracool dwarfs

### 1.1.1 Brown dwarfs and giant planets

The definition of what precisely defines a brown dwarf and what defines a planet is still disputed. The two main arguments rely on formation mechanisms (Padoan & Nordlund, 2004; Bonnell et al., 2007; Whitworth et al., 2007; Hennebelle & Chabrier, 2008) and the mass limits at which Hydrogen (stellar-brown dwarf separation) and Deuterium (IAU definition of the brown dwarf-planet separation) can undergo thermonuclear fusion (Burrows et al. 1997, Chabrier & Baraffe 2000, Burrows et al. 2001, Spiegel et al. 2011).

Although first predicted in 1963 (Kumar, 1963; Hayashi & Nakano, 1963) it took until 1995 for the detection of the first confirmed brown dwarfs, Gl 229B, (Nakajima et al., 1995) and Teide 1 (Zapatero-Osorio et al., 1996), and the very same day an announcement was made, the first exoplanet, 51 Peg b, had been discovered (Mayor & Queloz, 1995).

It soon became clear new spectral types were needed to categorise their properties in line with stellar populations; the "L" dwarfs (Martín et al., 1997; Kirkpatrick et al., 1999) and the "T" dwarfs (Burgasser et al., 1999; Kirkpatrick et al., 1999). In Kirkpatrick et al. (1999) they suggest the L dwarfs sequence represented effective temperatures ranging from ∼2000 K down to ∼1500 K with the coolest T dwarfs currently known having temperatures as low as 500 K (Burningham et al., 2008; Delorme et al., 2008; Leggett et al., 2009; Lucas et al., 2010; Liu et al., 2011). The discovery of seven ultracool brown dwarfs by Cushing et al. (2011) which were much fainter and

had colours and spectra which suggested a deviation from the T dwarfs led to the use of another spectral type, the "Y" dwarfs, as discussed by Kirkpatrick et al. (2012). With the discovery of "Y" dwarfs with estimated temperatures in the range of 250 - 500 K (e.g. Luhman, 2014), brown dwarfs now truly cover the full range of masses and temperatures between very low mass stars and planets.

Due to their low masses and low central temperatures, brown dwarfs never reach the temperature needed to sustain thermonuclear burning of Hydrogen (Kumar, 1963; Hayashi & Nakano, 1963) and are thus classed as substellar-mass objects, and are supported by electron degeneracy. As such brown dwarfs bridge the gap between the mass range of planets and stars (and can overlap in effective temperature, $T_{eff}$ ). Brown dwarfs, by definition, have masses below the Hydrogen burning mass limit, ∼0.075 to 0.080 $M_{\odot}$ or ∼80 to 90 Jupiter masses, $M_{Jup}$ (Baraffe et al., 2002). Some studies define the lower limit of brown dwarfs as those massive enough (∼ 11-16 $M_{Jup}$ depending on metallicity, Spiegel et al. 2011) to achieve the burning of Deuterium (Basri et al., 2000). An alternative way to split different types of substellar object is by their formation mechanism (e.g. Ma & Ge 2014).

The formation of brown dwarfs is discussed by Luhman (2012), and several methods are proposed (Bonnell et al., 2007; Whitworth et al., 2007). Formation can be attributed to:

1. Fragmentation of massive collapsing cores[1]
2. Ejection of smaller fragments from massive cores[1]
3. Interruption of accretion by photoionising-radiation-stripping[1]
4. Ejection of low-mass companions from gravitational fragmentation of circumstellar discs[1]
5. Turbulent compression and fragmentation of gas in molecular clouds[1]

These methods have some common ground (as well as some crucial differences) with models of planetary formation, which consist of two main formation mechanisms. The first is disc instability (Boss, 1997) where planets are formed by gravitational instability in planetary discs. The other method is core-accretion where planets form on a metallic core built from grains in the disc (Pollack et al., 1996; Ida & Lin, 2004; Alibert et al., 2005).

A debate still exists on what to call a brown dwarf and what to call a planet, and whether mass or formation mechanisms should be used for classification. However as stated by Luhman (2012) the Deuterium burning limit has little impact on the structure or evolution (Chabrier et al., 2007) and so cool brown dwarfs and warm-hot

[1]For further details see Luhman (2012) Section 3.1 and references there in.

giant exoplanets are observationally, if not physically, very similar. Figure 1.1 shows this point, giant planets and brown dwarfs can be taken observationally as very similar objects. Ultracool dwarfs (UCDs) are objects later in spectral type than ∼M7. UCDs include some old stars, and to a large extent brown dwarfs and warm-hot gaseous exoplanets. For the rest of this thesis I refer generically to UCDs as a practicality since my work is principally observational and involves assessing observational characteristics which are dictated mainly by $T_{eff}$ .

As of June 2015 there are 2,085 confirmed and 562 candidate UCDs known (Csizmadia et al., 2015), and there are at least an additional 998 (Skrzypek et al. 2016 present 998 new photometrically selected UCDs).

### 1.1.2 Complexities in UCD spectra

By virtue of their low-temperatures, UCD spectra are typified by the influence of combinations of complex molecular opacities, Figure 1.2a gives some insight into these sub-stellar chemical factories.

In addition to this, the condensation of species into clouds (dust) further complicate the situation (Burrows et al., 2001). Figure 1.2b shows examples of spectra for M, L, T dwarfs and Jupiter respectively, the differences are dominated by the absorption of different species at different temperatures across spectral type. Figure 1.3 shows a comparison between UCDs and M dwarfs both in terms of absolute flux (i.e. at the same distance) and relative flux (i.e. compared to the flux at 0.825$\mu$m ). Figure 1.2b and Figure 1.3 show the strong effects of molecular absorbers like methane and water vapour (for T dwarfs and Jupiter), and the strengthening of these molecules (along with reddening caused by dust) across the M-L transition.

These complications have made modelling UCDs very challenging, especially in the case of reproducing the strength of the water, methane and ammonia bands (at respectively lower temperatures, see the excellent review by Allard et al. 2012 and references therein). This is further complicated by non equilibrium chemistry (e.g. due to mixing from convection pushing hot fluid from the core into the atmosphere, Saumon et al. 2003) which alters the relative abundances of each species of molecule which can then differ substantially from the chemical equilibrium values.

### 1.1.3 The complicated nature of UCDs

Another complication is evolutionary cooling which means the observations of the $T_{eff}$ for these sources is degenerate with age, ranging from old low-mass stars through to

[2]X-shooter Spectral Library Chen et al. (2014). Accessed online at http://xsl.u-strasbg.fr/.

[3]SpeX Prism Spectral Libraries, maintained by Adam Burgasser at http://pono.ucsd.edu/~adam/browndwarfs/spexprism.

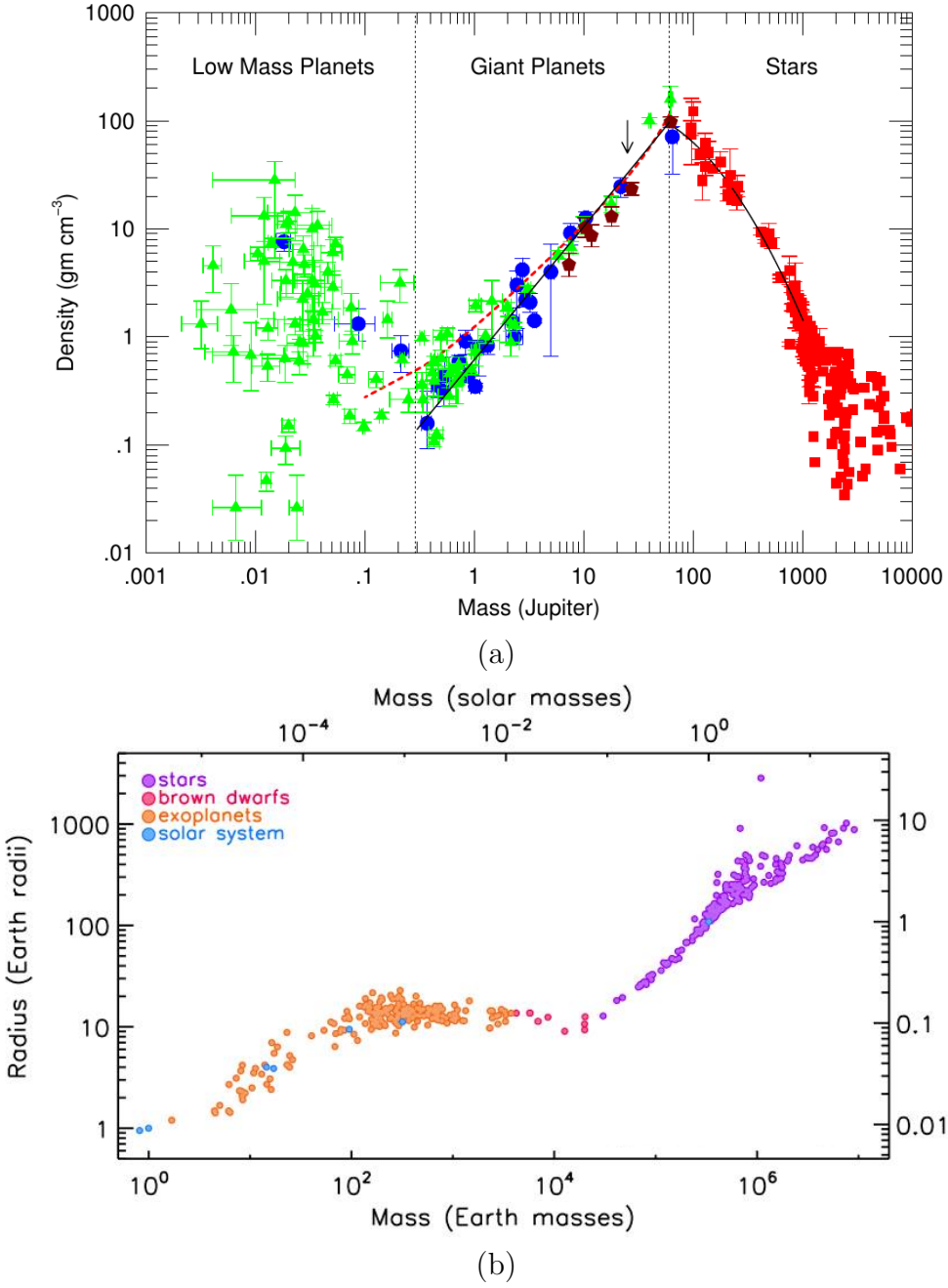


Figure. 1.1: (a) The density against mass relation for stars, brown dwarfs and giant planets (UCDs), and lower mass planets, the separation between star and brown dwarf is clear with the change from support by radiative pressure to support by electron degeneracy pressure. Figure from Hatzes & Rauer (2015), the black line represents the linear fit to UCDs from 0.35 to 60 times the mass of Jupiter. The dashed red line shows the mass-density relationship for H/He dominated giant planets taken from Fortney et al. (2007). (b) The radius against mass relation, for giant planets and brown dwarfs (UCDs) the radius is of order the radius of Jupiter ($\sim$0.1 $R_{\odot}$), with the largest (non stellar) UCDs having the smallest radii. Figure courtesy of Berta-Thompson (2014).

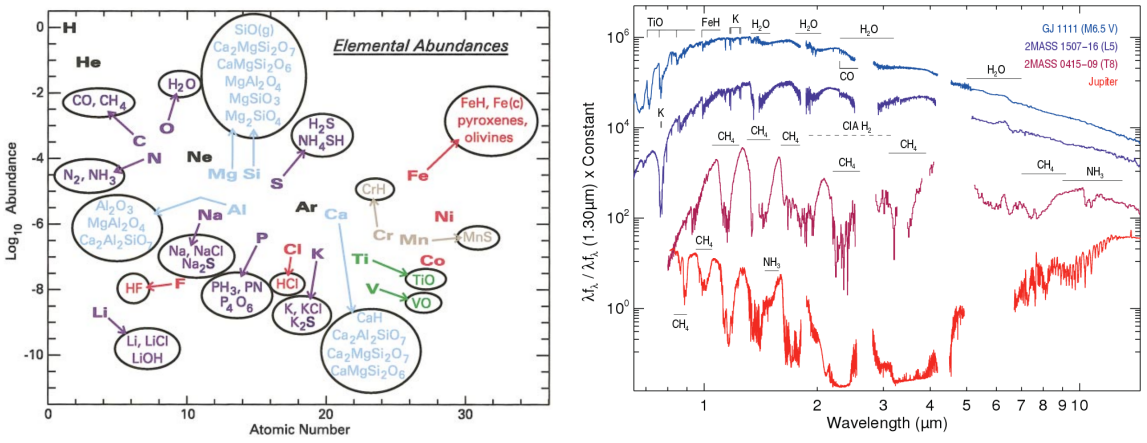


(a) (b)

Figure. 1.2: (a) Figure from Burrows et al. (2001) the abundance of elements is shown with balloons showing associated molecules (b) Figure from Burgasser (2011) showing the observed NIR-MIR spectra of top-to-bottom: M, L, T dwarfs and Jupiter. Data for Jupiter are from Rayner et al. (2009) and Kunde et al. (2004), M, L and T dwarf spectra are from Cushing et al. (2006) and references there in.

younger UCDs (e.g. in Nakajima et al. 1995, Delfosse et al. 1997, Burgasser et al. 1999, Kirkpatrick et al. 1999, Pinfield et al. 2003, Burgasser et al. 2004, Leggett et al. 2010, and Kirkpatrick et al. 2011) and down into the planetary regime (e.g. in Lucas et al. 2006, Caballero et al. 2007, Luhman & Muench 2008, Marsh et al. 2010, Lodieu et al. 2011, Delorme et al. 2012, Scholz et al. 2012). For example a 2,800 K object could be a young brown dwarf or could be an old low mass star, whereas a 2,100 K object could be a young giant planet or could be a few hundred $Myr$ old brown dwarf or a extremely old low mass star, and a cold 700 K object could be a young giant planet or could be a much older ($Gyr$) more massive object (see Figure 1.4). These equivalent $T_{eff}$ objects would share all observable properties (other than differences in environment, e.g. differing metallicity). This makes determining ages of UCDs extremely important for understanding their nature.

Observationally age can be estimated in several key ways, for example, younger UCDs (having lower surface gravity) can be used to distinguish two objects which have the same $T_{eff}$ (given metallicity constraints). This can be seen by a sharpening of the peak of H band spectrum, weakened alkali lines and enhanced metal-oxide absorption (Faherty 2014, e.g. Lucas et al. 2001, Gorlova et al. 2003, Luhman et al. 2004, McGovern et al. 2004, Allers et al. 2007, Rice et al. 2010, Rice et al. 2011, Cruz et al. 2009).

If one can detect Lithium in the atmosphere of a UCD an upper age estimate can be determined (e.g. see Faherty, 2014, and references therein). Lithium burning happens at cooler core temperatures than Hydrogen or Deuterium burning and thus can happen at a lower mass. As UCDs are fully convective this means objects above a mass limit of

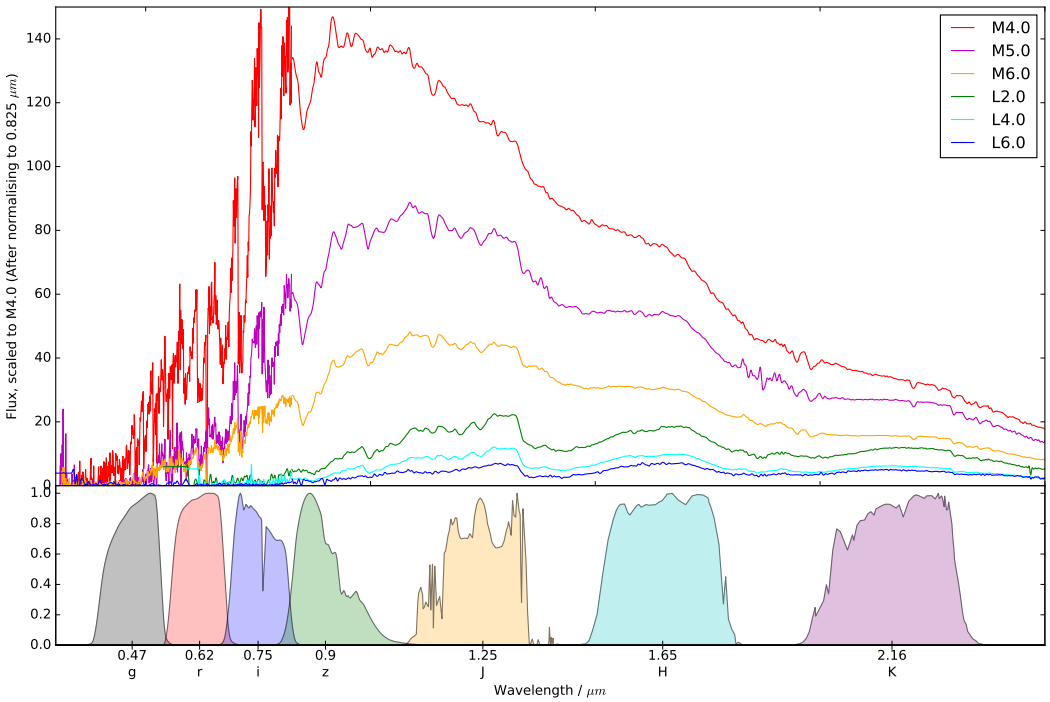


(a)

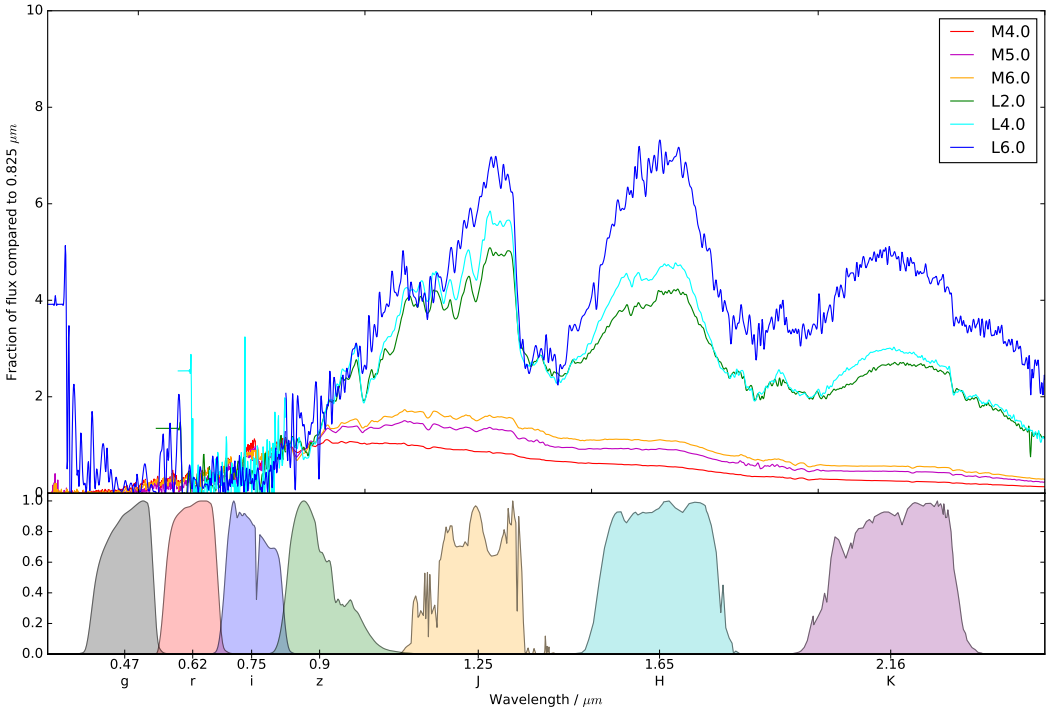


(b)

Figure. 1.3: Comparison between M dwarfs and L dwarfs in the optical and NIR. UCDs have little to no flux in the optical and have most of their flux in the NIR, whereas M dwarfs can be of order 100 times brighter in the peaks between the $z$ and $J$ bands and drop off at longer wavelengths. (a) The spectra are normalised at $0.825\mu$m then rescaled using absolute $J$ band magnitudes to show the expected flux of each type of object to show how the objects at the same distance would look. (b) The spectra are normalised at $0.825\mu$m to show the comparison of relative flux between objects. Optical M dwarf spectra from Chen et al. (2014)[2], NIR M dwarf spectra from Burgasser et al. (2004, 2008)[3], Optical L dwarf spectra from Day-Jones et al. (2013) and Marocco et al. (2015) and NIR L dwarf spectra from Burgasser et al. (2004, 2007)[3].

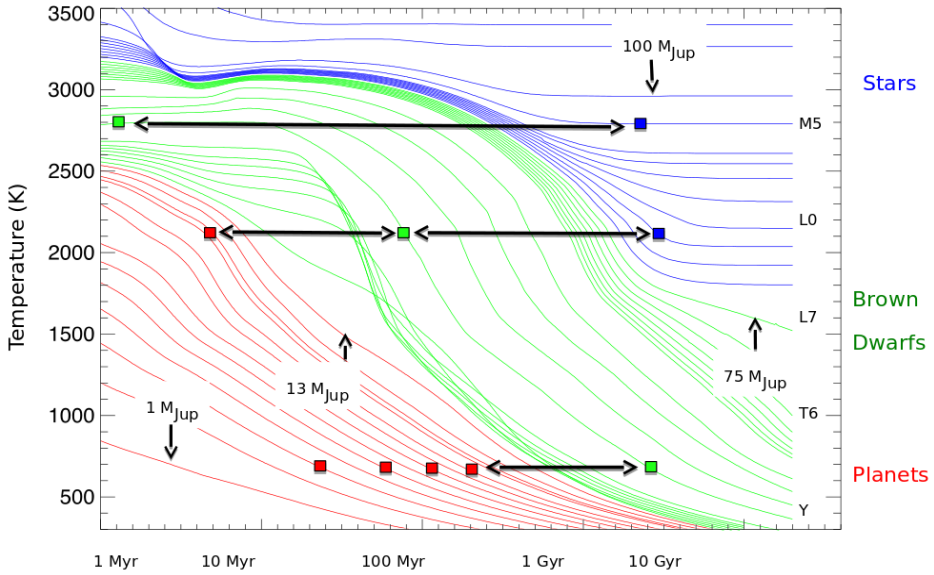


Figure. 1.4: Temperature-Age diagram from Faherty (2014) showing the evolution of low-mass stars (blue), UCDs (green) and planets (red), with model data from Burrows et al. (1997)) . Markers show the degeneracy found in observations. A 2,800 K objects could be a young brown dwarf or could be an old M dwarfs, whereas a 2,100 K object could be a young giant planet or could be a few hundred $Myr$ old brown dwarf or could be a extremely old low mass star.

$\sim$0.065$M_{\odot}$ (Rebolo et al., 1992; Magazzu et al., 1993) will fully deplete their reservoir of Lithium in less than 1 $Gyr$ (Faherty, 2014). Thus UCDs cooler than 2,700 K (Basri, 1998) with a Lithium detection must be lower in mass than 0.065$M_{\odot}$ and thus an upper limit in age can be determined for these objects (Faherty, 2014).

Another method to age date a UCD is to look at the UCDs kinematics (space motions in the form of UVW velocity distributions). These can be used to search for new members of well-studied moving groups with well known ages from higher mass members (velocity dispersions <1 km s$^{-}$1, e.g. $\beta$ Pictoris at $\sim$20 $Myr$ , TW Hydrae at $\sim$10 $Myr$ , Tucana Horologium at $\sim$30 $Myr$ , AB Doradus at $\sim$150 $Myr$ see Riedel 2014, Faherty 2014). UCDs are generally given a probability of membership exploiting statistical analysis such as using a Bayesian framework (e.g. the *Bayesian Analysis for Nearby Young AssociatioNs*, BANYAN and BANYANII from Malo et al. 2013 and Gagné et al. 2014 respectively).

A degeneracy also exists between surface gravity and metallicity (i.e. younger UCDs have a lower surface gravity and larger radii, Chabrier & Baraffe 2000, and larger metallicities produce a lower core temperature and thus a smaller radius, Burrows et al. 2001). This degeneracy coupled with the fact it is difficult to determine radii measurements of UCDs means there are only a few UCDs with measured radii, leading to inconsistencies between observations and current models (see Section 1.3).

In summary mass, radius, age and metallicity are extremely difficult to measure for

| Spectral type | Temperature K | Radius $R_\odot$ | Mass $M_\odot$ | Luminosity/100 $L_\odot$ | $M_V$ mag | log g [cgs] |
|---|---|---|---|---|---|---|
| M0.0 | 3800 | 0.62 | 0.60 | 7.2 | 9.34 | 4.63 |
| M1.0 | 3600 | 0.49 | 0.49 | 3.5 | 9.65 | 4.75 |
| M2.0 | 3400 | 0.44 | 0.44 | 2.3 | 10.12 | 4.79 |
| M3.0 | 3250 | 0.39 | 0.36 | 1.5 | 11.15 | 4.81 |
| M4.0 | 3100 | 0.26 | 0.20 | 0.55 | 12.13 | 4.91 |
| M5.0 | 2800 | 0.20 | 0.14 | 0.22 | 16.0 | 4.98 |
| M6.0 | 2600 | 0.15 | 0.10 | 0.09 | 16.6 | 5.09 |
| M7.0 | 2500 | 0.12 | ∼0.09 | 0.05 | 18.8 | 5.23 |
| M8.0 | 2400 | 0.11 | ∼0.08 | 0.03 | 19.8 | 5.26 |
| M9.0 | 2300 | 0.08 | ∼0.075 | 0.015 | 17.4 | 5.51 |

Table 1.1: Stellar properties of M dwarfs. Taken from Kaltenegger & Traub (2009) (original from Reid & Hawley (2005). Surface gravity, log g, is calculated using $log_{10}(m/r^2)$ in cgs units.

UCDs and as such these properties are vital for improving the understanding of UCDs.

## 1.2 M dwarfs

### 1.2.1 Stellar properties

M dwarf stars are the very low mass end of stellar formation sequence. Unlike higher mass stars, M dwarfs need to contract for tens to hundreds of $Myr$ before joining the main sequences by becoming hot enough for sustained Hydrogen burning (e.g. see review by Luhman, 2012, and references therein). M dwarfs range in mass from about half the mass of the sun down to around eight per cent the mass of the sun ($\sim 0.075$, the Hydrogen burning mass limit; Burrows et al. 1997, Chabrier & Baraffe 2000, see Table 1.1). One of the most important properties of M dwarfs is that they are the most numerous of all stars in the Galaxy (Reid & Cruz, 2002; Covey et al., 2008; Bochanski et al., 2010), this makes M dwarfs very important for understanding the mass function, and their formation and evolution.

### 1.2.2 Spectroscopy

The spectra of M dwarfs are dominated by molecular absorption (e.g. $TiO$, $VO$ in the optical and $H_2O$ in the infrared). M dwarfs come from many different populations, from very young M dwarfs in open clusters, to the Galactic disc, to the Galactic halo (where M dwarfs can be billions of years old). Modelling has always been more difficult in these low mass stars when compared to high mass stars due to incomplete molecular opacity data and due to the fully convective nature of these stars (see the review by

Allard et al. 1997, and references there in). Figure 1.3 shows a comparison between M dwarfs and UCDs both in terms of absolute flux (i.e. at the same distance) and relative flux (i.e. compared to the flux at 0.825$\mu$m ).

The complicated nature of these cool stars means observed photometry and their colours are intrinsically scattered by many factors including differences in temperature, surface gravity and composition, (e.g. in Burrows et al. 1997); rotation, (e.g. in McQuillan et al. 2014); and activity, (e.g. in Robertson et al. 2013), even between M dwarfs with the same spectral type. This means it is hard to define spectral standards for these objects. Attempts to overcome these complexities include relating these to calibration stars which have independently measured parameters (i.e. radii from interferometry, Boyajian et al. 2012, Mann et al. 2013b, Newton et al. 2015a, or companions to higher mass stars with well measured abundances, Bonfils et al. 2005, Johnson & Apps 2009, Rojas-Ayala et al. 2012, Mann et al. 2013a, Newton et al. 2014).

### 1.2.3 Activity and rotation

M dwarfs are known to be very active (Allard et al., 1997; Reid et al., 1999) and as for higher mass stars this magnetic activity appears to be linked to rotation. For the highest mass M dwarfs (<M3/M4) this activity is believed to come from the global dynamo which exists at the interface between the convective envelope and the inner region of the M dwarf (e.g. Ossendrijver 2003, Parker 1993, Charbonneau & MacGregor 1997, via Browning et al. 2010). However below ~0.3 $M_{\odot}$ the observational and theoretical understanding of where this activity comes from is far less clear, as an interface dynamo is not possible due to convective instability (Browning et al., 2010), e.g. this may come from a "distributed dynamo" due to convention and turbulence (see Shulyak et al., 2015, and references therein). Despite this many late M dwarfs have strong magnetic fields (~1 kG, West et al. 2015). This is still an open question, but regardless of how this process works it is clear from observations both low and high mass M dwarfs can have strong, large-scale magnetic fields. These can be probed directly using magnetically sensitive molecular line ratios such as $FeH$ (at 0.99 $\mu$m , Reiners & Basri, 2007) and Zeeman Doppler imaging (Donati et al., 2006).

Young M dwarfs, like their higher mass counterparts, are more active than older stars, therefore tracing and identifying magnetic activity is a key way to identify young M dwarfs (linked to rotation, i.e. from a star losing angular momentum from winds which subsequently slows rotation and thus magnetic activity, West et al. 2015). Due to M dwarfs being intrinsically faint and red H$\alpha$ is one way magnetic activity can be traced (H$\alpha$ appears as an emission feature around ~0.65 $\mu$m thus a fainter and redder spectrum does not mask the H$\alpha$ signature, Bopp & Schmitz, 1978; Walkowicz & Hawley, 2009; Bell et al., 2012). M dwarfs as they age also spin down due to magnetic braking (Mestel, 1968) and thus finding fast rotators is another way one can identify

youthfulness (in fact rotation increases due to gravitational contraction in their pre-main sequence phase, Rappaport et al. 2014).

### 1.2.4 Binarity

There is a clear observational trend that the fraction of stars which have companions depends on mass. Massive stars (O, A and B stars) have binary fractions of ∼80 per cent (Shatsky & Tokovinin, 2002; Kouwenhoven et al., 2007; Peter et al., 2012) where as FGK stars have binary fractions ranging from ∼46 percent to ∼67 per cent (Raghavan et al., 2010; Duquennoy & Mayor, 1991).

Low number statistics and observational bias make it difficult to robustly constrain the M dwarf binary fraction with varying mass-ratio and separation. However this trend seems to continue with a binary fraction between ∼26 per cent and ∼42 per cent in the early to mid M dwarf range and ∼10 to 30 per cent range for very low mass stars and UCDs (see Table 1.3 and Table 1.2). One of the largest M dwarf binary fraction analysis to date has been *the AstraLux large M dwarf Lucky Imaging Binary Survey* which studied 761 young, nearby late K and M dwarfs and found a binary fraction of 32±6 per cent (Bergfors et al., 2010; Janson et al., 2012), and 286 mid to late M dwarfs and found a binary fraction of 21 to 27 per cent (Janson et al., 2014). An overview of the trends in multiplicity can been seen in Table 1.2.

Binarity is very useful to constrain and infer M dwarf properties from (in general) the more well studied primary (i.e. taking the age and/or compositions from the higher mass primary). In addition very wide binaries can be used to probe the galactic dynamical evolution (due to their low binding energy, Tokovinin & Lépine, 2012). There is also an apparent drop of the number of wide systems at around 20,000 AU or ∼0.1 pc (See Caballero et al. 2012 and references therein). Wide binaries are especially interesting since despite this apparent drop they have been found wider than 20,000 AU (Jiang & Tremaine 2010, but these may be former binaries slowly drifting apart). M+M binaries are also important for providing constraints on stellar formation and dynamical evolution theories (see review by Duchêne & Kraus 2013 and recent work by Shan et al. 2015).

| Mass Range | MF/ CF Frequency | Mass Ratio Distribution | Orbital Period Distribution |
|---|---|---|---|
| $M_\star \lesssim 0.1\,M_\odot$ | $MF = 22^{+6}_{-4}\,\%$<br>$CF = 22^{+6}_{-4}\,\%$ | $\gamma = 4.2 \pm 1.0$ | Unimodal (log-normal?)<br>$\overline{a} \approx 4.5\,\mathrm{AU}$, $\sigma_{\log P} \approx 0.5$ |
| $0.1\,M_\odot \lesssim M_\star \lesssim 0.5\,M_\odot$ | $MF = 26 \pm 3\,\%$<br>$CF = 33 \pm 5\,\%$ | $\gamma = 0.4 \pm 0.2$ | Unimodal (log-normal?)<br>$\overline{a} \approx 5.3\,\mathrm{AU}$, $\sigma_{\log P} \approx 1.3$ |
| $0.7\,M_\odot \lesssim M_\star \lesssim 1.3\,M_\odot$ | $MF = 44 \pm 2\,\%$<br>$CF = 62 \pm 3\,\%$ | $\gamma = 0.3 \pm 0.1$ | Unimodal (log-normal)<br>$\overline{a} \approx 45\,\mathrm{AU}$, $\sigma_{\log P} \approx 2.3$ |
| $1.5\,M_\odot \lesssim M_\star \lesssim 5\,M_\odot$ | $MF \geq 50\%$<br>$CF = 100 \pm 10\,\%$ | $\gamma = -0.5 \pm 0.2$ | Bimodal<br>$\overline{P} \approx 10$ days & $\overline{a} \approx 350\,\mathrm{AU}$ |
| $8\,M_\odot \lesssim M_\star \lesssim 16\,M_\odot$ | $MF \geq 60\%$<br>$CF = 100 \pm 20\,\%$ | ... | ... |
| $M_\star \gtrsim 16\,M_\odot$ | $MF \geq 80\%$<br>$CF = 130 \pm 20\,\%$ | $\gamma^{P \leq 3000\,\mathrm{days}} = -0.1 \pm 0.6$<br>$\gamma^{a \geq 100\,\mathrm{AU}} = -0.5 \pm 0.1$ | Peak + power law<br>$\overline{P} \approx 5$ days |

Table 1.2: Table 1 from Duchêne & Kraus (2013). Summary of multiplicity properties for stars and UCDs. Where $MF$ is the multiplicity fraction (the fraction of stars which have a companion, Batten 1973), $CF$ is the companion fraction (the average number of companions per star system, e.g. Reipurth et al. 2014), $\gamma$ is the mass ratio ($\gamma = q_2/q_1$ where $q_2$ is the mass of the companion and $q_1$ is the mass of the primary), $a$ is the separation and $P$ is the period.

### 1.2.5 Cataloguing M dwarfs

One of the first general catalogues of M dwarfs dates back to nearly 70 years ago (Nassau & van Albada, 1949) in which 709 M type stars were found (627 M0 to M4). This work was followed by many trying to define dwarf spectral standards using the $TiO$ and $VO$ molecular bands between 6,000 $\AA$ and 9,000 $\AA$ (Boeshaar 1976, Keenan & McNeil 1976, 1989, Turnshek 1985, Boeshaar & Tyson 1985, Giampapa & Liebert 1986, McCarthy et al. 1988, Henry & Kirkpatrick 1990, Kirkpatrick et al. 1991). M dwarfs, especially late M dwarfs (along with UCDs) were thought to be one of the most plausible explanations for the missing mass (i.e. dark matter) in the Galaxy (Kirkpatrick, 1991).

This led to much investigation in to the low-mass luminosity and mass functions, but ultimately there was not enough contributing mass to explain the missing mass (e.g. Tinney, 1993). With the discovery of the first exoplanets and UCDs emphasis shifted more towards finding and characterising these even lower mass objects. However some study of M dwarfs remained mostly looking at how M dwarfs could be used to probe galaxy structure, due to their possible ancient nature (e.g. Kent et al., 1992; Weiland et al., 1994; Lépine & Leroy, 2000). There was also an interest in completing a census of the solar neighbourhood (within ∼25pc), the vast majority of which are M dwarfs, identified by having high proper motion (e.g. Scholz et al. 2000, Lépine et al. 2002, Gizis 1997, Gizis et al. 2000, Jahreiß et al. 2001, Reid & Cruz 2002, Lépine et al. 2003). This evolved in to a search for lower proper motion neighbours filling the local neighbourhood within 100 pc, with M dwarfs making up ∼75 per cent of all stars within 33 pc (Lépine, 2005).

In more recent years M dwarfs have become extremely important after the discovery that they too host exoplanets and hence new catalogues of bright M dwarfs have been a necessity (e.g. Gliese & Jahreiß, 1991; Lépine & Gaidos, 2011; Frith & Pinfield, 2013). M dwarfs make good exoplanet hosts due to their small size and intrinsic faintness. This leads to improved detection and measurement capabilities. Their closer-in habitable zones open up the possibility of studying cooler exoplanet companions and the latest studies suggest the majority should host at least one planet (Tuomi et al., 2014) making transiting systems around M dwarfs extremely valuable (e.g. Lohr et al., 2015).

As such surveys such as the continuing Kepler 2 campaigns (Howell et al. 2014, MEarth (Charbonneau et al., 2008), the *Transiting Exoplanet Survey Satellite* (TESS Ricker et al., 2014) and *Planetary Transits and Oscillation of stars* (PLATO 2 Rauer et al., 2014) are, and will be, monitoring M dwarfs for possible Earth twins as well as new and proposed NIR ground-based surveys such as the *Habitable-zone Planet Finder* (HPF Mahadevan et al., 2010), the *Calar Alto high-resolution search for M dwarfs with exo-earths with near-infrared and optical echelle spectrographs* (CARMENES, Quirrenbach et al., 2010), *Spectro-Polarimetre Infra-Rouge* (SPIRou Artigau et al., 2014), *Infrared Doppler instrument* (IRD Kotani et al., 2014) and *iLocator* (Crepp et al., 2014).

Accurate physical properties for M dwarfs are required to derive planetary parameters, thus furthering the interest of studying and characterising M dwarfs (e.g. Johnson et al. 2012, Mann et al. 2012, 2013b, Muirhead et al. 2012, 2014, Dressing & Charbonneau 2013, Mann et al. 2013c, Gaidos et al. 2014, Newton et al. 2014, 2015a, Alonso-Floriano et al. 2015, Bowler et al. 2015, Bergfors et al. 2016).

The known number of M dwarfs increased dramatically with the release of SDSS, specifically the 70,841 spectroscopic M dwarfs by West et al. (2011) and during the writing of this thesis the addition of ∼3 million faint M dwarfs, in *Motion Verified Red Stars* catalogue (MoVeRS, selected photometrically from SDSS, Theissen et al., 2016). The Gliese & Jahreiß (1991), West et al. (2011), Lépine & Gaidos (2011), Frith & Pinfield (2013) and Theissen et al. (2016) catalogues will be discussed further in Section 2.6.

| Primary | Companion and Info | Percentage | References |
|---|---|---|---|
| Stellar | UCD [RV] ($0 < \theta < 3AU$) | $\lesssim 0.5\%$ | Marcy & Butler (2000) |
| Stellar | Young LMS | $39 \pm 19\%$ | Vogt et al. (2014) |
| Stellar | UCD $5 < M_J < 70$ ($10 < \theta < 100AU$) | $1.0 - 3.1\%$ | Brandt et al. (2014) |
| F - G (135) | LMS/UCD | $\sim 65\%$ | Abt & Levy (1976) |
| Solar Type stars | LMS/UCD [RV] | $\sim 65\%$ | Duquennoy & Mayor (1991) |
| Solar Type stars | LMS/UCD [RV] ($\theta < 8AU$) | $\sim 19\%$ | Duquennoy & Mayor (1991) |
| G stars | LMS/UCD | $\sim 57$ | Fischer & Marcy (1992) |
| Solar Type stars | LMS/UCD [RV] | $\sim 56 \pm 2\%$ | Raghavan et al. (2010) |
| Solar Type Stars | LMS/UCD ($\theta > 2000AU$) | $> 4.4$ | Tokovinin & Lépine (2012) |
| Solar Type Stars | Young LMS [IM] | $62 \pm 14\%$ | Daemgen et al. (2014) |
| Solar Type Stars | Young LMS [IM] ($10 \lesssim \theta \lesssim 1500AU$) | $26.3^{+6.6}_{-4.9}\%$ | Daemgen et al. (2014) |
| Solar Type stars | BD [RV] | $\sim 8 \pm 6\%$ | Duquennoy & Mayor (1991) |
| Solar Type stars | BD [RV] ($\theta < 8AU$) | $< 2\%$ | Guenther et al. (2005) |
| Solar Type Stars | Young BD [IM] | $\sim 3.5 - 8.8\%$ | Daemgen et al. (2014) |
| Stellar | Young UCD | $7 \pm 15\%$ | Vogt et al. (2014) |
| Stellar | Young BD | $\sim 9\%$ | Vogt et al. (2014) |
| Stellar | Young BD ($\theta > 50AU$) | $\sim 6 \pm 4\%$ | Neuhäuser et al. (2003) |
| Stellar | $M_J$ [IM] ($> 10 - 30AU$) | $\sim 0\%$ | Maire et al. (2014) |
| F, G, K stars | BD ($100 < \theta < 1,000AU$) | $\sim 10\%$ | [1]Wilson et al. (2001) |
| F, G, K stars | BD ($1,000 < \theta < 10,000AU$) | $5 - 13\%$ | [1]Gizis et al. (2001) |
| F, G, K stars | BD ($0.1 < \theta < 1AU$) | $\lesssim 0.07\%$ | [1]Vogt et al. (2002) |
| F - K stars | BD ($28 < \theta < 1590AU$) | $3.2^{+3.1}_{-2.7}\%$ | Metchev & Hillenbrand (2009) |
| A - M stars (23) | UCD [HST] | 0% | [3]Schroeder et al. (2000) |
| A - M stars (50) | UCD [AO] | $2 - 4\%$ | [3]Chauvin et al. (2005a) |
| A - M stars (45) | UCD [HST] | $2 - 4\%$ | [3]Lowrance et al. (2005) |
| A - M stars (54) | UCD [AO] | 0% | [3]Biller et al. (2007) |
| B - M stars (150) | UCD [HST] | 0% | [3]Luhman et al. (2005) |
| G - M stars (28) | UCD [HST] | 0% | [3]Brandner et al. (2000) |

[1] via Pinfield et al. (2005) [2] via Burgasser et al. (2006b) [3] via Metchev & Hillenbrand (2009) [4] via Cheetham et al. (2015)

Table 1.3: Summary of some of the past binary fraction analysis for very low mass objects. Numbers in brackets in primary spectral type column indicate number of primary stars observed (where known). Square brackets in the companion column give an indication of observation type. $\theta$ is separation between the objects, $q = \frac{M_2}{M_1}$ is the mass ratio, HST is the Hubble Space Telescope, AO is Adaptive Optics, IM is Imaging, RV is radial velocity, UCD is Ultra cool/Sub-stellar Objects, BD is Brown Dwarfs, $M_J$ is Jupiter mass objects, LMS is Low Mass Stars, VLMS is Very Low Mass Stars and SD is Sub-Dwarfs; as defined within individual reference.

| Primary | Companion and Info | Percentage | References |
|---|---|---|---|
| G - M | BD [IM] ($75 < \theta < 300AU$) | $0.7 \pm 0.7\%$ | McCarthy & Zuckerman (2004) |
| G - M stars (28) | UCD [AO] | 0% | [3]Masciadri et al. (2005) |
| K - M SD (334) | LMS/UCD [AO] | $11.6 \pm 1.8\%$ | Ziegler et al. (2014) |
| ∼K - M (114) $\rho$Oph | LMS [AO] ($1.3 \lesssim \theta \lesssim 780AU$) | $44 \pm 6\%$ | Cheetham et al. (2015) |
| ∼K - M (114) $\rho$Oph | LMS [AO] ($1.3 \lesssim \theta \lesssim 41.6AU$) | $35 \pm 6\%$ | Cheetham et al. (2015) |
| ∼K - M uSco | LMS | $35^{+5}_{-4}\%$ | [4]Kraus et al. (2008) |
| ∼K - M T.Aur | LMS | $64^{+11}_{-9}\%$ | [4]Kraus et al. (2011) |
| ∼K - M (114) $\rho$Oph | UCD [AO] ($1.3 \lesssim \theta \lesssim 42AU$) | $< 12\%$ | Cheetham et al. (2015) |
| ∼K - M (114) $\rho$Oph | UCD [AO] ($1.3 \lesssim \theta \lesssim 780AU$) | $7^{+8}_{-5}\%$ | Cheetham et al. (2015) |
| ∼K - M (114) $\rho$Oph | UCD [AO] ($42 \lesssim \theta \lesssim 780AU$) | $4^{+5}_{-3}\%$ | Cheetham et al. (2015) |
| M dwarfs | UCD [IM] ($100 \lesssim \theta \lesssim 1400AU$) | $\lesssim 0.5\%$ | Hinz et al. (2002) |
| M stars (25) | UCD [AO] | $2 - 4\%$ | [3]Neuhäuser & Guenther (2004) |
| M dwarfs (205) | VLMS [IM] ($\sim 3 < \theta < 227AU$) | $27 \pm 3\%$ | Janson et al. (2012) |
| Field M stars | $q \geq 0.2$ ($1 < \theta < 2400AU$) | $42 \pm 9\%$ | Fischer & Marcy (1992) |
| M0-M2.5 (17) | VLMS/UCD | $24^{+13}_{-7}\%$ | Burgasser et al. (2007); Reid & Gizis (1997); Reid et al. (2003) |
| Early-type M stars | VLMS/UCD | $\sim 30 - 40\%$ | [2]Reid & Gizis (1997); Delfosse et al. (2004) |
| Early to mid M | BD ($0.001 < \theta < 0.01AU$) | $0 - 2\%$ | [1]Reid & Mahoney (2000) |
| Early to mid M | BD ($10 < \theta < 100AU$) | $1 - 3\%$ | [1]Oppenheimer et al. (2001) |
| Early to mid M | BD ($0.1 < \theta < 1AU$) | 1% | [1]Nidever et al. (2002) |
| Early to mid M | BD ($1.0 < \theta < 10.0AU$) | 1% | [1]Nidever et al. (2002) |
| mid to late M | Young BD ($\theta < 3AU$) | $18^{+20}_{-12}\%$ | Joergens (2008) |
| mid to late M | VLMS [IM] $q \gtrsim 0.4$ | 21% | Janson et al. (2014) |
| M3-M4.5 (45) | VLMS/UCD | $27^{+5}_{-7}\%$ | Burgasser et al. (2007); Reid & Gizis (1997); Reid et al. (2003) |
| M4 to M6 | Young BD [HST/AO] $\theta > 10AU$ | $15^{+5}_{-3}\%$ | Todorov et al. (2014) |
| M5-M9 (16) | VLMS/UCD | $31^{+13}_{-9}\%$ | Burgasser et al. (2007); Reid & Gizis (1997); Reid et al. (2003) |
| >M6 | Young BD [HST/AO] $\theta > 10AU$ | $4^{+3}_{-1}\%$ | Todorov et al. (2014) |
| Late M and L | T dwarfs | $\sim 0.7 - 3\%$ | Bardalez Gagliuffi et al. (2013) |
| Late M, L and T | BD ($1 < \theta < 10AU$) | $10 - 20\%$ | [1]Burgasser et al. (2003); Close et al. (2003); Reid et al. (2001) |
| Late M, L and T | BD ($0.01 < \theta < 0.1AU$) | $\lesssim 30\%$ | [1]Reiners (2004); Pinfield et al. (2003) |
| BD | BD | $12^{+7}_{-4}\%$ | Burgasser et al. (2006b) |
| Mid to late BD | Late BD | $< 16 - 25\%$ | Aberasturi et al. (2014) |

[1] via Pinfield et al. (2005) [2] via Burgasser et al. (2006b) [3] via Metchev & Hillenbrand (2009) [4] via Cheetham et al. (2015)

Table 1.3 (cont.): Summary of some of the past binary fraction analysis for very low mass objects.

| Name | $M_{\rm star}$ $M_\odot$ | $R_{\rm star}$ $R_\odot$ | $T_{\rm star}$ K | [Fe/H] | $P$ days | $e$ | $M_{\rm UCD}$ $M_{Jup}$ | $R_{\rm BD}$ $R_{Jup}$ | $\rho$ $gcm^{-3}$ | Ref. |
|---|---|---|---|---|---|---|---|---|---|---|
| 2M0535-05a[a] | | | | | 9.779621(42) | 0.3225±0.0060 | $56.7 \pm 4.8$ | 6.5±0.33 | 0.26±0.06 | 1 |
| 2M0535-05b[a] | | | | | 9.779621(42) | 0.3225±0.0060 | $35.6 \pm 2.8$ | 5.0±0.25 | 0.35±0.08 | 1 |
| CoRoT-3b | $1.37 \pm 0.09$ | $1.56 \pm 0.09$ | $6740 \pm 140$ | -0.02±0.06[b] | 4.25680(5) | 0.0 | $21.66 \pm 1.0$ | $1.01 \pm 0.07$ | 26.4±5.6 | 2 |
| CoRoT-15b | $1.32 \pm 0.12$ | $1.46^{+0.31}_{-0.14}$ | $6350 \pm 200$ | +0.1±0.2 | 3.06036(3) | 0 | $63.3 \pm 4.1$ | $1.12^{+0.30}_{-0.15}$ | 59±29 | 3 |
| CoRoT-33b | $0.86 \pm 0.04$ | $0.94^{0.14}_{-0.08}$ | $5225 \pm 80$ | +0.44±0.10 | 5.819143(18) | $0.0700 \pm 0.0016$ | $59.0^{+1.8}_{-1.7}$ | $1.10 \pm 0.53$ | 55±27 | 4 |
| KELT-1b | $1.335 \pm 0.063$ | $1.471^{+0.045}_{-0.035}$ | $6516 \pm 49$ | +0.052±0.079 | 1.217513(15) | $0.01^{+0.01}_{-0.007}$ | $27.38 \pm 0.93$ | $1.116^{+0.038}_{-0.029}$ | $24.5^{1.5}_{-2.1}$ | 5 |
| Kepler-39b[c] | $1.10^{+0.07}_{-0.06}$ | $1.39^{+0.11}_{-0.10}$ | $6260 \pm 140$ | -0.29±0.10 | 21.0874(2) | $0.121^{+0.022}_{-0.023}$ | $18.00^{+0.93}_{-0.91}$ | $1.22^{+0.12}_{-0.10}$ | $12.40^{+3.2}_{-2.6}$ | 6 |
| Kepler-39b[c] | $1.29^{+0.06}_{-0.07}$ | 1.40±0.10 | $6350 \pm 100$ | +0.10±0.14 | 21.087210(37) | $0.112 \pm 0.057$ | $20.1^{+1.3}_{-1.2}$ | $1.24^{+0.09}_{-0.10}$ | $13.0^{+3.0}_{-2.2}$ | 7 |
| KOI-189b[d] | $0.764 \pm 0.051$ | 0.733±0.017 | $4952 \pm 40$ | -0.07±0.12 | 30.3604467(5) | $0.2746 \pm 0.0037$ | $78.0 \pm 3.4$ | $0.998 \pm 0.023$ | 97.3±4.1 | 8 |
| KOI-205b | $0.925 \pm 0.033$ | $0.841 \pm 0.020$ | $5237 \pm 60$ | +0.14±0.12 | 11.7201248(21) | <0.031 | $39.9 \pm 1.0$ | $0.807 \pm 0.022$ | 75.6±5.2 | 9 |
| KOI-205b | $0.96^{+0.03}_{-0.04}$ | $0.87 \pm 0.020$ | $5400 \pm 75$ | +0.18±0.12 | 11.720126(11) | <0.015 | $40.8^{=1.1}_{-1.5}$ | $0.82 \pm 0.02$ | $90.9^{+7.2}_{6.8}$ | 6 |
| KOI-415b | $0.94 \pm 0.06$ | $1.15^{+0.15}_{-0.10}$ | $5810 \pm 80$ | -0.24±0.11 | 166.78805(22) | $0.698 \pm 0.002$ | $62.14 \pm 2.69$ | $0.79^{+0.12}_{-0.07}$ | $157.4^{+51.4}_{-52.3}$ | 10 |
| LHS 6343C[e] | $0.370 \pm 0.009$ | $0.378 \pm 0.008$ | $3130 \pm 20$ | +0.04±0.08 | 12.71382(4) | $0.056 \pm 0.032$ | $62.7 \pm 2.4$ | $0.833 \pm 0.021$ | 109±8 | 11 |
| WASP-30b | $1.166 \pm 0.026$ | $1.295 \pm 0.019$ | $6201 \pm 97$ | -0.08±0.10 | 4.156736(13) | 0 | $60.96 \pm 0.89$ | $0.889 \pm 0.021$ | 107.6±1.1 | 12 |

[1]Stassun et al. (2006), [2]Deleuil et al. (2008), [3]Bouchy et al. (2011a), [4]Csizmadia et al. (2015), [5]Siverd et al. (2012), [6]Bouchy et al. (2011b), [7]Bonomo et al. (2015), [8]Díaz et al. (2014), [9]Díaz et al. (2013), [10]Moutou et al. (2013), [11]Johnson et al. (2011), [12]Anderson et al. (2011).

*a:* 2M0535-05 is an extreme young eclipsing system in which two UCDs orbit each other.
*b:* [M/H] value is reported in the reference. Notice that $[M/H] \approxeq [Fe/H]$; Csizmadia et al. (2015) did not convert the inhomogeneous [Fe/H] to the same scale.
*c:* Also known as KOI-423b.
*d:* Díaz et al. (2014) concluded that KOI-189b can be either a high-mass UCD or a very low mass star, too, therefore its status is uncertain.
*e:* The UCD orbits companion A of a binary system, and data of the component A is given here. Star B has $M = 0.30 \pm 0.01 M_\odot$, $T_{\rm eff} = 3030 \pm 30$ K (Johnson et al., 2011)

Table 1.4: Table 1 from Csizmadia et al. (2015). Basic data of known transiting UCDs. $\rho$ is the mean density of the brown dwarf component and $e$ is the ellipticity.

## 1.3 UCDs in binary systems

As companions UCDs can be both revealing and informative. The statistical studies of UCD companions aids the theoretical study of low-mass star formation and provides constraints on the initial mass function (Parker & Reggiani, 2013; Chabrier et al., 2014). Specifically companion statistics can be used to decide between different formation processes. For wide binaries, for example, it is difficult to explain formation via dynamical processes[4] or disc fragmentation and is more likely to come from core fragmentation at very early stages (Chabrier et al., 2014). There is also a lack of 10 to 100 $M_{Jup}$ objects (the brown dwarf desert) in separation ranges covered by radial velocity surveys (see e.g. Kraus et al. 2008, Kraus et al. 2011, Cheetham et al. 2015). Observationally it has been found the frequency of companions increases for planetary mass companions but decreases for companions with larger mass (Howard et al., 2010). Giant planets are also thought to be less frequent around lower-mass stars than higher mass stars (Johnson et al., 2010) whereas in the same separation range UCD companions become more frequent around low-mass stars and other UCDs when compared to higher mass stars (Joergens, 2008).

Ultracool companions are also very useful as benchmark objects to test structure and atmospheric evolutionary models (Pinfield et al., 2006). To measure mass, UCDs need to be in a binary system where dynamical masses of UCDs can be measured (Bouy et al., 2004), using a combination of transits and radial velocity observations (Stassun et al., 2006), discussed in more detail in Section 1.3.4.

Age and composition can generally be inferred from the primary star (Leggett et al., 2010), and companion mass and radius constraints can sometimes come from radial velocity and light curve studies over multiple orbital periods (e.g. Agol et al., 2005; Cumming et al., 2008; Jones et al., 2015), via astrometry (e.g. with Gaia, de Bruijne, 2012), or via adaptive optics (e.g. Dupuy et al., 2010). Once these physical parameters can be directly measured they can be used for testing models of atmospheres and interiors (Baraffe et al., 2003; Burningham et al., 2009, 2011; Burrows et al., 2011; Luhman, 2012; Allard et al., 2012; Saumon et al., 2012; Burningham et al., 2013).

Of the 2,085 confirmed and 562 candidate UCDs known (as of June 2015), 427 are in binary or multiple systems (65 as companions to FGK stars and 10 of these are transiting), see Table 1.3 and the excellent table by Csizmadia et al. (2015), presented here in Table 1.4.

[4]However, as discussed in Faherty et al. 2010 scenarios such as where a UCD is a wide companion to a tight binary is affected by dynamical interactions.

### 1.3.1 UCD+UCD systems

The latter part of Table 1.3 shows the binary fraction for UCD+UCD systems at somewhere in the range of 10 to 30 per cent. Unresolved companions have been identified using a variety of observational techniques. Most UCD+UCD binaries are relatively close and wide companions are rare (only a few are known field UCDs with separations wider than ∼30 AU, i.e. Close et al. 2003, Bouy et al. 2003,Close et al. 2007,Burningham et al. 2010, and references within Burgasser et al. 2006b and Siegler et al. 2005). This rarity in wide companions is due to the weak binding energies, thus this fraction is higher in very young systems (i.e. Chauvin et al. 2004, Chauvin et al. 2005b, Mamajek 2005, Song et al. 2006). Close-in, high contrast systems are generally revealed through radial velocity variability searches, with much lower contrast systems (e.g. late M dwarf+UCD or UCD+UCD systems Burgasser et al. 2006a, 2010; Bardalez Gagliuffi et al. 2013, 2015) being more amenable to spectroscopic and photometric study (e.g. in Reid & Mahoney 2000, Reid et al. 2001, Oppenheimer et al. 2001, Nidever et al. 2002, Pinfield et al. 2003, Burgasser et al. 2003, Close et al. 2003, Reiners 2004, Burgasser et al. 2006b, Joergens 2008, Luhman 2012, Todorov et al. 2014, Manjavacas et al. 2016).

### 1.3.2 UCDs as companions to high mass stars

If one looks at the stellar primaries with UCD companions in Table 1.2 and Table 1.3 there is a steep drop in binary fraction from stars with stellar companions (i.e. M dwarfs above ∼20 per cent), and UCDs with UCD companions (again between 10 and 30 per cent), when compared to stars with UCD companions (∼0 and ∼10 per cent). This deficit in the frequency of brown dwarf companions is known as the brown dwarf desert. This desert has been attributed to selection effects and biases of the current observations, however work by Grether & Lineweaver (2006) verified this was probably not the case and a true deficit does exist around solar type stars. They compare the number of close stellar, brown and giant planet companions and find 11 per cent are stellar companions, less than 1 per cent are brown dwarf companions and 5 per cent are giant planet companions. This suggests a discontinuity in formation and the brown dwarf desert is where the stellar formation process tails off and the planetary formation process begins (Bate 2000, Boss 2002, Larson 2003, Kroupa & Bouvier 2003, Rice et al. 2003, Matzner & Levin 2005 via Grether & Lineweaver 2006, Ma & Ge 2014). This is also seen at wider separations where there are fewer than 50 wide (> 100 AU) comoving systems known (e.g. Gizis et al. 2001, Lafrenière et al. 2008, Faherty et al. 2010, 2011, Burningham et al. 2013, Gomes et al. 2013, Mužić et al. 2012, via Faherty 2014) corresponding to a wide binary fraction of 5 to 8 per cent (Burningham et al. 2013,Gomes et al. 2013).

### 1.3.3 UCDs as companions to M dwarfs

Observationally it is very difficult to measure a binary fraction. Many factors affect how many companions can be detected, and low numbers limit statistical studies over multiple parameter biases (i.e. separation and mass ratio, Parker & Reggiani, 2013; Oppenheimer, 2014). It is clear though the M dwarf-UCD companion fraction is low ($\lesssim$ 5%). Table 1.3 also shows a range of observational methods used to look for companions to stellar and UCD companions.

For lower luminosity primaries, the signature of additional unresolved objects (including companions and discs) becomes more pronounced, with an increased potential for identification through spectroscopic and photometric methods (e.g. Reid & Mahoney 2000, Reid et al. 2001, Oppenheimer et al. 2001, Nidever et al. 2002, Pinfield et al. 2003, Burgasser et al. 2003, Close et al. 2003, Reiners 2004, Burgasser et al. 2006b, Joergens 2008, Luhman 2012, Bardalez Gagliuffi et al. 2013, and Todorov et al. 2014). However, this is countered by fainter primaries being harder to detect. Therefore the ideal systems are those with primaries which are low luminosity whilst avoiding the tail end of the brightness distribution, with the companions being as bright as possible.

For separations of $\lesssim$100 AU the M dwarf+UCD companion fraction is low, possibly at the level of approximately one per cent (i.e. 2-4 per cent, via Adaptive optics; Neuhäuser & Guenther 2004; 0-2 per cent, $0.001<\theta<0.01$ AU, Reid & Mahoney 2000; 1-3 per cent, $10<\theta<100$ AU Oppenheimer et al. 2001; 1 per cent, $0.1<\theta<1$ AU, Nidever et al. 2002; and 1 per cent, $1.0<\theta<10.0$ AU Nidever et al. 2002, where $\theta$ is separation). Warm to hot giant exoplanets are not thought to be common companions to M dwarfs (Butler et al., 2004), and if found to exist would be an important test for planetary formation models (Lissauer et al., 1998), although this process would not be easy by core accretion mechanisms (Ida & Lin, 2005). However, as mentioned in Section 1.1.1 the maximum masses of giant exoplanets are similar to the lowest mass UCDs, so there is ambiguity when considering brown dwarf/exoplanet companions in this mass range.

UCDs are very faint compared to hotter stars and as such M dwarfs are the obvious primary stars to search for UCD companions as they are relatively cool and faint in comparison to other higher mass main sequence stars. As M dwarfs are the most numerous in the Galaxy even if UCD companions are rare, one maximises the number of possible candidates available. One also gets reduced glare from fainter M dwarfs when trying to detect faint UCD companions.

### 1.3.4 Measuring companion properties

#### Radial velocity

Two bodies gravitational bound to each other orbit a common centre-of-mass or barycentre. When the mass of one object is sufficiently larger (the primary) than the other

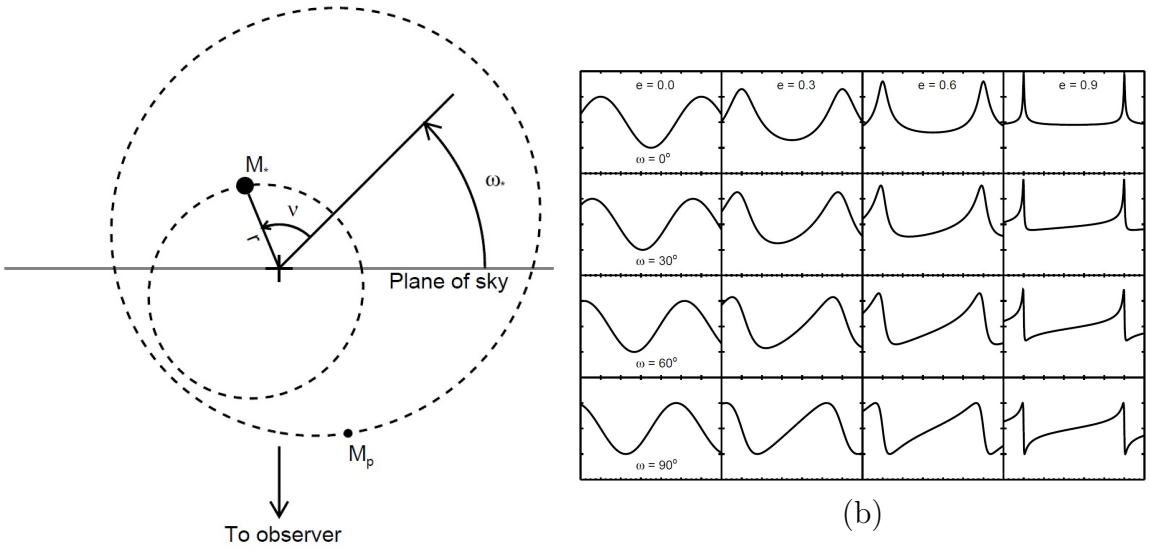


Figure. 1.5: Figures taken from Wright & Gaudi (2013), (a) a visual representation of the elements describing orbital motion in a binary system. $\omega$ is the argument of periastron and $\nu$ is the true anomaly with respect to the periastron, the closest point between the two bodies. (b) the effects of eccentricity, $e$, and argument of periastron, $\omega$, on the shape of a radial velocity curve with unit period, amplitude and unit time since periastron.

(the secondary) an apparent radial motion of the primary can be precisely measured through Doppler velocity measurements. From this motion the period, distance and shape of the orbit and orbiting mass can be found (Wright & Gaudi, 2013). Periodic radial velocity depends on the orbital period, the semi-amplitude of the signal (in units of velocity), the eccentricity of the orbit, the longitude of periastron for the star, the time since periastron, and the bulk velocity of the centre of mass of the system ($P$, $K$, $e$, $\omega$, $T_0$ and $\gamma$ respectively). $P$, $T_0$ and $K$ respectively set the period, phase and amplitude of the radial velocity curve with $\omega$ and $e$ setting the shape of the curve, see Figure 1.5.

This along with the inclination angle, $i$ (where $i = 0$ is an observed face-on counter-clockwise orbit) allows the mass function of the system to be measured. If one knows the mass of one of the objects and the inclination angle of the orbit the other mass can be worked out, or if the inclination angle is unknown, a minimum mass can be set as $M_2 \sin(i)$ (Wright & Gaudi, 2013). Thus if a radial velocity measurement can be made one can directly work out the minimum mass of the companion.

### Transit follow-up

When one luminous object passes in front of another a dimming of the signal is observed. For two bodies in orbit (the more massive being the primary, with radius $R_1$,

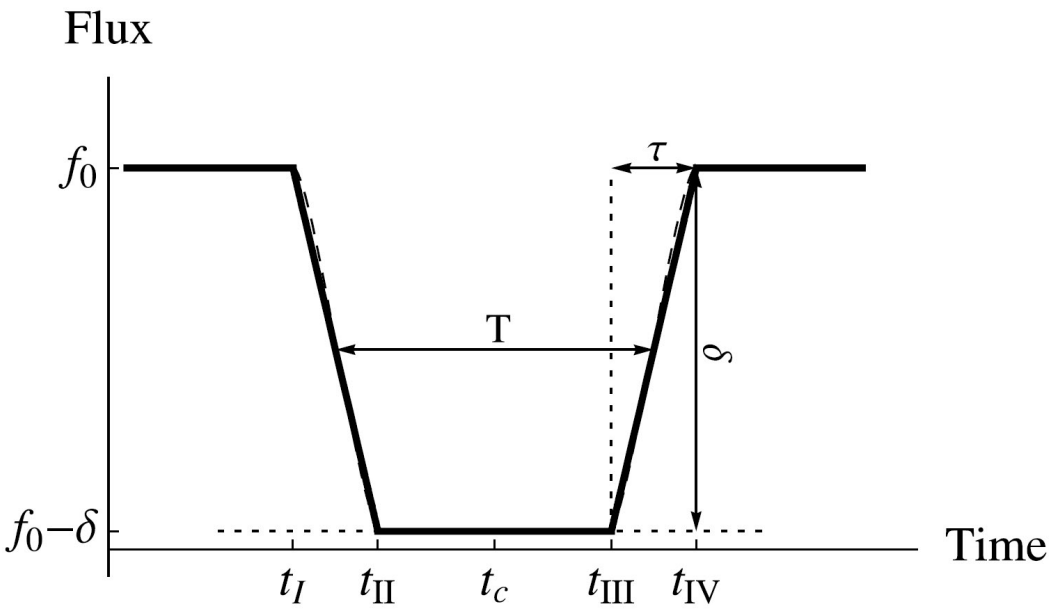


Figure. 1.6: Model transit light curve from Carter et al. (2008). $T$ is the full width half maximum, $FWHM$, of the light curve approximately equal to the duration of the transit, $f_0$ is the unocculted flux of the primary, $\tau$ is the ingress or egress time, $\delta$ is the transit depth and $t_I$, $t_II$, $t_c$, $t_III$, and $t_IV$ are the first, second, centre, third and fourth contact points respectively.

and the less massive being the secondary, with radius $R_2$) this dimming is periodic. The condition for obtaining a light curve from a transit is such that the projected separation between the secondary and the primary is less than the sum of the radii of both objects. A transit will occur when $b \leqslant 1+k$ where $k = \frac{R_2}{R_1}$ (Wright & Gaudi, 2013), see Figure 1.6. For derivation see Section 2 from Carter et al. (2008). The probability of a transit, $P_{tran}$, can be obtained by integrating over $i$ and assuming an isotropic orbit (Wright & Gaudi, 2013). Measuring the duration of transit, $T$, the ingress or egress time, $\tau$ and the depth of the transit, $\delta$, allows the calculation of the impact parameter, the equatorial crossing time, $T_{eq}$, and $k$, as shown by Wright & Gaudi (2013). By combining radial velocity and multiple transits it is possible to measure the orbital period and hence the mass fraction. By imposing external constraints on properties of the primary (spectroscopy, parallax or theoretical relations) it is possible to break the degeneracy and measure both inclination angle and hence the mass.

### Adaptive optics

The optimal resolution of a system is limited by the diffraction of electromagnetic waves. This diffraction limit is defined by the angle,

$$\alpha = 1.22\frac{\lambda}{D} \tag{1.1}$$

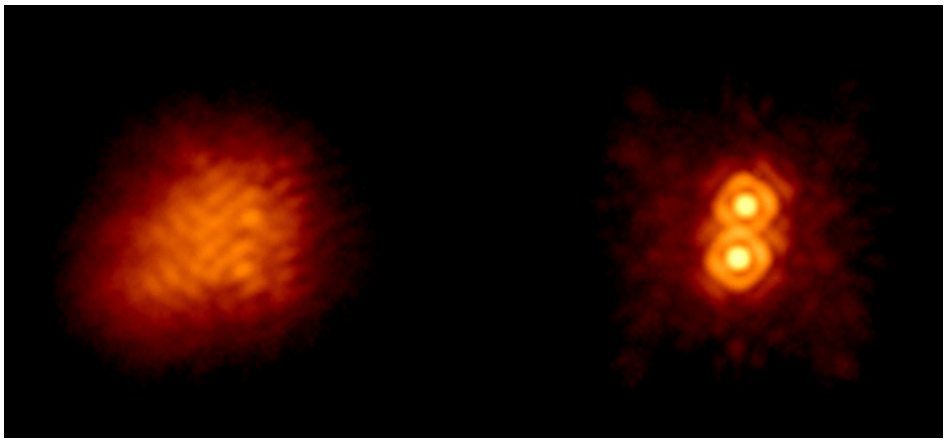

Figure. 1.7: Images taken by Chas Beichman and Angelle Tanner of JPL. The 0.3 arcsec separation binary star, IW Tau, left no adaptive optics, right adaptive optics (Group, 1999).

where $\lambda$ is the wavelength of light and $D$ is the diameter of the aperture. However, in practise, these limits are never reached in ground based observations due to turbulence in the atmosphere.

This is where adaptive optics is useful. By using a guide star or laser, atmospheric turbulence can be measured and is thus compensated for by fast steering mirrors and deformable mirrors (Roberts & Neyman, 2002). Adaptive optics means ground based observatories can compete with space-based telescopes, a typical improvement can be seen in Figure 1.7

For UCDs this has been used to aid direct imaging (e.g. Hinkley 2012) and calculating dynamical masses (e.g. Konopacky et al. 2010, Dupuy et al. 2011 and Montet et al. 2015).

| Survey | Band | Wavelength $\mu$m | PSF-FWHM *arcsec* | Mag. limit ($5\sigma$) *mag* | Notes |
|---|---|---|---|---|---|
| Tycho-2 | $B_{Tycho}$ | 0.4280 | 0.8-2.5 | 11.0 | *a* |
| SDSS | $g$ | 0.4686 | 1.3 | 22.2 | *b* |
| Tycho-2 | $V_{Tycho}$ | 0.5340 | 0.8-2.5 | 11.0 | *a* |
| SDSS | $r$ | 0.6165 | 1.3 | 22.2 | *b* |
| USNO-A2.0 | $R$ | 0.658 | - | >20 | *c* |
| SDSS | $i$ | 0.7481 | 1.3 | 21.3 | *b* |
| SDSS | $z$ | 0.8931 | 1.3 | 20.5 | *b* |
| 2MASS | $J$ | 1.25 | 2.9 | 16.55 | *d* |
| 2MASS | $H$ | 1.65 | 2.8 | 15.85 | *d* |
| 2MASS | $K_S$ | 2.16 | 2.9 | 15.05 | *d* |
| WISE | $W1$ | 3.4 | 6.1 | 16.5 | *e* |
| WISE | $W2$ | 4.6 | 6.4 | 15.5 | *e* |

[a] Høg et al. (2000) Magnitude limit at 99 per cent completeness
[b] Ahn et al. (2012) and http://www.sdss3.org/dr9/scope.php
[c] Assafin et al. (2001) and Monet (1998) via http://www.nofs.navy.mil/projects/pmm/USNOSA2doc.html
[d] Skrutskie et al. (2006), http://www.ipac.caltech.edu/2mass/releases/allsky/ and http://spider.ipac.caltech.edu/staff/roc/2mass/seeing/seesum.html (Magnitude limits quoted as $10\sigma$, $5\sigma \equiv$ 'mag at $10\sigma$' + 0.75)
[e] Wright et al. (2010) and http://wise2.ipac.caltech.edu/docs/release/allsky/expsup/

Table 1.5: Table summarising the surveys used in this thesis, band names are given as well as the photometric point spread function,PSF, size and photometric sensitivity limits. Catalogues used in this work are Tycho-2 (Høg et al., 2000), USNO-A2.0 (Monet, 1998), SDSS (Ahn et al., 2012), 2MASS protect(Skrutskie et al., 2006) and WISE (Wright et al., 2010) photometric bands used in this thesis.

## 1.4 The era of the mega surveys

The ultracool ($T_{eff}$<2500 K, >M7) field population has been greatly expanded over the last fifteen years using large-scale red and infrared surveys; *The Two Micron All-Sky Survey* (2MASS, Skrutskie et al., 2006), *The Sloan Digital Sky Survey* (SDSS, York et al., 2000), *The United Kingdom Infrared Telescope; Infrared Deep Sky Survey* (UKIDSS, Lawrence et al., 2007), *The Visible and Infrared Survey Telescope for Astronomy* (VISTA, Emerson & Sutherland, 2002) and *The Wide-Field Infrared Survey Explorer* (WISE, Wright et al., 2010). Table 1.5 summarises the multi-band photometric sensitivity limits which I used when selecting sources from these surveys

As well as large-scale photometric surveys the use of multi-object fibres, such as

[5] The 2MASS Atlas Image Gallery at IPAC accessed online at http://www.ipac.caltech.edu/2mass/gallery/
[6] NASA Jet Propulsion Laboratory (JPL) Photojournal accessed online at http://photojournal.jpl.nasa.gov/catalog/PIA15481

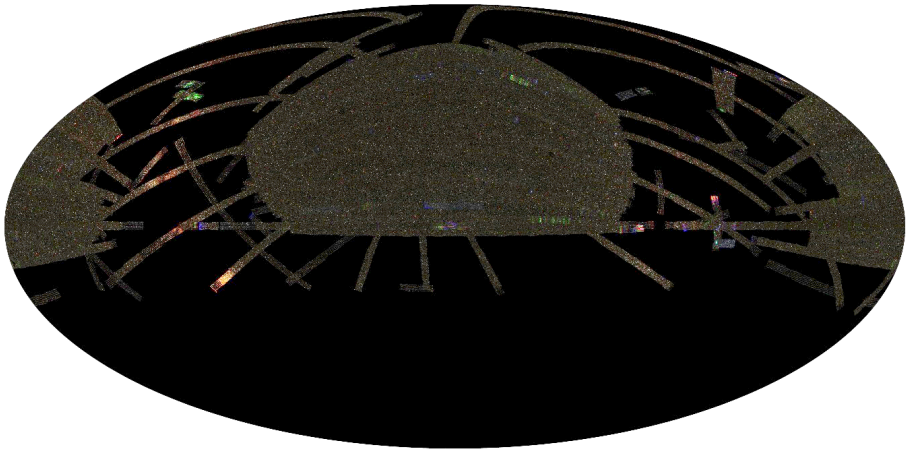

(a) The Sloan Digital Sky Survey SDSS

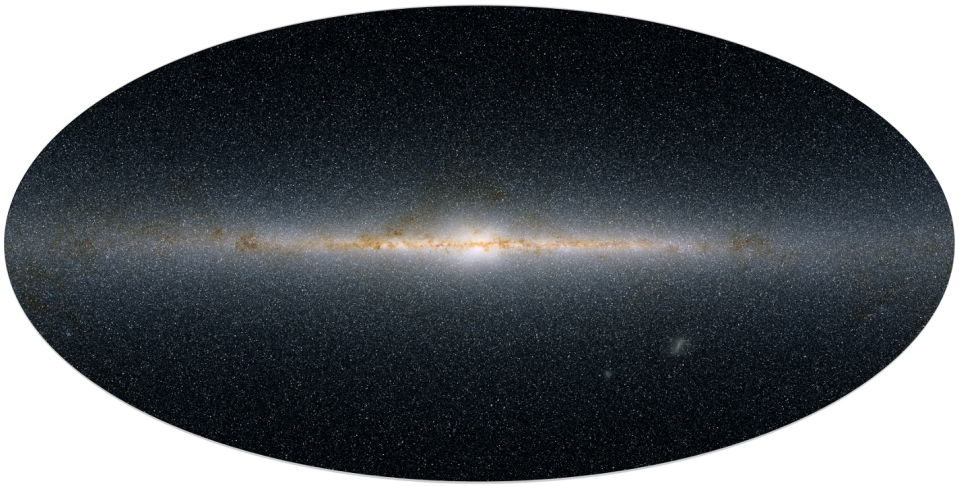

(b) The Two Micron All Sky Survey 2MASS

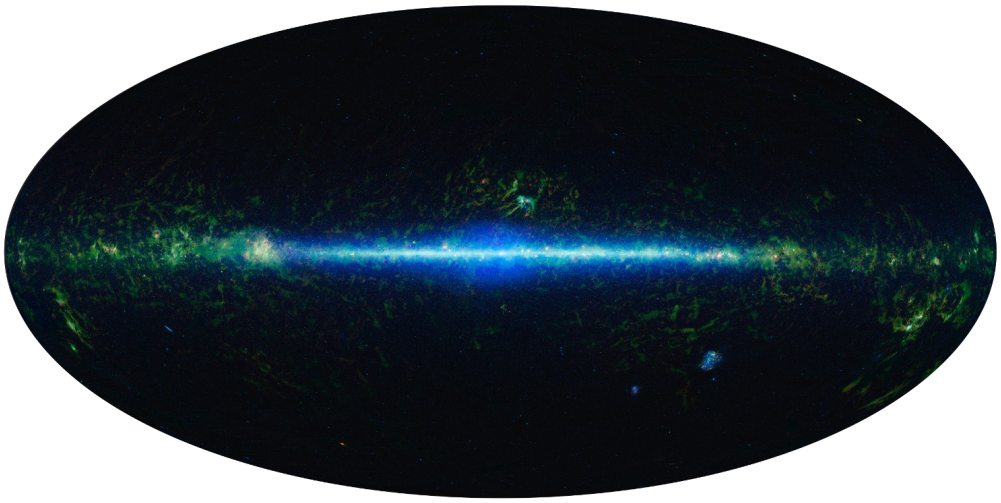

(c) The Wide-field Infrared Survey Explorer WISE All Sky Survey

Figure. 1.8: Images of the three large surveys used in this Thesis. (a) Aitoff protection centred around $\alpha = 180°$, $\delta = 0.0°$, created using the ALADIN (Bonnarel et al., 2000). (b) Galactic longitude/latitude Aitoff project taken from the 2MASS Atlas Image Gallery at IPAC[5]. (c) Galactic longitude/latitude Aitoff project taken from the NASA JPL Photojournal[6]

*The Large Sky Area Multi-Object Fibre Spectroscopic Telescope*(LAMOST Cui et al., 2012), has lead to huge numbers of stellar spectra becoming available.

### 1.4.1 The Two Micron All-Sky Survey

2MASS[13] was a ground-based near-infrared (NIR) all-sky survey, and as such, wavelength bands were significantly constrained by effects such as atmospheric transmission and ambient thermal background (Skrutskie et al., 2006). Thus the classical $K$ band used by (Johnson et al., 1962), not severely effected by thermal background emission, was chosen along with the $J$ and $H$ bands. The $J$ (1.25 $\mu$m ) and $H$ (1.65 $\mu$m ) have profiles which largely correspond to the classical $J$ and $H$ bands by Johnson et al. (1962). The so called "K-short", $K_s$ (2.16 $\mu$m ) band, is the exception, due to the exclusion of wavelengths longer than 2.31 $\mu$m to improve the reduction of thermal background (Skrutskie et al., 2006).

The 2MASS point source catalogue contains photometry for 470,992,970 objects and were observed at the Mt. Hopkins, Arizona facility between June 1997 and December 2000 in the North and at Cerro Tololo, Chile between March 1998 and February 2001. 2MASS achieved $10\sigma$ source sensitivities better than 15.8 magnitudes is $J$ band, 15.1 in $H$ band and 14.3 in $K_s$ band (see Figure 1.9) for PSFs of 2.9, 2.8 and 2.9 arcsec respectively (see Figure 1.10).

### 1.4.2 The Sloan Digital Sky Survey

As of the tenth data release, SDSS has observed 1,231,051,050 objects (of which 469,053,874 are unique and 260,562,744 are unique stars) using the Sloan Foundation 2.5-meter Telescope at the Apache Point Observatory in New Mexico from 1998 through to 2011. Unlike WISE and 2MASS it is a northern hemisphere only survey using five optical bands ($u$, $g$, $r$, $i$ and $z$ at 0.3551, 0.4686, 0.6165, 0.7481 and 0.8931$\mu$m respectively) to observe the sky. The 95 per cent completeness for points sources is 22.0, 22.2, 22.2, 21.3 and 20.5 with a median PSF FWHM in the r-band of 1.3 arcsec[9]. SDSS also has a range of spectroscopic surveys (BOSS, SEGUE-1, APOGEE and MARVELS). However, although SDSS provides spectroscopy for a selection of its sources (prioritised mainly for extragalactic science) and has been used for studying faint M dwarfs (e.g. West et al. 2011) I make use of a different spectroscopic survey which prioritises galactic targets (i.e. LAMOST, see section Section 1.4.4).

SDSS covers an area of around 14,555 square degrees and as such is smallest area covered by the three large surveys (hence my samples of objects are limited to the SDSS) regions (see Figure 1.11).

[7]Figure adapted from http://www.astro.caltech.edu/~jmc/2mass/v3/gp/analysis.html
[8]Figure adapted from spider.ipac.caltech.edu/staff/roc/2mass/seeing/seesum.html
[9]Accessed online at http://www.sdss3.org/dr9/scope.php

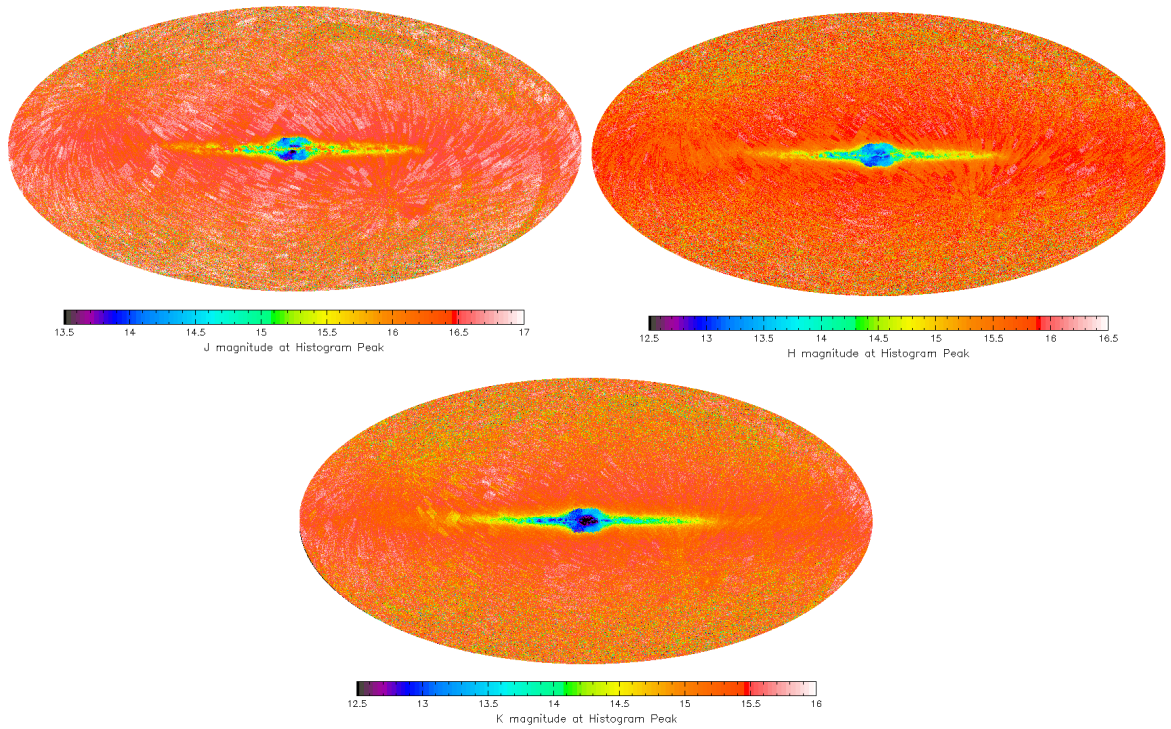


Figure. 1.9: 2MASS $J$ $H$ and $K_S$ $10\sigma$ sensitivity maps[7], average sensitivities better than 16.5 and 15.5 respectively (Wright et al., 2010).

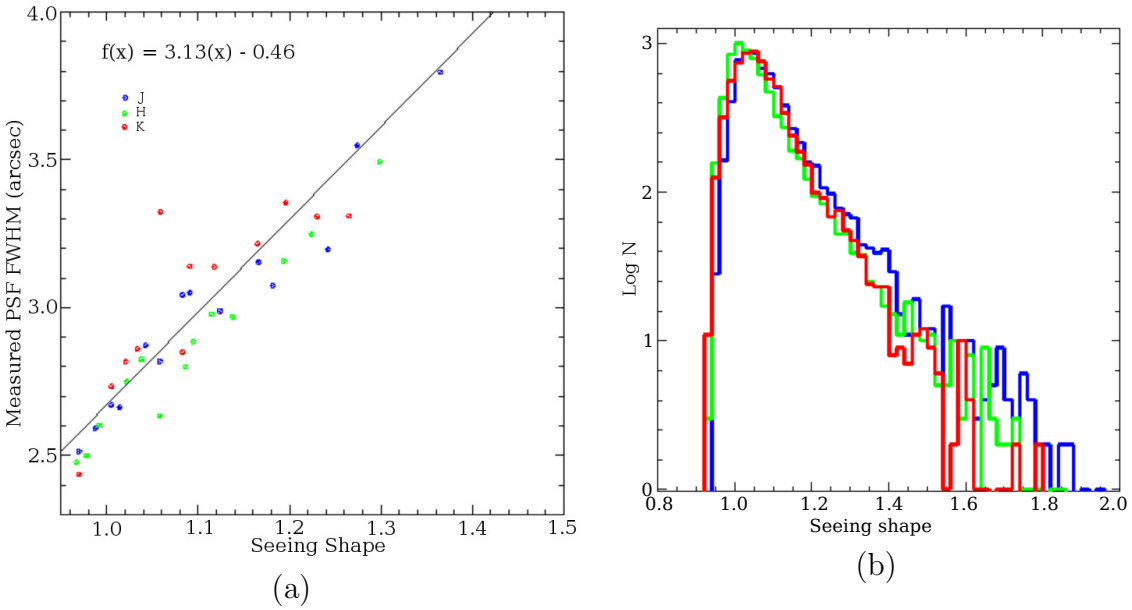


Figure. 1.10: Figures from 2MASS website[8]. As 2MASS is a ground-based telescope, PSF varies with seeing. (a) The seeing shape to PSF relation and (b) the distribution of seeing shapes for 2MASS bands $J$ (blue) $H$ (green) and $K_S$ (red). From the seeing shape medians of 1.07, 1.05 and 1.06 arcsec (FWHM) the 2MASS PSFs are 2.9, 2.8 and 2.9 arcsec respectively.

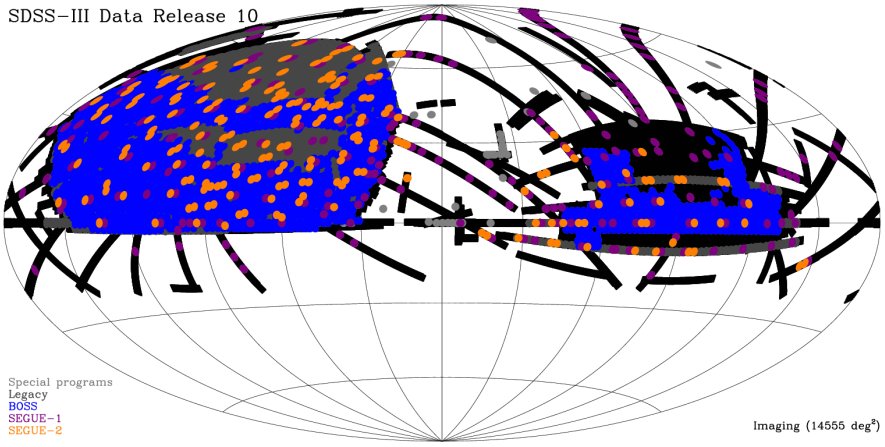


Figure. 1.11: The coverage of the tenth data release of SDSS which defines the sky coverage of the work in this thesis.

### 1.4.3 The Wide-Field Infrared Survey Explorer

WISE mapped the whole sky in four mid-infrared (MIR) bands $W1$, $W2$, $W3$ and $W4$ centred at 3.4, 4.6, 12 and 22 $\mu$m (Wright et al., 2010). This medium class explorer, a 40 cm Earth-orbiting telescope, provides MIR sensitivities across the sky. The $W1$ and $W2$ bands were designed specifically with UCDs in mind, to cover the 3.3 $\mu$m $CH_4$ absorption band and the region relatively free of opacity at 4.6 $\mu$m (see Figure 1.2b). This makes the $(W1 - W2)$ colours of UCDs extremely red, and due to this almost unique red colour, UCDs are relatively easy to identify (Kirkpatrick et al., 2011).

WISE completed two full sky passes, but due to depletion of the secondary cryogen tank, and then the primary tank, the second full sky pass is partly missing the $W3$ and $W4$ bands (Kirkpatrick et al., 2011). However $W1$ and $W2$ where unaffected and continued into a third sky pass. WISE also provides information on individual observations, and as such provides statistical information on profile fitting. This can be used as a measure of variability (Pinfield et al., 2013), see Section 3.2.3. The WISE all-sky source catalogue contains 563,921,584 objects and were observed between Jan 2010 and Aug 2010 (the full cryogenic mission phase) and achieved $5\sigma$ source sensitivities better than 16.5 magnitudes in $W1$ and 15.5 magnitudes in $W2$ (see Figure 1.12) for PSFs of 6.08 and 6.84 arcsec respectively (see Figure 1.13).

### 1.4.4 The Large Sky Area Multi-Object Fibre Spectroscopic Telescope

LAMOST (also known as the Guo Shoujing Telescope) is a uniquely designed telescope allowing up to 4,000 spectra to be observed in a single exposure. It originally had a limiting magnitudes as faint as $r = 19$ and a resolution of $R = 1800$ (Cui et al., 2012)

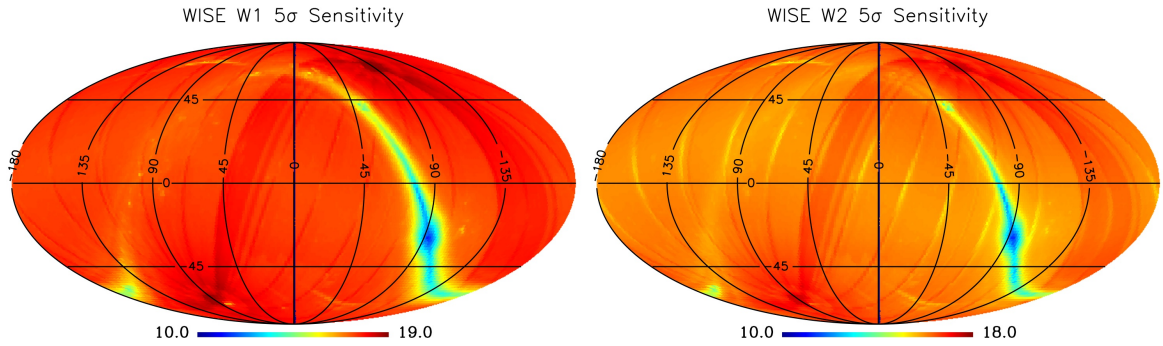


Figure. 1.12: WISE $W1$ and $W2$ $5\sigma$ sensitivity maps[10], average sensitivities better than 16.5 and 15.5 respectively (Wright et al., 2010).

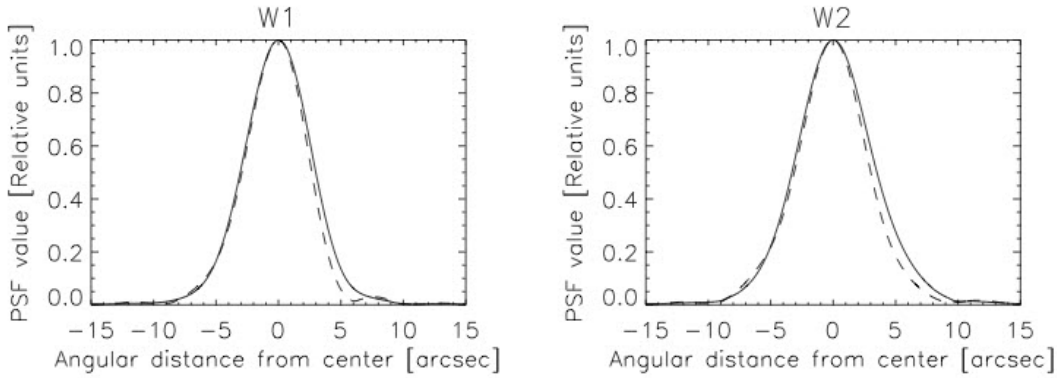


Figure. 1.13: Point spread functions (PSF) for WISE $W1$ and $W2$ bands through the major axes(Wright et al., 2010)[11]. The full width half maximums (FWHM) correspond to 6.08 and 6.84 arcsec respectively (Wright et al., 2010). The WISE PSFs are the largest out of the surveys I use and hence define my definition of unresolved within this PSF.

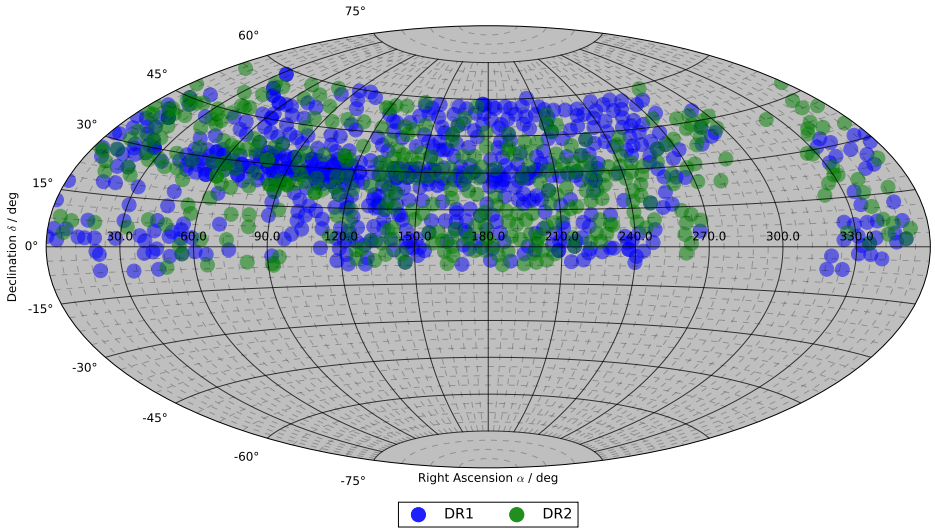


Figure. 1.14: The coverage of the first and second internal data releases of LAMOST.

but currently the limiting magnitude is closer to $r = 17$ (Lou, 2014).

The LAMOST spectrograph splits into a red (0.57-0.90$\mu$m ) and blue (0.37-0.59$\mu$m ) arm (Cui et al., 2012). However, both the blue arm and the far red end of the red arm suffer from skyline contamination and the overlap region between the two channel (0.57 and 0.59 $\mu$m ) should also be avoided, thus in general the use of LAMOST spectra should be limited to 0.6-0.8$\mu$m (Zhong et al., 2015a,b; Lou, 2014). The huge number of fibres available and the wide field of view (5° ) means LAMOST has obtained a vast number of spectra. As of pilot survey (Oct. 2011 to June 2012) the first (Sept. 2012 - June 2013) and second (Sept. 2013 - June 2014) internal data release the LAMOST catalogue has 4,136,482 spectra including 3,784,461 stars, 37,206 galaxies, 8,630 QSOs, and 306,185 unknowns[12] (see Figure 1.14).

## 1.5 Project Motivation

The aim of this thesis is to use a cross-match between WISE, 2MASS and SDSS to identify a large sample of M dwarfs (Chapter 2). Through the careful characterisation and quality control of these M dwarfs (and the use of LAMOST) I aim to identify rare systems (i.e. unresolved UCD companions, young M dwarfs, late M dwarfs and M dwarfs with common proper motion companions).

The identification of unresolved UCD companions relies on the intrinsic spectral differences between M dwarfs and UCDs (i.e. UCDs have much redder MIR-NIR colours

[10]Figure adapted from Section 6.3a wise2.ipac.caltech.edu/docs/release/allsky/expsup
[11]Figure adapted from Section 4.4c wise2.ipac.caltech.edu/docs/release/allsky/expsup
[12]Internal access was granted via my Chinese collaborators from IPERCOOL, grant number 247593 within the Marie Curie 7th European Community Framework Programme. Access to the first data release is public via http://dr1.lamost.org/

than M dwarfs). I used the fact close-in binaries (within the 6 arcsec WISE PSF) are unresolved, thus the colour of the binary is a combination of the colour of the M dwarf and UCD companion. To determine the nature of any companion I compared this combined colour to the colour of a similar isolated M dwarf. As UCDs are redder than M dwarfs in the NIR-MIR colour an M+UCD will have a MIR excess in colour when compared to the colour an isolated M dwarf. This MIR excess could be confused with other sources of reddening (i.e. interstellar reddening and/or photometric uncertainty) thus I aimed to minimise their contribution by using various quality cuts. I used the fact UCDs have little-to-no flux in the optical (see Figure 1.3) to select optical colours which identify M dwarfs which are very similar. I then modelled the MIR excess signal I expected from a UCD companion and choose specific colours to optimise this process. I carefully analysed the excess distribution, selected candidate M+UCD systems and looked at the properties of these candidates (Chapter 3).

These candidates need confirming, however this is a difficult process in itself. Therefore in Chapter 4 I discuss contamination in my M+UCD candidates and my attempts to reduce the contamination using optical spectra. In the rest of Chapter 4 I present a method to follow-up my M+UCD candidates, in an optimal manner, using colour similar control M dwarfs and a low resolution spectral difference approach.

In chapter 5 I present the other rare objects selected from my large M dwarf catalogue. Young objects (which have optical spectra) are selected using equivalent widths, and by rotation periods (for those which have Kepler 2 light curves). Late M dwarfs are selected via photometric (and reduced proper motion) and spectroscopic methods (again for those with optical spectra). Finally I use common proper motion cross-matching to search for physically bound systems where the other object can be a Tycho-2 (FGK) star (providing better constrained properties from the primary, as determining age and metallicity from M dwarfs is difficult compared to e.g. sun-like stars) or another one of my M dwarfs (for binary analysis).

I finish by discussing where this thesis is leading, with various avenues of follow-up and further characterisation of the M dwarfs. I discuss how upcoming surveys and missions could benefit from, and improve, the work presented here (Chapter 6).

The ultimate aim of finding these UCD companions to M dwarfs is their value for testing formation and evolutionary models and for furthering the understanding of these cool complicated objects. The real holy grail of this work would be finding UCDs which are sufficiently close to the M dwarf as to give a transit signal and thus provide the community with a unique set of benchmark systems. Carefully selected sub-samples of the young and late M dwarfs discussed in this thesis, if confirmed, would be good candidates for current and future exoplanet searches. The common proper motion systems also provide a set of opportunities to better characterise M dwarfs and the possibility of searching for exoplanet companions.

# Chapter 2: Catalogue construction

This chapter is a version of Section 2 of "A Method for Selecting M dwarfs with an Increased Likelihood of Unresolved Ultra-cool Companionship", Cook, Pinfield, Marocco, Burningham, Jones, Frith, Zhong, Luo, Qi, Lucas, Gromadzki, Day-Jones, Kurtev, Guo, Wang, Bai, Yi, & Smart, 2016a and is reproduced by permission of MNRAS.

The co-authors of the paper contributed in advice, guidance, ideas and private discussions only, everything else is my own original work. Chilean authorship is in part thanks to use of Chilean facilities and Chinese authorship relates to my access and use of the LAMOST catalogue.

## 2.1 Introduction

As a foundation for my analysis procedures, I constructed a large catalogue of M dwarf candidates with high quality WISE/2MASS/SDSS photometry. Through out this chapter I present plots showing a small sub sample from the evolving catalogue sample to illustrate aspects of the selection process (This small sample consists of a small area of sky, $\alpha = 9^h20^m0.0^s, \delta = +30°0^m0.0^s$ to $\alpha = 10^h0^m0.0^s, \delta = +40°0^m0.0^s$).

## 2.2 Survey band selection

I wanted to have the largest possible set of M dwarfs. As mentioned in Section 1.5 I make use of the all-sky nature of WISE and 2MASS. For reasons mentioned in Section 2.3.2 I limit myself to the northern hemisphere using SDSS in order to better gauge the spectral type of my M dwarfs.

I chose not to use SDSS $u$ band (0.3551 $\mu$m) due to its increased uncertainties (Padmanabhan et al., 2008) as I want high quality photometry only. I also chose not to use the WISE $W3$ and $W4$ bands due to the greatly reduced sensitivity (magnitude limit at $5\sigma$ of 11.40 for the 12 $\mu$m, $W3$ band, and 7.97 and for the 22 $\mu$m, $W4$ band; Wright et al., 2010) as I would not have detections for many of the M dwarf candidates, reducing the number further. This leaves me with access directly to the $g$, $r$, $i$, $z$, $J$, $H$, $K_S$, $W1$ and $W2$ (see Section 1.5) and indirectly to the V band (see Section 2.3.2).

## 2.3 Initial colour and photometric cuts

### 2.3.1 Combining WISE and 2MASS

I began by downloading[13] all 563,921,603 sources in the WISE All-Sky catalogue, of which 280,909,458 had 2MASS counterparts within three arcsec . I applied NIR colour cuts to help remove contaminating giant stars and earlier spectral type stars from the sample. I made use of the $(J-H)$ and $(H-K_S)$ colour constraints, see Figure 2.1 and Equation 2.1 (from Lépine & Gaidos, 2011, hereafter LG11). After these initial cuts 57,510,435 sources remained.

$$\begin{bmatrix} J-H & > & 0.72-1.2(H-K_s) \\ J-H & < & 0.85-0.6(H-K_s) \\ J-H & > & 0.40 \\ H-K_s & > & 0.10 \\ H-K_s & < & 0.40 \end{bmatrix} \tag{2.1}$$

### 2.3.2 V band - the $(V-J)$ cut in spectral type

The photometric colour cuts of Section 2.3.1 are sufficient to select M type stars, however as discussed later in Section 3.4 I required only spectral types later than ∼M3.5. Lépine et al. (2013) present a photometric spectral type estimation via $(V-J)$ (see equation 12; Lépine et al., 2013, presented here in Equation 2.2), and I use this to define my cut in spectral type as a colour cut in $(V-J)$ .

$$Spt(V-J) = -32.79 + 20.75(V-J) - 4.04(V-J)^2 + 0.275(V-J)^3 \tag{2.2}$$

Using $(V-J)$ meant it was necessary to obtain a V band measurement, to complement the J band magnitude from 2MASS for my sample. The 2MASS data gives an indication of visual or red magnitudes via the VR_M_OPT column. This is either a Johnson V magnitude $(V_J)$ derived from $B_T$ and $V_T$ using Equation 2.3 (from Høg et al., 2000, marked with column $a$ = "$T$") or a photographic blue magnitude from USNO-A2.0 (marked with column $a$ = "$U$" Monet, 1998).

$$V_J = V_T - 0.09(B_T - V_T) \tag{2.3}$$

[13] Access to data releases via http://irsa.ipac.caltech.edu

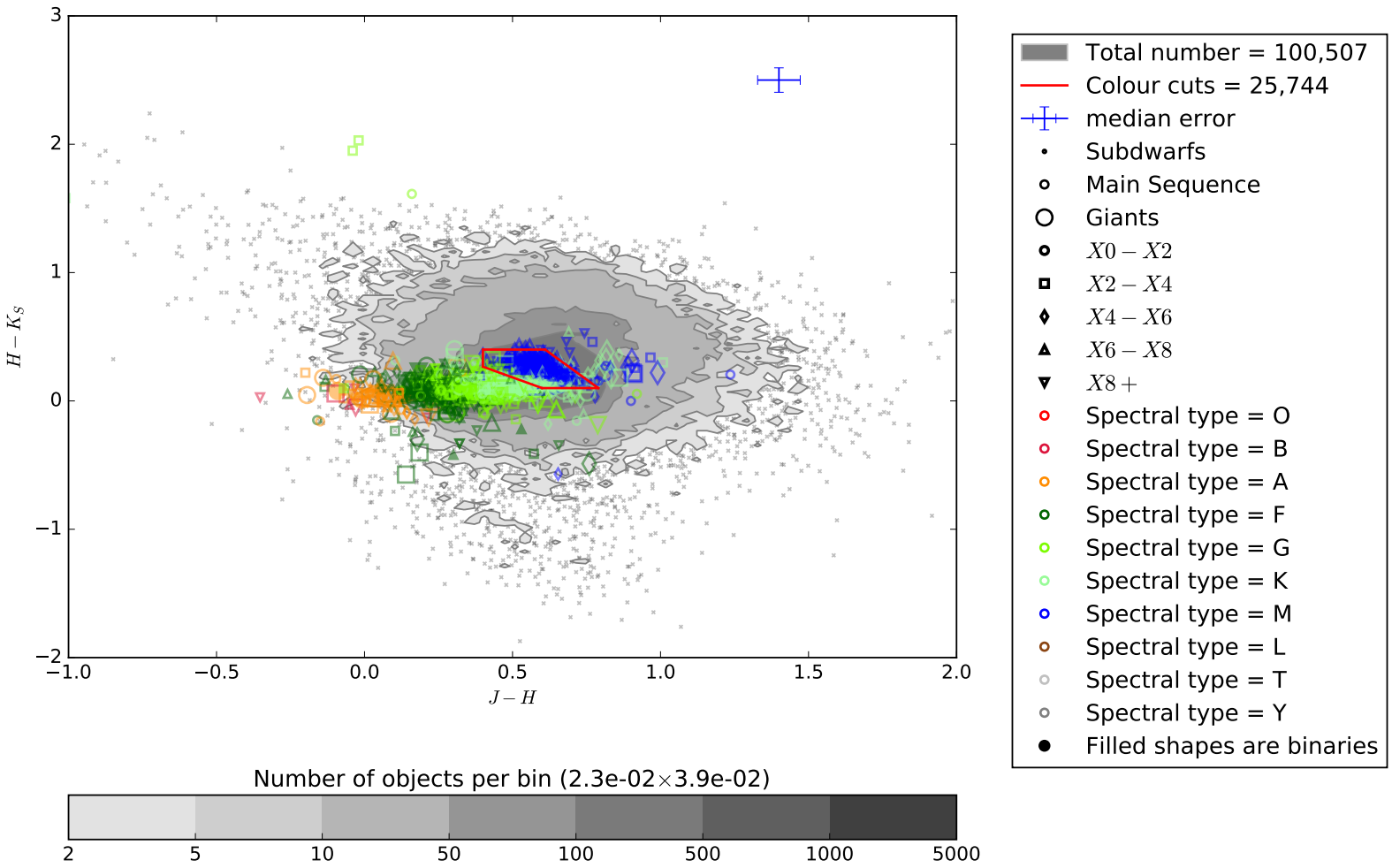


Figure. 2.1: The LG11 colour cuts applied to a small area of sky ($\alpha = 9^h20^m0.0^s, \delta = +30°0^m0.0^s$ to $\alpha = 10^h0^m0.0^s, \delta = +40°0^m0.0^s$) to show the size of the area selected. Over plotted on my distribution is a sample from the *Gliese and 2MASS Cross Identifications Catalogue* by Stauffer et al. (2010) to show that this cut truly selects M dwarfs and rejects other spectral types of stars. Difference shapes represent the different spectral subtypes, different sizes represent sub-dwarfs, main sequence and giant stars, colours represent different spectral classes.

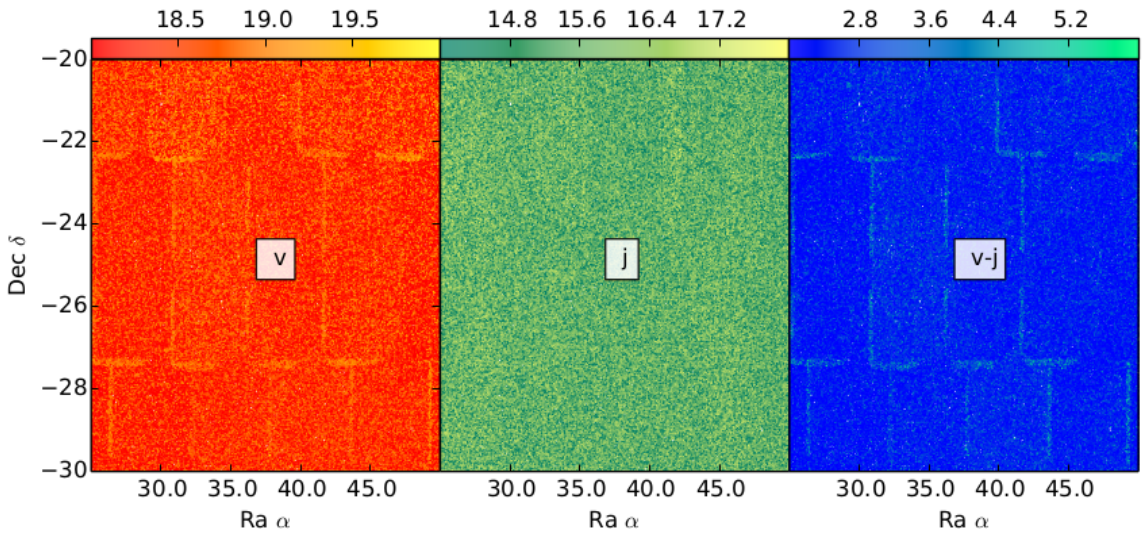


Figure. 2.2: The boundary problem found in USNO-A2.0, it appears that the V band plates overlap and thus cause an over density in found sources, possibly due to increased depth or duplication of sources. This and the large uncertainties in USNO lead to me choosing to use SDSS (via $(g-r)$ ) instead of using the V band magnitude from USNO-A2.0.

Any sources marked as USNO-A2.0 were R band magnitudes, and were converted to V band magnitudes using my own colour-colour polynomial quadratic fit (presented in Equation 2.4) which was determined using a sample of M dwarfs from Gliese & Jahreiß (1991).

$$V_{USNO} = -0.0291(R-J)^2 + 1.197(R-J) + 0.756 + J \tag{2.4}$$

Few M dwarfs had Tycho-2 V band magnitudes and the V band estimate from USNO-A2.0 suffered from problems around the boundaries of some fields (which I attribute to overlapping plates, see Figure 2.2) and rather large uncertainties (see Figure 2.3).

In contrast, the cross-match with SDSS would give me access to the V band via the $(g-r)$ to $(V-g)$ transformation[14] of Jordi et al. (2006). Although this limits my sample to the northern hemisphere the photometry is much less uncertain thus I chose to use SDSS to obtain my V band magnitude over that of Tycho-2/USNO-A2.0 V band measurement.

$$V_{SDSS} = (-0.565 \pm 0.001)(g_{SDSS} - r_{SDSS}) - (0.016 \pm 0.001) + g_{SDSS} \tag{2.5}$$

[14]SDSS photometric transformationsavailable via https://www.sdss3.org/dr8/algorithms/sdssUBVRITransform.php

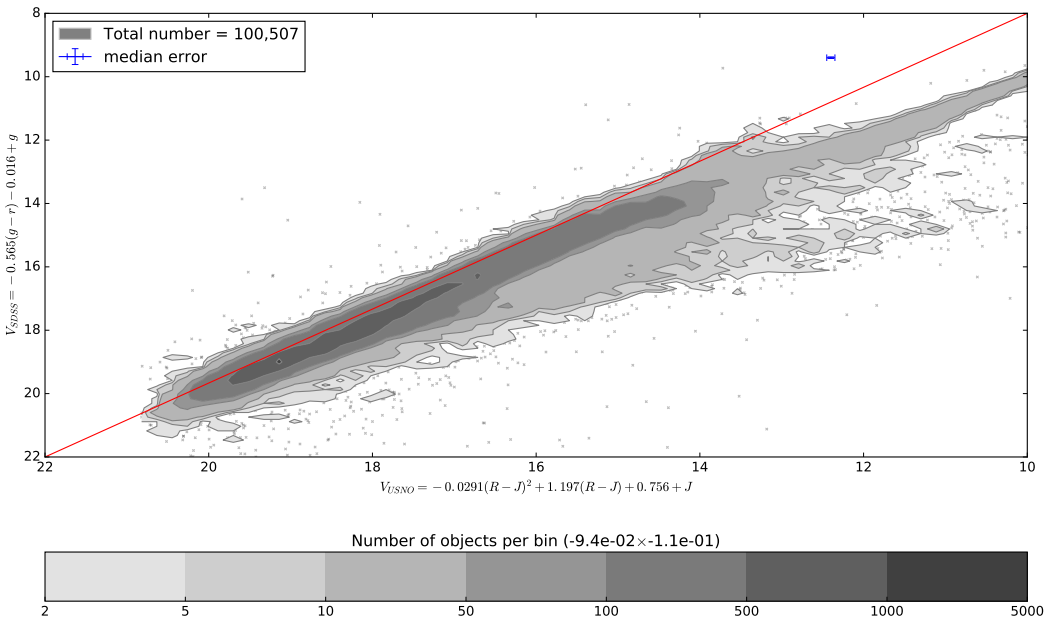


Figure. 2.3: The comparison between $V_{SDSS}$ and $V_{USNO}$. The uncertainties in $V_{SDSS}$ are far less than that of $V_{USNO}$ with more variation in V band towards fainter magnitude. This could be related to the boundary effect see in Figure 2.2. The trend strays at bright magnitudes due to saturation (∼14 for SDSS).

### 2.3.3 The addition of SDSS

Due to requiring a V band measurement (Section 2.3.2) it was necessary to locate sources which had a nearby associated SDSS source. I cross-matched the catalogue with the *Tenth Data Release of SDSS*[15](DR10, Ahn et al., 2012) (using the WISE coordinates and cross-matched using three arcsec separation, equivalent to the WISE PSF[16]). Of my 57 million sources, 9,944,123 sources had SDSS photometry and were flagged as stars (*type* = 6 in DR10 PhotoObjAll). I calculated an estimate of the V band magnitudes (see Equation 2.5) and removed all sources which have an estimated spectral type earlier than ∼M3.5 (equivalent to a $(V-J)$ >4.0, see Figure 2.4 and Section 3.4 for explanation). This was a slightly redder cut than LG11 which aimed to remove stars earlier than K7 dwarfs with $(V-J)$ >2.7.

This left 1,352,931 sources with estimated spectral type M3.5 or later. I decide to check the V band magnitude from SDSS against the V band measurements from USNO-A2.0, the comparison can be seen in Figure 2.3.

To reduce the number of sources which had poor photometry I rejected sources

[15]Access via http://skyserver.sdss3.org/CasJobs/

[16]Note that the later rejection of any source that had more than one 2MASS within six arcsec (Section 2.4) meant there was no need to be concerned about matching the wrong SDSS object.

whose one-sigma photometric uncertainties were greater than 0.1 (for $V$, $J$, $H$, $K$, $W1$ and $W2$). This left a total of 704,723 sources. I impose more strict photometric requirements for the excess analysis in Section 3.2.

## 2.4 Reduced proper motion

Reliable, accurate proper motions ($\mu$) allows the separation of dwarf stars from background stars and galaxies through reduced proper motion. I therefore cross-matched the sample with the *Position and Proper Motion Extended-L*[13] catalogue (PPMXL Roeser et al., 2010). A total of 691,421 of the 704,723 sources had proper motion measurements thus I decided not to use any additional proper motion catalogues. Any sources without proper motions in PPMXL were rejected as possible contaminants.

$$H_V = V + 5log(\frac{\mu}{\text{arcsec yr}^{-1}}) + 5 \tag{2.6}$$

I selected only sources whose proper motion uncertainties were less than 25 per cent ($4\sigma_\mu$) of the measured value. Of those sources with proper motion, 464,655 met the $4\sigma_\mu$ cut. Reduced proper motion (see Equation 2.6) was then calculated and possible contamination rejected following the same approach as LG11, see Equation 2.7.

$$H_V > 2.2(V - J) + 2.0 \tag{2.7}$$

This offers a good balance between contamination rejection and M dwarf retention. LG11 estimated associated M dwarf rejection rates of no more than 1.1 per cent. After the reduced proper motion cut 450,440 M dwarf candidates remained, Figure 2.5 shows the cut in reduced proper motion applied to a small area of the sky. I used the 2MASS proximity flag (PROX), to make sure none of my M dwarfs had another 2MASS counterpart within six arcsec . This avoids source blending which can affect photometric accuracy. This left a total of 440,694 sources in the full M dwarf candidate catalogue.

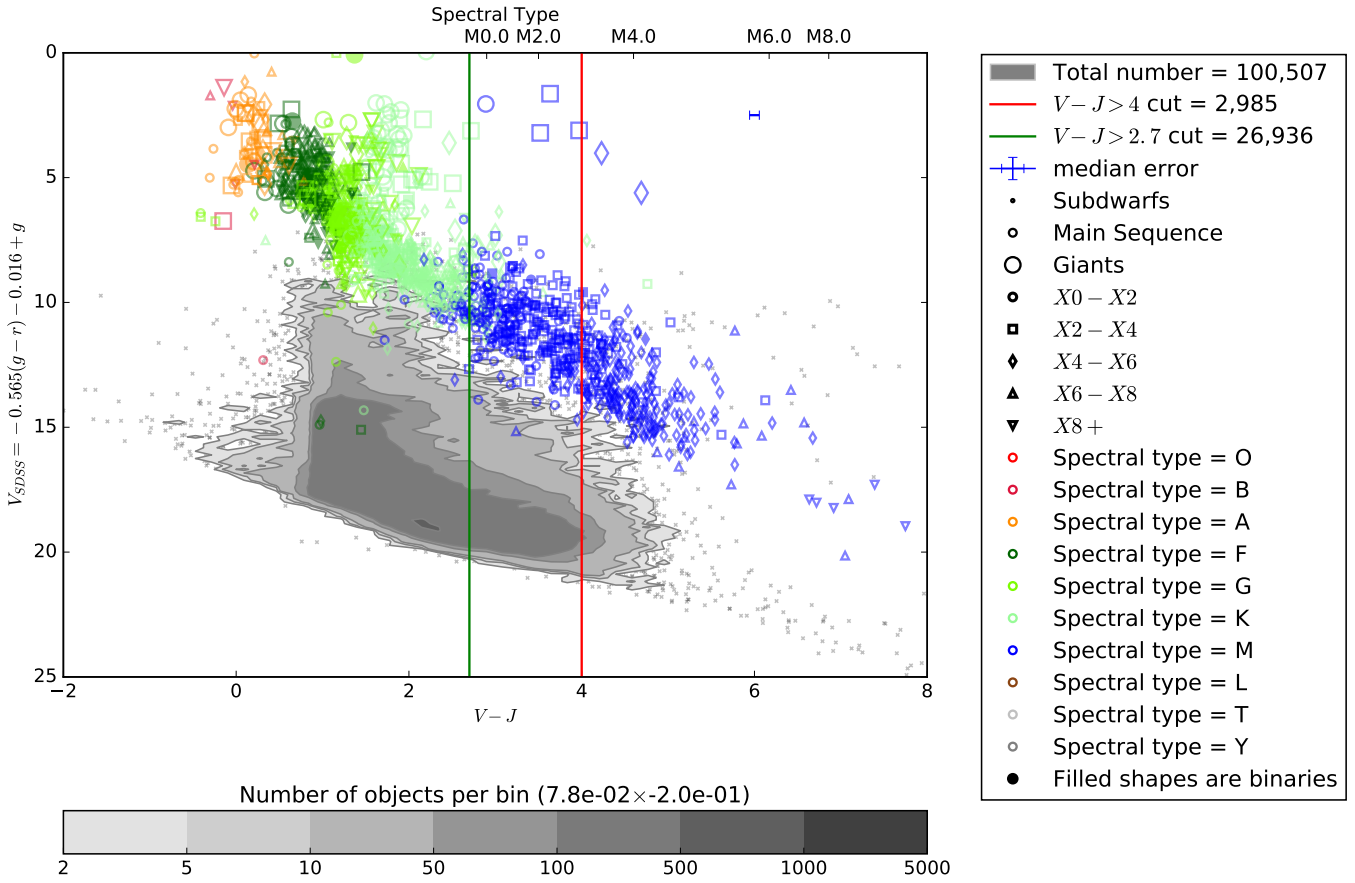


Figure. 2.4: The $(V-J)$ cuts applied to a small area of sky ($\alpha = 9^h20^m0.0^s, \delta = +30°0^m0.0^s$ to $\alpha = 10^h0^m0.0^s, \delta = +40°0^m0.0^s$) to show the size of $(V-J)$ cut. Spectral type is calculated using Equation 2.2. This is compared to the $(V-J)$ cut of LG11 ($(V-J)$ >2.7). This plots demonstrates that I remove a vast number of sources by selecting sources later than M3.0 but may still have some contamination from giants (the brightest sources). Over plotted on my distribution is a sample from the *Gliese and 2MASS Cross Identifications Catalogue* by Stauffer et al. (2010) to show that this cut truly selects M dwarfs and rejects other spectral types of stars. Note the catalogue by Stauffer et al. (2010) is much brighter than my catalogue due to the use of the Gliese catalogue. Difference shapes represent the different spectral subtypes, different sizes represent sub-dwarfs, main sequence and giant stars, colours represent different spectral classes.

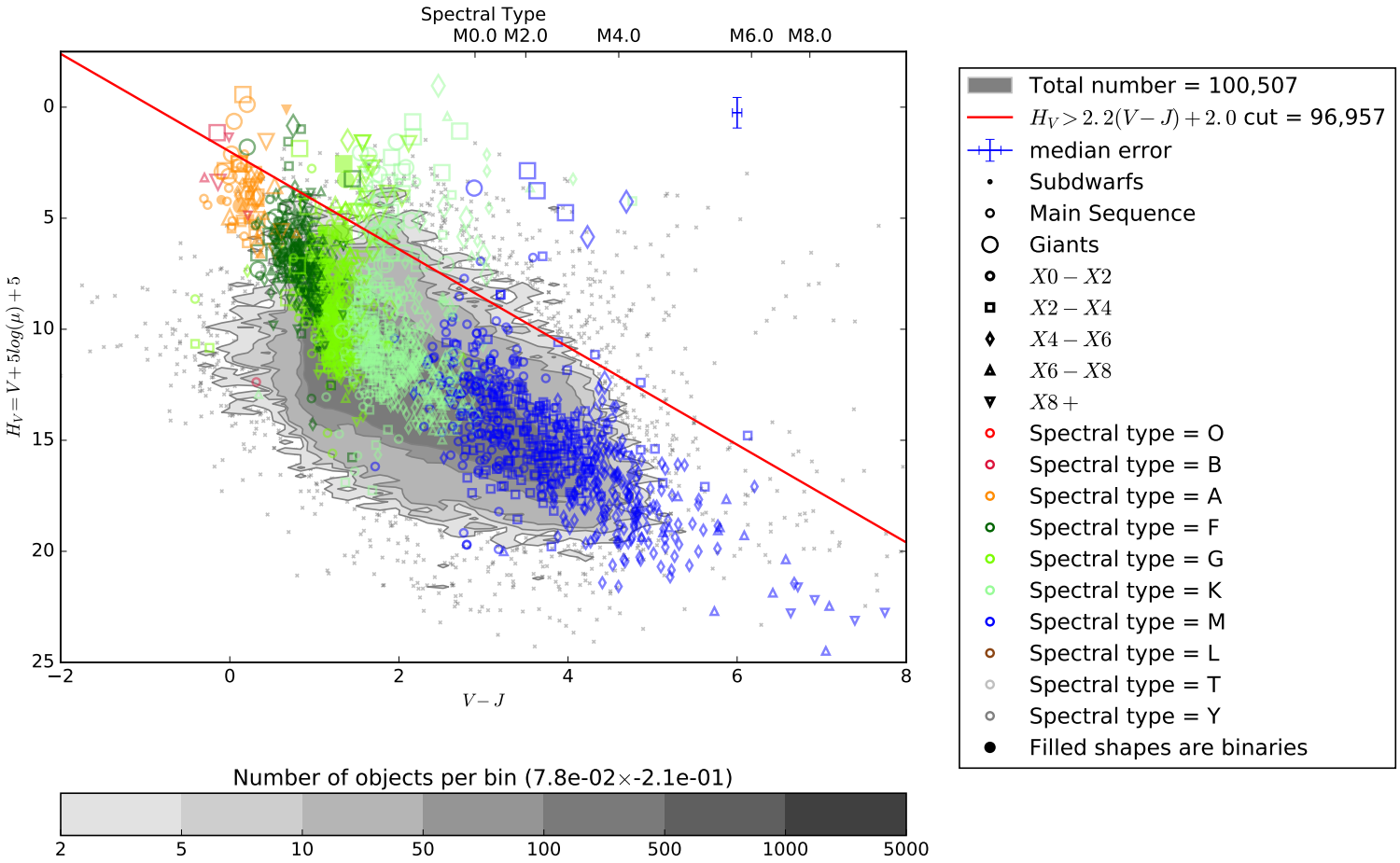


Figure. 2.5: The reduced proper motion cuts applied to a small area of sky ($\alpha = 9^h20^m0.0^s, \delta = +30°0^m0.0^s$ to $\alpha = 10^h0^m0.0^s, \delta = +40°0^m0.0^s$) to show the size of the reduced proper motion cut. Spectral type is calculated using Equation 2.2. This shows that the vast majority of sources are kept using this cut but the brightest slow moving sources are rejected as possible giant stars or background galaxies. Over plotted on my distribution is a sample from the *Gliese and 2MASS Cross Identifications Catalogue* by Stauffer et al. (2010) to show that this cut truly selects dwarf stars and the giant stars are clearly seen as rejected. Difference shapes represent the different spectral subtypes, different sizes represent sub-dwarfs, main sequence and giant stars, colours represent different spectral classes.

## 2.5 Summary of the catalogue construction

The catalogue started with the WISE catalogue (563,921,603 sources). This was cross-matched with 2MASS (to three arcsec ) leaving 280,909,458 sources. Next I applied basic colour cuts from LG11 designed to select M dwarfs (this left 57,510,435 sources). As I required optical photometry I cross-matched with SDSS leaving 9,944,123 sources. This enabled the cut in $(V-J)$ $((V-J) > 4)$ designed to target M dwarfs later in spectral type than M3 (this left 1,352,931 sources). I then applied basic photometric accuracy cuts and removed any source with errors greater than 0.1 magnitudes, and removed any objects with more than one 2MASS source within six arcsec (this left 670,819). Also I required proper motions (for reduced proper motion cuts), thus I cross-matched with PPMXL, performed $4\sigma$ uncertainty cuts and reduced proper motion cuts (a proxy for distance, to remove as much giant contamination as possible via the LG11 reduced proper motion cuts) this, when combined with the accuracy cuts produced my full M dwarf candidate catalogue of 440,694 sources. Figure 2.6 shows a flow diagram summarising the initial selection process.

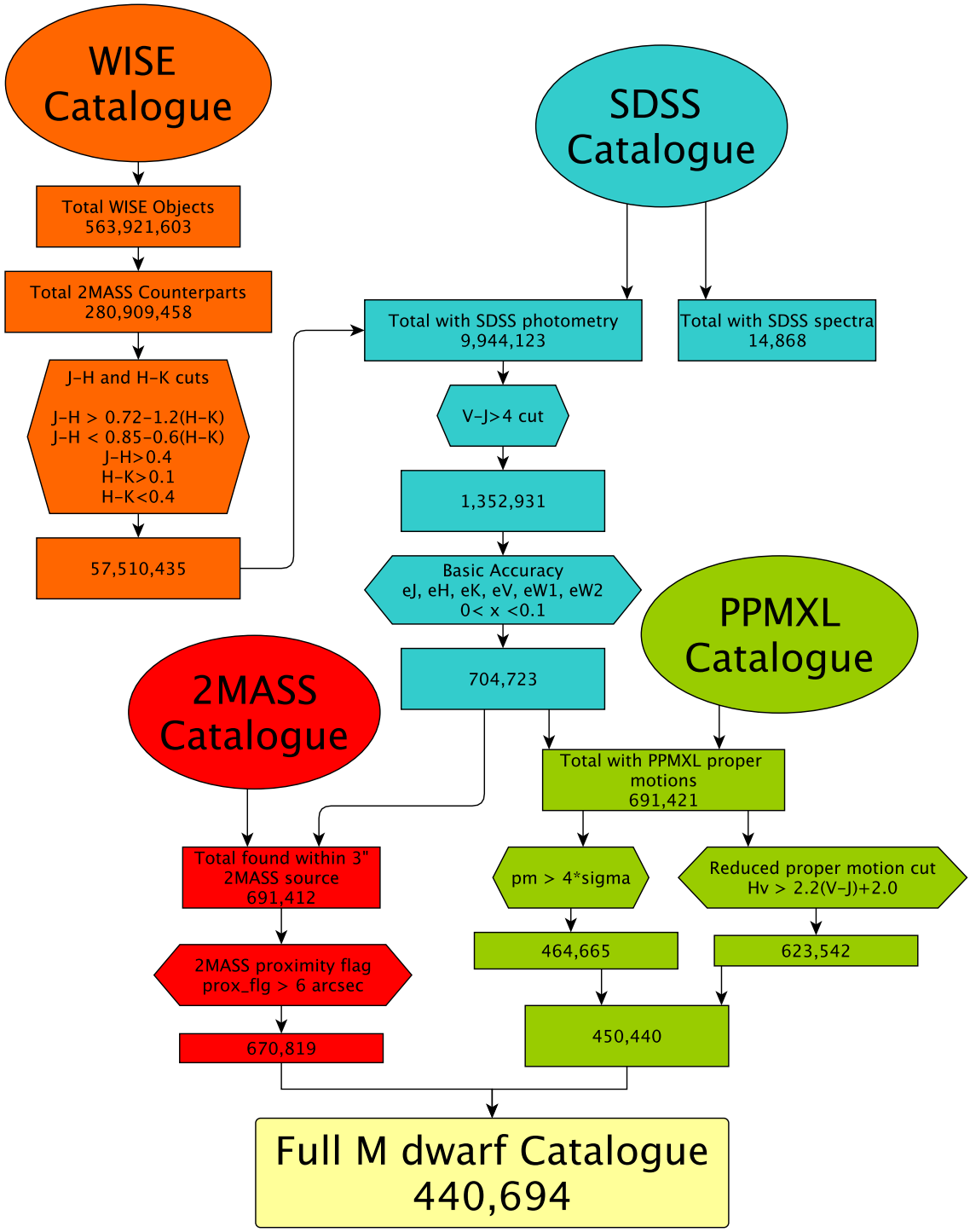


Figure. 2.6: Flow chart to summarise the process involved in making my full M dwarf candidate catalogue.

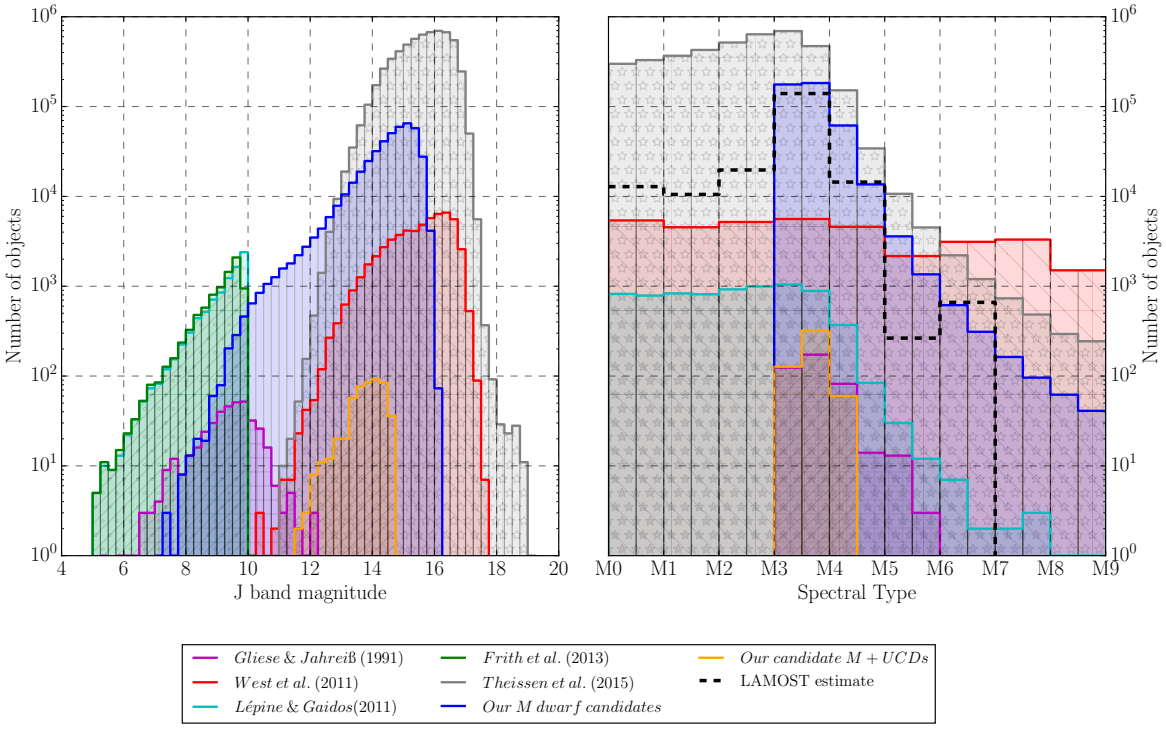


Figure. 2.7: Histograms comparing the J band magnitudes (left) and spectral type (right) of my full M dwarf candidate catalogue and the catalogues of Gliese & Jahreiß (1991); West et al. (2011), LG11, Frith & Pinfield (2013) and Theissen et al. (2016). The dashed black line on the spectral type histogram shows the estimated M dwarf spectral type distribution from the LAMOST sample analysis (see Section 2.7). Spectral types for my candidates were calculated photometrically $(V - J)$ by the equations presented in LG11 (Equation 2.2). Frith & Pinfield (2013) does not give a spectral type estimate nor V band magnitudes in order for an $(V - J)$ estimation thus there was no spectral type data for the Frith & Pinfield (2013) catalogue. West et al. (2011) give integer spectral types thus I assume a flat distribution and split these equally between whole and half integer bins (i.e. N M dwarfs in the M0 - M1 bin becomes N/2 M dwarfs in the M0 - M0.5 bin and N/2 M dwarfs in the M0.5 - M1 bin).

## 2.6 Catalogue properties

The comparison in J magnitude and the spectral type comparison can be seen in Figure 2.7. My full M dwarf candidate catalogue complements other catalogues of M dwarfs, including M dwarf catalogues from Gliese & Jahreiß (1991); West et al. (2011), LG11, Frith & Pinfield (2013) and Theissen et al. (2016). My catalogue is not a continuation of the Frith & Pinfield (2013) nor LG11 catalogues due to my use of the SDSS catalogue (thus restricted to the northern hemisphere).

My catalogue is brighter than the recent MoVeRS catalogue (Theissen et al., 2016) due to their cuts in SDSS of $r > 16$. The MoVeRS catalogue also goes two orders of magnitude deeper than my catalogue due to my quality cuts and my requirement of a W2 detection. It should be noted my M dwarfs consist only of M dwarfs later than

M3, and this is not true for the other catalogues compared in Figure 2.7. My full M dwarf candidate catalogue fills in the gap in M dwarf candidates between the bright Frith & Pinfield (2013) and LG11 catalogues and the fainter West et al. (2011) and Theissen et al. (2016) catalogues.

The dashed black line on the spectral type histogram shows the estimated M dwarf spectral type distribution from the LAMOST sample analysis (Cui et al. 2012; Luo et al. 2012; Zhao et al. 2012, see Section 2.7), the LAMOST estimates show the $(V-J)$ cut does an imperfect job at selecting later than M3 dwarfs, and shows the spectral type distribution goes out to at least M7 (although $(V-J)$ scatter may suggest a contingent of later types I have yet to confirm). I select against earlier M dwarfs, and the West et al. (2011) and Theissen et al. (2016) catalogues continues to dominate numerically for the latest spectral type M dwarfs. My catalogue spectral type distribution is as expected with a cut off seen at M3 due to our $(V-J)$ cuts and falling off with later spectral types (due to the intrinsic faintness of later type dwarfs compared with earlier type dwarfs).

At the bright extreme the M dwarf frequency of my catalogue falls below those of the Gliese & Jahreiß (1991), LG11 and Frith & Pinfield (2013) catalogues, due mainly to the restriction of using SDSS. My catalogue dominates numerically in the magnitude range $J = 10-13$, but does not go as deep as the West et al. (2011) or Theissen et al. (2016) catalogues.

I estimated distances using the Bochanski et al. (2010) $M_R$ fits to $(r-z)$ and $(r-i)$ (see Equation 2.8, Equation 2.9 and Equation 2.10). Note there are colour range restrictions for these fits (Bochanski et al., 2010) but these are only used as a rough estimate of distance and note these were modified due to an erratum (see Bochanski et al., 2012). The bulk of my full M dwarf candidate catalogue lies between 100 and 200 pc consistent with M dwarfs of spectral type M3 to M5 for these magnitudes.

In summary my catalogue (of 440,694 sources) fills a gap in magnitude space between the bright (nearby) catalogues and the larger fainter catalogues (due to differing approaches on photometric cuts). My catalogue consists mainly of M dwarfs of spectral type M3 - M5 between 12th and 15th magnitude in the 2MASS J band (equivalent to distances of approximately 100 to 300 pc, and proper motions, in general, between 0.02 and 0.1 arcsec $yr^{-}1$).

$$M_r = 5.190 + 2.474(r-z) + 0.4340(r-z)^2 - 0.08635(r-z)^3 \quad \text{valid for: } 0.5 < (r-z) < 4.53 \tag{2.8}$$

$$M_r = 5.025 + 4.548(r-i) + 0.4175(r-i)^2 - 0.18315(r-i)^3 \quad \text{valid for: } 0.62 < (r-i) < 2.82 \tag{2.9}$$

$$M_r = 4.748 + 8.275(i-z) + 2.2789(i-z)^2 - 1.5337(i-z)^3 \quad \text{valid for: } 0.32 < (i-z) < 1.85 \tag{2.10}$$

## 2.7 Sources of contamination and bias in the full M dwarf candidate catalogue

I expect my full M dwarf candidate catalogue to contain non-M dwarf contamination for two main reasons. Scatter in the $(V-J)$ colours will lead to the inclusion of some earlier types (<M3). These will mostly be early M dwarfs but could include some F, G and K stars. Reduced proper motion uncertainty is also expected to lead to a low level of giant stars contamination as previously discussed in Section 2.4.

### 2.7.1 Spectral types from SIMBAD

To assess the contamination levels I cross-matched my full M dwarf candidate catalogue with SIMBAD[17] catalogue (cross-matched to three arcsec). In total there were 20,286 matches with my full M dwarf candidate catalogue. Of these 7,360 had spectral types from SIMBAD. From this I gauged the contamination from early (FGK) stars, M giant stars, and white dwarfs. The full catalogue has ∼1.3 per cent contamination from these sources. It should however be noted some of the spectral types carry little information, e.g. only as an M-type star (∼1.4 per cent), and thus I may slightly underestimate the contamination from sources such as M giant stars. SIMBAD also shows a bias toward the brighter stars in my sample, thus my fainter catalogue may contain more contamination from fainter sources. In my full M dwarf candidate catalogue I find thirteen (∼0.2 per cent) white dwarfs are cool enough to be selected by my initial selection process. I also find twenty-two (∼0.3 per cent) of my full M dwarf candidate catalogue have white dwarf companions, twenty (∼0.3 per cent) are known M+M binaries, and one is a known M+L binary. These spectral types are presented in Table 2.1 and Table 2.2.

### 2.7.2 Object classifications from SIMBAD

I also used the SIMBAD cross-match to count the source classifications given and to group them by type. From this I gauged the contamination from sources classified as galaxies, variable stars and white dwarfs as ∼2.7 per cent for my full M dwarf candidate catalogue. As with spectral type some of the source classifications carry little

[17]SIMBAD database accessible at http://simbad.u-strasbg.fr/simbad (Wenger et al., 2000)

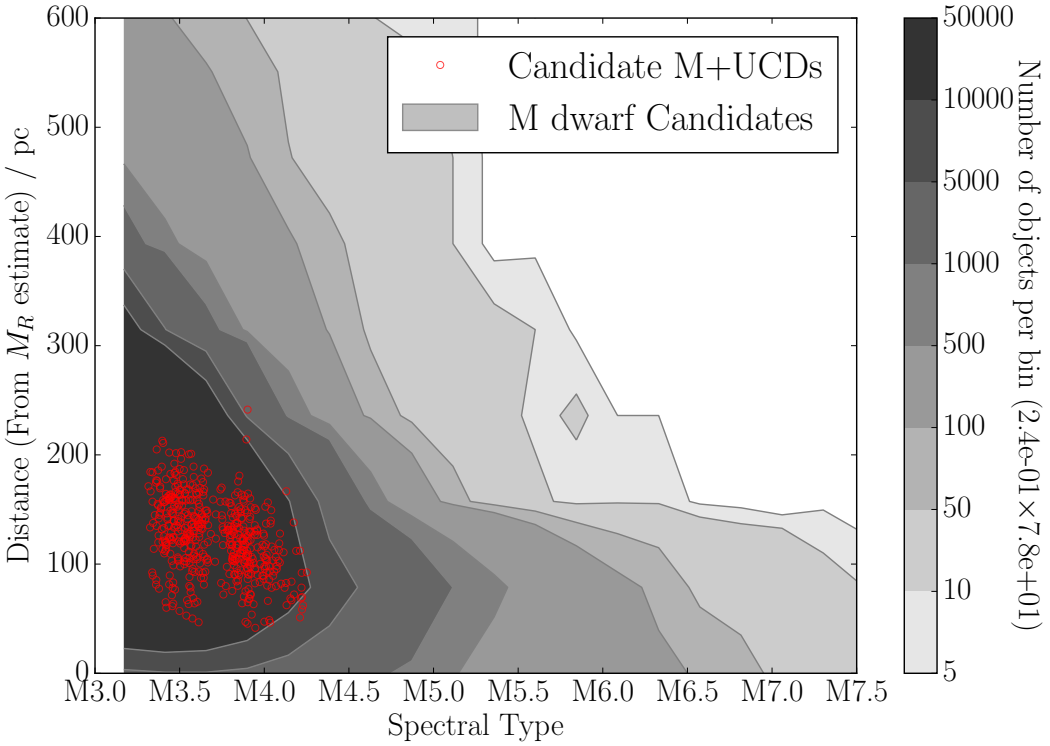


Figure. 2.8: Distribution in estimated spectral type-distance space. Spectral types from Lépine et al. (2013)'s fit to $(V - J)$. Distance was estimated using Bochanski et al. (2010)'s $M_R$ fits to $(r - z)$ and $(r - i)$ (averaged).

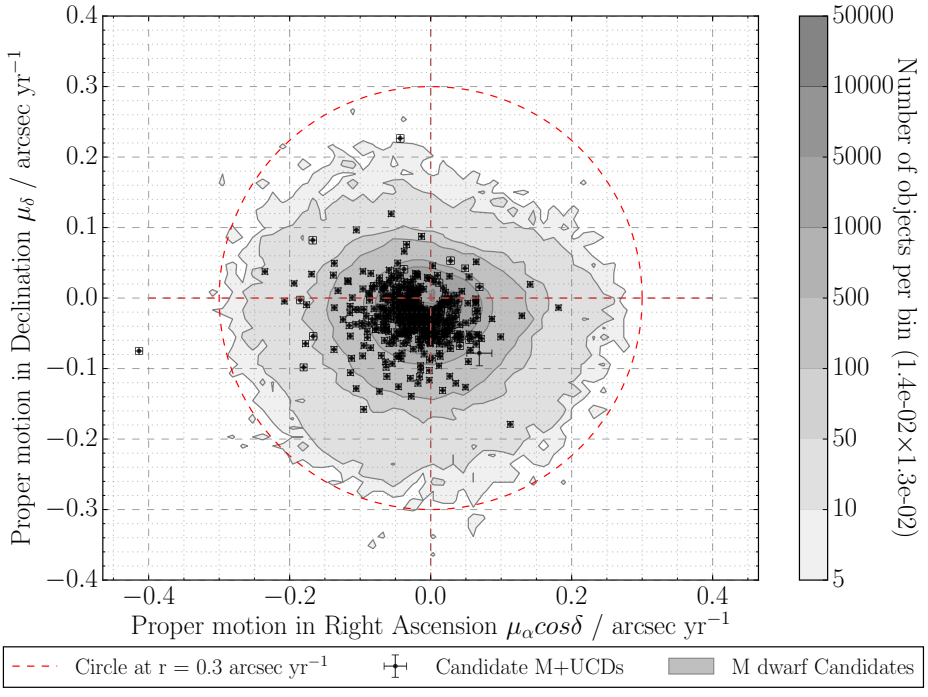


Figure. 2.9: A proper motion vector-point-diagram showing the overall distribution of M dwarfs in my catalogue as well as my M+UCD candidates. Distributions are skewed towards the bottom left due to SDSS being a northern hemisphere survey, and in the candidates case being localised around the northern galactic cap. The M+UCD candidates are all within 300 mas yr$^{-1}$ due to the catalogue cross-matching radii selected.

information (i.e. classified only as being stars or as being in an association or a cluster) therefore I also take this contamination as a rough estimate. These classifications are presented in Table 2.3.

### 2.7.3 Spectral types from LAMOST

I obtain additional optical spectral types by exploring data from LAMOST and I repeated this exercise with the LAMOST DR1 and DR2a1[18] catalogue spectral types (again cross-matched to three arcsec ). In total there were 9,262 sources with spectral types in my full M dwarf candidate catalogue. From this I gauged the contamination from early-than-M stars and white dwarfs. The full catalogue has ∼9.6 per cent contamination from these sources, however it should be noted the LAMOST general catalogue does not distinguish between giant stars and dwarfs nor between spectral types of the double stars thus the contaminations is a rough estimate. In my full M dwarf candidate catalogue I find eight (∼0.1 per cent) white dwarfs are cool enough to be selected by my initial selection process. These classifications are presented in Table 2.4. There is an apparent 3 per cent contamination of the sample by G type stars that is not seen in the SIMBAD selection. This is due to LAMOST preferentially observing G type stars over other types of stars (over 40 per cent of the LAMOST catalogue comprises of G type stars compared to only 17 per cent K type dwarfs and less than 5 per cent M type stars), this combined with the intrinsic faintness of later types (i.e. K and M type stars are fainter and thus less are observed by LAMOST) and the mass function of early type stars (i.e. the more massive the star the less numerous) leads to the large apparent number of contaminating G type stars in our M dwarf catalogue.

### 2.7.4 Summary of contamination in the full M dwarf candidate catalogue

My full M dwarf candidate catalogue contains very little non-M dwarf contamination (less than 5 per cent). However, the $(V - J)$ cuts seem to do an imperfect job of selecting all later than M3 dwarfs, thus more cuts are required to make sure my analysis uses M dwarfs later than M3 for finding M+UCD systems (see Section 3.2). These numbers should be taken as a broad estimate at best, the SIMBAD cross-matches only represent the brighter stars in my catalogue and thus contamination for the fainter objects may be worse, and the LAMOST cross-matches suffer from catalogue selection effects, such as the preferential selection of G type stars.

[18]Later in this thesis the full DR2 is used however at this point only the first semester of DR2 was available.

| Group | SIMBAD spectral type selected for group | Number in full candidate catalogue | Number in excess sample | Number in candidate M+UCDs |
|---|---|---|---|---|
| Total | - | 440,694 | 36,898 | 1,082 |
| Total (with SIMBAD) | - | 7,360 | 1,475 | 32 |
| White dwarf | *DA, DA.7, DA1.1, DA1.7, DA2.9, DA3, DA3.3, DA3.5, DB, DC..., DC-DQ* | 13 (0.18%) | 1 (0.07%) | 0 |
| White dwarf binaries | *D+M, DAM, DA+M, DA+dM, DA+dM:, DA+dMe, DA+M3V, DA+M4, DB+..., DB+M, DB+M3 DO+M, DC+M, DC+dM* | 22 (0.30%) | 0 | 0 |
| F | *F9.5* | 1 (0.01%) | 0 | 0 |
| G | *G:, G2III* | 2 (0.03%) | 0 | 0 |
| K | *K, K:, K..., K/M* | 15 (0.20%) | 1 (0.07%) | 0 |
| early K | *K3, K4, K4.5, K4/5* | 9 (0.12%) | 0 | 0 |
| late K | *K4V:, K5, K5V, K5Ve K5.3, K5/M0, K6, K6V, K6Ve, K6.5, K7, K7V, K8, K9V* | 56 (0.76%) | 0 | 0 |
| M | *M, M:, MV:, MV, MV:e* | 145 (1.97%) | 36 (2.44%) | 0 |
| M0 - <M1 | *M0V:, M0Vk, M0, M0V, M0e, M0.4, M0.5, M0.5V, M0.6, M0.8* | 38 (0.52%) | 2 (0.14%) | 0 |
| M1 - <M2 | *M1V, M1, M1.0, M1.0V, M1e, M1.5, M1.5V* | 48 (0.65%) | 1 (0.07%) | 0 |
| M2 - <M3 | *M2, M2.0, M2V, M2.0V, M2e, M2V:, M2.3, M2.4, M2.4V, M2.5, M2.5V, M2.6, M2.7, M2.8, M2.9, M2/3* | 169 (2.30%) | 24 (1.63%) | 0 |
| M3 - <M4 | *M3.0, M3, M3e, M3V, M3V:, M3.0V, M3.1, M3.2, M3.3, M3.3V, M3.4, M3.5, M3.5V, M3.5e, M3.6, M3.7, M3.8, M3.9, M3..., M3:, M3-4* | 1099 (14.93%) | 159 (10.78%) | 7 (21.86%) |
| M4 - <M5 | *M4V, M4.0V, M4, M4.0, M4.1, M4.2, M4.25V, M4.3, M4.3V, M4.4, M4.4V, M4.5, M4.5V, M4.6, M4.6V, M4.7, M4.7v..., M4.75, M4.75V, M4.8, M4.9, M4-5, M4..., M4:V* | 2663 (36.18%) | 642 (43.53%) | 13 (40.63%) |

Table 2.1: Statistics on SIMBAD spectral types for the cross-match between the full M dwarf candidate catalogue, the excess sample and the M+UCD candidates with SIMBAD. Note some spectral types have no luminosity class, e.g. 'V', and thus for these sources I cannot identify whether they are dwarfs or giant stars (and thus whether these sources contribute to the contamination)

| Group | SIMBAD spectral type selected for group | Number in full candidate catalogue | Number in excess sample | Number in candidate M+UCDs |
|---|---|---|---|---|
| Total | - | 440,694 | 36,898 | 1,082 |
| Total (with SIMBAD) | - | 7,360 | 1,475 | 32 |
| M5 - <M6 | *M5, M5e, M5V, M5.0, M5.0V, M5V:, M5Ve, M5.1, M5.2, M5.2, M5.3, M5.4, M5.4V, M5.5, M5.5V, M5.7, M5.9, M5.9V, M5..., M5V:e...* | 1189 (16.15%) | 330 (22.37%) | 12 (37.5%) |
| M6 - <M7 | *M6, M6.0, M6.0V, M6e, M6V, sdM6, M6-M6.25, M6.1, M6.2v..., M6.3, M6.4, M6.5, M6.5V, M6e...* | 1053 (14.31%) | 173 (11.73%) | 0 |
| M7 - <M8 | *M7.0, M7, M7V, M7.0V, M7.5* | 735 (9.99%) | 100 (6.78%) | 0 |
| M8 - <M9 | *M8, M8V* | 74 (1.01%) | 1 (0.07%) | 0 |
| >M9 | *M9V* | 4 ( 0.05%) | 0 | 0 |
| early L | *L0, L1.5* | 2 (0.03%) | 0 | 0 |
| M giants | *M3III* | 1 (0.01%) | 0 | 0 |
| M + M binaries | *M0+M1, M2+M3, M2+M5, M2.5+M3.5, M2.5+M4.0, M3+M3, M3+M4, M3.5+M4.0, M3+WD, M4+M4, M4+WD, M4.2+M4.3, M4.5+M5.5, M5.0+M6.0, M6+WD* | 20 (0.27%) | 5 (0.07%) | 0 |
| M + L binaries | *M80v+L3.0V* | 1 (0.01%) | 0 | 0 |
| Non contaminated sources | *M, M0 - <M1 to M9> early L, D+M, M+M binaries, M+L binaries* | 7,263 (98.68%) | 1,473 (99.86%) | 32 (100.00%) |
| Contaminated sources | *D, F, G, K, early K, late K, M3 Giants* | 97 (1.32%) | 2 (0.14%) | 0 |

Table 2.2: Table 2.1 continued. Statistics on SIMBAD spectral types for the cross-match between the full M dwarf candidate catalogue, the excess sample and the M+UCD candidates with SIMBAD. Note some spectral types have no luminosity class, e.g. 'V', and thus for these sources I cannot identify whether they are dwarfs or giant stars (and thus whether these sources contribute to the contamination)

| Group | LAMOST spectral types selected for group | Number in full candidate catalogue | Number in excess sample | Number in candidate M+UCDs |
|---|---|---|---|---|
| Total | - | 440,694 | 36,898 | 1,082 |
| Total with LAMOST spectral types | - | 9,262 | 1,851 | 41 |
| A | *A0, A1IV, A1V, A2V, A4III, A6V, A7IV* | 8 (0.09%) | 0 | 0 |
| D | *WD, WDMagnetic* | 8 (0.09%) | 1 (0.05%) | 0 |
| F | *F0 F2 F3 F4 F5 F6 F7 F9* | 42 (0.45%) | 6 (0.32%) | 0 |
| G | *G0 G1 G2 G3 G4 G5 G6 G7 G8 G9* | 286 (3.09%) | 33 ( 1.78%) | 1 (2.44%) |
| early K | *K0 K1 K2 K3 K4* | 44 (0.48%) | 1 (0.05%) | 0 |
| late K | *K5 K7* 503 (5.43%) | 3 (0.16%) | 0 | |
| M0 - <M1 | *M0 M0V* | 540 (5.83%) | 2 (0.11%) | 0 |
| M1 - <M2 | *M1* | 442 (4.77%) | 2 (0.11%) | 0 |
| M2 - <M3 | *M2 M2V* | 827 (8.93%) | 110 (5.94%) | 2 (4.88%) |
| M3 - <M4 | *M3* | 5,874 (63.42%) | 1,505 (81.31%) | 33 (80.49%) |
| M4 - <M5 | *M4* | 607 (6.55%) | 154 (8.32%) | 5 (12.20%) |
| M5 - <M6 | *M5* | 11 (0.12%) | 2 (0.11%) | 0 |
| M6 - <M7 | *M6* | 28 (0.30%) | 8 (0.43%) | 0 |
| M7 - <M8 | *M7* | 0 | 0 | 0 |
| M8 - <M9 | *M8* | 0 | 0 | 0 |
| >M9 | *M9* | 2 (0.02%) | 0 | 0 |
| double star | *DoubleStar* | 40 (0.43%) | 7 (0.38%) | 0 |
| Non contaminated sources | double star, M0 - <M1 to M9>, early L | 8,371 (90.38%) | 1807 (97.62%) | 40 (97.56%) |
| Contaminated sources | D, A, F, G, early K, late K | 891 (9.62%) | 44 (2.38%) | 1 (2.44%) |

Table 2.3: Statistics on LAMOST source classifications for the cross-match between the full M dwarf candidate catalogue, the excess sample and the M+UCD candidates with LAMOST. Note spectral types are only given to integer spectral types and giant stars and dwarfs are not distinguished.

| Group | SIMBAD Object Types selected for group | Number in full candidate catalogue | Number in excess sample | Number in candidate M+UCDs |
|---|---|---|---|---|
| Total | - | 440,694 | 36,898 | 1,082 |
| Total with SIMBAD cross-matches | - | 20,286 | 3,928 | 66 |
| Potential M dwarfs | *PM*, low-mass*, star, *inCl, Candidate_low-mass** | 17,670 (87.10%) | 3624 (92.26%) | 55 (83.33%) |
| White dwarfs | *WD*, Candidate_WD** | 29 (0.14%) | 2 (0.05%) 0 | 0 (0.00%) |
| Brown dwarfs | *brownD*, Candidate_brownD** | 45 (0.22%) | 8 (0.20%) | 0 (0.00%) |
| X-ray sources | *X* | 303 (1.49%) | 96 (2.44%) | 1 (1.52%) |
| Infrared sources | *IR, IR<10μ m* | 1035 (5.10%) | 92 (2.34%) | 8 (12.12%) |
| Known multiple systems | **in**, **, EB*Algol, EB*, multiple_source, SB* | 584 (2.88%) | 68 (1.73%) | 1 (1.52%) |
| Extragalactic | *Galaxy, EmG, GinGroup, GinCl, QSO_Candidate* | 196 (0.97%) | 29 (0.74%) | 1 (1.52%) |
| Variable stars | *V*, RotV*, Flare*, RRLyr* | 321 (1.58%) | 7 (0.18%) | 0 (0.00%) |
| Other sources | *Unknown Transient DkNeb SNR? HII Blue Symbiotic* Inexistant RGB** | 22 (0.11%) | 2 (0.05%) | 0 (0.00%) |
| Non contaminated sources | Blue source, Radio source, Brown dwarfs, Young stellar Objects, Infrared sources, Known multiple systems, Unknown, Potential M dwarfs, X-ray sources | 19733 (97.27%) | 3890 (99.03%) | 65 (98.48%) |
| Contaminated sources | Not an source, Symbiotic Star, ISM, White dwarfs, Extragalactic, Variable stars, Red Giant Branch Star | 553 (2.73%) | 38 (0.97%) | 1 (1.52%) |

Table 2.4: Statistics on SIMBAD source classifications for the cross-match between the full M dwarf candidate catalogue, the excess sample and the M+UCD candidates with SIMBAD. Note some source classifications, e.g. 'star', carry little information and hence contamination levels may be underestimated.

# Chapter 3: Selecting M dwarfs with mid-infrared excess

This chapter is a version of Section 3 of "A Method for Selecting M dwarfs with an Increased Likelihood of Unresolved Ultra-cool Companionship", Cook, Pinfield, Marocco, Burningham, Jones, Frith, Zhong, Luo, Qi, Lucas, Gromadzki, Day-Jones, Kurtev, Guo, Wang, Bai, Yi, & Smart, 2016a and is reproduced by permission of MNRAS.

The co-authors of the paper contributed in advice, guidance, ideas and private discussions only, everything else is my own original work. Chilean authorship is in part thanks to use of Chilean facilities and Chinese authorship relates to my access and use of the LAMOST catalogue.

## 3.1 Introduction

To facilitate my search for M dwarfs with MIR excess I identified a sub-sample from within my M dwarf catalogue, using more stringent and additional constraints (hereinafter the 'excess sample'). My colour excess signal could be confused with interstellar reddening and/or photometric uncertainty, thus I aim to minimise their contribution. With an estimated three per cent excess from an unresolved companion (see Section 3.4) I required all uncertainties to be less than this level. Reddening and photometric uncertainty cuts were designed to achieve or better this requirement, while maintaining a sufficiently high number of candidate M dwarfs.

## 3.2 Catalogue sub-sample for excess studies

### 3.2.1 Reddening cuts

To enable reddening cuts I obtained extinction information from dust maps (Schlegel et al., 1998), and updated the extinctions using Schlafly & Finkbeiner (2011). I required little to no reddening, comparable to the uncertainties in the photometric data and reddening in the NIR minus MIR colours, (e.g. $E(J-W1)$ ) and required reddening to be less than two per cent in $E(J-W2)$ .

I used Equation 3.1 (from Equation 2, Massa & Savage, 1989) and thus derived Equation 3.2, where $\frac{A_\lambda}{A_V}$ was calculated by taking the weighted average of cubic splines fits to $\frac{A_\lambda}{A_V}(\lambda^{-1})$ from Cardelli et al. (1989), Fitzpatrick (1999) and Schlegel et al. (1998) for an $R_V$ of 3.1 (see Table 3.1 and Figure 3.1). Using Equation 3.2 extinction was

| Colour | $\frac{A_\lambda}{A_V}(CCM)$ | $\frac{A_\lambda}{A_V}(F99)$ | $\frac{A_\lambda}{A_V}(SFD)$ | $\frac{A_\lambda}{A_V}(\bar{x})$ |
|---|---|---|---|---|
| $J$ | 0.282 ± 0.047 | 0.277 ± 0.034 | 0.282 ± 0.017 | 0.281 ± 0.015 |
| $H$ | 0.180 ± 0.030 | 0.171 ± 0.028 | 0.180 ± 0.011 | 0.179 ± 0.010 |
| $W1$ | 0.056 ± 0.009 | 0.064 ± 0.291 | 0.056 ± 0.003 | 0.056 ± 0.003 |
| $W2$ | 0.035 ± 0.006 | 0.041 ± 0.188 | 0.035 ± 0.002 | 0.035 ± 0.002 |

Table 3.1: Weighted average of cubic splines fits to $\frac{A_\lambda}{A_V}(\lambda^{-1})$ from Cardelli et al. (1989), Fitzpatrick (1999) and Schlegel et al. (1998) shown in Figure 3.1. Here $R_V = 3.1$ and $\bar{x}$ is the weighted average of the three estimations.

| Colour | $E(\lambda_1 - \lambda_2)$ | $A_V(CCM)$ | $A_V(F99)$ | $A_V(SFD)$ | $A_V(\bar{x})$ |
|---|---|---|---|---|---|
| $(H - W1)$ | 0.01 | 0.081 ± 0.004 | 0.093 ± 0.017 | 0.080 ± 0.001 | 0.081 ± 0.001 |
| $(H - W2)$ | 0.01 | 0.069 ± 0.003 | 0.077 ± 0.005 | 0.069 ± 0.001 | 0.069 ± 0.001 |
| $(J - W1)$ | 0.01 | 0.044 ± 0.003 | 0.047 ± 0.005 | 0.044 ± 0.001 | 0.044 ± 0.001 |
| $(J - W2)$ | 0.01 | 0.040 ± 0.003 | 0.042 ± 0.002 | 0.041 ± 0.001 | 0.041 ± 0.001 |
| $(H - W1)$ | 0.02 | 0.161 ± 0.007 | 0.187 ± 0.034 | 0.161 ± 0.003 | 0.162 ± 0.002 |
| $(H - W2)$ | 0.02 | 0.137 ± 0.005 | 0.154 ± 0.011 | 0.138 ± 0.002 | 0.138 ± 0.002 |
| $(J - W1)$ | 0.02 | 0.089 ± 0.005 | 0.094 ± 0.009 | 0.089 ± 0.002 | 0.089 ± 0.002 |
| $(J - W2)$ | 0.02 | 0.081 ± 0.004 | 0.085 ± 0.004 | 0.081 ± 0.002 | 0.081 ± 0.001 |
| $(H - W1)$ | 0.03 | 0.242 ± 0.011 | 0.280 ± 0.050 | 0.242 ± 0.004 | 0.243 ± 0.004 |
| $(H - W2)$ | 0.03 | 0.206 ± 0.008 | 0.232 ± 0.016 | 0.207 ± 0.003 | 0.207 ± 0.003 |
| $(J - W1)$ | 0.03 | 0.133 ± 0.008 | 0.141 ± 0.014 | 0.133 ± 0.003 | 0.133 ± 0.003 |
| $(J - W2)$ | 0.03 | 0.121 ± 0.007 | 0.127 ± 0.007 | 0.122 ± 0.002 | 0.122 ± 0.002 |

Table 3.2: Using Equation 3.2 and $A_\lambda/A_V$ (from Table 3.1) I estimated $A_V$ values from Cardelli et al. (1989, CCM), Fitzpatrick (1999, F99) and Schlegel et al. (1998, SFD). Here $R_V = 3.1$ and $\bar{x}$ is the weighted average of the three estimations. Note errors from CCM are described as a lower limit only.

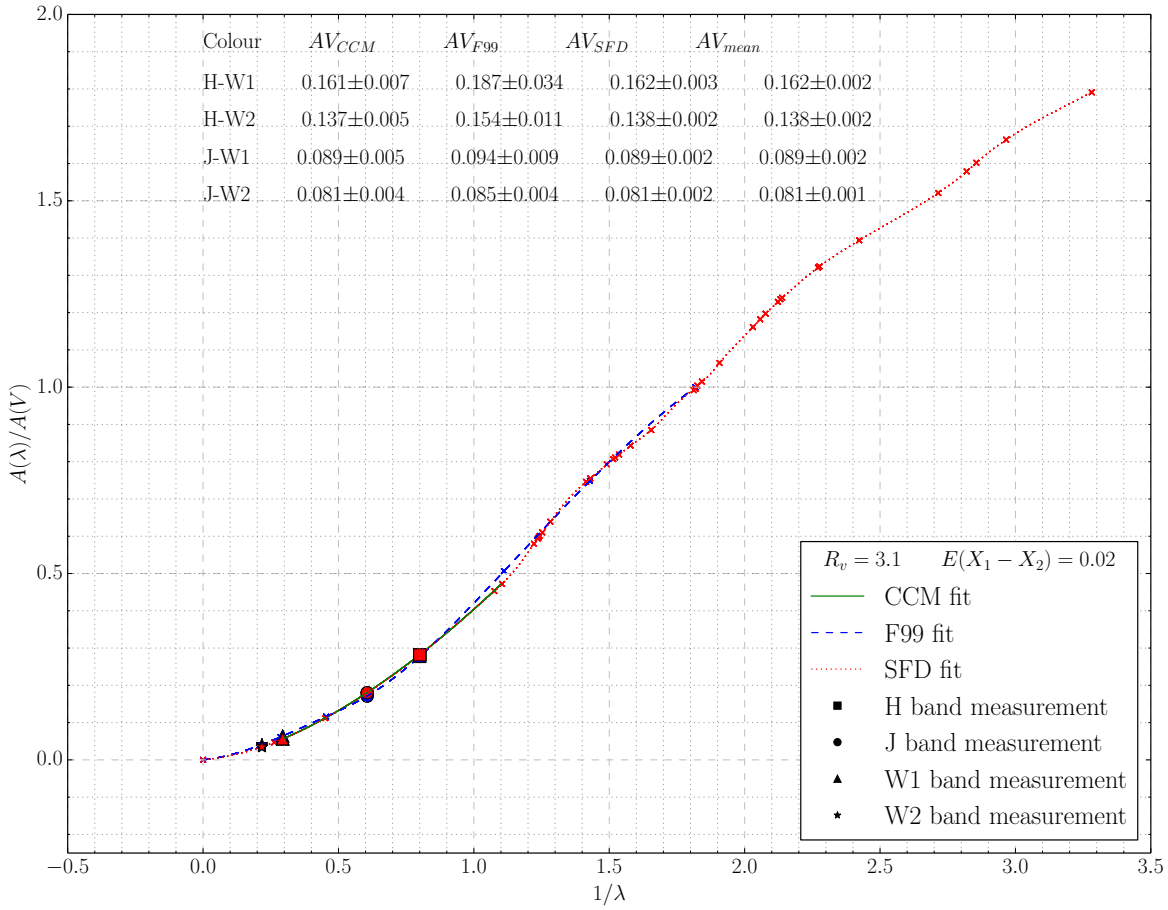


Figure. 3.1: Comparison between the Cardelli et al. (1989, CCM), Fitzpatrick (1999, F99) and Schlegel et al. (1998, SFD) for $E(J-W1)$, $E(J-W2)$, $E(H-W1)$, and $E(H-W2)$ equal to 0.02 for an $R_V$ of 3.1.

calculated. Note, I also tested $R_V$ values of 2.1 and 4.1 but at these tiny values of extinction are indistinguishable from an $R_V$ of 3.1.

$$A_{\lambda 1} - A_{\lambda 2} = E(\lambda_1 - \lambda_2) \tag{3.1}$$

$$A_V = E(\lambda_1 - \lambda_2)\left[\frac{A_{\lambda 1}}{A_V} - \frac{A_{\lambda 2}}{A_V}\right]^{-1} \tag{3.2}$$

After the reddening cuts 138,572 of the original 440,694 M dwarfs were retained en route towards my excess sample. Figure 3.2 shows the reddening cuts for $(J-W2)$ applied to a small area of sky.

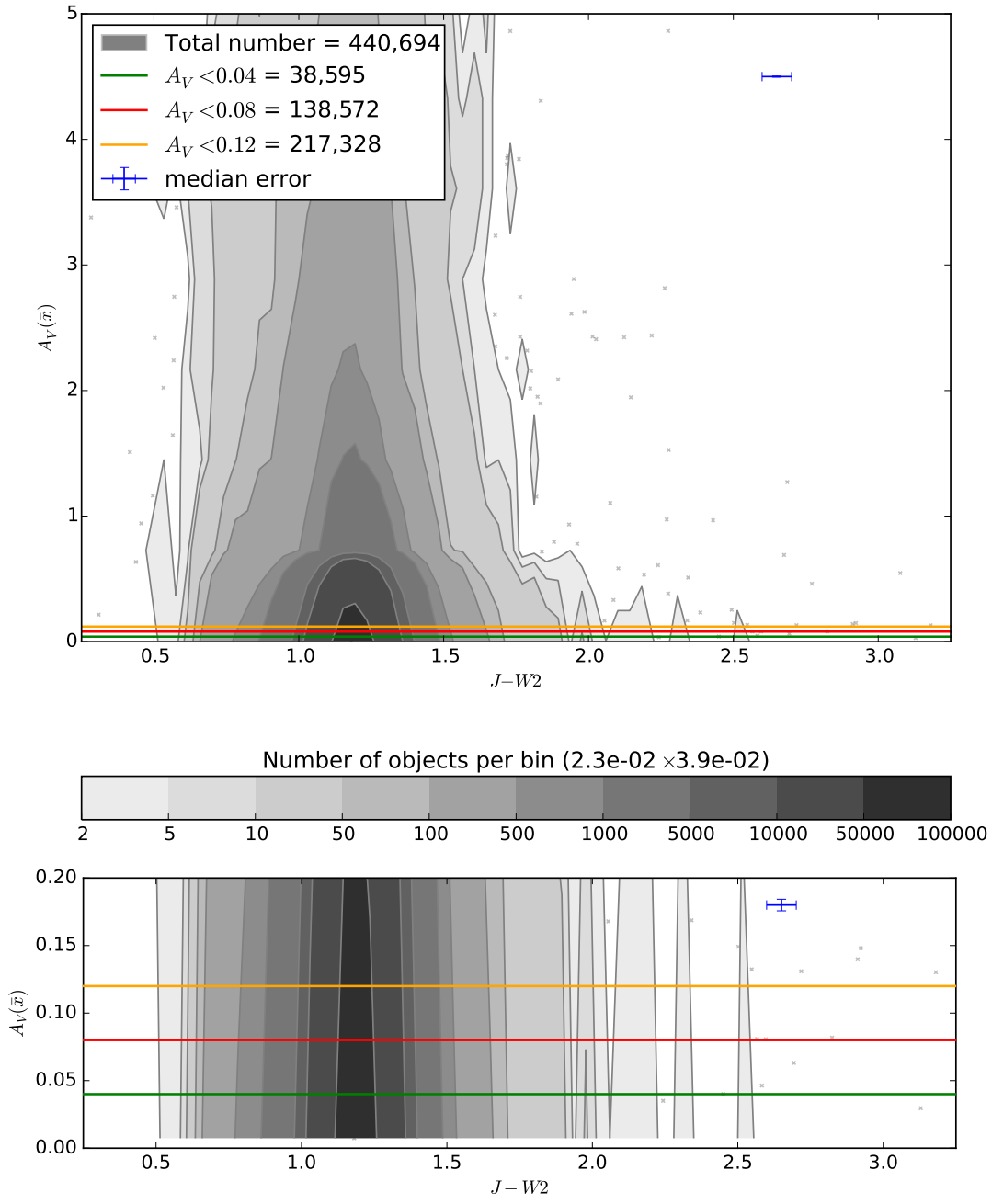


Figure. 3.2: The reddening cuts applied to a small area of sky ($\alpha = 9^h20^m0.0^s, \delta = +30°0^m0.0^s$ to $\alpha = 10^h0^m0.0^s, \delta = +40°0^m0.0^s$) to show the size of various reddening cut (for $(J-W2)$ ). Top shows the main $A_\mathrm{v}$ distribution, bottom shows a zoomed in version at low $A_\mathrm{v}$ .

### 3.2.2 Photometric quality cuts

To ensure high quality photometry I required photometric magnitudes:

- had uncertainties better than 0.04 in $g$, $r$, $i$ and $z$ (413,944 sources in the full M dwarf candidate catalogue; see Figure 3.3a).
- had uncertainties better than 0.04 in $V$, $J$, $H$, $K$, $W1$ and $W2$ (150,307 sources in the full M dwarf candidate catalogue; see Figure 3.3b).
- had unsaturated $g$ and $r$ photometry ($g$ >14, $r$ >14, York et al., 2000, 439,202 sources in the full M dwarf candidate catalogue; see Figure 3.4a).
- had WISE photometry unblended (flags $na = 0$ and $nb = 1$; 416,330 sources in the full M dwarf candidate catalogue; see Figure 3.4b).
- had SDSS photometry not registering as an extended source (flag ext_flg= 0; 435,087 sources in the full M dwarf candidate catalogue; see Figure 3.5a).
- had an SDSS score[19] greater than 0.5 (407,962 sources in the full M dwarf candidate catalogue; see Figure 3.5b).
- were not flagged[20] as too close to the edge of their frames (using the *EDGE* flag; 431,431 sources in the full M dwarf candidate catalogue; see Figure 3.6a).
- were not flagged[20] as using photometry from bad images (using the *PEAKCENTER*, *NOTCHECKED* and *DEBLEND_NOPEAK*; 439,641, 429,979 and 419,436 sources respectively in the full M dwarf candidate catalogue; see Figure 3.6b, Figure 3.7a, and Figure 3.7b respectively).
- were not flagged[20] as having photometry from images containing saturated pixels (*SATURATED*; 416,889 sources in the full M dwarf candidate catalogue; see Figure 3.8a).
- were not flagged[20]as having more than 20 per cent of the PSF flux interpolated (using the *PSF_FLUX_INTERP* flag; 380,868 sources in the full M dwarf candidate catalogue; see Figure 3.8b).

Combining all of these cuts left 103,482 M dwarf candidates. A comparison between the sample before (440,694) and after (103,482) these photometric quality cuts can be seen in Figure 3.9. One can see that these photometric quality cuts really do remove a lot of the scatter in colour. Although I reject over three quarters of the M dwarfs all outliers (i.e. where there was one object per 0.12×0.12 mag squared colour bin) are removed, thus making my sample extremely clean.

[19]The 'score' is a number between zero and one rating the quality of an SDSS image field, see http://www.sdss3.org/dr10/algorithms/resolve.php

[20]I chose which SDSS flags to use by assessing the quality flags for photometric outliers in my sample. Detailed information on these flags can be found at https://www.sdss3.org/dr9/algorithms/photo_flags.php.

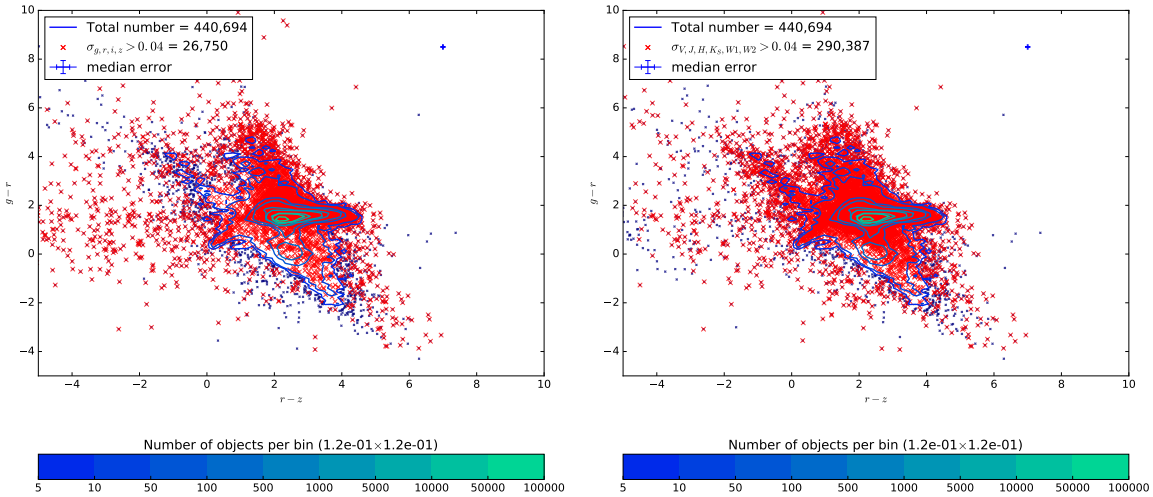


(a) (b)

Figure. 3.3: Colour-colour diagram, $(r-z)$ against $(g-r)$ showing the cuts for (a) $\sigma_{g,r,i} < 0.04$ and (b) $\sigma_{V,J,H,K_S,W1,W2} < 0.04$, rejected objects are shown with red crosses, grey contours are the full M dwarf distribution.

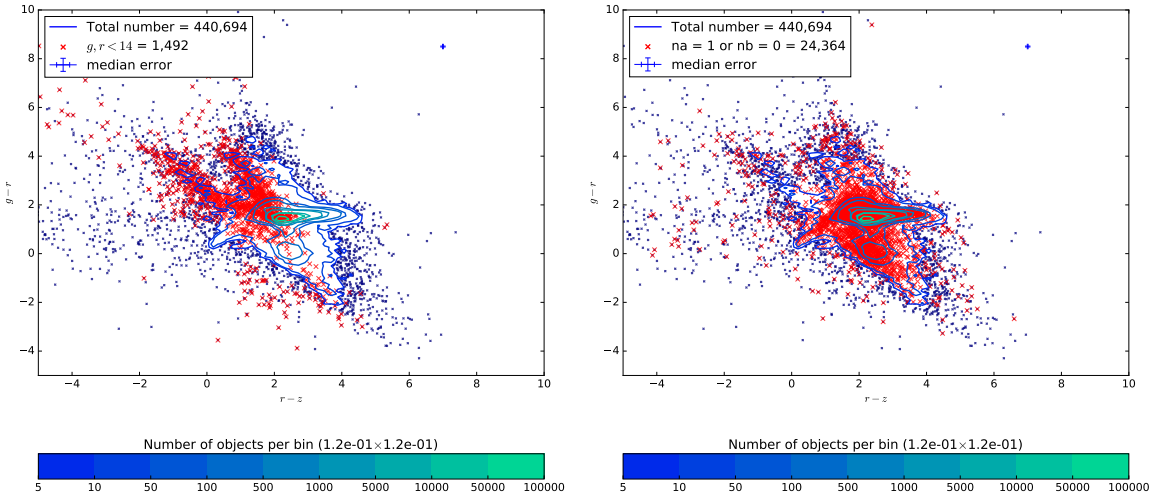


(a) (b)

Figure. 3.4: Colour-colour diagram, $(r-z)$ against $(g-r)$ showing the cuts for (a) $g, r > 14$ and (b) '$na = 0$ and $nb = 1$', rejected objects are shown with red crosses, grey contours are the full M dwarf distribution.

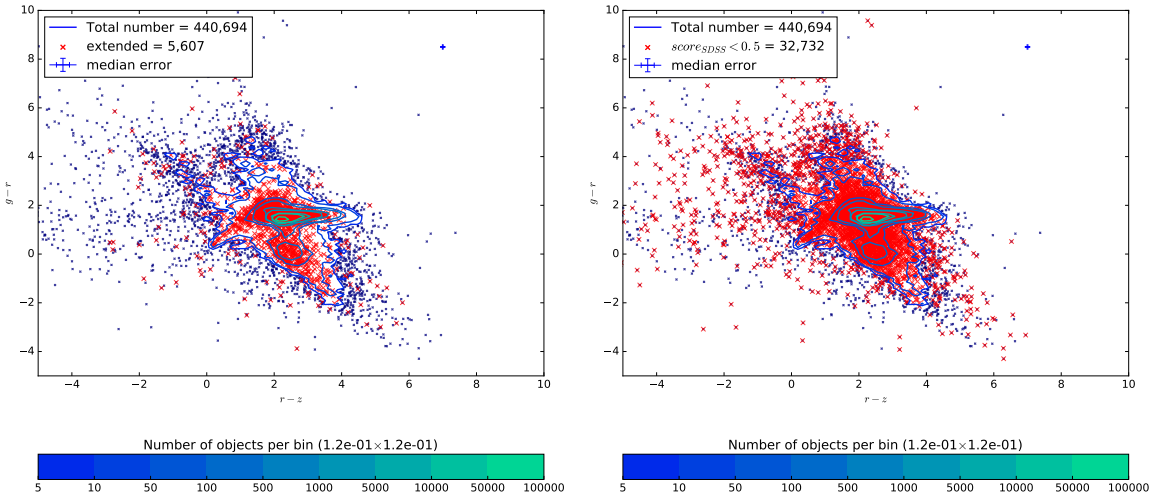


(a) (b)

Figure. 3.5: Colour-colour diagram, $(r-z)$ against $(g-r)$ showing the cuts for (a) 'ext_flg= 0' and (b) SDSS score $> 0.5$, rejected objects are shown with red crosses, grey contours are the full M dwarf candidate catalogue distribution.

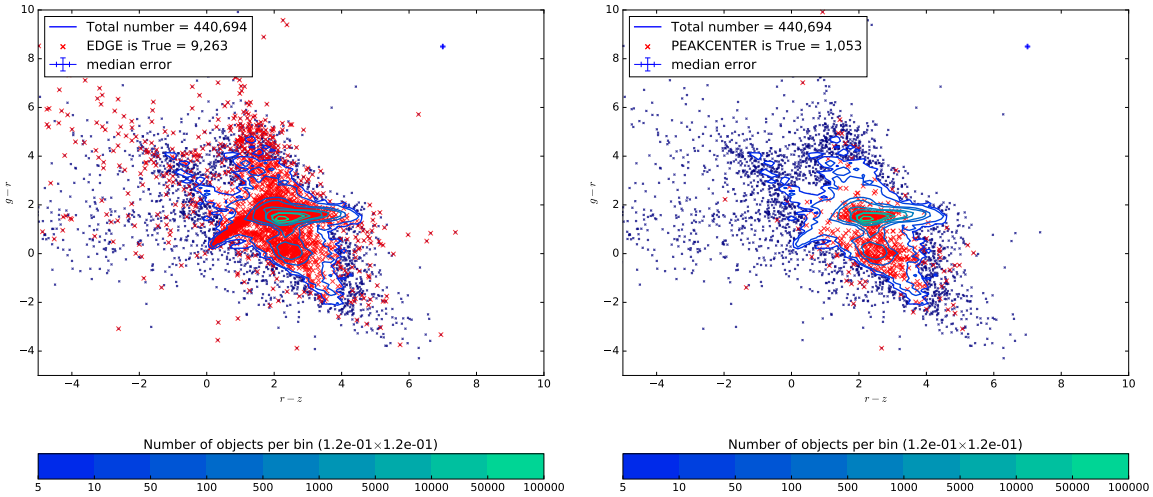


(a) (b)

Figure. 3.6: Colour-colour diagram, $(r-z)$ against $(g-r)$ showing the cuts for (a) SDSS flag *EDGE* and (b) SDSS flag *PEAKCENTER*, rejected objects are shown with red crosses, grey contours are the full M dwarf candidate catalogue distribution.

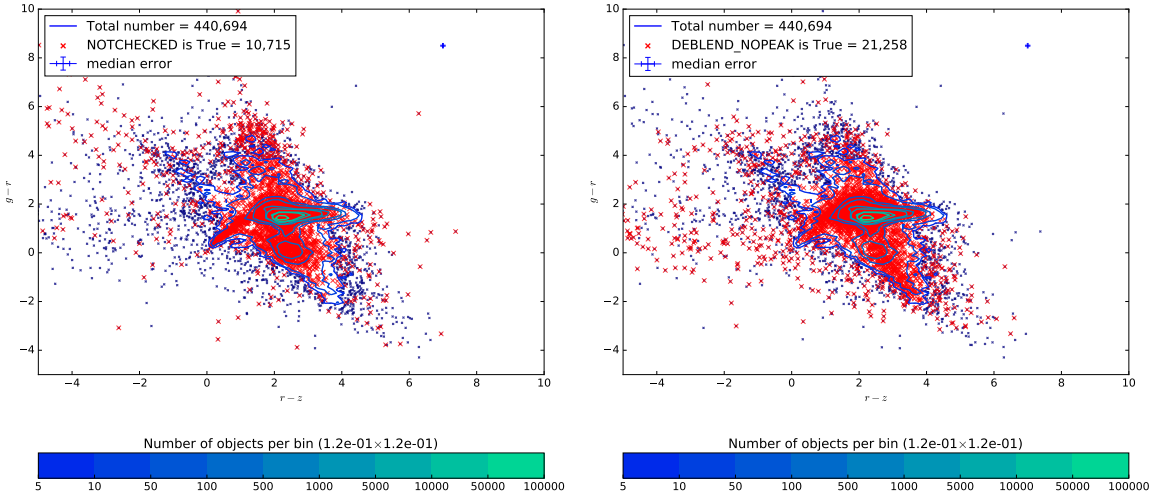


(a) (b)

Figure. 3.7: Colour-colour diagram, $(r-z)$ against $(g-r)$ showing the cuts for (a) SDSS flag *NOTCHECKED* and (b) SDSS flag *DEBLEND_NOPEAK*, rejected objects are shown with red crosses, grey contours are the full M dwarf candidate catalogue distribution.

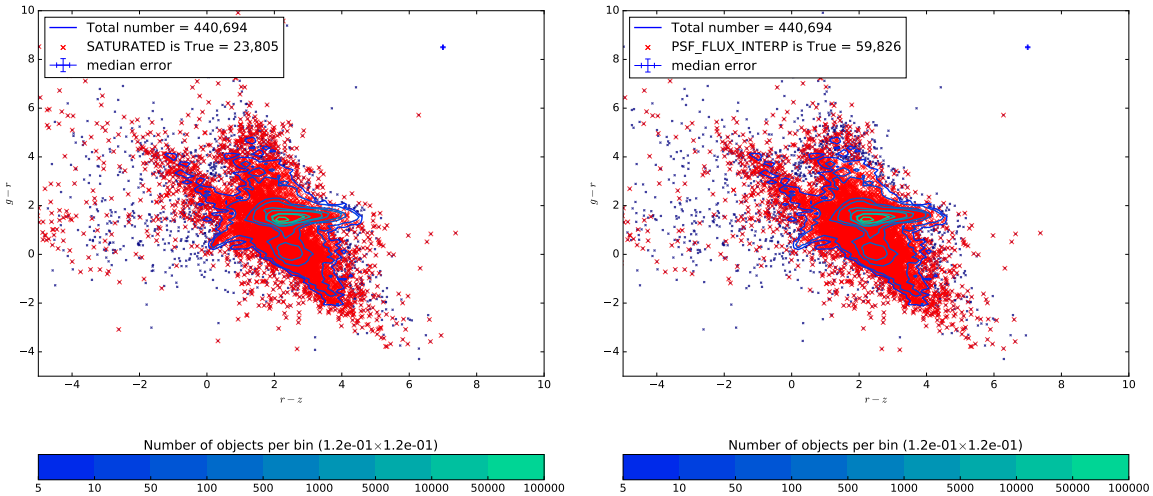


(a) (b)

Figure. 3.8: Colour-colour diagram, $(r-z)$ against $(g-r)$ showing the cuts for (a) SDSS flag *SATURATED* and (b) SDSS flag *PSF_FLUX_INTERP*, rejected objects are shown with red crosses, grey contours are the full M dwarf candidate catalogue distribution.

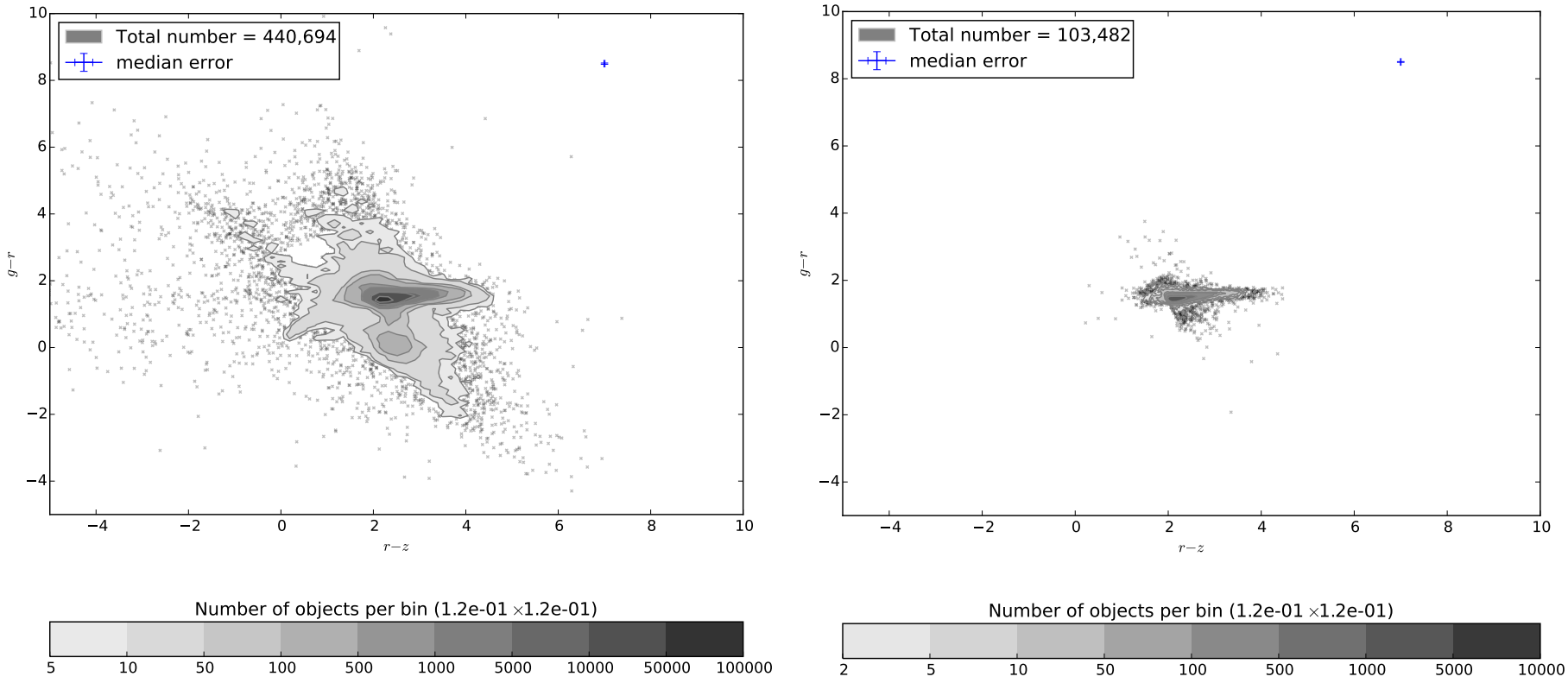


Figure. 3.9: Comparison between the M dwarf sample before (a) and after (b) the photometric quality cuts were applied, showing the extent of the "cleaning" process described in Section 3.2.2.

### 3.2.3 Removing variable sources

An additional check is possible to make sure none of the M dwarfs show short or long period variability, thus making them unusable for detecting excess. Pinfield et al. (2014) present a WISE cut, facilitated by the multi-epoch WISE measurements, in which M dwarfs are rejected if they lie above,

$$\log(w2sigp1 - w2sigmpro) = 1.3 - 1.38\log(w2snr) \tag{3.3}$$

where $w2sigp1$ is the standard deviation of the population of W2 fluxes measured on the individual frames, $w2sigmpro$ is the integrated flux uncertainty and $w2snr$ is the profile-fit measurement SNR (Pinfield et al., 2014). The WISE photometry covers several orders of magnitude for variation. From hours to days (covering activity due to flares and spots) and between groups of photometric observation (covering longer period variations), therefore most sources of variability should be removed using a rejection such as this (and thus should not be mistaken as excess candidates). These measurements are acquired from the WISE database[21]. This process was repeated for the $W1$ measurements. A total of 967 of my full M dwarf candidate catalogue were found to be variable in $W2$ and a further 66 were found to be variable in $W1$. The variable M dwarfs were set aside as interesting objects, though they are not studied further in this thesis.

### 3.2.4 The final excess sample

To further reduce contamination and provide as higher quality catalogue as possible for finding M+UCD systems I applied further cuts to the full M dwarf candidate catalogue. I applied reddening cuts equivalent to $A_V < 0.08$ or $E(J-W2) < 0.02$ which left 138,572 of my 440,694 M dwarf candidates. Then applied photometric quality cuts, requiring uncertainties better than 0.04 in all bands and high quality photometry (using flags provided in the WISE, 2MASS and SDSS catalogues). Combining these cuts left 103,482 of my 440,694 M dwarf candidates. As an additional cut we used WISE measurements to reject variable sources (following the procedure presented by Pinfield et al. 2014). Combining the reddening, quality and variability cuts left 36,898 M dwarf candidates in my excess sample.

These cuts effectively remove the galactic plane from my excess sample (one M dwarf is within galactic latitude of $\pm 15°$ and 255 M dwarfs, 0.7 per cent, are within galactic latitude of $\pm 20°$). Figure 3.11 shows the sky distribution of the full M dwarf candidate catalogue and the excess sample of M dwarfs, dominated by the SDSS foot-

[21] Access to data releases via http://irsa.ipac.caltech.edu

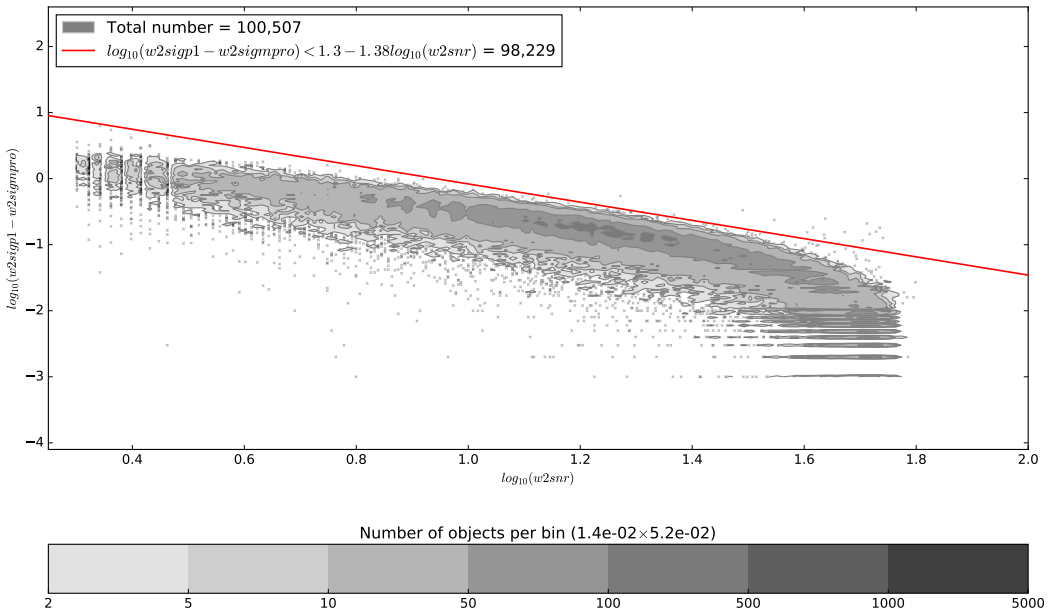


Figure. 3.10: The WISE variability cuts were applied to a small area of sky ($\alpha = 9^h20^m0.0^s, \delta = +30°0^m0.0^s$ to $\alpha = 10^h0^m0.0^s, \delta = +40°0^m0.0^s$), here shown for W2 (see Equation 3.3).

print and the reddening cut (Section 3.2.1) respectively. Figure 3.12 shows a flow diagram summarising of the excess sample selection process .

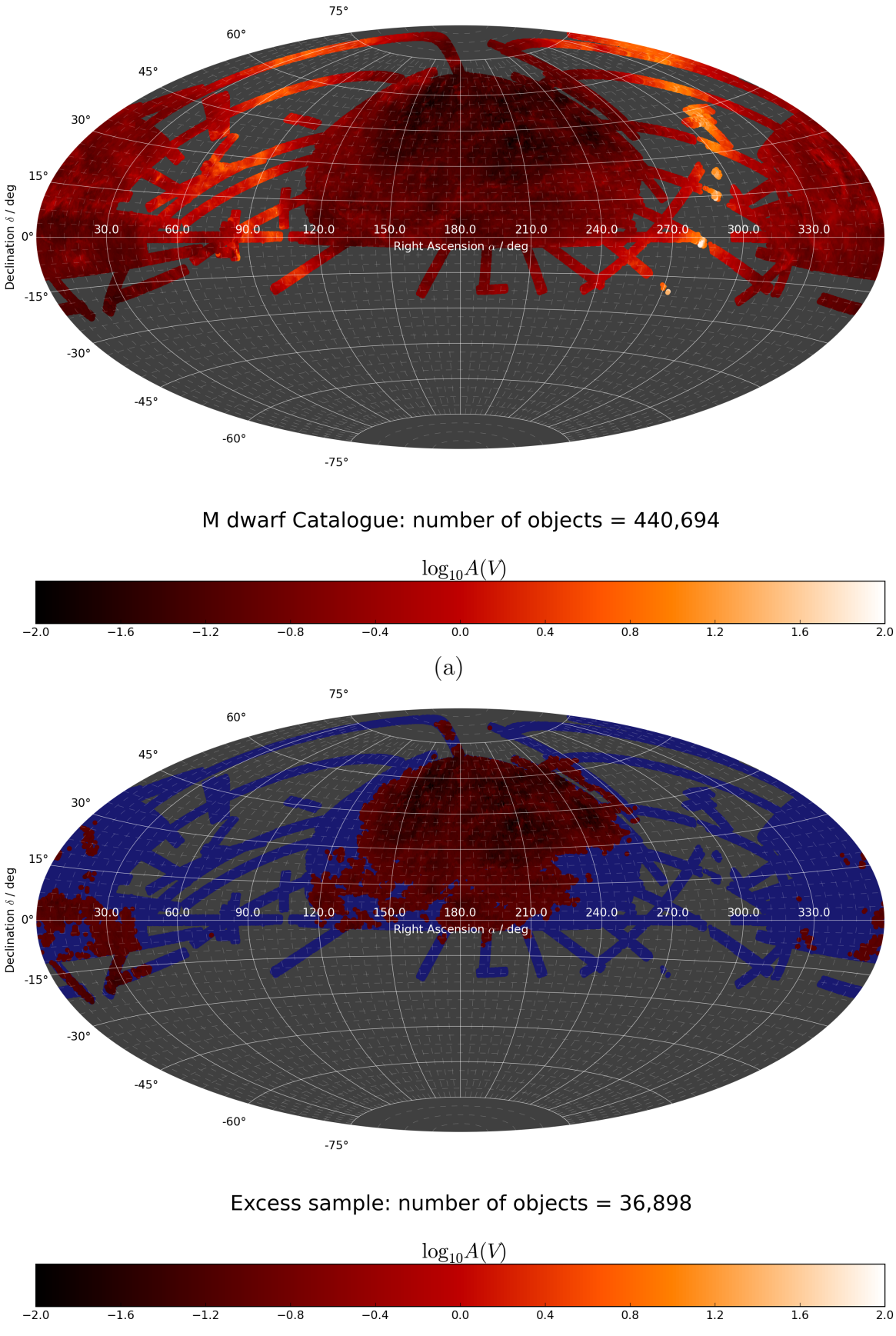


Figure. 3.11: Sky plot to show (a) the full M dwarf candidate catalogue and (b) the excess sample of M dwarfs. The full M dwarf candidate catalogue is dominated by the SDSS footprint and the excess sample is dominated by the reddening cuts applied in Section 3.2.1.

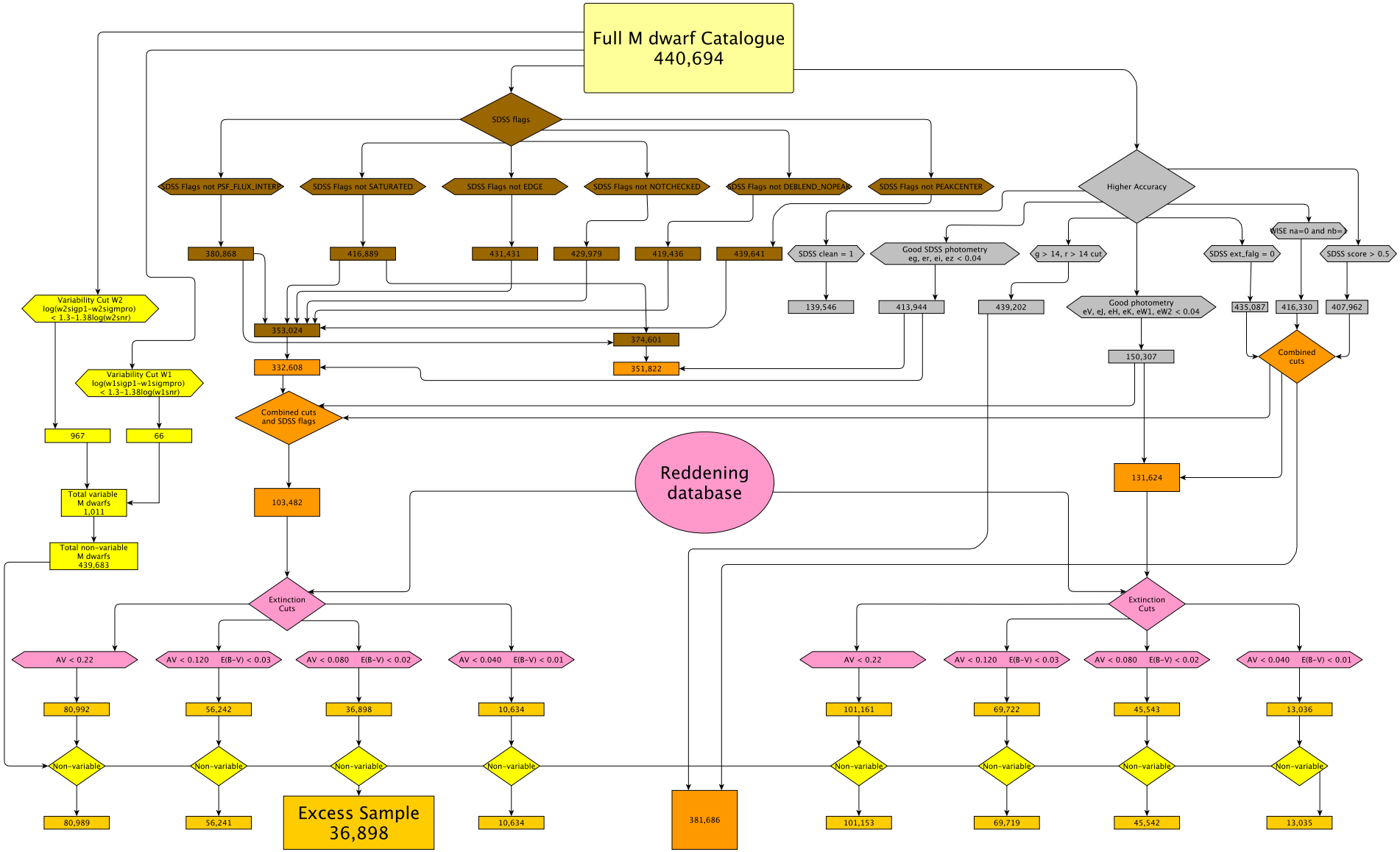


Figure. 3.12: Flow chart to summarise the process involved in making my excess sample.

## 3.3 Simulating photometry

Although M dwarf colours are intrinsically scattered at some level (see Section 1.2), the effects of adding an unresolved binary companion may be well determined. As a tool in my analysis I thus simulated M dwarf and UCD photometry which I used to interpret the observational parameter-space of the excess sample.

### 3.3.1 Simulating M dwarfs

For M dwarfs I constructed a probabilistic fitting routine which I applied to an M dwarf sample constructed using the following catalogues: *The Spectroscopic Catalog of The 1,564 Brightest (J <9) M-dwarf Candidates in the Northern Sky*[22] (selected from the *SUPERBLINK proper-motion catalogue*; Lépine et al., 2013), *The Database of Ultra-cool Parallaxes*[23] (from Dupuy & Liu, 2012), and *The Preliminary Version of the Third Catalog of Nearby Stars* (Gliese & Jahreiß, 1991).

Polynomials were fit to a variety of (colour and magnitude) data-points using a Bayesian approach (using EMCEE[24] and the fitting routine used by Foreman-Mackey et al. 2013 and Hogg et al. 2010). The probabilistic fitting routine allowed the polynomial parameters ($a_i = a_1, a_2, ..., a_n$) to vary as well as allowing the variance to vary[25], represented below by $f$. The probability distribution was assumed Gaussian and is shown in Equation 3.4.

$$\ln p(y|x, \sigma, model, f) = -\frac{1}{2}\sum_{i=1}^{n}\frac{(y_n - model_n)^2}{s_n^2} + \ln(2\pi s_n^2) \tag{3.4}$$

where $s$ is the total uncertainty comprising of the fixed measured uncertainty ($\sigma$) and a parameter that was allowed to vary within the model ($f$) such that $s_n^2 = \sigma_n^2 + f^2(model_n)^2$, and $model_n = \sum_{i=0}^{m} a_i x_n^i$.

The best polynomial fit found to simulate absolute J band magnitude, $M_J$, from spectral subtype, $spt$, for spectral subtype in the range M1 $\geq spt \geq$ M8 was a cubic fit (Equation 3.5).

$$M_J = -(0.014^{+0.002}_{-0.002})spt^3 + (0.17^{+0.02}_{-0.02})spt^2 + (0.13^{+0.05}_{-0.06})spt + (5.81^{+0.05}_{-0.04}) \pm 0.375 \tag{3.5}$$

where the $\pm 0.375$ was added to simulate the maximum deviation due to binaries in my sample[26] (see Figure 3.13).

[22] Accessed on-line at http://heasarc.gsfc.nasa.gov/W3Browse/all/bnmdspecat.html
[23] Accessed on-line at https://www.cfa.harvard.edu/~tdupuy/plx
[24] PYTHON implementation (Goodman & Weare, 2010) affine invariant MCMC ensemble sampler
[25] See http://dan.iel.fm/emcee/current/user/line/ for a full example
[26] The maximum brightness of an unresolved binary for two stars of equal brightness giving a factor of two in flux (in magnitudes equivalent to $-2.5\log_{10}(2) \approx -0.75 \rightarrow \pm 0.375$ uncertainty).

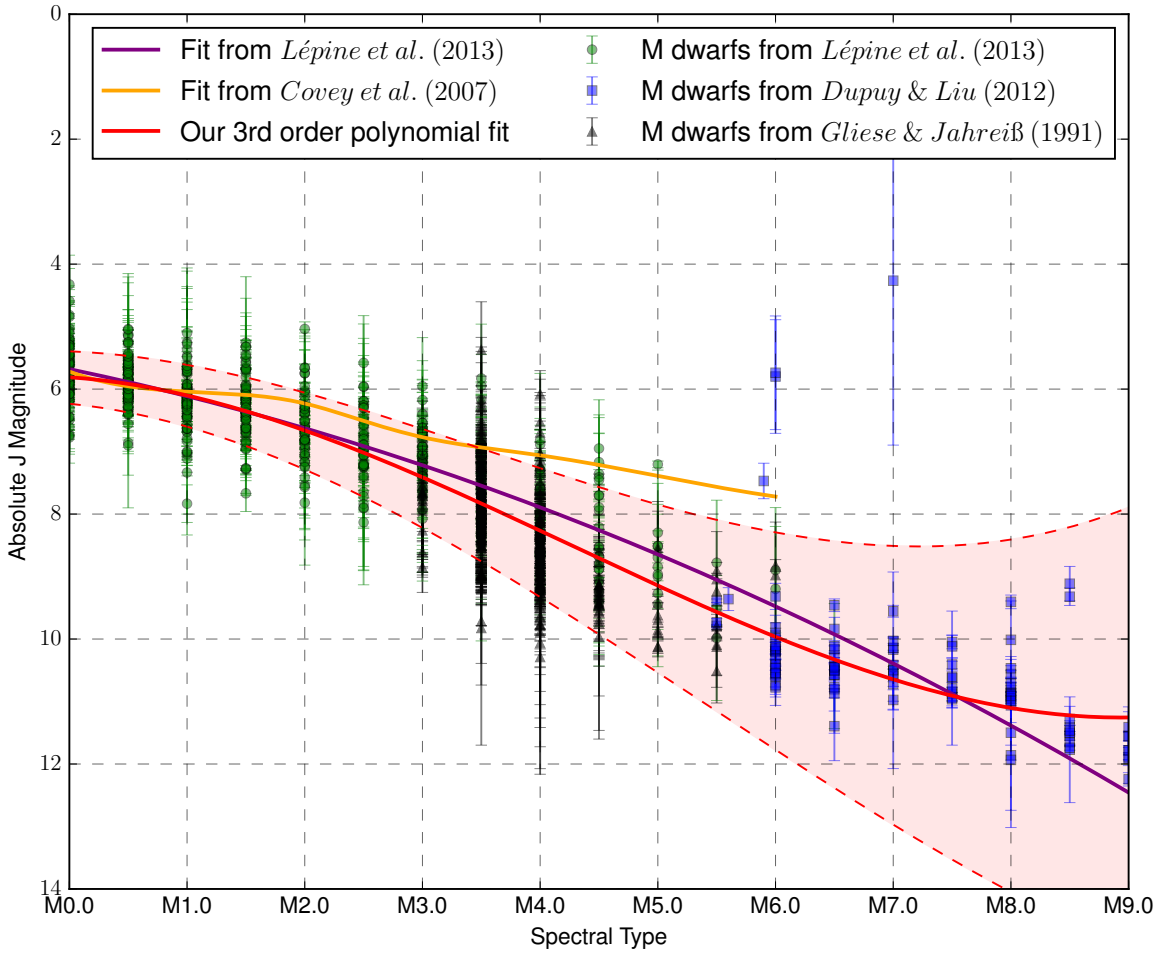


Figure. 3.13: Absolute magnitude against spectral type for sample of well measured M dwarfs (from Lépine et al. 2013; Gliese & Jahreiß 1991 and Dupuy & Liu 2012). Shown in purple is the fit Lépine et al. (2013) proposed, in yellow is an interpolated fit of data from Covey et al. (2007) and in red is my spectral type fit (see Equation 3.5), shaded regions show outer most bounds of the simulated photometric uncertainties and the added uncertainty due to the contribution of an unresolved equal binary (±0.375 magnitudes[26]).

I thus determined relationships between the $M_J$-NIR and $M_J$-MIR colours which led to synthetic absolute magnitudes in the $J$, $H$, $K$, $W1$, and $W2$ bands (See Figure 3.14 and Figure 3.15). In addition I used the synthesised colour-colour relations from Covey et al. (2007) to generate SDSS magnitudes, making use of cubic spline fits for spectral types M0.5, M1.5, M3.5, M4.5, M5.5 (See Table 3 from Covey et al., 2007). The simulated photometry is plotted with the simulated UCD photometry in Figure 3.16 and a summary of the photometry is given in Table 3.5.

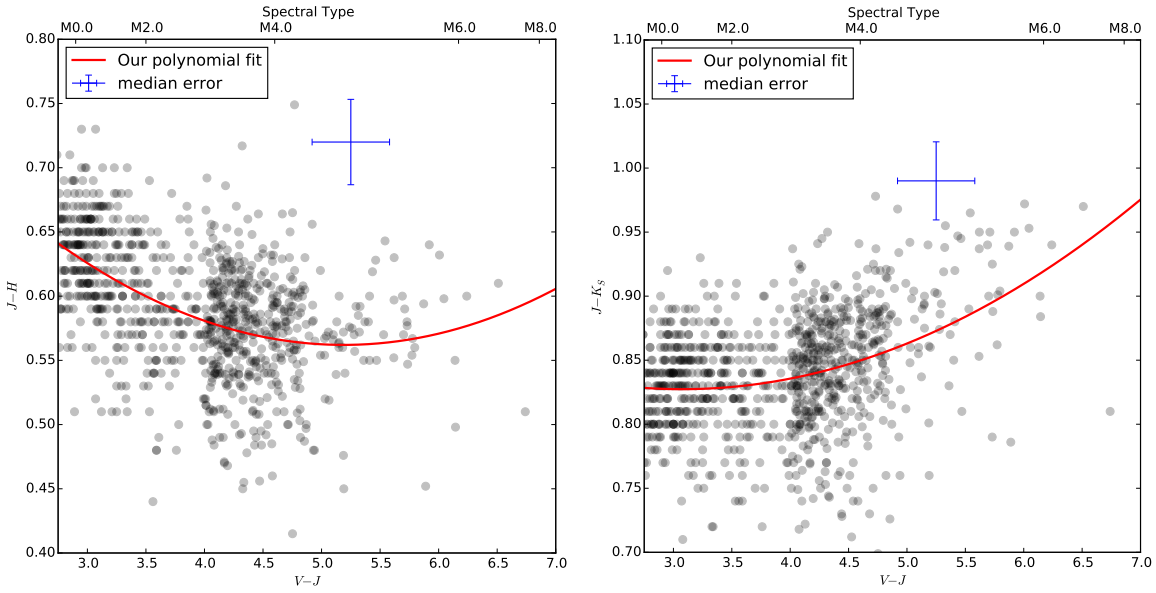


(a) (b)

Figure. 3.14: Polynomial fit results using the probabilistic fitting routine mentioned in Section 3.3.1. Using (a) the fit between $(V-J)$ and $(J-H)$ and (b) the fit between $(V-J)$ and $(J-K_S)$ and Figure 3.13 I was able to work out absolute $H$ and $K_S$ magnitudes.

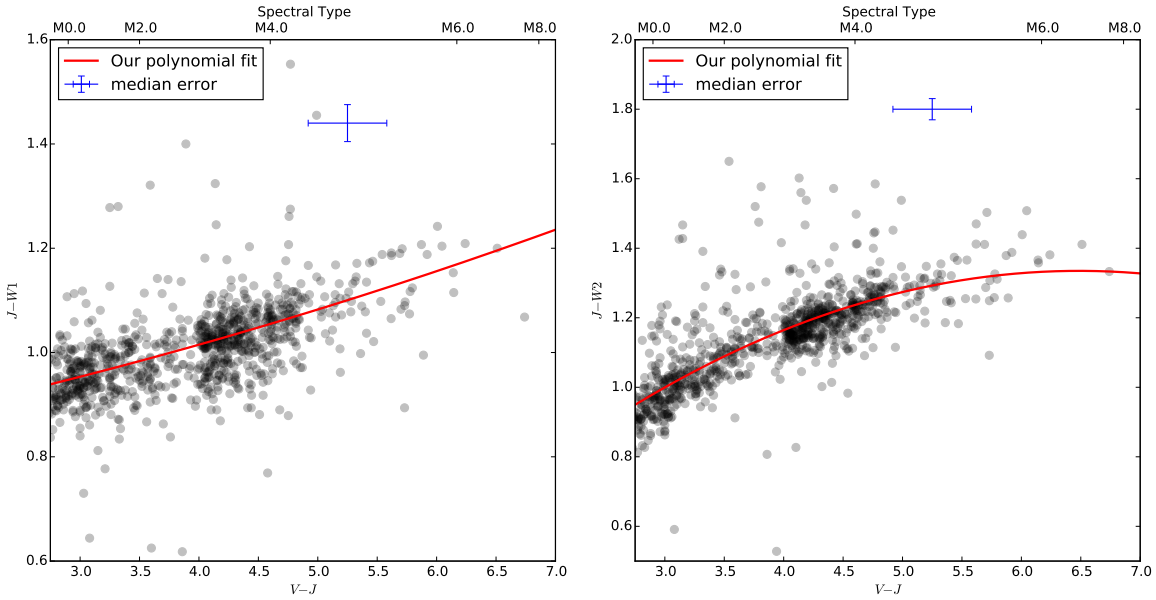


(a) (b)

Figure. 3.15: Polynomial fit results using the probabilistic fitting routine mentioned in Section 3.3.1. Using (a) the fit between $(V-J)$ against $(J-W1)$ and (b) the fit between $(V-J)$ against $(J-W2)$ and Figure 3.13 I was able to estimate the absolute $W1$ and $W2$ magnitudes.

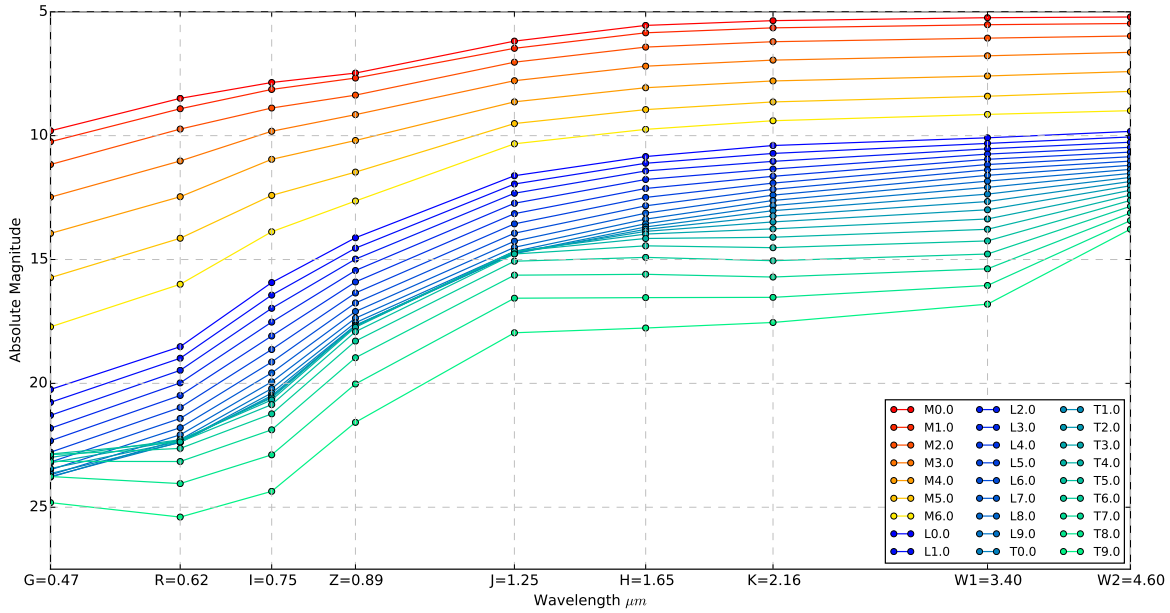


Figure. 3.16: Absolute magnitude against wavelength, for simulated M dwarf and UCD photometry as calculated by the fits in Table 3.3 and Table 3.4.

### 3.3.2 Simulating UCDs

For the UCDs, Dupuy & Liu (2012) present a set of polynomials for $J$, $H$, $K$, $W1$, and $W2$ (see Table 3.4). I use these to simulate the NIR and MIR photometric bands. The optical photometric bands were estimated using the synthetic SDSS colours ($(u-g)$, $(g-r)$, $(r-i)$, $(i-z)$ and $(z-J)$; see Table 3.4a and Figure 3.17 and Figure 3.18). Figure 3.17 and Figure 3.18 show the polynomial fits for the various colours as a function of $(V-J)$. The fit was generated using the probabilistic fitting routine (used in this Section 3.3.1) on data from Hawley et al. (2002); Chiu et al. (2006) and Dupuy & Liu (2012) cross-matched with 2MASS and SDSS. From these simulated colours and using $J$ from the Dupuy & Liu (2012) polynomial fit I was able to calculate $z$ (from $(z-J)$) and thus $i$, $r$, $g$ and $u$. This simulated photometry is plotted with the simulated M dwarf photometry in Figure 3.16 and a summary of the photometry is given in Table 3.5.

| y | x | $c_0$ | $c_1$ | $c_2$ | $c_3$ |
|---|---|---|---|---|---|
| $M_J$ | *spt* | $(+5.81^{+0.05}_{-0.04}) \pm 0.375$ | $(+1.28^{+0.55}_{-0.55})\times10^{-1}$ | $(+1.76^{+0.20}_{-0.17})\times10^{-1}$ | $(-1.37^{+0.16}_{-0.15})\times10^{-2}$ |
| $(J-H)$ | $(V-J)$ | $(+9.20^{+0.37}_{-0.36})\times10^{-1}$ | $(-1.38^{+2.55}_{-2.93})\times10^{-1}$ | $(+1.33^{+0.23}_{-0.23})\times10^{-2}$ | ... |
| $(J-K_S)$ | $(V-J)$ | $(+9.18^{+0.41}_{-0.36})\times10^{-1}$ | $(-0.59^{+0.99}_{-1.38})\times10^{-1}$ | $(+0.96^{+0.25}_{-0.22})\times10^{-2}$ | ... |
| $(J-W1)$ | $(V-J)$ | $(+8.05^{+0.91}_{-0.74})\times10^{-1}$ | $(+4.05^{+4.26}_{-4.01})\times10^{-2}$ | $(+0.30^{+0.55}_{-0.12})\times10^{-2}$ | ... |
| $(J-W2)$ | $(V-J)$ | $(+1.74^{+1.27}_{-1.01})\times10^{-1}$ | $(+3.58^{+0.56}_{-0.59})\times10^{-1}$ | $(-2.76^{+4.77}_{-6.18})\times10^{-2}$ | ... |

(a)

| colour | fit | M0 | M1 | M2 | M2.5 | M3 | M4 | M5 | M6 |
|---|---|---|---|---|---|---|---|---|---|
| $(u-g)$ | spline | 2.65 | 2.72 | 2.59 | 2.74 | 2.67 | 3.13 | 3.05 | 2.99 |
| $(g-r)$ | spline | 1.31 | 1.33 | 1.43 | 1.47 | 1.46 | 1.48 | 1.59 | 1.72 |
| $(r-i)$ | spline | 0.64 | 0.78 | 0.85 | 1.01 | 1.20 | 1.51 | 1.73 | 2.12 |
| $(i-z)$ | spline | 0.38 | 0.46 | 0.52 | 0.63 | 0.67 | 0.76 | 0.94 | 1.24 |
| $(z-J)$ | spline | 1.29 | 1.20 | 1.33 | 1.32 | 1.37 | 1.56 | 1.96 | 2.31 |

(b)

Table 3.3: M dwarf synthetic photometry generation: **a:** Colour-colour fits ($y = \sum_{i=0}^{N} c_i x^i$) were produced for $M0.0 - M6.0$ dwarfs using my probabilistic fitting routine (Equation 3.4) using the data from Lépine et al. (2013); Gliese & Jahreiß (1991) and Dupuy & Liu (2012). **b:** Synthetic SDSS colours from Covey et al. (Table 3; 2007) were used to generate synthetic SDSS photometry ($u$, $g$, $r$, $i$ and $z$) using a cubic spline for the missing spectral types ($M0.5$, $M1.5$, $M3.5$, $M4.5$, $M5.5$).

| y | $c_0$ | $c_1$ | $c_2$ | $c_3$ | $c_4$ | $c_5$ | $c_6$ | rms |
|---|---|---|---|---|---|---|---|---|
| $J$ | $-9.68\times10^{+0}$ | $+8.16\times10^{+0}$ | $-1.33\times10^{+0}$ | $+1.12\times10^{-1}$ | $-4.83\times10^{-3}$ | $+1.01\times10^{-4}$ | $-7.85\times10^{-7}$ | 0.40 |
| $H$ | $-1.18\times10^{+1}$ | $+9.00\times10^{+0}$ | $-1.50\times10^{+0}$ | $+1.29\times10^{-1}$ | $-5.81\times10^{-3}$ | $+1.29\times10^{-4}$ | $-1.11\times10^{-6}$ | 0.40 |
| $K$ | $+1.10\times10^{+1}$ | $-8.67\times10^{-1}$ | $+1.34\times10^{-1}$ | $-6.42\times10^{-3}$ | $+1.07\times10^{-4}$ | ... | ... | 0.43 |
| $W1$ | $+7.15\times10^{+0}$ | $+3.55\times10^{-1}$ | $-4.38\times10^{-3}$ | $-3.34\times10^{-4}$ | $+1.58\times10^{-5}$ | ... | ... | 0.39 |
| $W2$ | $+7.47\times10^{+0}$ | $+1.92\times10^{-1}$ | $+1.14\times10^{-2}$ | $-8.82\times10^{-4}$ | $+1.79\times10^{-5}$ | ... | ... | 0.35 |

(a)

| y | $c_0$ | $c_1$ | $c_2$ | $c_3$ |
|---|---|---|---|---|
| $(u-g)$ | $(+6.29^{+7.23}_{-2.74})\times10^{+0}$ | $(-1.02^{+1.59}_{-3.32})\times10^{+0}$ | $(+5.24^{+8.37}_{-1.93})\times10^{-2}$ | $(-0.09^{+0.15}_{-0.33})\times10^{-2}$ |
| $(g-r)$ | $(+0.99^{+5.26}_{-8.81})\times10^{-1}$ | $(+2.61^{+5.04}_{-0.69})\times10^{-1}$ | $(-0.98^{+1.71}_{-4.16})\times10^{-2}$ | ... |
| $(r-i)$ | $(+2.74^{+0.32}_{-0.27})\times10^{+0}$ | $(+0.81^{+4.40}_{-2.54})\times10^{-2}$ | $(-0.23^{+0.31}_{-0.59})\times10^{-2}$ | ... |
| $(i-z)$ | $(+1.70^{+0.65}_{-0.55})\times10^{+0}$ | $(-0.90^{+0.16}_{-0.31})\times10^{-1}$ | $(+1.31^{+1.10}_{-0.97})\times10^{-2}$ | $(-0.03^{+0.03}_{-0.08})\times10^{-2}$ |
| $(z-J)$ | $(+2.08^{+9.40}_{-0.86})\times10^{-1}$ | $(+4.05^{+1.48}_{-1.06})\times10^{+0}$ | $(-2.15^{+3.24}_{-5.02})\times10^{-2}$ | $(+0.04^{+0.02}_{-0.02})\times10^{-2}$ |

(b)

Table 3.4: UCD synthetic photometry generation: **(a)** Table adapted from table 14 - Coefficients of polynomial fits to absolute magnitudes (Dupuy & Liu, 2012), where $y$ is the simulated photometry, $y = \sum_{i=0}^{N} c_i x^i$ and $x$ is spectral type. For these simulated brown dwarfs $Spt(L0) : x = 10$ to $Spt(Y0) : x = 30$. **(b)** $u$, $g$, $r$, $i$ and $z$ were estimated using the synthetic SDSS colours from (Covey et al., 2007) and J from (a), $y = \sum_{i=0}^{N} c_i x^i$, where $x$ is spectral type. The fit was generated using the probabilistic fitting routine on data from Hawley et al. (2002); Chiu et al. (2006) and Dupuy & Liu (2012) cross-matched with 2MASS and SDSS.

| *SpT* | $V$ | $g$ | $r$ | $i$ | $z$ | $J$ | $H$ | $K_s$ | $W1$ | $W2$ |
|---|---|---|---|---|---|---|---|---|---|---|
| M0.0 | 9.05 | 9.80 | 8.49 | 7.85 | 7.47 | 6.18 | 5.55 | 5.36 | 5.24 | 5.21 |
| M0.5 | 9.22 | 9.98 | 8.67 | 7.92 | 7.47 | 6.29 | 5.66 | 5.47 | 5.34 | 5.30 |
| M1.0 | 9.48 | 10.25 | 8.92 | 8.14 | 7.68 | 6.48 | 5.85 | 5.65 | 5.52 | 5.47 |
| M1.5 | 9.84 | 10.63 | 9.26 | 8.47 | 8.01 | 6.73 | 6.11 | 5.90 | 5.77 | 5.70 |
| M2.0 | 10.34 | 11.17 | 9.74 | 8.89 | 8.37 | 7.04 | 6.43 | 6.21 | 6.06 | 5.98 |
| M2.5 | 10.97 | 11.82 | 10.35 | 9.34 | 8.71 | 7.39 | 6.79 | 6.56 | 6.40 | 6.29 |
| M3.0 | 11.64 | 12.48 | 11.02 | 9.82 | 9.15 | 7.78 | 7.20 | 6.95 | 6.78 | 6.64 |
| M3.5 | 12.34 | 13.18 | 11.72 | 10.35 | 9.65 | 8.20 | 7.62 | 7.37 | 7.18 | 7.02 |
| M4.0 | 13.09 | 13.95 | 12.47 | 10.96 | 10.20 | 8.64 | 8.07 | 7.79 | 7.59 | 7.41 |
| M4.5 | 13.92 | 14.80 | 13.28 | 11.66 | 10.82 | 9.08 | 8.51 | 8.22 | 8.01 | 7.81 |
| M5.0 | 14.82 | 15.73 | 14.14 | 12.41 | 11.47 | 9.51 | 8.95 | 8.64 | 8.41 | 8.21 |
| M5.5 | 15.76 | 16.71 | 15.06 | 13.17 | 12.10 | 9.93 | 9.36 | 9.04 | 8.79 | 8.61 |
| M6.0 | 16.73 | 17.72 | 16.00 | 13.88 | 12.64 | 10.33 | 9.75 | 9.40 | 9.14 | 8.99 |
| L0.0 | 19.25 | 20.25 | 18.52 | 15.93 | 14.12 | 11.62 | 10.84 | 10.40 | 10.09 | 9.83 |
| L1.0 | 19.74 | 20.77 | 18.99 | 16.44 | 14.54 | 11.95 | 11.12 | 10.72 | 10.31 | 10.05 |
| L2.0 | 20.25 | 21.29 | 19.47 | 16.97 | 14.98 | 12.33 | 11.43 | 11.04 | 10.53 | 10.27 |
| L3.0 | 20.76 | 21.81 | 19.98 | 17.53 | 15.44 | 12.73 | 11.77 | 11.35 | 10.75 | 10.47 |
| L4.0 | 21.27 | 22.32 | 20.49 | 18.09 | 15.91 | 13.15 | 12.13 | 11.64 | 10.96 | 10.67 |
| L5.0 | 21.74 | 22.78 | 20.97 | 18.63 | 16.35 | 13.56 | 12.49 | 11.92 | 11.17 | 10.85 |
| L6.0 | **22.17** | **23.18** | 21.42 | 19.14 | 16.76 | 13.94 | 12.83 | 12.17 | 11.38 | 11.03 |
| L7.0 | **22.51** | **23.49** | 21.79 | 19.58 | 17.10 | 14.26 | 13.13 | 12.40 | 11.60 | 11.20 |
| L8.0 | **22.76** | **23.69** | 22.08 | 19.94 | 17.37 | 14.51 | 13.37 | 12.62 | 11.84 | 11.36 |
| L9.0 | **22.91** | **23.78** | **22.27** | 20.21 | 17.55 | 14.67 | 13.56 | 12.82 | 12.09 | 11.52 |
| T0.0 | **22.96** | **23.76** | **22.37** | 20.39 | 17.65 | 14.75 | 13.69 | 13.03 | 12.36 | 11.69 |
| T1.0 | **22.91** | **23.64** | **22.39** | 20.49 | 17.69 | 14.76 | 13.78 | 13.24 | 12.66 | 11.85 |
| T2.0 | **22.81** | **23.44** | **22.35** | 20.55 | 17.68 | 14.72 | 13.86 | 13.48 | 12.99 | 12.02 |
| T3.0 | **22.67** | **23.20** | **22.29** | 20.59 | 17.68 | 14.67 | 13.97 | 13.76 | 13.36 | 12.20 |
| T4.0 | **22.57** | **22.99** | **22.28** | 20.67 | 17.74 | 14.67 | 14.15 | 14.10 | 13.78 | 12.40 |
| T5.0 | **22.56** | **22.85** | **22.36** | 20.86 | 17.91 | 14.78 | 14.45 | 14.52 | 14.25 | 12.61 |
| T6.0 | **22.72** | **22.88** | **22.62** | 21.23 | 18.29 | 15.07 | 14.91 | 15.05 | 14.78 | 12.85 |
| T7.0 | **23.14** | **23.15** | **23.15** | 21.87 | 18.96 | 15.63 | 15.60 | **15.71** | 15.38 | 13.12 |
| T8.0 | **23.91** | **23.76** | **24.05** | **22.88** | 20.02 | **16.56** | **16.54** | **16.53** | 16.05 | 13.43 |
| T9.0 | **25.13** | **24.81** | **25.40** | **24.36** | 21.57 | **17.96** | **17.77** | **17.54** | **16.80** | 13.78 |

Table 3.5: The final absolute magnitudes for each spectral type (*SpT*) from the simulation of photometry process. Photometry is available for any subtype but not shown for UCDs of half-integer subtype (for clarity). $V = V(g - r)$ is calculated using Equation 2.5 as with my full M dwarf candidate catalogue. Note those in bold font should not be used as actual values, as they are below the $5\sigma$ limit (see Table 1.5) for the photometry set. These are only used and presented as a guide to the extrapolated photometric values/sensitivity limits of the survey data (sensitivity to a UCD companion diminishes before this becomes a problem).

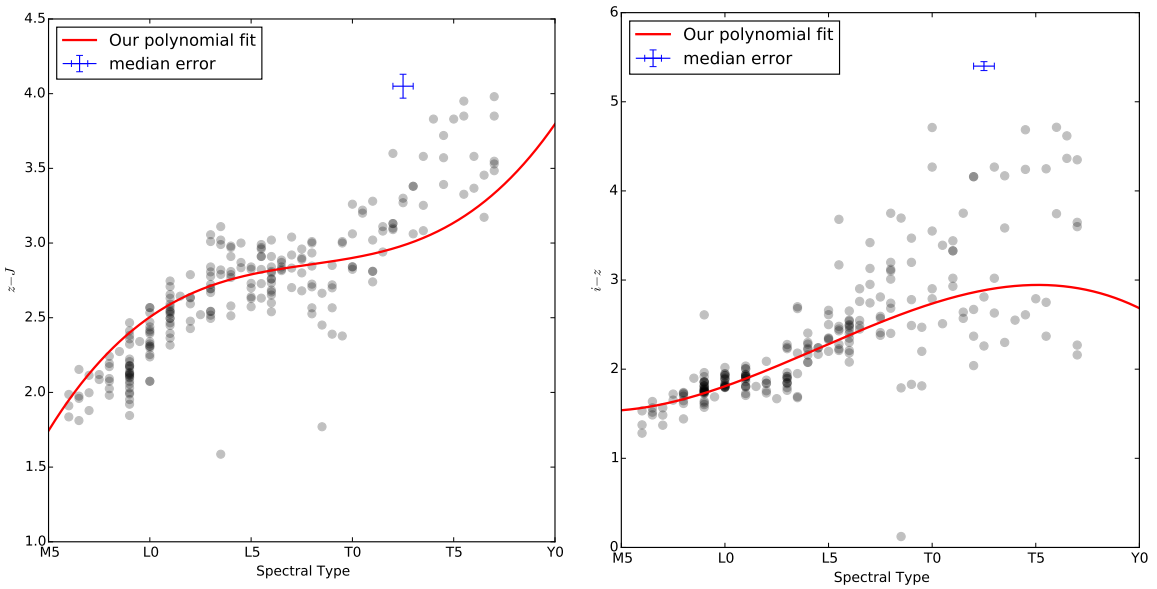


(a) (b)

Figure. 3.17: Polynomial fit results using the probabilistic fitting routine mentioned in Section 3.3.1. Using (a) the fit between spectral type against $(z-J)$ and $J$ from the Dupuy & Liu (2012) polynomial fit I was able to estimate the absolute $z$ magnitude. Using the $z$ band magnitude and (b) the fit between spectral type and $(i-z)$ I was able to estimate the absolute $i$ magnitudes.

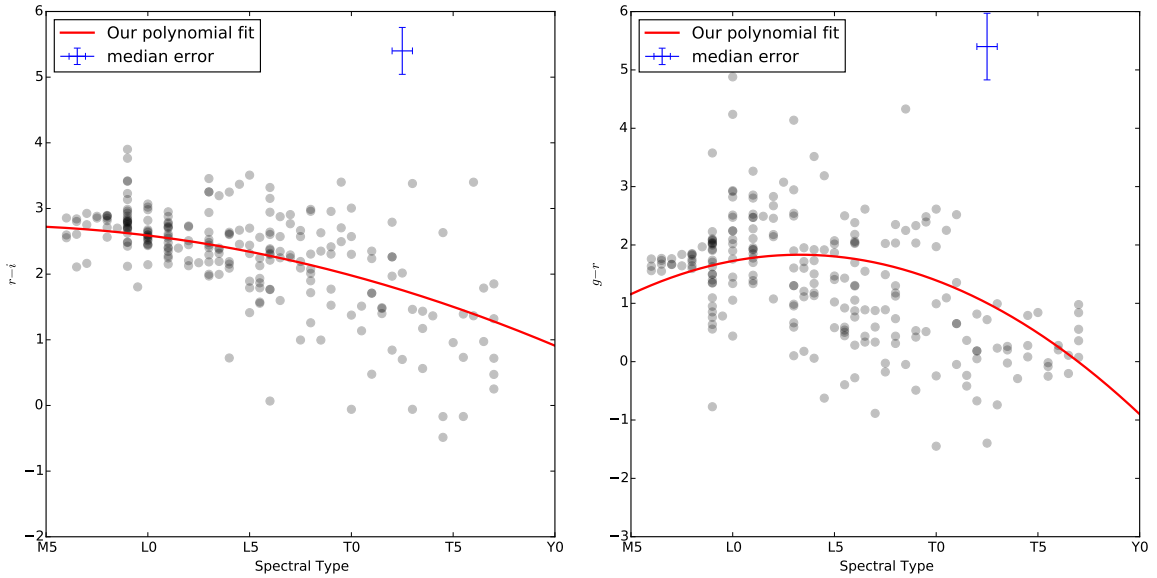


(a) (b)

Figure. 3.18: Polynomial fit results using the probabilistic fitting routine mentioned in Section 3.3.1. Using (a) the fit between spectral type against $(r-i)$ and $i$ from the spectral type and $(i-z)$ polynomial fit I was able to estimate the absolute $r$ magnitude. Using the $r$ band magnitude and (b) the fit between spectral type against $(g-r)$ I was able to estimate the absolute $g$ magnitudes.

## 3.4 Choosing the optimal colours for analysis of the excess sample

To optimise the photometric analysis of my excess sample I used my simulated M dwarf and UCD photometry to synthesize M+UCD photometry (see Equation 3.6). This enabled me to estimate the expected changes in colour due to the presence of unresolved UCD companions, as well as the expected changes in colour due to spectral type variation.

$$M_{\mathrm{M+UCD}} = -2.5log_{10}\left(10^{-0.4M_{\mathrm{M\ dwarf}}} + 10^{-0.4M_{\mathrm{UCD}}}\right) \tag{3.6}$$

where $M_M$ is the M dwarf photometry and $M_{UCD}$ is the UCD photometry.

### 3.4.1 Combining the simulated photometry

Using the simulated M+UCD systems I was able to give an indication of which (M+UCD) colours were sensitive to a specific primary M dwarf and which colours were sensitive to a specific UCD companion. The colour excess (Equation 3.7) was plotted against companion spectral type (see Figure 3.19 to Figure 3.23).

$$\text{Simulated Colour Excess} = Colour_{\mathrm{M+UCD}} - Colour_{\mathrm{M\ dwarf}} \tag{3.7}$$

The level of colour excess was compared to mean uncertainty level of my M dwarf sample and thus sensitivity of a certain colour to the addition of a companion could be gauged. From Figure 3.19 to Figure 3.23 it is also clear early M dwarfs (∼M3.0) are too bright for a companion to be detected in the colours I tested (hence my cut in $(V-J)$ in Section 2.3.2) and also puts a limit on how late in spectral type my companion can be (no later than ∼T0).

From the simulated M+UCD systems I was also able to gauge how sensitive colours were to the primary M dwarf. Plotting the colour of a M+UCD system against primary spectral type gave an indication to which colours are good at differentiating M dwarf spectral types (See Figure 3.24 to Figure 3.28). I used the gradient of these as a quantitative measure of primary sensitivity.

I defined 'companion sensitive' (CS) colours as those which are sensitive to the presence of unresolved companions but are insensitive to variations in primary spectral type. I also defined 'primary sensitive' (PS) colours as those which are sensitive to changes in the primary spectral type, but are insensitive to the presence of unresolved UCD companions.

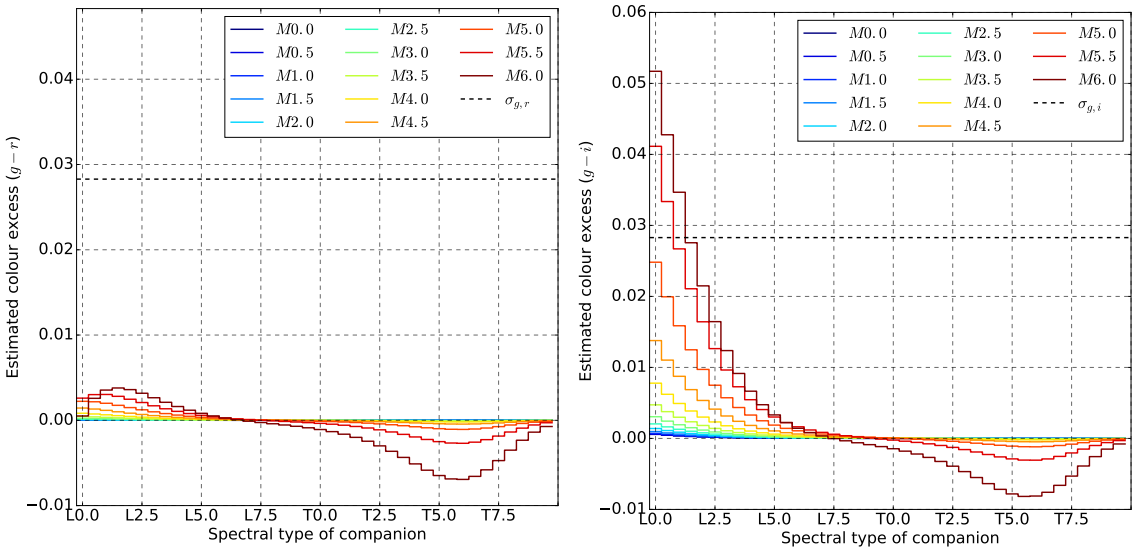


(a) (b)

Figure. 3.19: Expected colour excess for simulated M0 + UCD to M6 + UCD for (a) $(g-r)$ and (b) $(g-i)$: both chosen PS colours. The dashed line shows the average colour uncertainties for these colours in my catalogue.

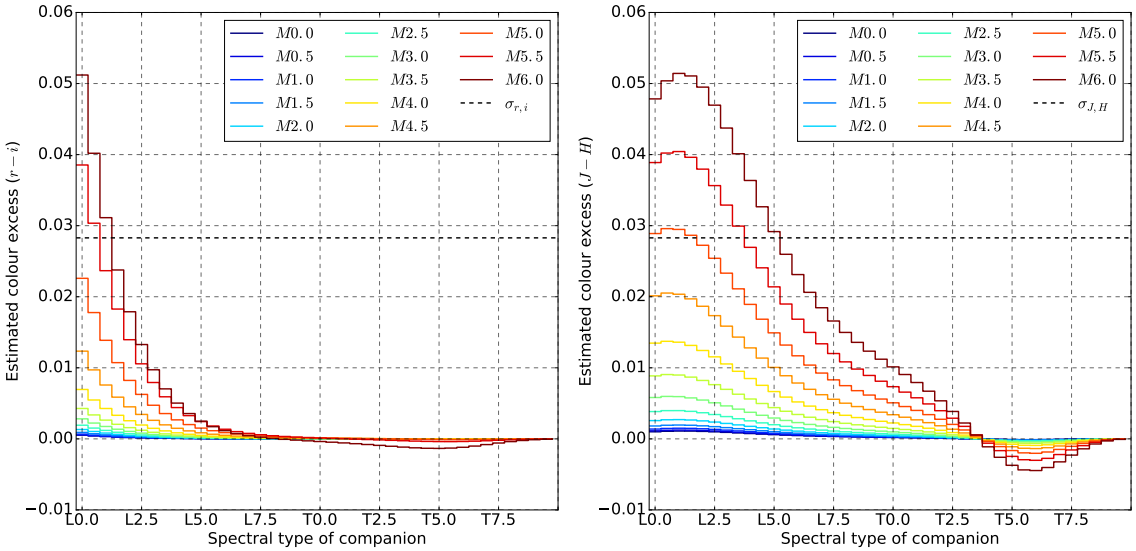


(a) (b)

Figure. 3.20: Expected colour excess for simulated M0 + UCD to M6 + UCD for (a) $(r-i)$: an identified PS colour and (b) $(J-H)$: neither a chosen PS nor CS colour. The dashed line shows the average colour uncertainties for these colours in my catalogue.

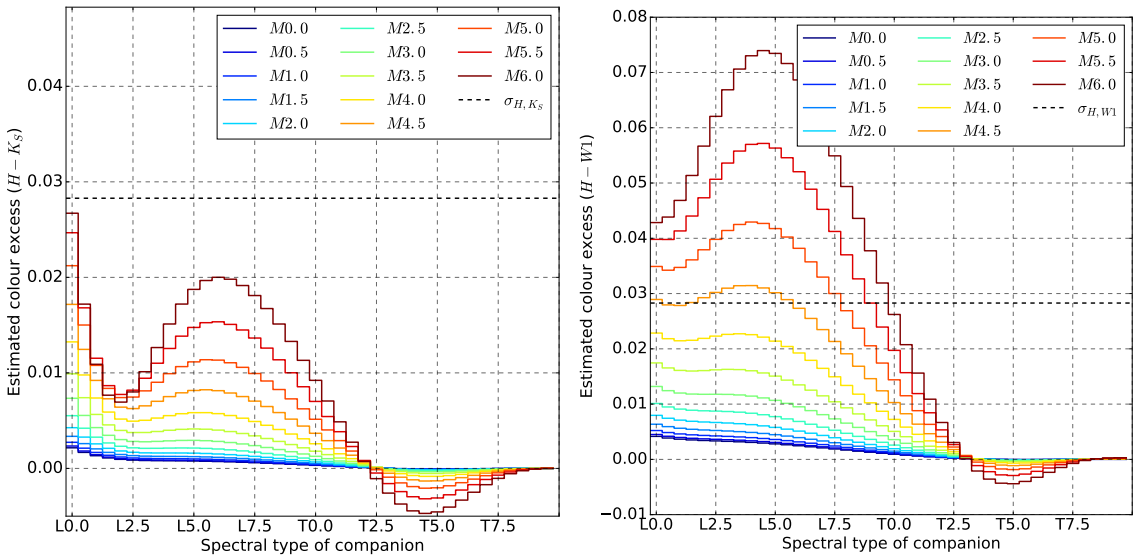


(a) (b)

Figure. 3.21: Expected colour excess for simulated M0 + UCD to M6 + UCD for (a) $(H-K_S)$: neither a chosen PS nor CS colour and (b) $(H-W1)$: a chosen CS colour. The dashed line shows the average colour uncertainties for these colours in my catalogue.

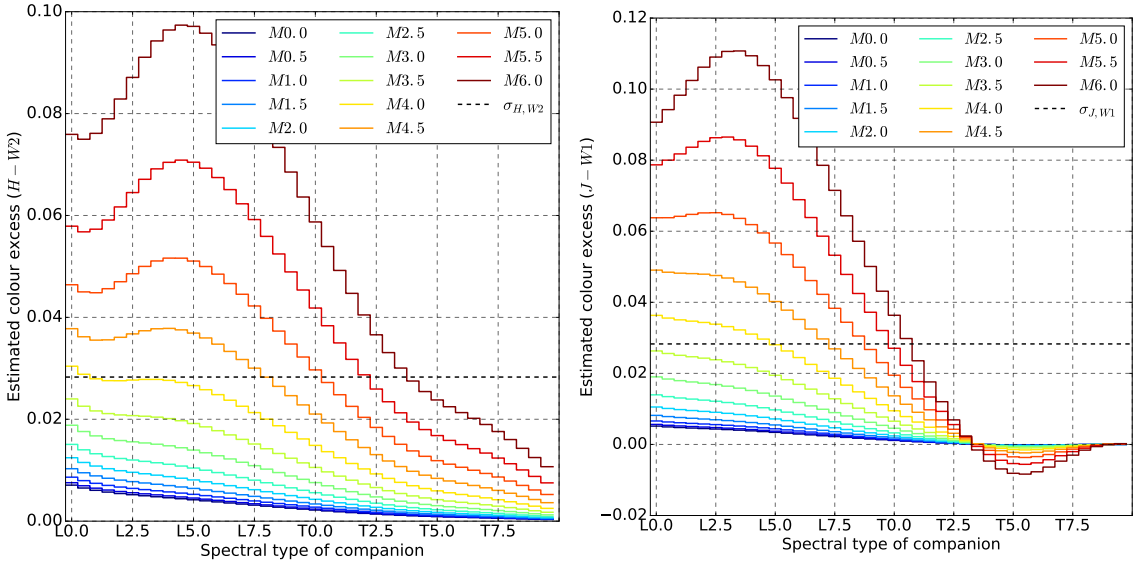


(a) (b)

Figure. 3.22: Expected colour excess for simulated M0 + UCD to M6 + UCD for (a) $(H-W2)$ and (b) $(H-W1)$: both chosen CS colours. The dashed line shows the average colour uncertainties for these colours in my catalogue.

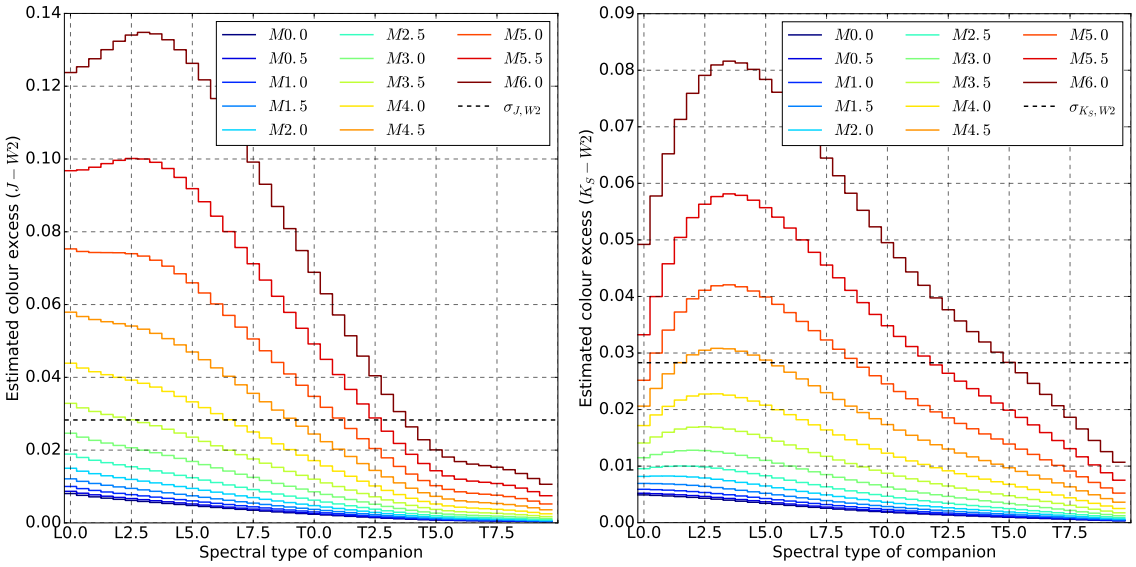


(a) (b)

Figure. 3.23: Expected colour excess for simulated M0 + UCD to M6 + UCD for (a) $(J-W2)$ and (b) $(K_S-W2)$: both chosen CS colours. The dashed line shows the average colour uncertainties for these colours in my catalogue.

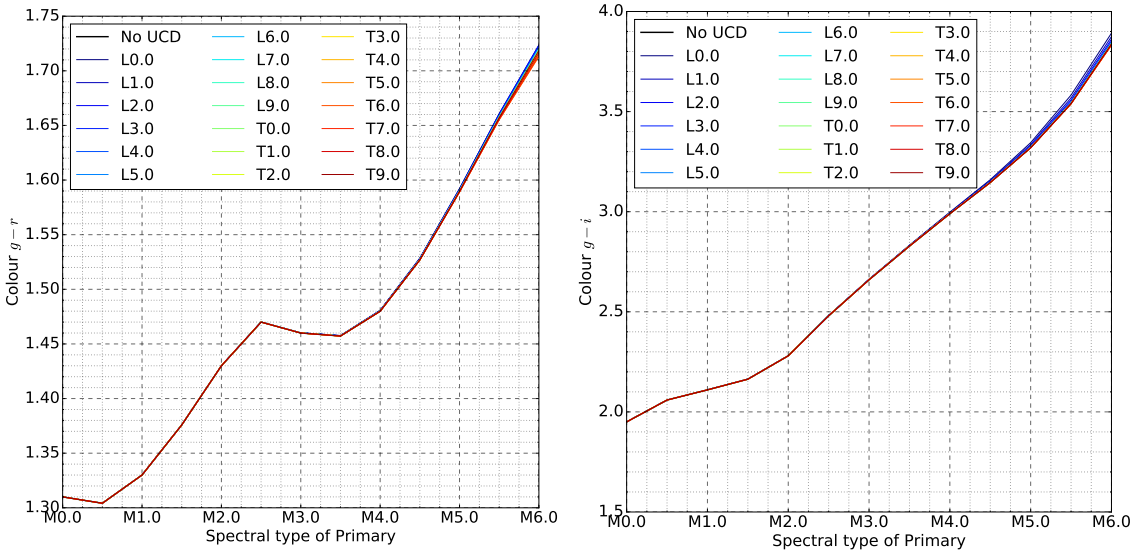


(a) (b)

Figure. 3.24: Expected primary colour variation in (a) $(g-r)$ and (b) $(g-i)$ as a function of primary spectral type for simulated M dwarf+UCD unresolved binary systems. A large change in colour with primary spectral type without a large change across companion spectral type identifies a good colour for identifying M dwarfs.

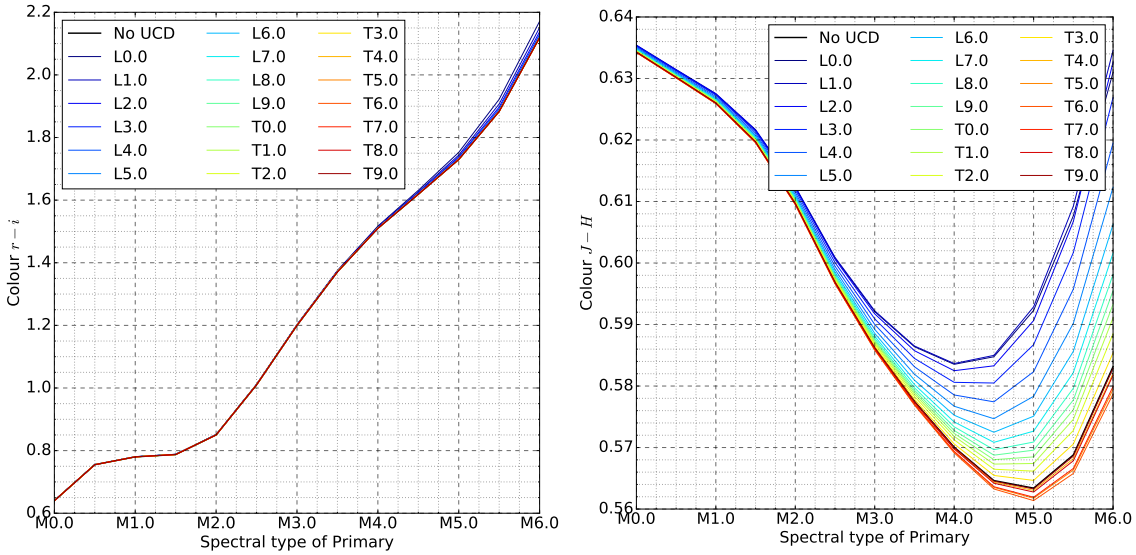


(a) (b)

Figure. 3.25: Expected primary colour variation in (a) $(r-i)$ and (b) $(J-H)$ as a function of primary spectral type for simulated M dwarf+UCD unresolved binary systems. A large change in colour with primary spectral type without a large change across companion spectral type identifies a good colour for identifying M dwarfs.

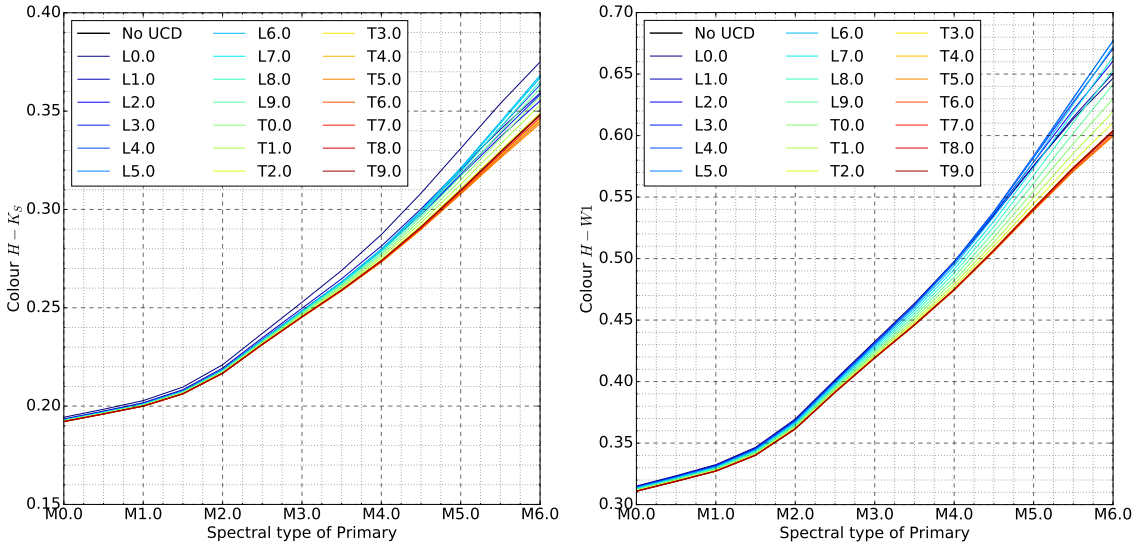


(a) (b)

Figure. 3.26: Expected primary colour variation in (a) $(H-K_S)$ and (b) $(H-W1)$ as a function of primary spectral type for simulated M dwarf+UCD unresolved binary systems. A large change in colour with primary spectral type without a large change across companion spectral type identifies a good colour for identifying M dwarfs.

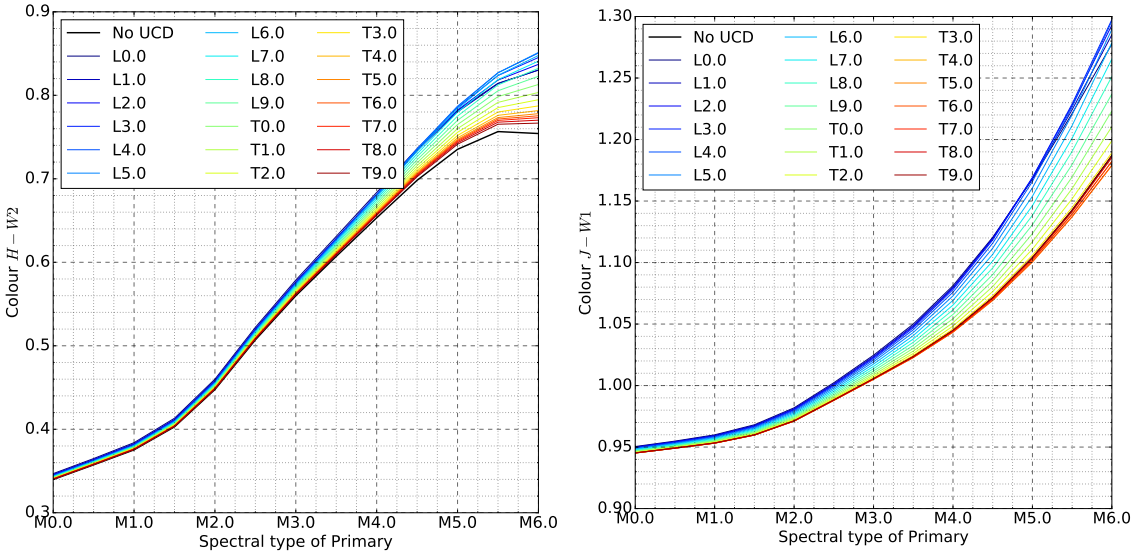


(a) (b)

Figure. 3.27: Expected primary colour variation in (a) $(H-W2)$ and (b) $(J-W1)$ as a function of primary spectral type for simulated M dwarf+UCD unresolved binary systems. A large change in colour with primary spectral type without a large change across companion spectral type identifies a good colour for identifying M dwarfs.

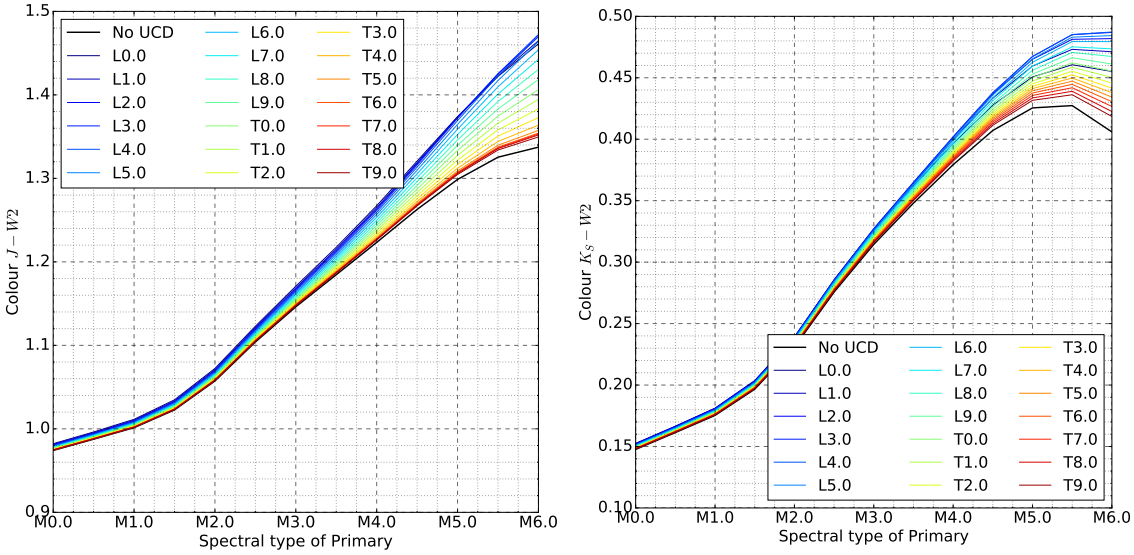


(a) (b)

Figure. 3.28: Expected primary colour variation in (a) $(J-W2)$ and (b) $(K_S-W2)$ as a function of primary spectral type for simulated M dwarf+UCD unresolved binary systems. A large change in colour with primary spectral type without a large change across companion spectral type identifies a good colour for identifying M dwarfs.

### 3.4.2 Selecting the optimal colours

Figure 3.29 shows the colour excess due to a companion (companion sensitivity), against the change in primary colour for Δspectral type= 1.0 (primary sensitivity). The results were averaged for L0-L4 companions and for M3-M6 primaries. Using this plot as a guide I selected the CS colours and PS colours. In addition I also considered sensitivity to metallicity when selecting PS colours (see West et al. 2011 and Newton et al. 2014), even when there was little sensitivity to spectral type.

$$\Delta(g-r) = 0.01 \quad \Delta(g-i) = 0.01 \quad \Delta(r-i) = 0.01 \tag{3.8}$$

My final selection of CS colours ($(J-W2)$, $(J-W1)$, $(H-W2)$, $(H-W1)$, and $(K_S-W2)$) are shown in yellow in Figure 3.29. They all have primary sensitivity below 0.1 mag, and companion sensitivity above 0.03 mag.

My selected PS colours ($(g-r)$, $(g-i)$, and $(r-i)$) are shown in green, and all have secondary sensitivity below 0.01 mag (see Equation 3.8). The $(r-i)$ and $(g-i)$ colours have good sensitivity to spectral type, while $(g-r)$ is sensitive to metallicity (West et al., 2011).

### 3.4.3 Comparison to spectroscopic colours

Using spectra from the SpeX Prism Spectral Libraries[27] I combined M dwarf and UCD NIR spectra (one SpeX spectra for each primary and each secondary) to simulate M dwarf + UCD unresolved binary systems. From the spectra of the M dwarfs and of the M dwarf + UCD unresolved binary systems the contribution due to the addition of a UCD was calculated (see Equation 3.9).

$$Colour(1,2) = M_1 - M_2 = -2.5log_{10}\left(\frac{\int F_\lambda \tau_1(\lambda)d\lambda}{\int F_{0,1}\tau_1(\lambda)d\lambda}\frac{\int F_{0,2}\tau_2(\lambda)d\lambda}{\int F_\lambda \tau_2(\lambda)d\lambda}\right) \tag{3.9}$$

where $F_\lambda$ is the flux from the spectrum, $\tau_1(\lambda)$ is the transmission profile of band 1, and $F_{0,1}$ is the zero-point flux of band 1[28].

Figure 3.30 complements the simulated photometric excesses in Figure 3.29. Note the excesses in Figure 3.29 are the mean colour excess across M3 to M6 and L0 to L4, and thus appear diluted when compared to the peak excess (around L2). The

[27] SpeX Prism Spectral Libraries, maintained by Adam Burgasser at http://pono.ucsd.edu/~adam/browndwarfs/spexprism.

[28] 2MASS bands from http://www.ipac.caltech.edu/2mass/releases/allsky/doc/sec6_4a.html and WISE bands from http://wise2.ipac.caltech.edu/docs/release/allsky/expsup/sec4_4h.html

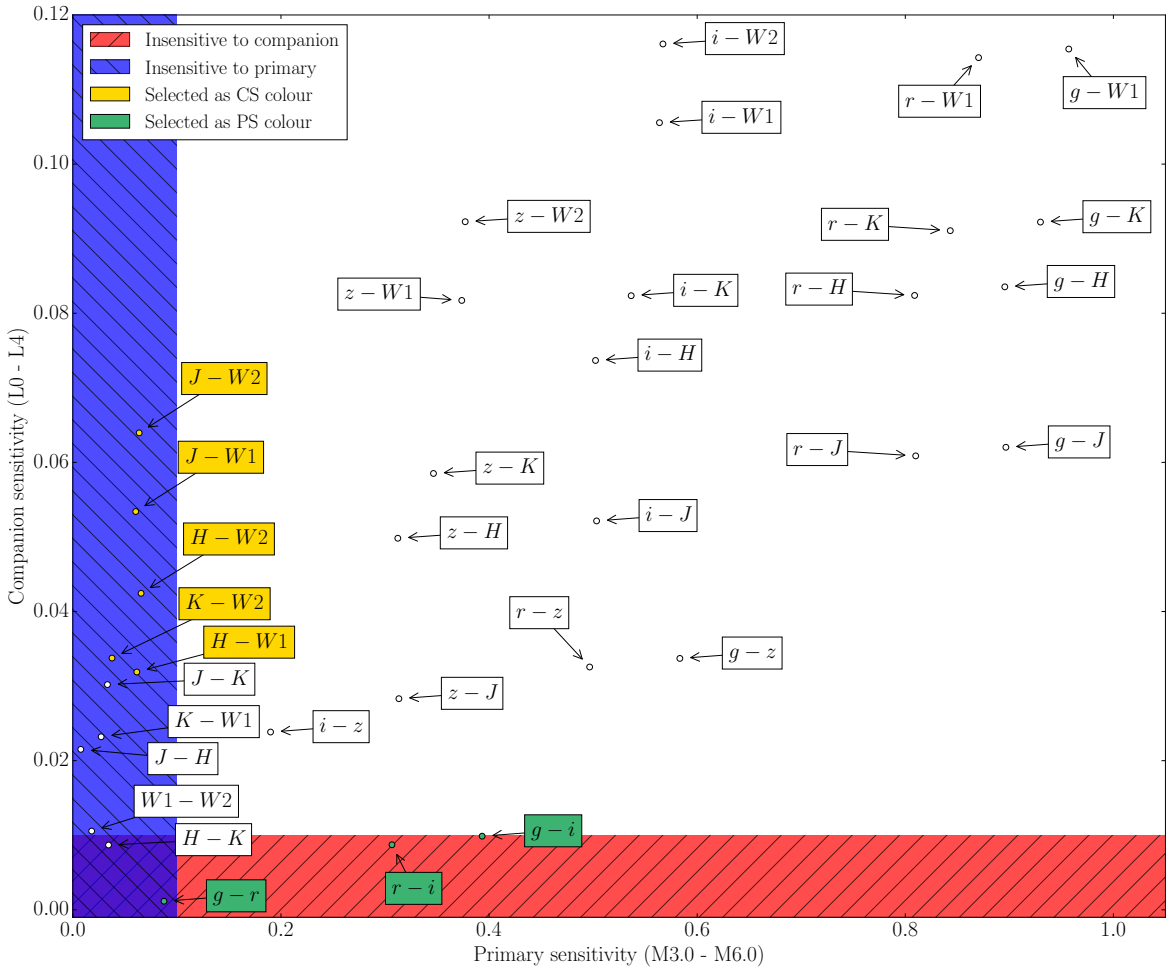


Figure. 3.29: Colour excess due to a companion (companion sensitivity) against the change in primary colour (primary sensitivity). The results from Section 3.3 have been averaged for L0-L4 companions, and for M3-M6 primaries. These are expected to be the most common systems my analysis will identify. Regions which are insensitive to companions and to spectral type variations are shaded blue and red respectively. my chosen CS and PS colours, see text, are indicated in yellow and green respectively) .

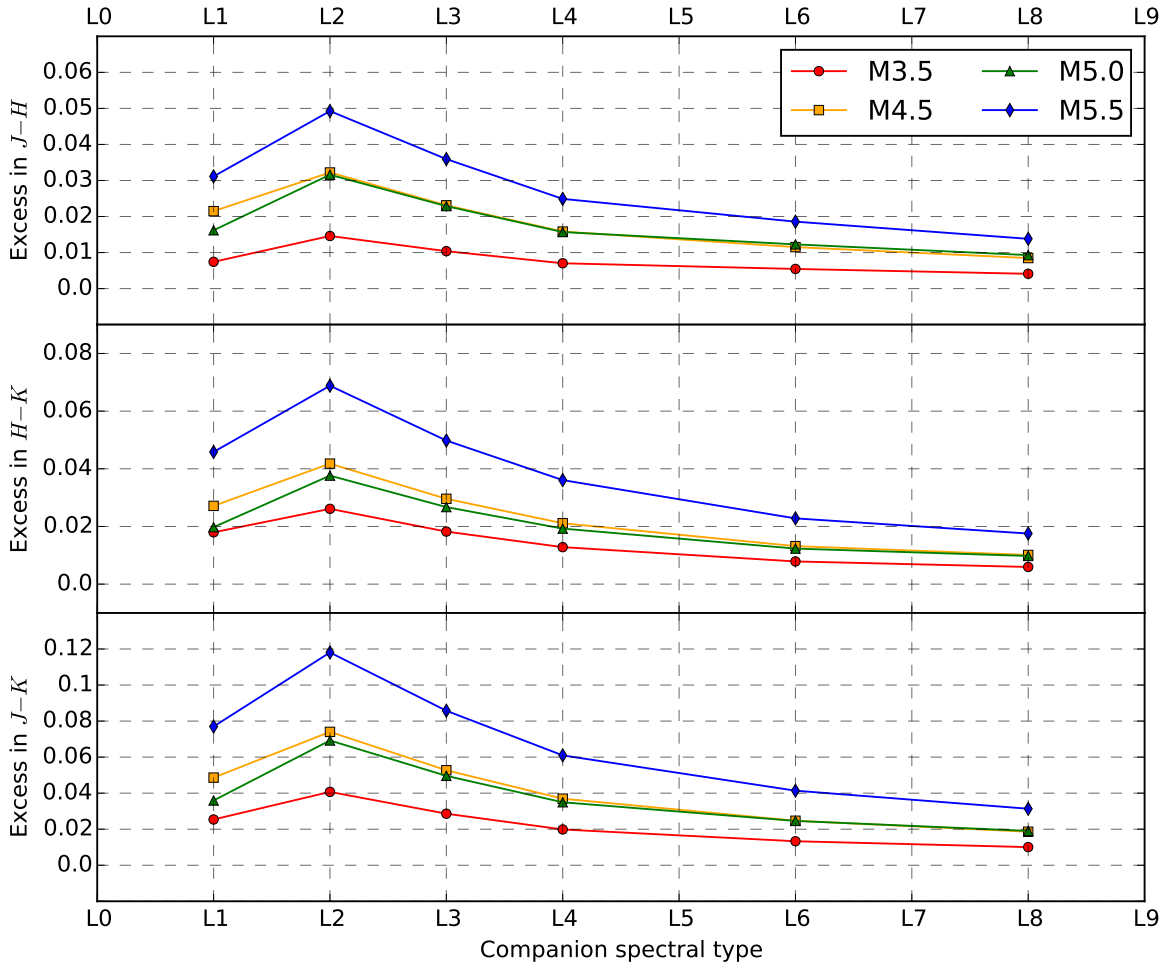


Figure. 3.30: Using spectra from SpeX[27] I combined M dwarf and UCD NIR spectra to simulate M dwarf+UCD unresolved binary systems. I calculated the $(J-H)$, $(H-K_S)$ and $(J-K_S)$ colours for each and compared them to the colours of the isolated M dwarfs. The excess seen is complimentary to the photometric simulations (Figure 3.29 where I average over M3 to M6 and L0 to L4).

peak excess around L2 is also seen in Figure 3.19 to Figure 3.23 thus validating my photometric simulations spectroscopically.

There is good agreement between the photometric and spectroscopic values of $(J-H)$ excess (an average excess of ∼0.02 in both the photometric and spectroscopic case) and small differences in $(J-K_S)$ (an average excess of ∼0.03 in the photometric simulation and ∼0.05 in the spectroscopic case) and $(H-K_S)$ (an average excess of ∼0.01 in the photometric simulation and ∼0.03 in the spectroscopic case). The small differences in values of the excess are based on the fact that Figure 3.19 to Figure 3.23 are average SEDs based on photometric simulations and the spectroscopic simulations are based on individual M dwarf and UCD spectra and thus there is some intrinsic scatter due to differing properties of M dwarfs and UCDs that may mean the spectra used are not completely representative of the whole population. Our photometric and colour uncertainties are of order 0.01 magnitudes, our photometric simulation uncertainties are at least of order 0.01 so these values are consistent when uncertainties are taken into account.

## 3.5 The colour excess distribution

### 3.5.1 Identifying excess using multi-colour parameter space

In order to estimate the NIR-MIR excess of the candidate M dwarfs in my excess sample I defined a three-dimensional colour parameter-space using the chosen PS colours $(g-r)$, $(r-i)$ and $(g-i)$. For each candidate M dwarf (target M dwarf) in my excess sample I then defined a tiny sub-volume within this PS colour-space[29], centred on the target M dwarf colours and with a size of ±0.01 in each colour (see Figure 3.31, Figure 3.32 and Figure 3.33)[29]. I then established 'no companion' comparison colours[29] for each candidate by selecting all excess sample members within a target M dwarf's PS colour sub-volume, and measured the mean CS colours in this volume. This approach assumes the vast majority of the excess sample are M dwarfs without UCD companions, and thus the 'no companion' comparison colours should provide a good zero excess reference from which the MIR excess of target M dwarfs can be estimated.

I required at least 20 comparison objects[29] in a target M dwarf's PS colour sub-volume (this was the case for 22,579 members of the excess sample), and measured the MIR excess using the most sensitive of my CS colours $(J-W2)$. The resulting excess distribution is shown in Figure 3.35 and Figure 3.36, against $(V-J)$, a proxy for spectral type.

[29]Colour sub-volume size, PS colours, CS colours, and the minimum number of comparison objects per sub-volume were extensively tested using a wide range of numerical values for each, the full process was repeated to maximise the number of candidates in a box while keeping the sub-volumes sufficiently small as to still be defined as similar in colour.

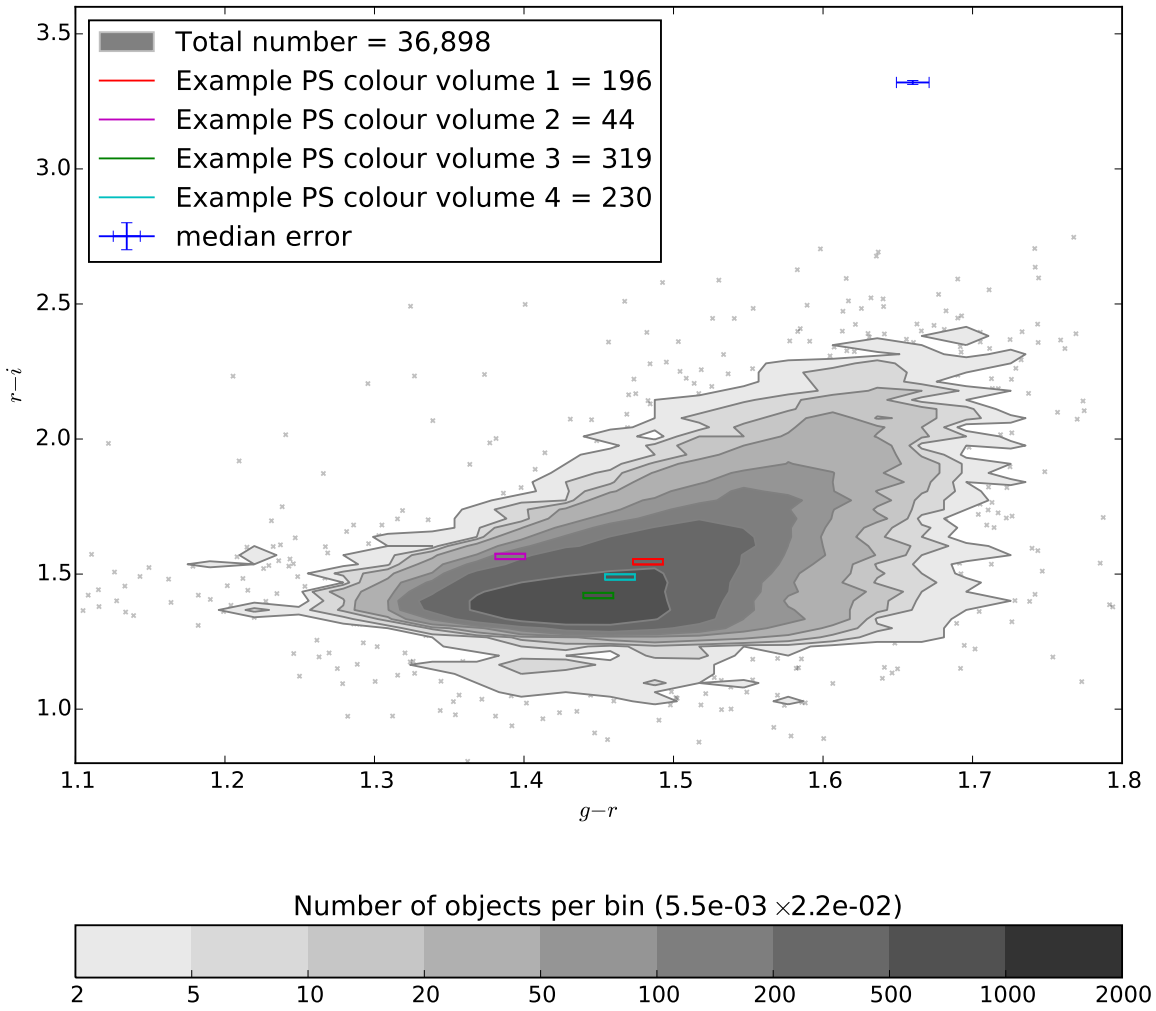


Figure. 3.31: Colour-colour contour diagrams for $(g-r)$ against $(r-i)$ for the populations of M dwarfs used in the multi-colour-space analysis. Boxes represent example targets and their respective PS colour volumes. These volumes are used to define similar M dwarfs, the colour volume means and standard deviations are used to calculate colour excess compared to those in each target colour volume. This process was undertaken for each M dwarf, except those which had less than 20 M dwarfs in their colour volume.

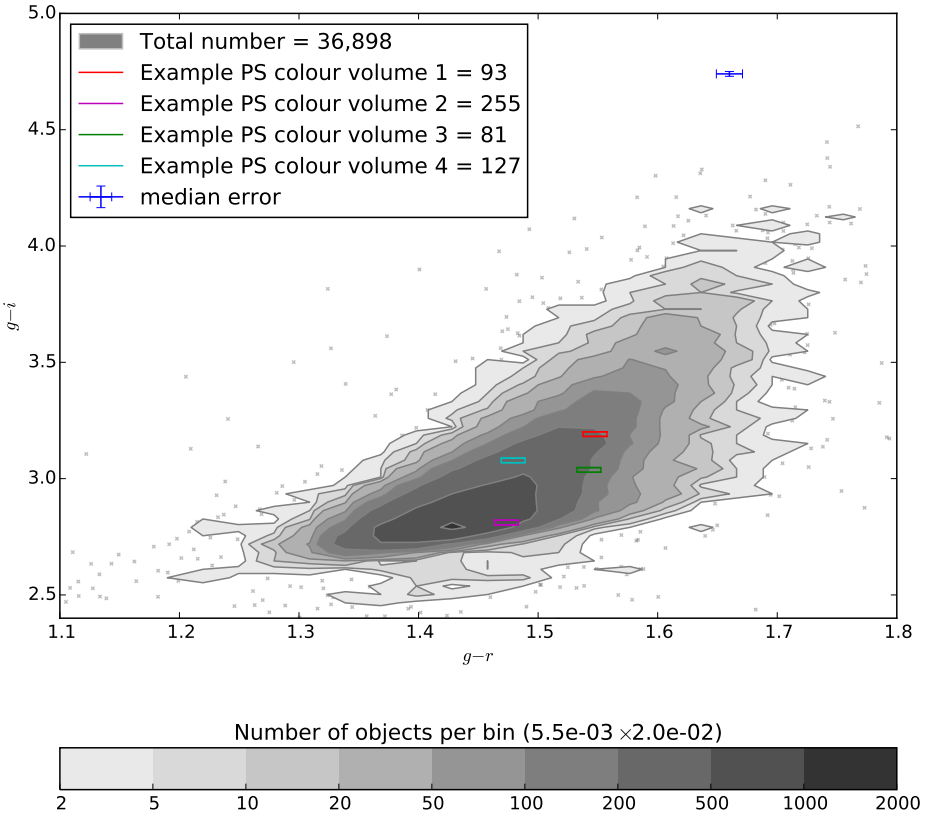


Figure. 3.32: Same as Figure 3.31 for $(g-r)$ against $(g-i)$.

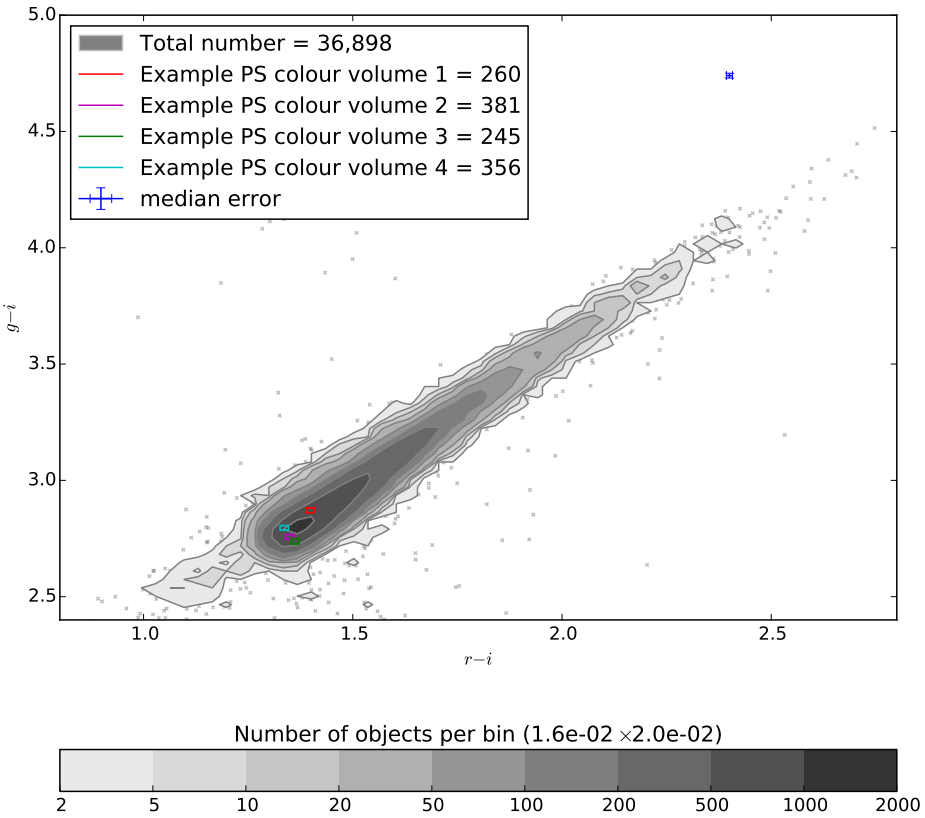


Figure. 3.33: Same as Figure 3.31 for $(r-i)$ against $(g-i)$.

Figure 3.36 also shows the selection contours which will be discussed in Section 3.5.3, the excess distribution of the sample lies generally in the range -0.15 to +0.15, and the excess values of M dwarfs with L dwarf companions lie at the upper end of this range (see Section 3.5.3 and the L dwarf excess vectors shown in Figure 3.36 as a guide).

### 3.5.2 Is there an excess population?

Figure 3.34a shows the histogram of my excess measurements. Overall it is similar to a Gaussian distribution, but it has some asymmetries. Firstly it is apparent the peak of this histogram is found at a slightly negative excess value which seems unexpected. However, I believe this bias is introduced by my analysis method, and results from the finite size and distribution of the PS colour sub-volumes. The number density of objects varies across the sub-volumes in my multi-colour parameter-space, leading to average values which can be slightly different to the central value. I suggest, on average, this effect leads to the small negative offset which is seen. For my symmetry analysis I offset the histogram by $\sim$+0.003 magnitudes to remove this offset.

To assess the symmetry of the histogram I reflected the negative side of the distribution in the Y-axis and subtracted this from the positive distribution (see Figure 3.34a). Although the histogram is fairly symmetrical, it contains an important feature. The positive wing has relatively lower frequencies (compared to the negative wing) for excesses of 0-0.05, and has relatively higher frequencies for excesses of 0.05-0.15 (an excess bump). To assess the nature of this excess bump I carried out a comparison analysis using the $(H - K_S)$ colour as my CS colour (instead of $(J - W2)$ see Figure 3.34b).

This comparison analysis should not be sensitive to companion excesses, or indeed to spectral type variations (see Figure 3.29), but should produce a distribution I expect in the absence of any significant excess (albeit with some scatter due to a metallicity spread). The $(H - K_S)$ excess distribution is much more symmetrical than the $(J - W2)$ distribution. The mirror-subtracted trace for the $(H - K_S)$ excesses is close to zero with a few short-range deviations. This contrasts with the bump feature seen when excess values are calculated using $(J - W2)$ , and thus supports the idea the bump is caused by a population of M dwarfs with MIR excess, rather than by some unidentified bias in my analysis method.

The mid-IR excess bump represents $\sim$2 per cent of my excess sample, and I thus expect unresolved M+UCD systems to only form a fraction of this population (see further treatment in Section 3.5.3).

During the viva process it was noted that a median instead of a mean of the M dwarfs in each targets sub volume (to calculate the excess in each colour) would be more appropriate for selecting the "representative" colour of each sub volume. Post

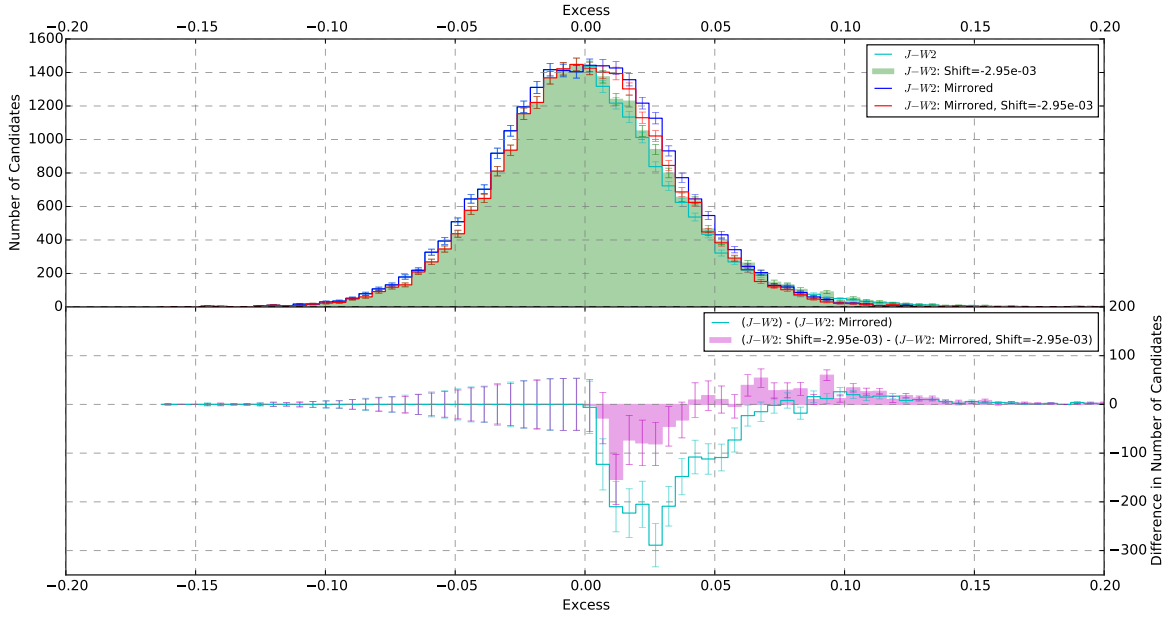


(a)

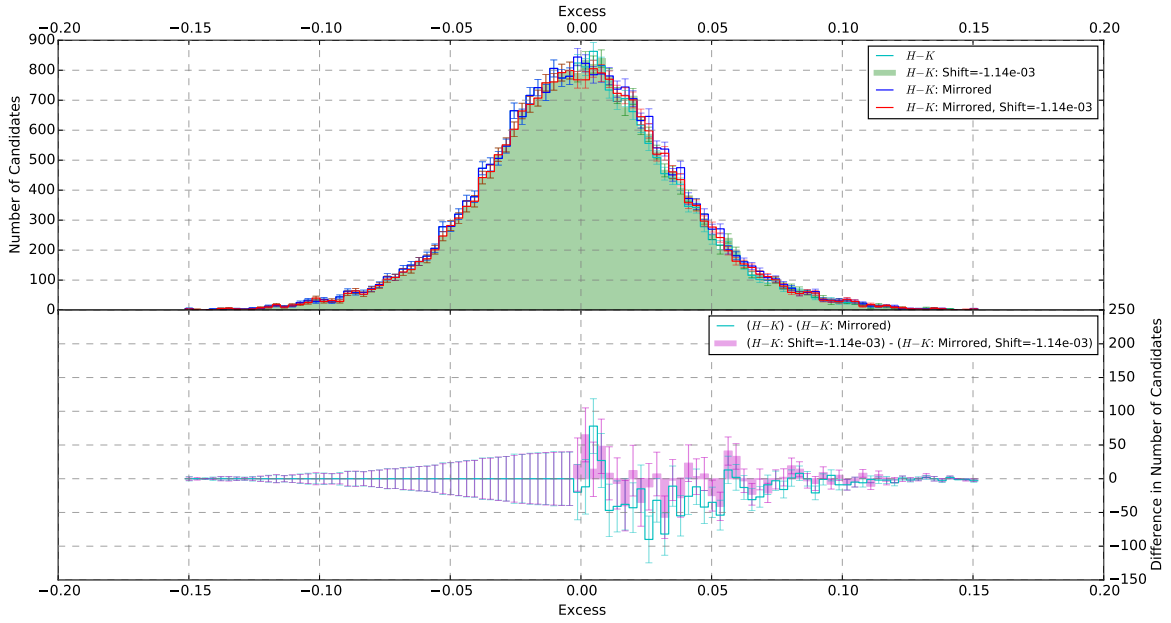


(b)

Figure. 3.34: The histogram of my excess distribution, compared to a mirrored deficit (negative) distribution. (a) Assuming the deficit section of the excess $(J-W2)$ distribution is from Gaussian, random or likewise symmetric contamination process (and not from a UCD companion), I show the histogram of my excess distribution, compared to a mirrored deficit (negative) distribution around zero (non-shifted, magenta) and around an overall deficit value of -0.0030 (shifted, red). (b) The excess $(H-K_S)$ distribution (an independent colour which also shows a low sensitivity to companions and spectral type, see Figure 3.29, shown in cyan and blue for non-shifted and shifted respectively). The residuals of $(J-W2)$ and $(H-K_S)$ are also shown in red (lower panels of (a) and (b) respectively). The positive bump at a $(J-W2)$ excess of >0.05 magnitudes is evidence of processes contributing to making the targets redder than their mean PS colour volume colour, including M dwarfs with unresolved UCD companions and is not seen in my companion insensitive $(H-K_S)$ residuals.

viva this was confirmed, in addition to this the distribution of excess calculated using the median instead of the mean removed the need for the shift in mirroring process (this shift, as explained above was due to the distribution not being Gaussian, and thus a median is preferable over using a mean). The overall number of objects selected and sample produced is not affected due to this shift (and thus difference between mean and median values) being very small.

### 3.5.3 Excess selection contours

In order to identify M dwarfs likely to have MIR excess consistent with unresolved UCD companions, I used my simulated M dwarf and UCD photometry (from Section 3.3). As a starting point I took the photometry of my excess sample to represent a population without any unresolved UCD companions. This assumes UCD companions are reasonably rare, which is consistent with previous constraints (see Section 1) and my interpretation of the excess bump feature. I then simulated unresolved UCD companions around a randomly selected fraction ($\beta$) of my sample by modifying the M dwarf colours to account for L2 companions (since I expect the most significant UCD reddening from companions in the range ∼L0-L3; see Section 3.3). I used these simulated M dwarfs to map out a so-called 'improvement' parameter-space. I define improvement to be the factor by which the probability increases of detecting a M+UCD system (normalising this by the input binary fraction makes an improvement of one equal to the probability of randomly selecting an M+UCD from a sample of M dwarfs).

$$Improvement = \frac{N_{SB}}{N_T}\frac{1}{\beta} \tag{3.10}$$

where $N_{SB}$ is the total number of simulated M+UCD unresolved binary systems present in a small box, $N_T$ is the total number of M dwarfs present in a small box ($N_T = N_D - N_{SS} + N_{SB}$), and $\beta$ is the simulated binary fraction. Here $N_D$ is the number of original M dwarfs in the small box and $N_{SS}$ is the number of simulated M+UCD unresolved binary systems present in the small box before the UCDs were added. The small box is centred on each bin in a grid covering the distribution (see Figure 3.35) and thus a grid of improvements covering the entire parameter-space was calculated.

I calculated improvement values across the excess $(V - J)$ parameter-space of my excess sample using a box-smoothed approach and running my simulation 1,000 times to smooth out the random noise. Figure 3.35 shows the 'improvement' levels (colour-scaled) across the excess $(V - J)$ parameter-space. The box size I used for smoothing is indicated in the upper left of the diagram.

A set of improvement contours were defined to aid selection of potential M+UCD binaries. These are shown in Figure 3.36, where the contours range from 3.0-8.0. I

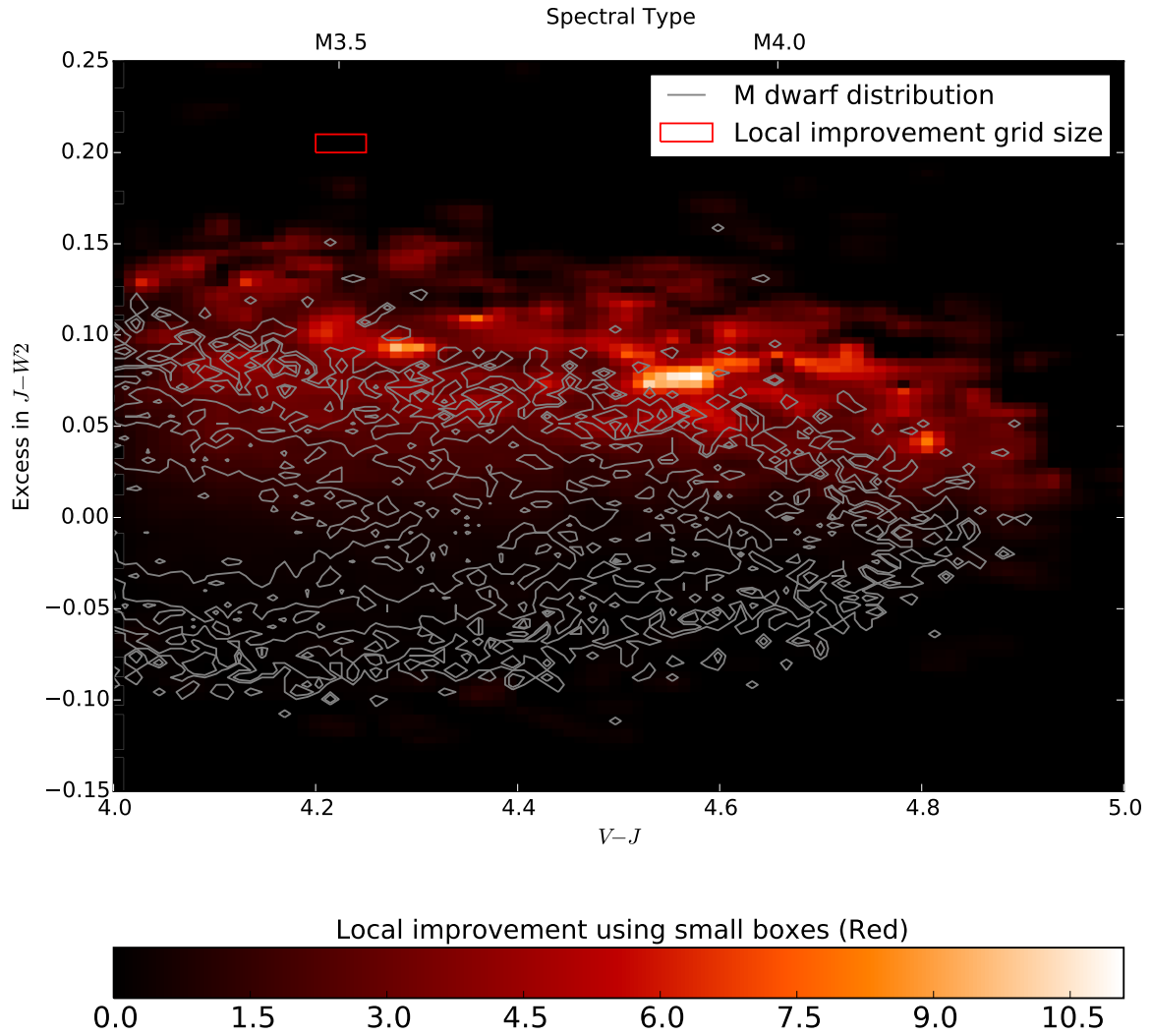


Figure. 3.35: Excess distribution of my sample of M dwarfs after the colour-space analysis (for the CS colour $(J - W2)$ ). The colour distribution represents the local improvement grid created simulating M dwarf+UCD unresolved binary systems through the multi-colour-space analysis. The red box shows the size of the improvement grid used.

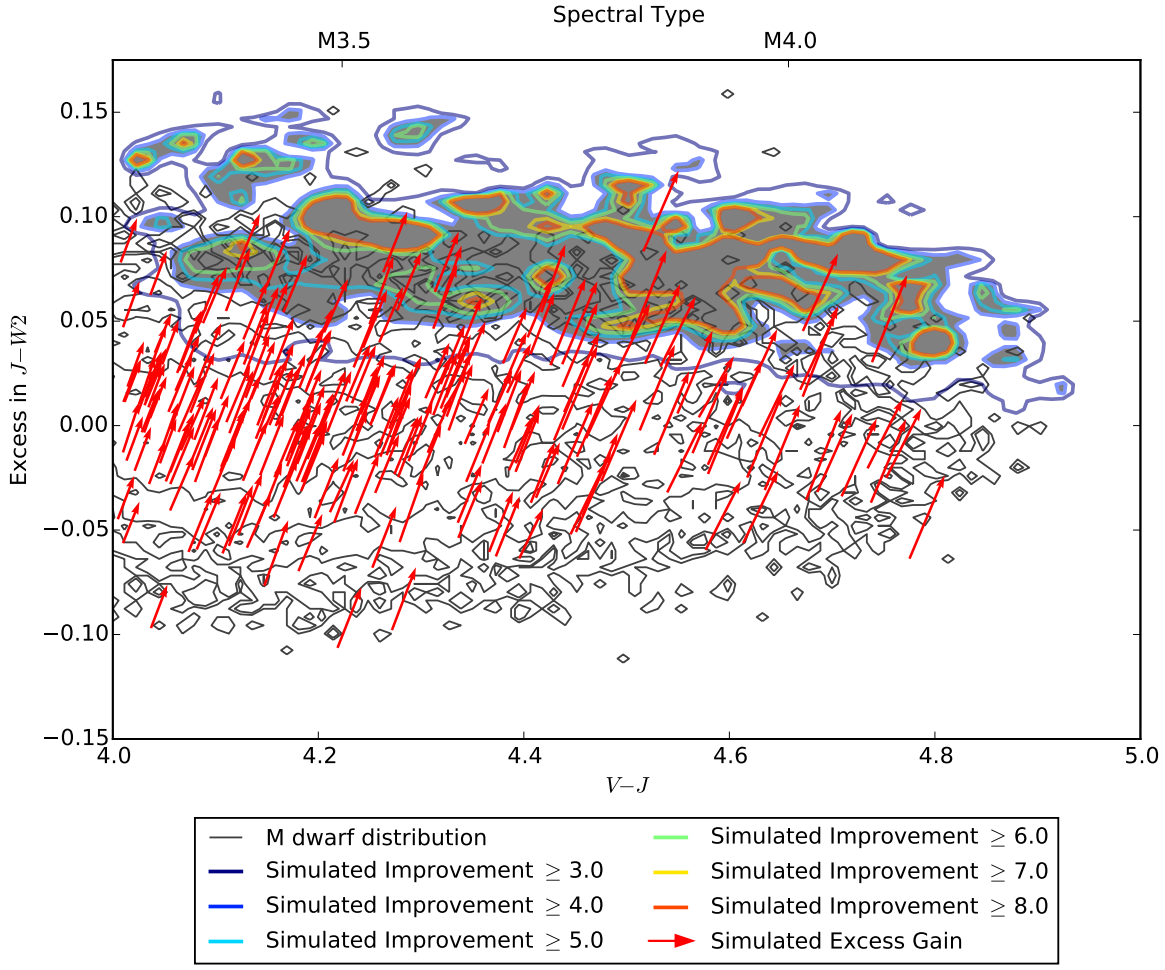


Figure. 3.36: The local improvement grid was used to define contours of improvement (coloured contours). For comparison the excess gained (in $(J-W2)$ ) by a sample of M dwarfs is shown. For comparison the effect of adding unresolved UCD companions to M dwarfs is indicated with red arrows. The shaded region is the final selected contour equivalent to an improvement of $\geq$4 over randomly selecting an M dwarf from my full catalogue of M dwarf candidates

| Colour | $Imp \geq 3$ | $Imp \geq 4$ | $Imp \geq 5$ | $Imp \geq 6$ | $Imp \geq 7$ | $Imp \geq 8$ |
|---|---|---|---|---|---|---|
| $(J-W1)$ | 1,800 | 654 | 330 | 169 | 110 | 83 |
| $(J-W2)$ | 2,934 | 1,082 | 511 | 269 | 128 | 82 |
| $(H-W1)$ | 705 | 176 | 85 | 34 | 26 | 15 |
| $(H-W2)$ | 1,095 | 301 | 118 | 57 | 23 | 17 |
| $(K_S-W2)$ | 616 | 221 | 98 | 34 | 14 | 8 |

Table 3.6: Using a locally defined improvement, $Imp$, based on my simulated M dwarf+UCD unresolved binary systems, contours of improvement were defined (i.e. $Imp \geq 3$) and the numbers of M dwarfs in excess/$(V-J)$ space which fell inside a contour were recorded. The simulated binary fraction, ($\beta$) in this case was $\beta = 0.01$ (1 per cent).

required improvement ≥4 for my final selection, and this region is shaded in grey. I used these contours to select my M+UCD candidates and the numbers of M dwarfs selected can be seen in Table 3.6, for a simulated binary fraction of 0.01 (1 per cent). For $(J-W2)$ and $\beta$=0.01 this led to 1,082 objects which constitutes my 'M+UCD candidates sample'.

### 3.5.4 Measuring improvement in detection

By varying the fraction of simulated binaries added ($\beta$, Section 3.5.3) I was able to estimate the expected yield of M+UCD candidates at certain improvement levels. The binary fraction for mid-type M dwarfs with a UCD companion is rather uncertain, so I present a range of estimates for $\beta$=0.2-8 per cent. I ran the same selection method as above to create additional candidate M+UCD samples for the various levels of simulated unresolved binary injection. I counted the number of candidates found for each binary fraction and show this in Figure 3.37. The higher the binary fraction the lower my yield, this is expected because more of my reference PS colour M dwarfs have companions thus diluting the colour excess detectable. For a binary fraction of 0.01 I expect over 1,000 M+UCD candidates for $(J-W2)$.

### 3.5.5 Predicting candidate companion subtype

To estimate the subtypes of the expected companions I ran the same selection method again as above to create additional candidate M+UCD samples, except this time varying the spectral type of the companion I added (L0-T4 companions in steps of two subtypes). Figure 3.38 shows the result for the number of candidate M+UCD systems with a binary fraction of 0.01. For comparison I show the predictions when a range of other CS colours are used instead, but including, $(J-W2)$. $(J-W2)$ yields the most candidate M+L dwarf systems because it is the most sensitive to M+L unresolved binaries. If the companion distribution is flat, similar to the field population

(See Figures 11 and 12 from Cruz et al., 2003) I can use Figure 3.38 to predict roughly my expectation of companion subtypes. I expect up to 60 per cent of my M+UCD candidates to have companions of spectral subtype earlier than L3 and ∼35 per cent to be later L dwarfs. The remaining ∼5 per cent may be late L dwarfs or early T dwarfs.

### 3.5.6 Summary of selecting M dwarfs with MIR excess

I took my full M dwarf candidate catalogue of 440,694 sources and applied more stringent photometric constraints in order to produce a sample to search for M dwarfs with MIR excess. After experimenting with different reddening cuts I chose to remove all sources with $A_V > 0.08$ equivalent to a $E(J-W1)$ of 0.02 (leaving 138,572 sources) and removed sources flagged as having bad photometry (e.g. saturated sources, poor observation and/or variation, leaving 36,898 M dwarfs, that constitute my excess sample).

I then simulated photometry (of both M dwarfs and UCDs) in order to select colours that would be sensitive to a UCD companion (PS colours, used to search for excess) and to select colours that would be insensitive to a UCD companion (CS colours, used to define similar M dwarfs). I selected the colours $(g-r)$, $(g-i)$ and $(r-i)$ as my CS colours, and $(J-W1)$, $(J-W2)$, $(H-W1)$, $(H-W2)$ as well as $(K_S-W2)$ as my PS colours using my photometry simulation (that was subsequently compared to a spectroscopic simulation using SpeX spectra).

The next stage was to search for excess in the PS colours using the CS colours to define sub volumes of similar M dwarfs. This was done and the distribution of excesses (shown for $(J-W2)$) were found and verified using a mirrored deficit approach. M dwarfs were selected as candidates by using a improvement statistic such that M dwarfs in areas where it was deemed to be more than four times as likely as randomly selecting M dwarfs with UCD companions were selected. For $(J-W2)$ I selected 1,082 such M dwarfs which constitute my M+UCD candidate systems. Once I had my sample I analysed how the fraction of simulated binaries added affected how many candidates I produced, and predicted yields on number of each UCD subtype based on varying the UCD subtype used simulations.

Figure 3.39 shows a summary of the excess sample selection process.

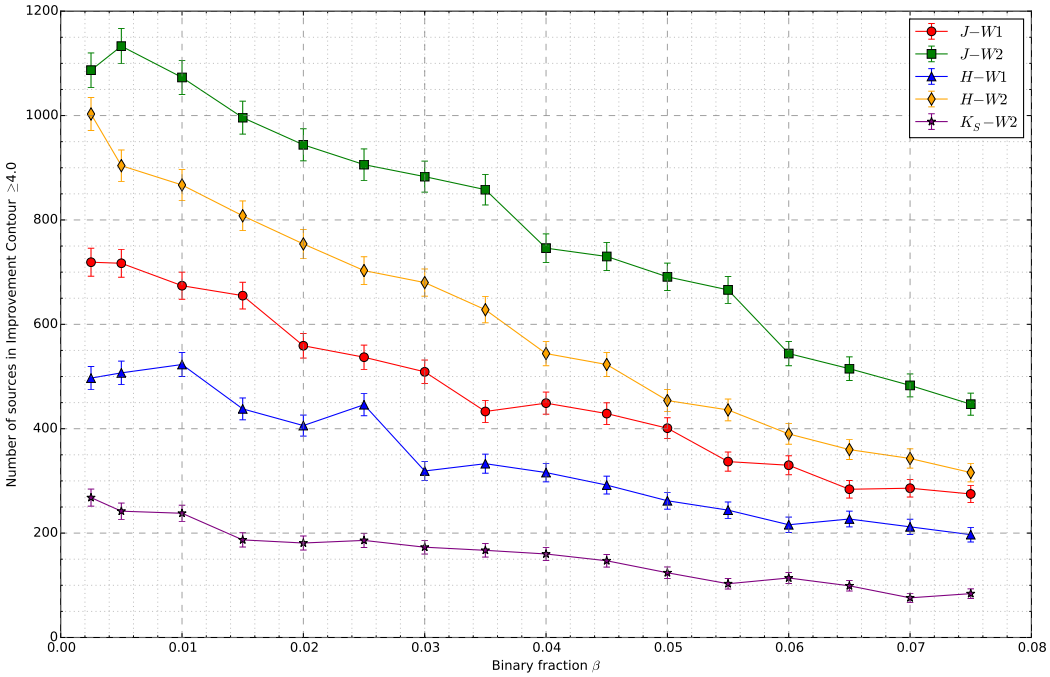


Figure. 3.37: After varying the initial binary fraction of my simulated companion systems, the final detected fraction was calculated and thus the yield of M+UCD candidates was calculated and the improvement over randomly selecting M dwarf was defined for each CS colour. Plot shows M+UCD candidates for an improvement $\geq 4$. $(J-W2)$ yields the most M+UCD candidate systems.

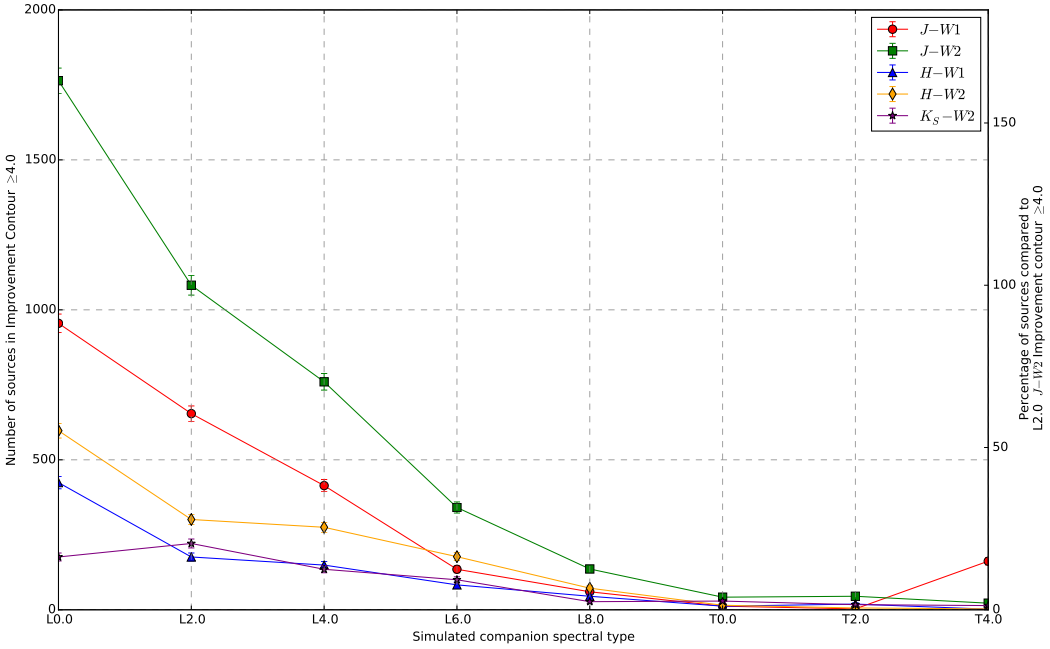


Figure. 3.38: After varying the simulated companion subtype between L0 and T4 I was able to gain insight into the possible companion spectral type distribution. As with Figure 3.37, $(J-W2)$ yields the most M+UCD candidate systems.

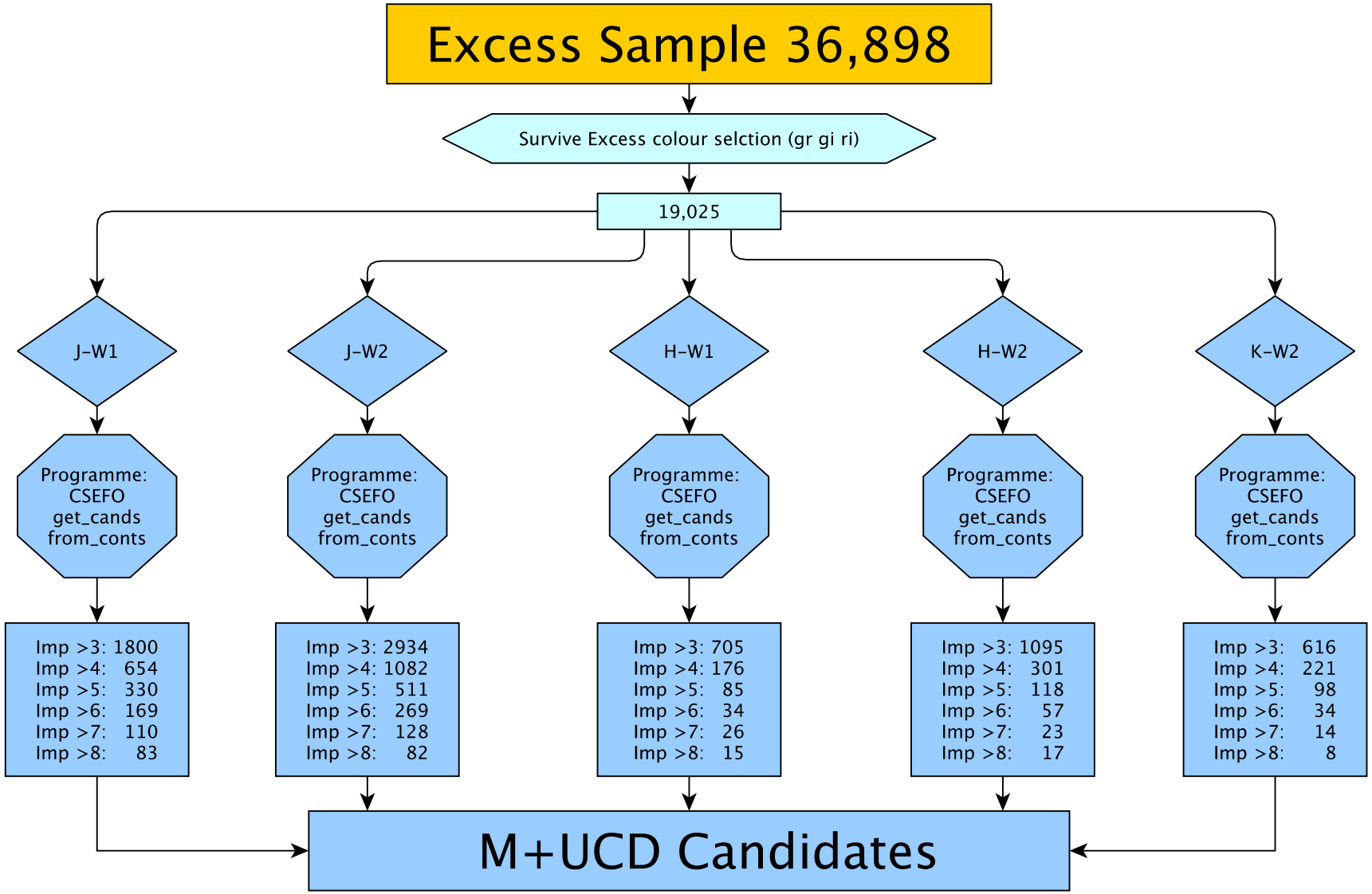


Figure. 3.39: Flow chart to summarise the process involved in selecting my final M+UCD candidates.

# Chapter 4: Follow-up of Unresolved Ultra-cool Companions to M dwarfs

## 4.1 Introduction

In Chapter 3 I showed how I selected my excess sample of 36,898 M dwarfs from my full M dwarf candidate catalogue of 440,496 M dwarfs, and how I then selected 1,082 M+UCD candidates from amongst the excess sample. Up to now all this work has been achieved using past observations. However, the best way to confirm these candidates is to follow them up with new observations. This, like finding these objects in the first place, is difficult due to the UCD's faintness and proximity to the host M dwarfs. These objects should be easily detectable by the largest telescopes, however with over 1,000 M+UCD candidates this would require a large amount of resources, for a rather uncertain number of real M+UCD candidates. Therefore it is important to find a method of follow-up which requires as little resources as possible. It is also important to try to reduce and understand the contaminants amongst the M+UCD candidates as much as possible before any observations are done. In this chapter I discuss the various types of contamination I expect in my sample (Section 4.2) and try to reduce the contamination in Section 4.3. I spend the rest of this chapter describing a method I developed to confirm my M+UCD candidates and to give some indication of the likely spectral types I will be able to confirm through my follow-up, while trying to optimise and minimise the observations required for confirmation.

## 4.2 Contamination in the excess sample and candidate M+UCDs

I select M dwarfs as M+UCD candidates based on their red colour. However a UCD companion is not the only process which can make an M dwarf redder. The M+UCD candidates may include a variety of contaminating objects such as unseen blended background or foreground objects (within the largest spatial resolution element of my photometric data; the ∼six arcsec full-width-at-half-maximum, FWHM, of the WISE $W2$ point-spread function, PSF), M+M binaries (where the cooler companion causes an excess), M dwarfs in regions of local reddening (not picked up by my reddening assessments), and M dwarfs with some low level of disc emission. These objects will be mixed with M dwarfs whose colours have scattered to the red due to photometric

uncertainty. In this section I discuss the types and level of contamination I expect amongst the M+UCD candidates.

### 4.2.1 Spectral types from SIMBAD

Out of the 36,898 sources in the excess sample there were 3,928 sources with entries in SIMBAD matches and 66 of the 1,082 M+UCD candidates with entries in SIMBAD (both using three arcsec cross-matches, covering the WISE $W2$ FWHM). Of these 1,475 and 32 respectively had spectral types from SIMBAD. From this I gauged the contamination from early (FGK) stars, M giants, and white dwarfs (from spectral type alone). My excess sample has a contamination of ∼0.14 per cent from these sources and there was no contamination from these sources found in my candidate M+UCDs (see Table 2.1 and Table 2.2). It is also interesting to note I find 1.7 per cent of my excess sample are classified as known multiple or binary systems. It should however be noted, as with the full catalogue, some of the spectral types are defined only as M type star (∼1.35 per cent) and thus I may slightly underestimate my contamination from M giants.

### 4.2.2 Classifications from SIMBAD

I counted the source classifications given in SIMBAD and grouped them (see Table 2.4). From this I gauged the contamination from galaxies, variable stars and white dwarfs (from classifications alone) as ∼0.97 per cent for my excess sample and ∼1.52 per cent for my candidate M+UCDs. As for the assessment of SIMBAD spectral types, some of the source classifications are not specific enough to gauge possible contamination (e.g. classifications including "star" , "in an association" or "in a cluster") therefore I take these contaminations as rough estimates.

### 4.2.3 Spectral types from LAMOST

I repeated this exercise with the LAMOST DR1 and DR2 catalogue (see Section 1.4.4) using the spectral types found using their modified HAMMER routine (Cui et al., 2012, again with a three arcsec cross-match). In total there were 1,851 with spectral types out of my 36,898 excess sample and 41 with spectral types out of my 1,082 candidate M+UCDs. From this I gauged the contamination from early stars, multiple stars and white dwarfs. My excess sample has a contamination of ∼2.38 per cent from these sources and there was a ∼2.44 per cent contamination from these sources found in my candidate M+UCDs (see Table 2.3). However, as with the full catalogue, it should be noted the LAMOST general catalogue does not distinguish between giant stars and dwarfs nor between spectral types of the double stars thus my contaminations are a rough estimate.

### 4.2.4 Contamination from discs

Circumstellar discs around M dwarfs can be approximated quite well by a black-body of temperature, $T_{eff}$ and of extent $R$. These discs are heated by the central star and as such cannot exceed the stellar temperature unless some other process is involved. One way discs are found is to look for MIR excess (for M dwarfs e.g. Esplin et al., 2014; Theissen & West, 2014; Luhman & Mamajek, 2012).

Esplin et al. (2014) investigate the excess signal via MIR continuum emission from warm circumstellar dust. They define a boundary (see Figure 2 from Esplin et al., 2014) above which stars have an excess signal due to this warm dust. Theissen & West (2014) compliment this with a polynomial fit (see Table 1 Theissen & West, 2014) to the M dwarf main sequence with $(W1-W3)$ and $(W2-W3)$ as functions of $(r-z)$ from SDSS. My M dwarfs lie well below the region in which M dwarfs are know to have circumstellar discs lie (Figure 3 from Theissen & West 2014 and plotted for my M dwarfs in Figure 4.2), and mostly lie out of the region defined by Esplin et al. (2014, see Figure 4.1). Luhman & Mamajek (2012) also present a boundary in $(K_S-W2)$ colour-spectral type space, however their boundaries lies significantly above my distribution and the boundary of Esplin et al. (2014), thus having no overlap with my M+UCD candidates.

To investigate the effects of circumstellar reddening further, I investigated ways in which warm disks (of various size) might give excess values that could contaminate my selection of M+UCD candidates.

$$B_\lambda = \frac{2hc^2}{\lambda^5}\frac{1}{exp(hc/\lambda k_B T_{eff}) - 1} \tag{4.1}$$

$$F_\lambda = \pi B_\lambda \tag{4.2}$$

$$F_\lambda(d) = F_\lambda \frac{\Sigma_{disc}}{\Sigma_{\text{sphere}}} \tag{4.3}$$

where $B_\lambda$ is the spectral radiance, $F_\lambda$ is the flux, $F_\lambda(d)$ is the flux as observed from a distance $d$, $\Sigma_{disc} = \pi(R^2_{outer} - \pi R^2_{inner})$ is the surface area of the disc with inner radius $R_{inner}$ and outer radius $R_{outer}$, and $\Sigma_{sphere} = 4\pi d^2$ is the surface area of a sphere at radius $d$, the distance of observation (taken to be 10 pc).

I made a grid of 250 values of $0.5 < log(\frac{T_{eff}}{K}) < 3.6$ and 250 values of $-3.5 < log(\frac{\text{extent of disc}}{AU}) < 4.5$ (where Extent of disc $\approx R_{outer}$ as I set $R_{inner} = R_*$). From these 62,500 $T_{eff}$ and Extent of disc combinations I added a black-body as described

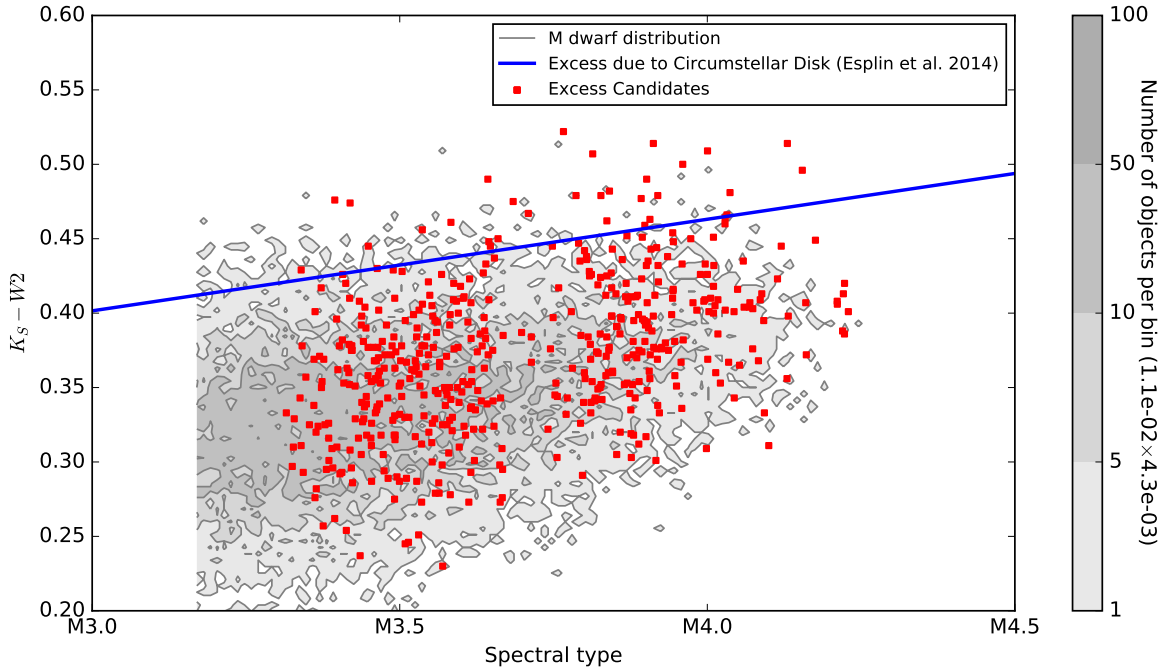


Figure. 4.1: Following the work by Esplin et al. (2014) I show possible excess due to circumstellar discs. Esplin et al. (2014) use $(K_S - W2)$ to define a boundary above which stars have possible excess due to circumstellar discs. Most of my M+UCD candidates lie below this line.

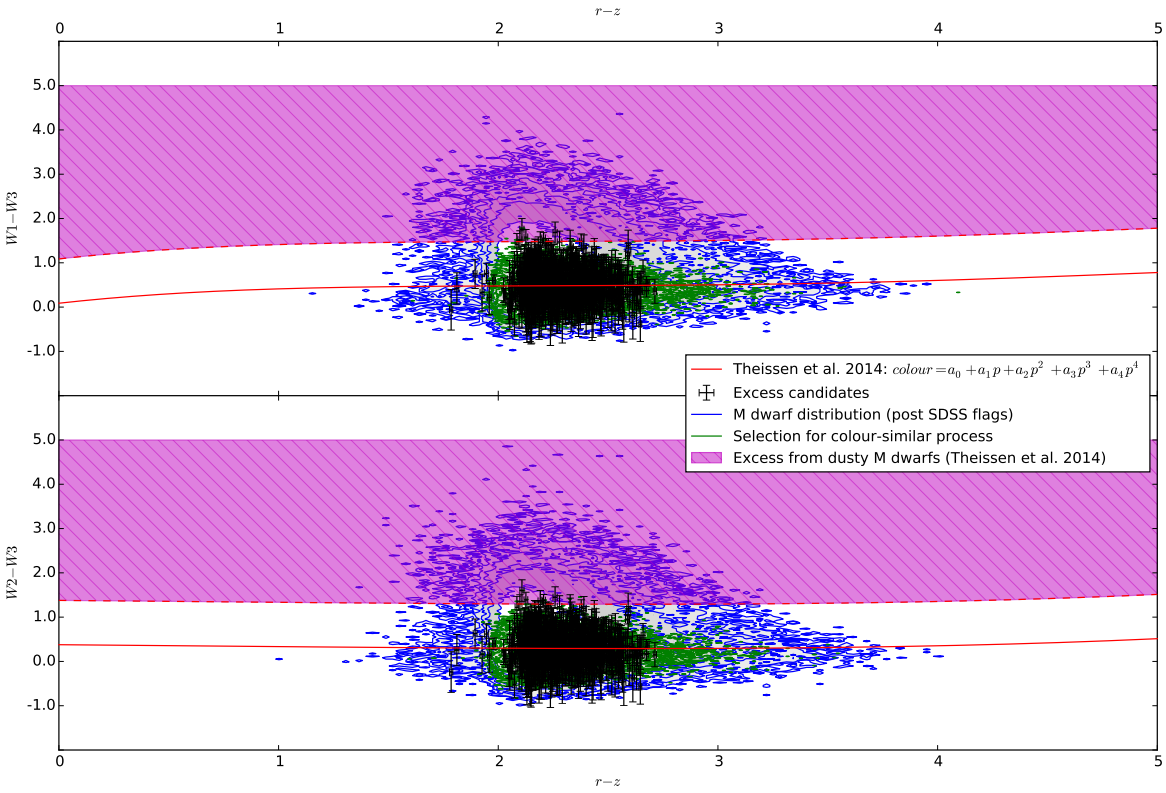


Figure. 4.2: Theissen & West (2014) fit for M dwarfs (red line) as a function $(W2 - W3)$ against $(r - z)$, and $(W1 - W3)$ against $(r - z)$. Shown in the shaded region the cut defined by Theissen & West (2014) for excess due to dusty M dwarfs. All my M+UCD candidates (in black) lie below this cut as do the M dwarfs which form my excess sample (in green).

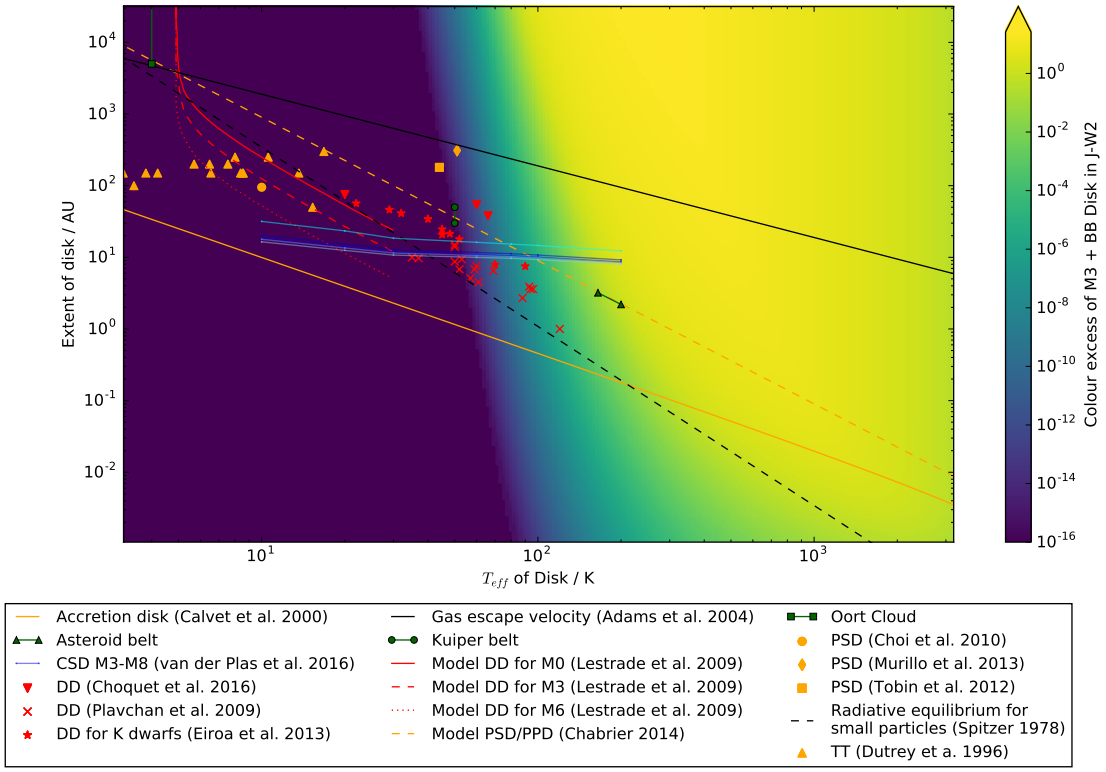


Figure. 4.3: Simulations of the colour excess from an M dwarf with an added black-body of temperature, $T_{eff}$ and surface area $= \pi(\text{extent})^2$ for colour excess in $(J - W2)$. Over plotted are literature examples of circumstellar discs, CSD, debris discs, DD, protostellar discs, PSD, and T-Tauri stars, TT (Plavchan et al. 2009, Eiroa et al. 2013, Choquet et al. 2016, Choi et al. 2010, Tobin et al. 2012, Murillo et al. 2013) and models (Lestrade et al. 2009, Calvet et al. 2000, van der Plas et al. 2016, Adams et al. 2004, Chabrier et al. 2014, Spitzer 1978). Note the solar system objects (Asteroid belt, Kuiper belt and Oort Cloud) are plotted as comparisons to warmer stars and as such M dwarf levels of excess would be much lower.

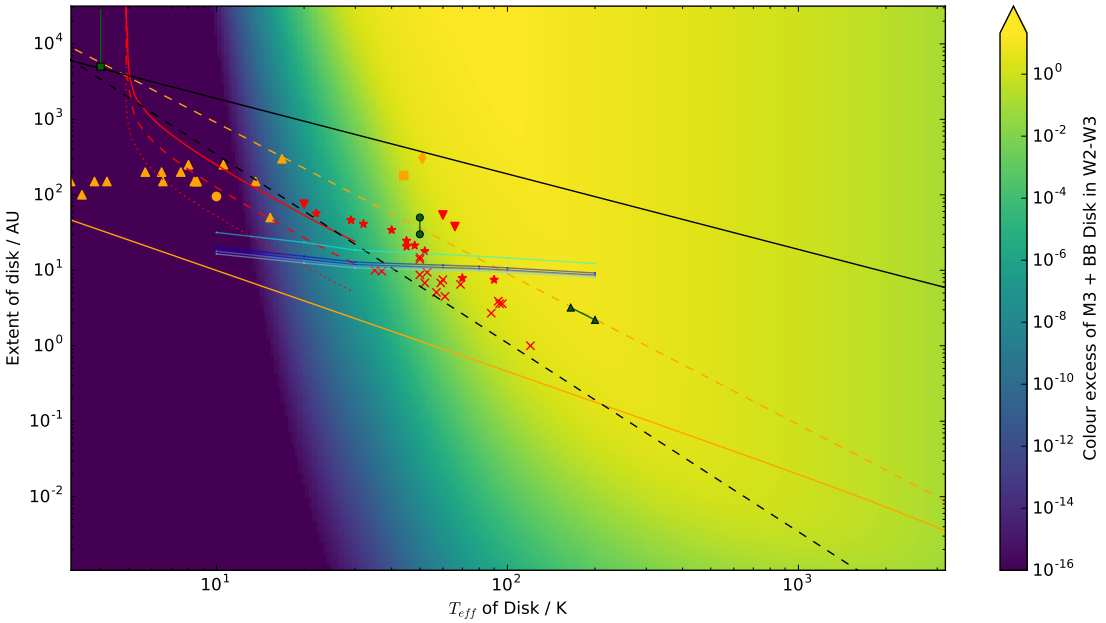


Figure. 4.4: Same as Figure 4.3 but for colour excess in $(W2 - W3)$

in equations Equation 4.1, Equation 4.2 and Equation 4.3 to the M dwarf BT-Settl (CIFIST2011_2015 Baraffe et al., 2015).[30] model (smoothed to 5,000 bins for faster computation between 0 and 30 $\mu$m, and normalised to 10 pc). For each point in the grid the colour excess ($Colour_{disc} - Colour_{Mdwarf}$) was calculated for $(J-H)$, $(H-W1)$, $(H-W2)$, $(J-W1)$, $(J-W2)$ and $(W2-W3)$ where colour is calculated in Equation 4.4.

$$Colour(1,2) = M_1 - M_2 = -2.5log_{10}\left(\frac{\int I_\lambda \tau_1(\lambda)d\lambda}{\int I_{0,1}\tau_1(\lambda)d\lambda}\frac{\int I_{0,2}\tau_2(\lambda)d\lambda}{\int I_\lambda \tau_2(\lambda)d\lambda}\right) \tag{4.4}$$

where $I_\lambda$ is the flux from the spectrum, $\tau_1(\lambda)$ is the transmission profile of band 1, and $I_{0,1}$ is the zero point flux of band 1[31].

To these grids I added data from the literature for known circumstellar discs, CSD, debris discs, DD, around low-mass stars (from Plavchan et al. 2009, Eiroa et al. 2013, Choquet et al. 2016) protostellar discs, PSD, around low-mass stars (from Choi et al. 2010, Tobin et al. 2012, Murillo et al. 2013), low-mass T-Tauri stars, TT (from Dutrey et al. 1996) and from the solar system (Asteroid belt, Kuiper belt and Oort cloud). I also added some models of debris discs from Lestrade et al. (2009) for M0, M3 and M6 dwarfs; a model of accretion discs from Calvet et al. (2000), models of circumstellar discs for M3 to M8 dwarfs from van der Plas et al. (2016), a model of gas escape velocity from Adams et al. (2004), a model of PSD and proto-planetary discs, PPD from Chabrier et al. (2014) and a model of radiative equilibrium for small particles by Beckwith et al. (1990) and Spitzer (1978).

I used these to show how much colour excess discs at given $T_{eff}$ and extent would add to an M dwarf assuming they were blackbodies. Figure 4.3 and Figure 4.4 show these grid points plotted for an M4 dwarf with the comparison to the literature.

As a very red $(W2-W3)$ colour is a clear signature of a disc I also plotted $(W2-W3)$ against colour excess in $(J-W2)$ for all my M dwarfs in the full M dwarf candidate catalogue with a $W3$ detection (non-upper limit) and for my M+UCD candidates which have a $W3$ detection (see Figure 4.5). Figure 4.5 shows there are no major outliers and therefore no obvious discs present in my M+UCD candidates.

In addition to this analysis, discs around late-K and M dwarfs seem to be rare and only present around very young M dwarfs (see Deacon et al., 2013, and references therein). Even if these rare discs exist from work presented above (Esplin et al. 2014; Theissen & West 2014; Luhman & Mamajek 2012, Figure 4.1, Figure 4.3 and Figure

[30] Accessed online at https://phoenix.ens-lyon.fr/Grids/BT-Settl/

[31] 2MASS bands from http://www.ipac.caltech.edu/2mass/releases/allsky/doc/sec6_4a.html and WISE bands from http://wise2.ipac.caltech.edu/docs/release/allsky/expsup/sec4_4h.html

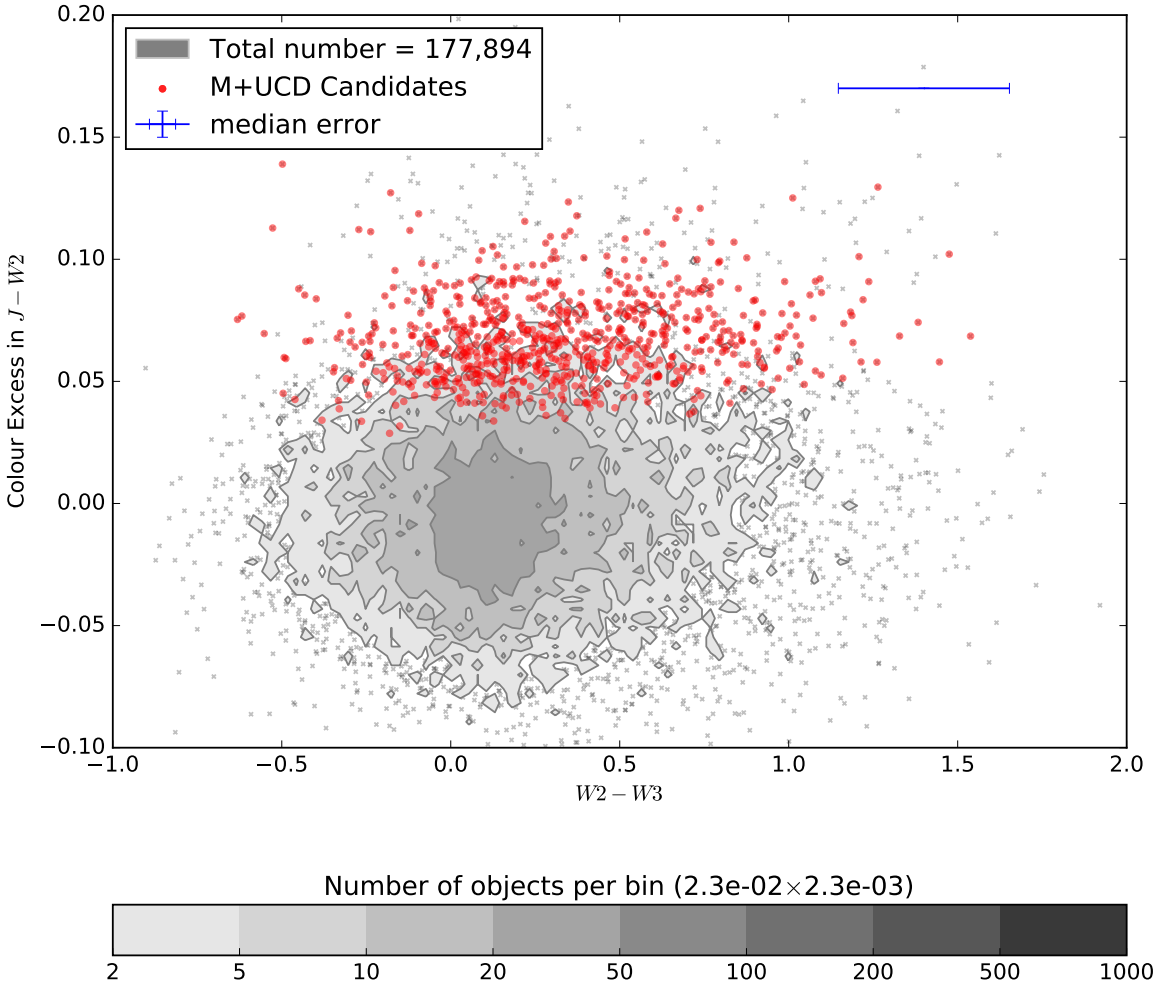


Figure. 4.5: Colour excess in $(J-W2)$ against $(W2-W3)$ for all my M dwarfs in the full M dwarf candidate catalogue and for my M+UCD candidates which have a $W3$ detection. This plot shows that The distribution of my M+UCD candidates is consistent with my over all distribution of M dwarfs in $(W2-W3)$ and thus there are no obvious candidates that have extremely large $(W2-W3)$ colour (i.e. there are no signatures of a circumstellar discs in my M+UCD candidates).

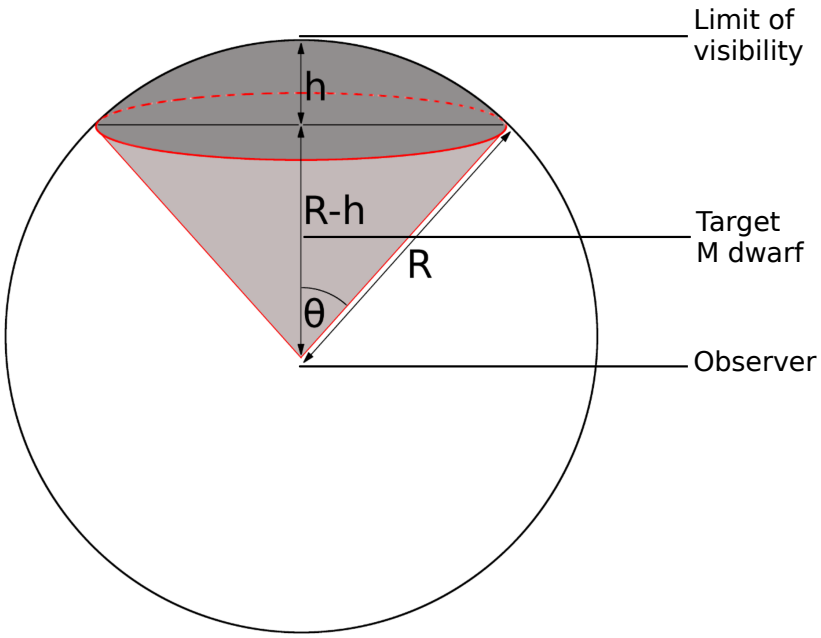


Figure. 4.6: Geometry of a spherical cone.

4.4) it is clear only exceptionally warm or large discs would give the colour excess required to be mistaken for one of my M+UCD candidates.

### 4.2.5 Contamination from chance aligned red objects

Foreground or background objects which appear redder than my M dwarfs and are randomly aligned within the WISE PSF will cause an M dwarf to look redder. I explore the various red objects, foreground and background objects which can redden my M dwarfs. In the following sections I look at foreground and background M dwarf and brown dwarfs (Section 4.2.6), background giants (Section 4.2.7) and galaxies (Section 4.2.8). Although line of sight dust (local reddening) could also redden my M dwarfs, it is not clear how this can be easily modelled so I do not attempt this.

To calculate how many reddened objects are expected to contaminate my M dwarfs I defined a spherical cone (Weisstein, 1999) with volume, $Vol$ (see Figure 4.6). Any objects inside this spherical cone (centred around my M dwarf) appear blended due to the size of the M dwarfs PSF. This cone can also be used to calculate the density of objects in a certain area of sky, given a magnitude limit (and hence maximum distance; see Equation 4.5, Equation 4.6, Equation 4.7 and Equation 4.8).

$$Vol = \frac{2}{3}\pi R^2 h \tag{4.5}$$

$$R - h = Rcos(\theta) \qquad h = R - Rcos(\theta) \tag{4.6}$$

$$Vol = \frac{2}{3}\pi R^3(1 - cos(\theta)) \tag{4.7}$$

$$\rho = \frac{N}{Vol} = \frac{N}{(\frac{2}{3}\pi R^3(1 - cos(\theta))} \tag{4.8}$$

where $Vol$ is the volume of the spherical cone, $R$ is the distance from the observer to the limit of visibility, $N$ is the number of objects in the volume, and $\theta$ is the angular size of the cone.

As well as being present within the PSF of WISE objects need to contribute a sufficient amount of flux to give an excess in $(J - W2)$ similar to adding a UCD to my M dwarfs. I define sufficient $(J - W2)$ excess to mean 5 per cent colour excess (see Figure 3.35 and Figure 3.36). Using the definition of the limit of colour excess (Equation 4.9) and adding my target M dwarf and red contaminating object in flux space (Equation 4.10) and leads to Equation 4.11 and Equation 4.12, which is the limiting magnitude given a specific M dwarf and a specific $(J - W2)$ of the contaminating object.

$$(m_{J(M+B)} - m_{W2(M+B)}) - (m_{J(M)} - m_{W2(M)}) > E \tag{4.9}$$

$$m_{J(M+B)} = -2.5log_{10}(10^{-0.4m_{J(M)}} + 10^{-0.4m_{J(B)}}) \tag{4.10}$$

$$m_{J(B)} = -2.5log_{10}\left(\frac{10^{-0.4(E+m_{J(M)})} - 10^{-0.4m_{J(M)}}}{1 - 10^{-0.4(E+(J-W2)_M-(J-W2)_B)}}\right) \tag{4.11}$$

$$m_{W2(B)} = -2.5log_{10}\left(\frac{10^{-0.4(m_{J(M)}-E)} - 10^{-0.4m_{W2(M)}}}{1 - 10^{-0.4((J-W2)_B-E-(J-W2)_M)}}\right) \tag{4.12}$$

where $m_{J(M+B)}$ and $m_{W2(M+B)}$ are the $J$ and $W2$ magnitudes of the combined M dwarf and red contaminating object, $m_{J(M)}$ and $m_{W2(M)}$ are the $J$ and $W2$ magnitudes of a specific M dwarf target, $(J - W2)_B$ is the colour of the red contaminating object and $m_{J(B)}$ is the limiting magnitude of the red contaminating needed to cause an Excess of $E$ (0.05 for my sample).

Using Equation 4.11 and Equation 4.12 I calculated the limiting magnitudes a red contaminating object would need to have to sufficiently redden one of the M dwarfs.

I chose not to apply extinction to the limiting magnitude due to the small amount of difference this would make (with an $A_V < 0.08$ and mean values of $\frac{A_\lambda}{A_V}$ of 0.179 for $J$ and 0.056 for $W2$, see Table 3.1, the extinction is of order 0.01 in $J$ and 0.005 in $W2$).

These calculations (Section 4.2.6 to Section 4.2.8) are only order of magnitude calculations and are over simplified due to assumptions such as uniform space density (e.g. neglecting Galactic scale height effects).

### 4.2.6 Chance alignment of brown dwarfs and M dwarfs

For chance alignments of brown dwarfs and M dwarfs I took spatial densities from the literature (Reid et al. 2007, Phan-Bao et al. 2003, Phan-Bao et al. 2008, Cruz et al. 2007, Marocco et al. 2015, Burningham et al. 2013) and calculated the $(J - W2)$ colour of the M dwarfs and brown dwarfs from my simulated photometry (see Section 3.3), these values are presented in Table 4.1.

Using $(J - W2)$ from Table 4.1 I calculated the maximum distance brown dwarfs and M dwarfs could add sufficient flux to my target M dwarf (using Equation 4.11 and Equation 4.12) this value was used if it was brighter than the limiting magnitude in 2MASS or WISE, otherwise the $1.25\sigma$ 2MASS/WISE limit (18.05/17.00) was used instead (see Table 1.5 where I add 1.5 to convert from $5\sigma$ to $1.25\sigma$). This number was calculated for each of my 36,898 target M dwarfs.

Then using Equation 4.8 I estimated the number of brown dwarfs or M dwarfs chance aligned with each of my target M dwarfs. Taking the sum of the number of objects for each of my target M dwarfs gave the total number of contaminating brown dwarfs and M dwarf expected in my M+UCD candidates. My M+UCD candidates occupy an excess region between 0.05 and 0.15 in colour excess of $(J - W2)$. Therefore I also subtract off those objects which have an excess greater than 0.15 to give a final number of objects. The results are shown in Table 4.1 and I expect a total of no more than two of my 36,898 sources to be reddened due to a chance alignment with a foreground or background M dwarf or brown dwarf.

| spectral type | $M_J$ | $M_{W2}$ | $(J-W2)$ | spatial density | $M_{J(limit)}$ | $M_{W2(limit)}$ | Medium objects per target M dwarf | Total objects $0.05 < E < 0.15$ | Ref. |
|---|---|---|---|---|---|---|---|---|---|
| | mag | mag | mag | $\times 10^{-3}$ pc$^{-3}$ | mag | mag | | | |
| M2 - M5 | 7.0 - 9.5 | 5.9 - 8.5 | 1.1 - 1.3 | 76 | 12.39 - 13.87 | 11.29 - 12.57 | $1.20\times10^{-4}$ | 1.59 | a |
| M6 - M8 | 10.3 - 11.0 | 9.0 - 9.4 | 1.3 - 1.6 | 4.62 | 13.87 - 16.05 | 12.57 - 14.45 | $4.41\times10^{-6}$ | 0.18 | b |
| M8 - L3.5 | 11.0 - 12.9 | 9.4 - 10.6 | 1.6 - 2.3 | 3.28 | 16.05 - 17.70 | 14.45 - 15.39 | $3.13\times10^{-6}$ | 0.12 | c |
| L0 - L3 | 11.6 - 12.9 | 9.8 - 10.9 | 1.8 - 2.3 | 1.7±0.4 | 16.69 - 17.70 | 14.89 - 15.39 | $1.70\times10^{-6}$ | 0.05 | d |
| L4 - L6.5 | 13.1 - 14.1 | 10.7 - 11.1 | 2.4 - 3.0 | 0.85±0.55 and 1.00±0.64 | 17.85 - 18.68 | 15.43 - 15.68 | $6.30\times10^{-7}$ | 0.02 | e |
| L7 - T0.5 | 13.3 - 14.8 | 11.2 - 11.8 | 3.1 - 3.0 | 0.73±0.47 and 0.85±0.55 | 18.80 - 18.70 | 15.70 - 15.68 | $3.79\times10^{-7}$ | 0.01 | e |
| T1 - T4 | 14.7 - 14.8 | 11.9 - 12.5 | 2.8 - 2.3 | 0.74±0.48 and 0.88±0.56 | 18.42 - 17.69 | 15.62 - 15.39 | $1.33\times10^{-7}$ | 0.00 | e |
| T6 - T6.5 | 14.7 - 15.3 | 12.6 - 13.0 | 2.1 - 2.3 | 0.39±0.22 to 0.71±0.40 | 17.34 - 17.69 | 15.24 - 15.39 | $2.43\times10^{-8}$ | 0.00 | f |
| T7 - T7.5 | 15.6 - 16.0 | 13.1 - 13.3 | 2.5 - 2.7 | 0.56±0.32 to 1.02±0.64 | 18.01 - 18.29 | 15.51 - 15.59 | $2.51\times10^{-8}$ | 0.00 | f |
| T8 - T8.5 | 16.6 - 17.2 | 13.4 - 13.6 | 3.2 - 3.6 | 2.05±1.21 to 3.79±2.24 | 18.92 - 19.39 | 15.72 - 15.79 | $8.33\times10^{-8}$ | 0.00 | f |

Table 4.1: Results of the chance alignments of M dwarfs and brown dwarfs. Shown are the simulated M dwarf absolute photometry and $(J-W2)$ colour, taken from Section 3.3, and the spatial densities taken from the literature (a. Reid et al. 2007, b. Phan-Bao et al. 2003, c. Phan-Bao et al. 2008, d. Cruz et al. 2007, e. Marocco et al. 2015, f. Burningham et al. 2013). Note space densities from Marocco et al. (2015) are stated for binary fractions of 26±13 and 14±10 respectively, and space densities from Burningham et al. (2013) are stated from a minimum to maximum value and I take the worst case scenario in each case to calculate the contamination. Also calculated are the limiting magnitudes to give a five per cent excess in $(J-W2)$ and thus the number of chance alignments of brown dwarfs and M dwarfs per target M dwarf and in total for my excess sample. Note if the limiting magnitude was greater than the $1.25\sigma$ detection limit of 2MASS or WISE, the 2MASS/WISE limit (18.05/17.00) was used instead (see Table 1.5 where I add 1.5 to convert from $5\sigma$ to $1.25\sigma$).

### 4.2.7 Change alignment of M giants

For M giants I downloaded all Milky Way stars from the *10th version of the Gaia Universe Model Snapshot* (GUMS-10, Milky Way stars in GUMS.MW Robin et al., 2012)[32]. The GUMS.MW catalogue gives simulated stellar properties such as spectral type, luminosity class and distance, as well as the predicted Gaia $G$ magnitude to simulate objects present in the future Gaia data releases.

From this catalogue I selected all the M giants (selecting M spectral type stars and luminosity classes I, II and III) with galactic latitude, $b > 40°$, this left 4,966 M giants. I selected those with $G < 9$ (to select a complete sample at known distance) which left 3,022 M giants in my M giant sample.

To work out a density I needed a maximum distance a $G < 9$ M giant can be observed at (and thus needed the absolute magnitude of M giants in $G$ band). Converting $G$ in to $M_G$ (via $M_G = G - 5log_{10}(distance) + 5$) and taking the faintest possible $M_G$ value for my M giant sample (thus the worst case scenario for my density) I estimated the maximum distance Gaia could detect M giants to was 6,983 pc. Thus the average density of M giants per parsec$^3$ in a spherical cone of radius, $R = 6,983pc$, $\rho_{Mgiant}$ is $1.1866\times^{-8}$M Giants $pc^{-3}$ (using Equation 4.8).

To calculate the number of chance alignments of M giants with one of my M dwarfs I needed the maximum distance I could detect M giants out to in 2MASS/WISE. For this I needed the absolute magnitude of M giants. Using Equation 4.13, Equation 4.14 and Equation 4.15 (Smart, 2013) I calculated an equation for J in terms of G and $(J - K_S)$ (see Equation 4.13 to Equation 4.17)[33] where I take the $(J - K_S)$ values for M giants from Straižys & Lazauskaitė (Table 3 2009).

$$B_J = J + 4.9816 - 0.38945670(J - K_S) \tag{4.13}$$

$$\begin{aligned} R_F &= J + 2.6997 - 0.46257863(J - K_S) \\ M &= R_F - J = 2.6997 - 0.46257863(J - K_S) \end{aligned} \tag{4.14}$$

$$\begin{aligned} G =& R_F + 0.0045 + 0.3623(B_J - R_F) - 0.1783(B_J - R_F)^2 \\ &+ 0.0080(B_J - R_F)^3 \end{aligned} \tag{4.15}$$

[32] Accessed online at http://dc.zah.uni-heidelberg.de/__system__/dc_tables/show/tableinfo/gums.mw

[33] Equations from Smart (2013), accessed via ftp://cdsarc.u-strasbg.fr/pub/cats/I%2F324/Gaia-C3-TN-OATO-RLS-004-01.pdf and use transformations by Hog et al. 'Guide to the Tycho-2 Catalog' http://www.astro.ku.dk/~erik/Tycho-2/ and Jordi (2009)

$$\begin{aligned} L =& B_J - R_F \\ L =& J + 4.9816 - 3.8946 \times 10^{-1}(J - K_S) - J - 2.6997 + \\ & 4.6258 \times 10^{-1}(J - K_S) \\ L =& 7.3122 \times 10^{-2}(J - K_S) + 2.2819 \end{aligned} \tag{4.16}$$

$$\begin{aligned} J =& G - M - 0.0045 + 0.3623L - 0.1783L^2 + 0.0080L^3 \\ J =& G - 3.1278 \times 10^{-6}(J - K_S)^3 + 6.6052 \times 10^{-4}(J - K_S)^2 + \\ & 4.8645 \times 10^{-1}(J - K_S) - 2.6976 \end{aligned} \tag{4.17}$$

For a $(J - K_S)$ of 1.11 (average of the $(J - K_S)$ values for M giants from Table 3 of Straižys & Lazauskaitė 2009) and an absolute $G$ magnitude of -0.61 I calculate an absolute J band magnitude of -2.7668. Feeding this in to the equation for distance ($d_J = 10^{-0.4(M_J - m_j)}$) where $m_j$ is the $1.25\sigma$ limit of 2MASS (see Table 1.5 where I add 1.5 to convert from $5\sigma$ to $1.25\sigma$) gives a distance of $\sim$200 $Mpc$. This distance is far beyond the reach of the Milky Way, thus I chose to use the maximum distance looked through by the excess sample. Where I use Equation 4.18 taking $b_{min} = 40°$ and $h_z$ =1200 pc as stated in the GUM.MW simulation (Table 2 from Robin et al., 2012). This gave a distance of 1,867 pc.

$$d_{max} = \frac{h_z}{sin(b_{min})} \tag{4.18}$$

The number of chance aligned giants then comes directly from Equation 4.8, where $\rho_{Mgiant}$ is 1.2×$^{-8}$M Giants $pc^{-3}$, $\theta$ = six arcsec and $R = dmax$ =1867 pc. Hence the number of chance alignments of giant stars which are sufficiently red per M dwarf is $6.8\times10^{-8}$. With 36,898 M dwarfs in my excess sample I estimate 0.003 M giants chance alignments my excess sample.

### 4.2.8 Change alignment of red galaxies

For galaxies I started with the simulation from Henriques et al. (2012)[34]. Henriques et al. (2012) use the semi-analytic models of Guo et al. (2011) which simulate the evolution of haloes and sub-haloes within them. These models are implemented on two large dark matter simulations, the Millennium Simulation (Springel et al., 2005) and Millennium-II Simulation (Boylan-Kolchin et al., 2009).

[34] Accessed online at http://gavo.mpa-garching.mpg.de/Millennium/Help/databases/henriques2012a/database.

This gave me access to distance, $J_{AB}$, the Spitzer [4.5$\mu$m] band (also in the AB system, and assumed for simplicity to have a similar band-pass to $W2$). I chose to only count galaxies initially brighter than the WISE $W2$ 1.25$\sigma$ limit (see Table 1.5 where I add 1.5 to convert from 5$\sigma$ to 1.25$\sigma$) of 17 and a $(J-W2)$ colour redder than 1.17 (the bluest colour my M+UCD candidates appear to be). These needed to be converted into the AB system, for $W2$ this was done using Equation 4.19 from Jarrett et al. (2011)[35] and for $J$ this was done using Equation 4.20 from Blanton & Roweis (2007)[36]. This led to a $(J-W2)$ conversion shown in Equation 4.21, and the cuts were then applied to the simulations by Henriques et al. (2012) as in Equation 4.22. This left 11,903 galaxies in my sample of red galaxies.

$$J_{AB} = J_{Vega} + 0.91 \tag{4.19}$$

$$W2_{AB} = W2_{Vega} + 3.339 \tag{4.20}$$

$$(J-W2)_{AB} = (J-W2)_{Vega} - 2.429 \tag{4.21}$$

$$[4.5\mu\mathrm{m}] < 20.4 \qquad J - [4.5\mu\mathrm{m}] > -1.259 \tag{4.22}$$

Galaxies can be red for a number of reasons, (i.e. galaxies can be red because they are dusty, which reddens starlight and also emits in the infrared and via reddening due to redshift), to keep the estimation of contamination as simple as possible I use my sample of red galaxies to model the spread in $(J-W2)$ observed. I took the minimum, mean and maximum values of the $(J-W2)$ galaxy distribution and calculated the limiting magnitude in $J$ band (using Equation 4.11 and Equation 4.12) which would give an excess of 5 per cent. This value was used as a new cut to the galaxy sample if it was brighter than the 1.25$\sigma$ limiting magnitude in 2MASS (see Table 1.5 where I add 1.5 to convert from 5$\sigma$ to 1.25$\sigma$), otherwise the 1.25$\sigma$ 2MASS/WISE band limit (18.05/17.00) was used. The number of objects left gave the density of objects out to the limiting magnitude in which the galaxies would redden my M dwarfs by 5 per cent (see Table 4.2).

There were two ways to convert this number into a number of objects change aligned

[35] Accessed via http://wise2.ipac.caltech.edu/docs/release/prelim/expsup/sec4_3g.html#WISEZMA

[36] Accessed via http://www.astronomy.ohio-state.edu/~martini/usefuldata.html

| | unit | minimum | mean | maximum |
|---|---|---|---|---|
| $(J-W2)$ | mag | 1.43 | 2.65 | 3.93 |
| $M_{J(limit)}$ | mag | 15.15 | 18.22 | 19.76 |
| $M_{W2(limit)}$ | mag | 13.72 | 15.57 | 15.83 |
| $1.25\sigma$ 2MASS limit | mag | 18.05 | 18.05 | 18.05 |
| $1.25\sigma$ WISE limit | mag | 17 | 17 | 17 |
| Number of red galaxies in Survey | | 39 | 898 | 1207 |
| Density of red galaxies | $Mpc^{-3}$ | 0.001 | 0.015 | 0.020 |
| Number of objects per target M dwarf | | $1.74\times10^{-4}$ | $4.00\times10^{-3}$ | $5.37\times10^{-3}$ |
| Total objects in with $E > 0.05$ | | 10 | 143 | 175 |
| Number of extended ($\theta > 3''$) | | 10 | 21 | 21 |
| Total objects with $E > 0.15$ | | 0 | 28 | 42 |
| Total non-extended objects $0.05 < E < 0.15$ | | 0 | 94 | 112 |

Table 4.2: Table showing the limiting magnitudes to give a five per cent excess in $(J-W2)$ and thus the number of chance alignments of galaxies per target M dwarf and in total for my excess sample. Note if the limiting magnitude was greater than the $1.25\sigma$ detection limit of 2MASS or WISE, the 2MASS/WISE limit (18.05/17.00) was used instead (see Table 1.5 where I add 1.5 to convert from $5\sigma$ to $1.25\sigma$).

with one of my M dwarfs. Taking all galaxies to be at infinite distance one can simply divide the area of the WISE PSF (six arcsec ) by the area of the survey (1.4°×1.4°), however for consistency I also work out a density of galaxies and use the spherical cone analysis. Using the sample of galaxies I calculated the minimum, mean and maximum absolute $J$ band magnitudes and thus the minimum, mean and maximum values for the distance of these galaxies. Then using Equation 4.7, I estimated a density, and the number of galaxies per M dwarf, and in the total excess sample (of 36,898 M dwarfs) by using Equation 4.8. All results for the minimum, mean and maximum values can be seen in Table 4.2.

In my selection process (Chapter 2 and Chapter 3) any galaxy which looked extended to 2MASS or WISE was rejected as a contaminant and thus rejected from my excess sample. I thus also need to remove any galaxies in my sample which are extended and thus already rejected from amongst my M dwarfs. To do this I use the hydrodynamic cosmological simulation from Figure 3 of Naab et al. (2009) to define a relationship between redshift, $z$ and extent of the galaxy (see Equation 4.23).

$$\left[\frac{\text{Extent}}{kpc}\right] = -1.1551 log_{10}(z) + 1.2985 \qquad \text{correlation} = -0.97 \tag{4.23}$$

However one must be careful in converting extent of a galaxy as the angular size varies as a function of redshift (see Equation 4.24, Equation 4.25, Equation 4.26, Equation 4.27 from Equation 7.33, 7.37, 7.31 and 7.11 Ryden 2003 respectively),

$$\theta = \left[\frac{\text{Extent}}{d_A}\right]^{rad} \tag{4.24}$$

$$d_A = \frac{d_L}{(1+z)^2} \tag{4.25}$$

$$d_L \approx \frac{c}{H_0} z \left(1 + \frac{1+q_0}{2} z\right) \tag{4.26}$$

$$q_0 = \Omega_{r,0} + 0.5\Omega_{m,0} - \Omega_{\Lambda,0} \tag{4.27}$$

where $d_A$ is the angular diameter distance, $d_L$ is the luminosity distance, $z$ is the redshift, $\theta$ is in radians, $H_0$ =72 km s$^{-1}$ Mpc$^{-1}$, $q_0$ = -0.55 is the deceleration parameter

for $\Omega_{\Lambda,0} = 0.7$, $\Omega_{m,0} = 0.3$ and $\Omega_{r,0} = 0$ for a nearly flat universe. Combining Equation 4.24, Equation 4.25 and Equation 4.26 with Equation 4.23 gives an equation for $\theta = \theta(z)$. Taking the PSF of 2MASS as three arcsec this is equivalent to galaxies of redshift smaller than 0.05 as being possibly extended and thus already rejected.

My M+UCD candidates occupy an excess region between 0.05 and 0.15 in colour excess of $(J - W2)$. Therefore I also subtract off those objects which have an excess greater than 0.15 to give a final number of objects. Hence the number of chance alignments is $4{\times}10^{-3}$ per M dwarf. With 36,898 M dwarfs in my excess sample I estimate a worst case scenario of between 94 and 112 of my excess sample may be reddened by chance alignments with red galaxies.

### 4.2.9 Change alignment from random offsets

Another way I gauge possible contamination from red objects was to randomly offset my excess sample by 2° at random angles. This movement to a random location should simulate the possibility of finding a chance aligned object. I then cross-matched these offset points with WISE (out to 6 arcsec totalling 3,073 of 36,898 matches) and with 2MASS (out to 3 arcsec totalling 464 of the 3,073 matches). I was then able to work out $(J - W2)$ colour of these objects. From this I added the object back to my M dwarfs $(J - W2)$ (using Equation 3.6) and thus was able to calculate the objects colour excess. Of the 464 objects which had a random object with both a WISE and 2MASS detection, 105 had an positive non-zero excess and 38 had an excess between 0.05 and 0.15 (equivalent to my improvement contour constraints). Thus a total of 0.285 per cent and 0.103 per cent of my M dwarf in my excess sample had chance alignments (out of the total 36,898). This means that out of my 1,082 M+UCD candidates I would have 105 objects (9.70 per cent) that were just chance alignments that would produce a positive non-zero excess and 38 objects (3.51 per cent) that would produce an excess than matched my contour criteria and be selected by my approach. Thus I can expect a contamination from chance alignments of around 3.5 per cent and no worse than ∼9.5 per cent.

### 4.2.10 Visual inspection of the M+UCD candidates

As part of my reduction in contamination I visually inspected[37] my M+UCD candidates in SDSS ($g$, $r$), in 2MASS ($J$, $H$), in WISE ($W1$, $W2$ and $W3$) and where possible in UKIDSS $J$ (Lawrence et al., 2007, 2013) and the DSS2 red band. I flagged any object which was obviously blended by a galaxy, by a diffraction spike from a bright nearby star, both of which are obvious contamination. I also flagged any object blended by

[37] This was much quicker by using the Python module Astroquery SkyView http://dx.doi.org/10.6084/m9.figshare.805208

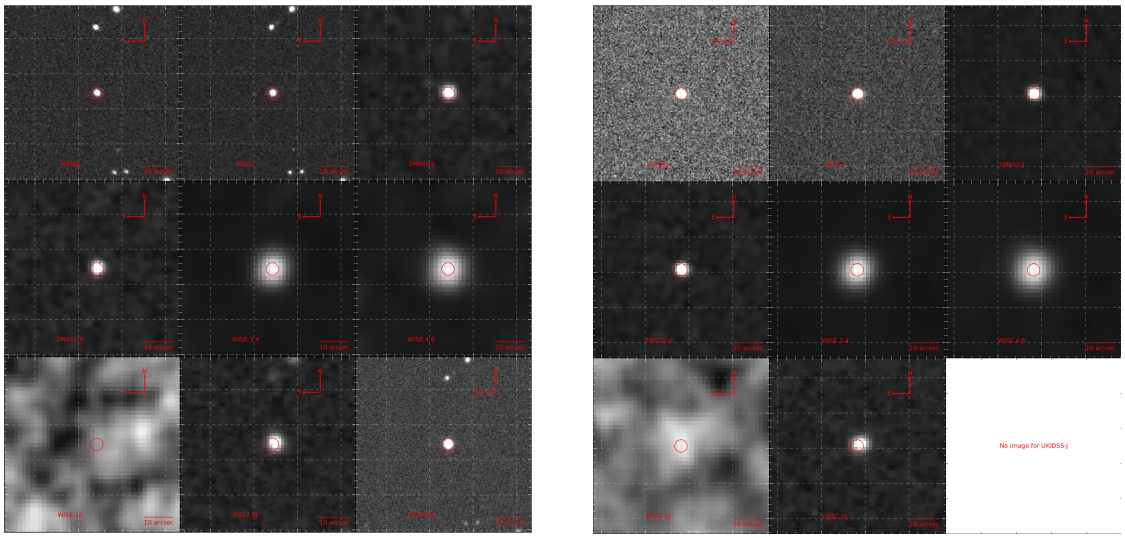

(a) (b)

Figure. 4.7: Visual inspection of (a) WISE J082013.57+073241.2 and (b) WISE J024125.18-064759.2, examples of clean M dwarfs. Images from SDSS ($g$, $r$), 2MASS ($J$, $H$), WISE ($W1$, $W2$), UKIDSS $J$ and the DSS2 red band. Note nearby optical sources may not contribute in the WISE bands.

a nearby object, these are also probably contamination but are not removed from my catalogue completely. Example of two clean visual inspections can be seen in Figure 4.7a and b. In Figure 4.8a I show a blend with a diffraction spike which probably caused this M dwarf to be selected and in Figure 4.8b I show an object which appear separate in the optical bands but blended in WISE.

Of my 1,082 M+UCD candidates I flagged:

- 161 (14.88 per cent) as having nearby sources within the size of the WISE PSF and being possible blends.
- 29 (2.68 per cent) as having identifiable nearby galaxies as possible blends.
- 3 (0.28 per cent) as having possible contamination from the diffraction spikes of nearby bright stars.
- 11 (1.02 per cent) as having other problems (i.e. no images or too faint to see in the images)

These number seem high, however although any of these blended sources may contribute to the reddening of my M dwarfs they also might not (since the effects of the blend on the data quality are not known directly) and thus I use this number as a rough estimate of possible blended contamination. The visual inspection of the UKIDSS images (143 of the 1,082 had UKIDSS images) also showed 27 close blends. Twenty five of these nearby objects have UKIDSS photometry (obtained by cross-matching with

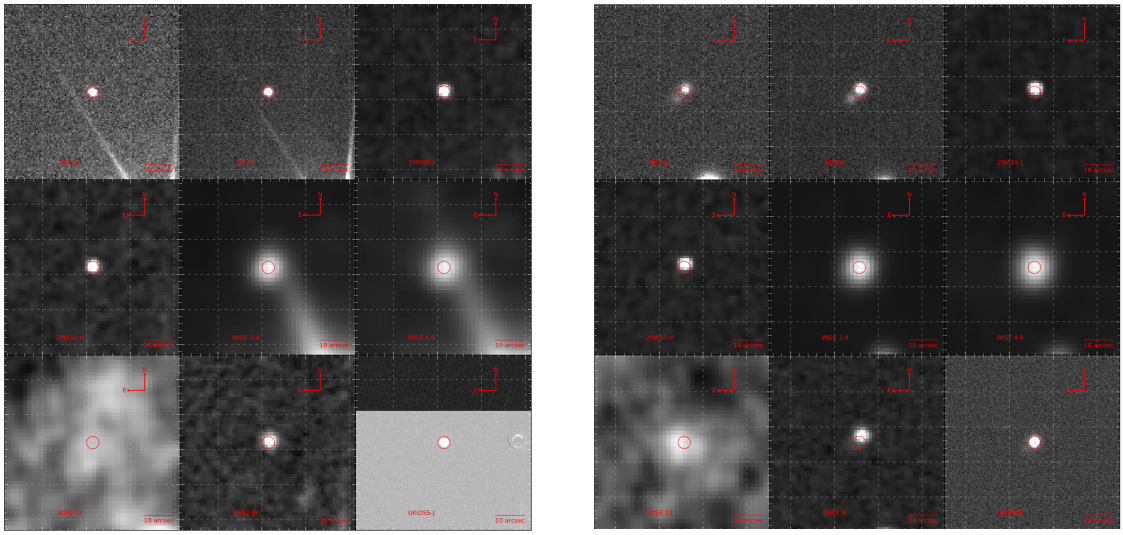

(a) (b)

Figure. 4.8: Visual inspection of (a) WISE J005433.85-002209.5: example of a diffraction spike and probably causing this M dwarf to be selected as a M+UCD candidate (b) WISE J113642.43-010917.3: example of a object blended with my selected M dwarf. Images from SDSS ($g$, $r$), 2MASS ($J$, $H$), WISE ($W1$, $W2$), UKIDSS $J$ and the DSS2 red band. Note nearby optical sources may not contribute in the WISE bands.

*UKIDSS Large Area Survey*, UKIDSS LAS, Lawrence et al. 2007, 2013). I then located any UKIDSS source which was within the WISE PSF and found 31 other sources around my 25 objects with UKIDSS photometry. Nineteen of these were flagged as galaxies using the PGalaxy[38] flag greater than 0.5, two such examples are shown in Figure 4.9, however as some of these nearby sources are blended with my M dwarfs they may be misclassified as galaxies.

To gauge an upper limit on how many galaxies might be in my M+UCD candidates I cross-matched them with UKIDSS LAS (again within the WISE six arcsec PSF), 247 had matches with my 1,082 M+UCD candidates. Around these 247 M dwarfs were 175 sources detected within the WISE PSF, of which 85 were flagged as galaxies (PGalaxy>0.5). Thus an upper limit on the number of galaxies would be 372 (34.4 per cent), however as I discussed in Section 4.2.8, one needs to take into account many of these galaxies will not have the correct $(J - W2)$ to give a colour excess that could mimic an unresolved UCD companion.

[38]PGalaxy is calculated by combining individual detection classifications in the source merging process see http://wsa.roe.ac.uk/www/gloss_p.html#lassource_pgalaxy for the definition

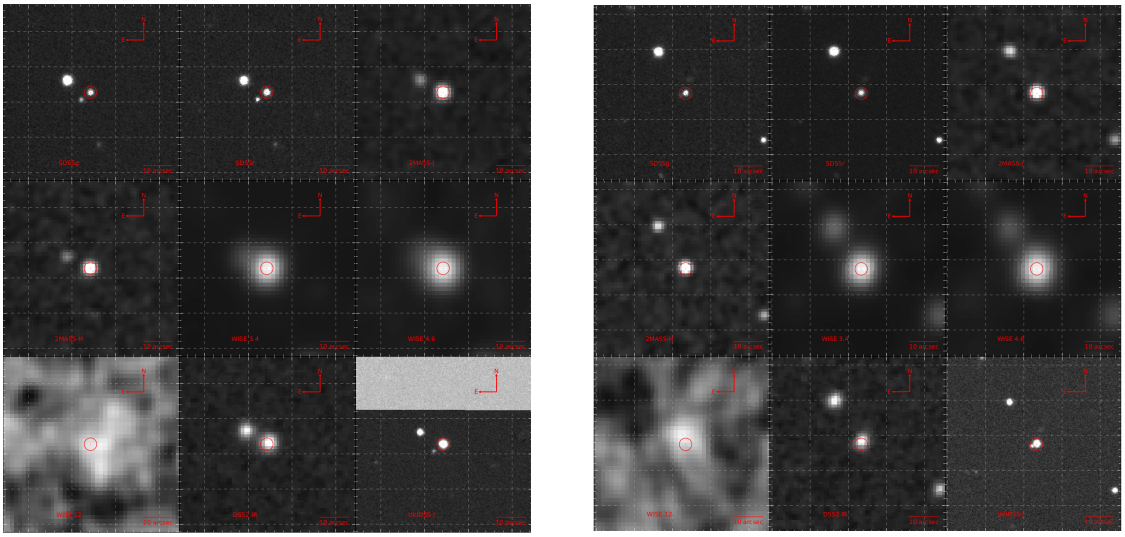

(a) (b)

Figure. 4.9: Visual inspection of (a) WISE J081928.57+070015.2 and (b) WISE J163829.66+293756.8: example of two M dwarfs with a close UKIDSS detected blend. Images from SDSS ($g$, $r$), 2MASS ($J$, $H$), WISE ($W1$, $W2$), UKIDSS $J$ and the DSS2 red band. Note nearby optical sources may not contribute in the WISE bands.

### 4.2.11 Summary of contamination in the excess sample and candidate M+UCDs

Similarly to my full M dwarf candidate catalogue, I cross-matched my excess sample and M+UCD candidates with both SIMBAD and LAMOST. The SIMBAD/LAMOST cross-match shows my additional cuts have successfully removed nearly all contamination from early type stars (with a slight contamination still from M dwarfs earlier than M3). This contamination from early M dwarfs is explored further in Section 4.3. Next I explored the type of objects that could give a false positive excess signal in my M+UCD candidates, this included exploring M dwarfs with discs, and contamination from chance alignments with other brown dwarfs and M dwarfs, with background M giants, with galaxies and in general for chance alignments of red objects. From this analysis I found that I can expect a contamination from chance alignments of around 3.5 per cent and no worse than ∼9.5 per cent (mostly from chance alignments with red galaxies).

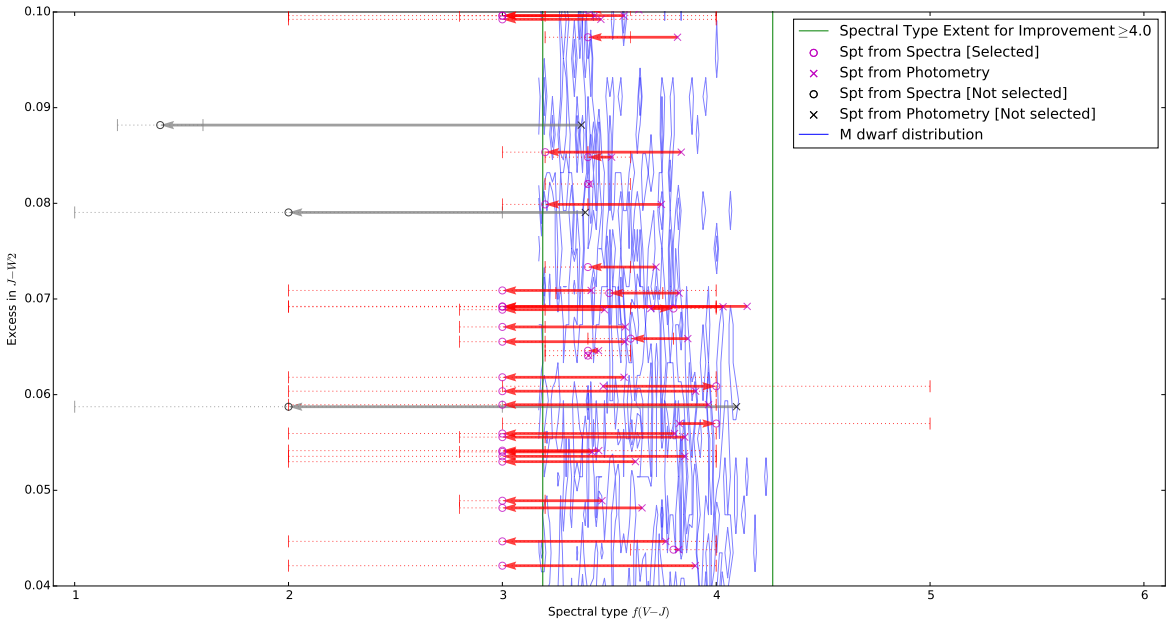


Figure. 4.10: Identification of M+UCD candidates with well measured optical spectral types conforming to my selection criteria. Any candidate was rejected from my sample if its spectral type is inconsistent with the limits expected from the excess/$(V-J)$ contours (converting the limits of the contours in excess/$(V-J)$ space into spectral type using Equation 12 from Lépine et al. (2013). Spectral types come from LAMOST DR1 and DR2 (uncertainties of $\pm 1$) or using the method by Zhong et al. (2015a) on the LAMOST DR1 catalogue (uncertainties of $\pm 0.5$, if more than one spectral type exists a weighted mean was used).

## 4.3 Using optical spectral types to reduce contamination

I obtained optical spectral types of my sample to strengthen the $T_{eff}$ constraints associated with my relative excess measurements. This has been done, in part, by exploring data from LAMOST. Provided in the LAMOST general catalogues are spectral types which quote uncertainties of $\pm 1$ spectral type, using a modified version (Luo et al., 2004) of the HAMMER code (Covey et al., 2014). I combined these with spectral types obtained using the method by Zhong et al. (2015a, uncertainties quoted at $\pm$ 0.5 spectral types), such that I used any of the spectral types available. If more than one existed I used a weighted mean (see Equation 4.28).

$$\bar{x} = \frac{\sum w_i x_i}{\sum w_i} \qquad \sigma^2_{\bar{x}} = \frac{1}{\sum w_i} \qquad w_i = \frac{1}{\sigma_i^2} \tag{4.28}$$

where $\bar{x}$ is the weighted mean, $\sigma_{x_i}$ is the uncertainties on spectral type defined above on $x_i$, and $x_i$ is an individual spectral type.

Thus I identified a sample of M+UCD candidates with well measured optical spec-

| Improvement | Excess Candidates | Has any* optical spectral type | Selected by cut |
|---|---|---|---|
| $\geq 3$ | 2,934 | 129 | 102 |
| $\geq 4$ | 1,082 | 47 | 38 |
| $\geq 5$ | 511 | 25 | 17 |
| $\geq 6$ | 269 | 16 | 12 |
| $\geq 7$ | 128 | 6 | 6 |
| $\geq 8$ | 82 | 5 | 5 |

*Any optical spectral type refers to a target either having a LAMOST dr1 or dr2 spectra type using a modified version (Luo et al., 2004) of the *Hammer* code (Covey et al., 2014) and/or a spectral type using the method by (Zhong et al., 2015a) on the dr1 catalogue.

Table 4.3: After cross-matching my candidates with LAMOST DR1 and DR2 I was able to reduce contamination by obtaining optical spectral types of my sample.

tral types, conforming to my selection criteria. The identification of unwanted M dwarfs was done by transposing the excess/$(V-J)$ contours into excess/spectral type limits (converting the limits of the contours in excess/$(V-J)$ space into spectral type using Equation 12 from Lépine et al. 2013). Figure 4.10 shows the case where I accepted any spectral type (within its associated uncertainties) which falls inside the converted contour limits. The results of this selection are shown in Table 4.3.

Of the 1,082 M+UCD candidates having colour excess in $(J-W2)$, 47 have spectral types and of which 38 are selected by my optical spectra type cut (20 per cent rejected). Figure 4.11 shows a flow diagram summarising the optical spectral type selection process.

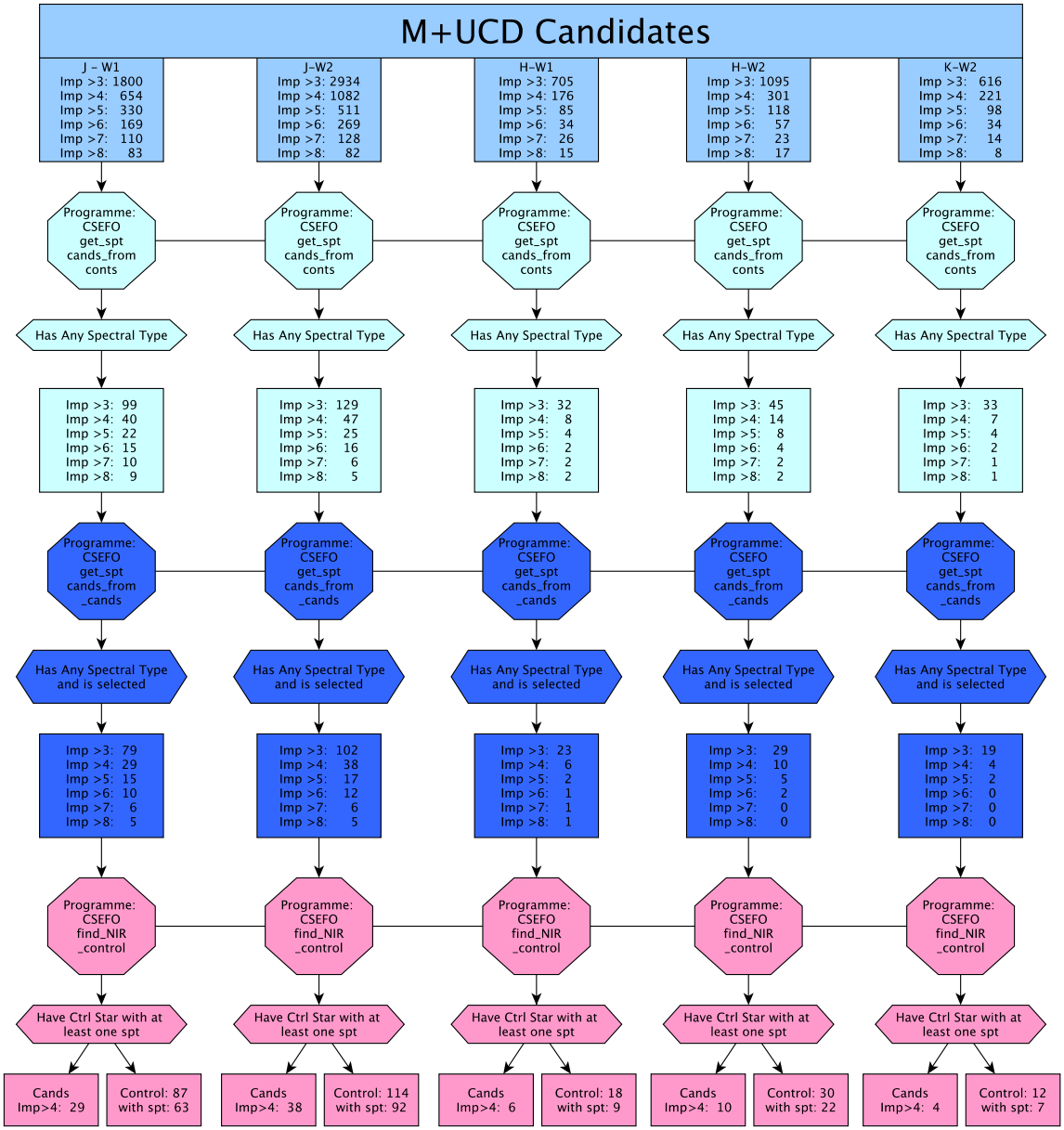


Figure. 4.11: Flow chart to summarise the optical spectral type selection process.

## 4.4 Colour-similarity applied to spectra

For this and the following sections in this chapter it is useful to define nomenclature to explain the naming conventions given to the various M dwarf, UCD and colour variant described in this chapter, these are defined in Table 4.4.

I identified a small set of colour-similar SpeX[39] spectra, within the limits of my colour-similar criteria (Equation 3.8 and the definition of PS colour from Section 3.4). I took two colour-similar M dwarfs ($M_A$ and $M_B$ ) and created simulated M dwarf+UCD systems (i.e. $M_A + UCD = M_{A[UCD]}$ ). I then subtracted them (i.e. $M_A - M_B = M_{A-B}$ and $M_{A[UCD]} - M_B = M_{A_{[UCD]}-B}$ ) and compared the residuals. This showed if the M dwarfs were "colour-similar" according to me definition (see Figure 4.12).

Two M dwarfs of similar colour and/or spectral type do not have identical spectra, due to small changes in their stellar properties (see Section 1 for a discussion on M dwarf colour scatter). To simulate this I artificially changed the colour of my M dwarfs by injecting a scale factor to each spectral pixel such that the $(J-H)$ colour changes by $\Delta(J-H)$ simulating differences due to small changes in the spectrum from differing stellar properties.

Specifically if all the colour change in $(J-H)$ was due to the J-band (the most extreme case) this scale factor becomes $1+\Delta(J-H)$ in the J-band and remains unchanged (equal to 1) everywhere else. This artificial continuum was then smoothed with a simple cubic spline and multiplied by the spectrum to create a slight variation of the original spectrum. I refer to this as a colour-variant ( i.e. a colour-variant to $M_A$ would be $M_{A[CV]}$ , see Figure 4.13). Figure 4.14 shows how this variation in colour changes an example spectrum (and its subtraction) and Figure 4.15 and Figure 4.16 show how this variation in colour changes with changing primary and companion spectral type.

I could then test whether I could detect a UCD given the change in colour by subtracting the system from a colour-variant version of the same M dwarf (i.e. $M_{A[UCD]-A[CV]} = M_{A[UCD]} - M_{A[CV]}$ ) and comparing it to a similar spectral subtraction of the lone M dwarf and a colour-variant version of the same M dwarf (i.e. $M_A - M_{A[CV]} = M_{A-A[CV]}$ ). This is analogous to a synthetic version of Figure 4.12 and can be seen in Figure 4.14.

## 4.5 Band selection

Although in some cases it was possible to determine by eye whether $M_{A[UCD]-A[CV]}$ was distinguishable from $M_{A-A[CV]}$ , I wanted a quantitative means to establish this. I

[39] SpeX Prism Spectral Libraries, maintained by Adam Burgasser at http://pono.ucsd.edu/~adam/browndwarfs/SpeXprism.

| Nomenclature | Description | Colour Variant | Binary |
|---|---|---|---|
| $M_A$ | M dwarf 1 | - | - |
| $M_B$ | M dwarf 2 | - | - |
| $M_{A[CV]}$ | A colour variant of M dwarf 1 | ✓ | - |
| $M_{B[CV]}$ | A colour variant of M dwarf 2 | ✓ | - |
| $M_{A[UCD]}$ | An unresolved system, consisting of a UCD and $M_A$ | - | ✓ |
| $M_{B[UCD]}$ | An unresolved system, consisting of a UCD and $M_B$ | - | ✓ |
| $M_{A[UCD,CV]}$ | An unresolved system, consisting of a UCD and $M_{A[CV]}$ | ✓ | ✓ |
| $M_{B[UCD,CV]}$ | An unresolved system, consisting of a UCD and $M_{B[CV]}$ | ✓ | ✓ |
| $M_{A-B}$ | The residuals after subtraction of the spectra $M_A$ and $M_B$ | - | - |
| $M_{A_{[UCD]}-B}$ | The residuals after subtraction of the spectra $M_{A[UCD]}$ and $M_B$ | - | ✓ |
| $M_{A[CV]-B}$ | The residuals after subtraction of the spectra $M_{A[CV]}$ and $M_B$ | ✓ | - |
| $M_{A-A}$ | The residuals after subtraction of the spectra $M_A$ and $M_A$ | - | - |
| $M_{A-A[CV]}$ | The residuals after subtraction of the spectra $M_A$ and $M_{A[CV]}$ | ✓ | - |
| $M_{A[UCD]-A[CV]}$ | The residuals after subtraction of the spectra $M_{A[UCD]}$ and $M_{A[CV]}$ | ✓ | ✓ |
| $M_{A[UCD]-A}$ | The residuals after subtraction of the spectra $M_{A[UCD]}$ and $M_A$ | - | ✓ |
| $M_{A[UCD,CV]-B}$ | The residuals after subtraction of the spectra $M_{A[UCD]}$ and $M_B$ | ✓ | ✓ |
| $M_{A[UCD,CV]-A}$ | The residuals after subtraction of the spectra $M_{A[UCD]}$ and $M_A$ | ✓ | ✓ |
| $M_{A[Smoothed]}$ | A version of $M_A$ where the spectrum has been smoothed by a Gaussian smoothing function | - | - |
| $M_{A[UCD,Smoothed]}$ | A version of $M_{A[UCD]}$ where the spectrum has been smoothed by a Gaussian smoothing function | - | ✓ |
| $M_{A[CV,Smoothed]}$ | A version of $M_{A[CV]}$ where the spectrum has been smoothed by a Gaussian smoothing function | ✓ | - |

Table 4.4: Naming system for synthetic systems discussed in this chapter.

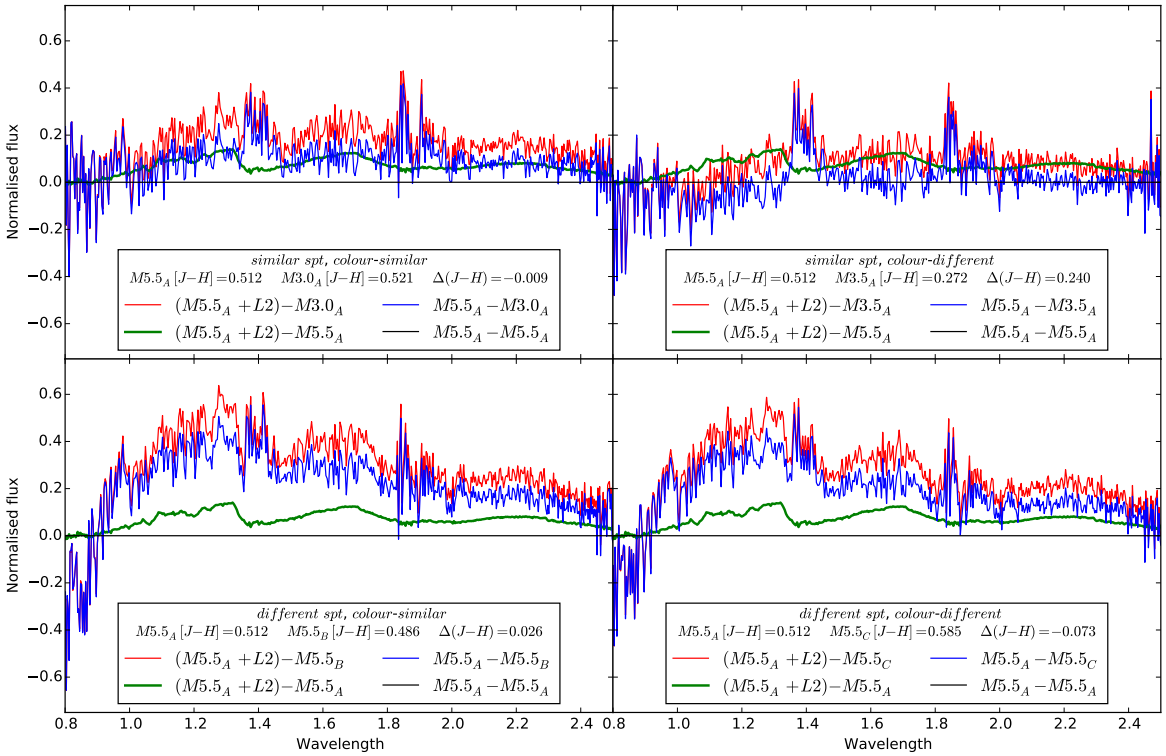


Figure. 4.12: Spectral subtractions were used to show if my definition of colour-similar M dwarfs holds for any particular M dwarf pairing. An L2 dwarf spectrum was added to the spectrum of one of the M dwarfs (i.e. $M_A + L2 = M_{A[UCD]}$ ) and then the spectrum of the other colour-similar M dwarf ($M_B$ ) was subtracted (red curve). The result was compared to the ideal case (where $M_{A[UCD]}$ was subtracted from $M_A$ , i.e. $M_{A[UCD]}$ - $M_A = M_{A[UCD]-A}$ , green curve) and the case where no UCD companion was present ($M_{A-B} = M_A$ - $M_B$ , blue curve). M dwarfs are deemed colour-similar if their difference spectrum is significantly less than my synthetic M dwarf-UCD system subtraction. All spectra were accessed from the SpeX Prism Spectral Libraries. $M5.5_A$ from Burgasser et al. (2004) and, $M3_A$, $M4.5_A$, $M4.5_B$, $M5.5_B$ and $M5.5_c$ from Kirkpatrick et al. (2010).

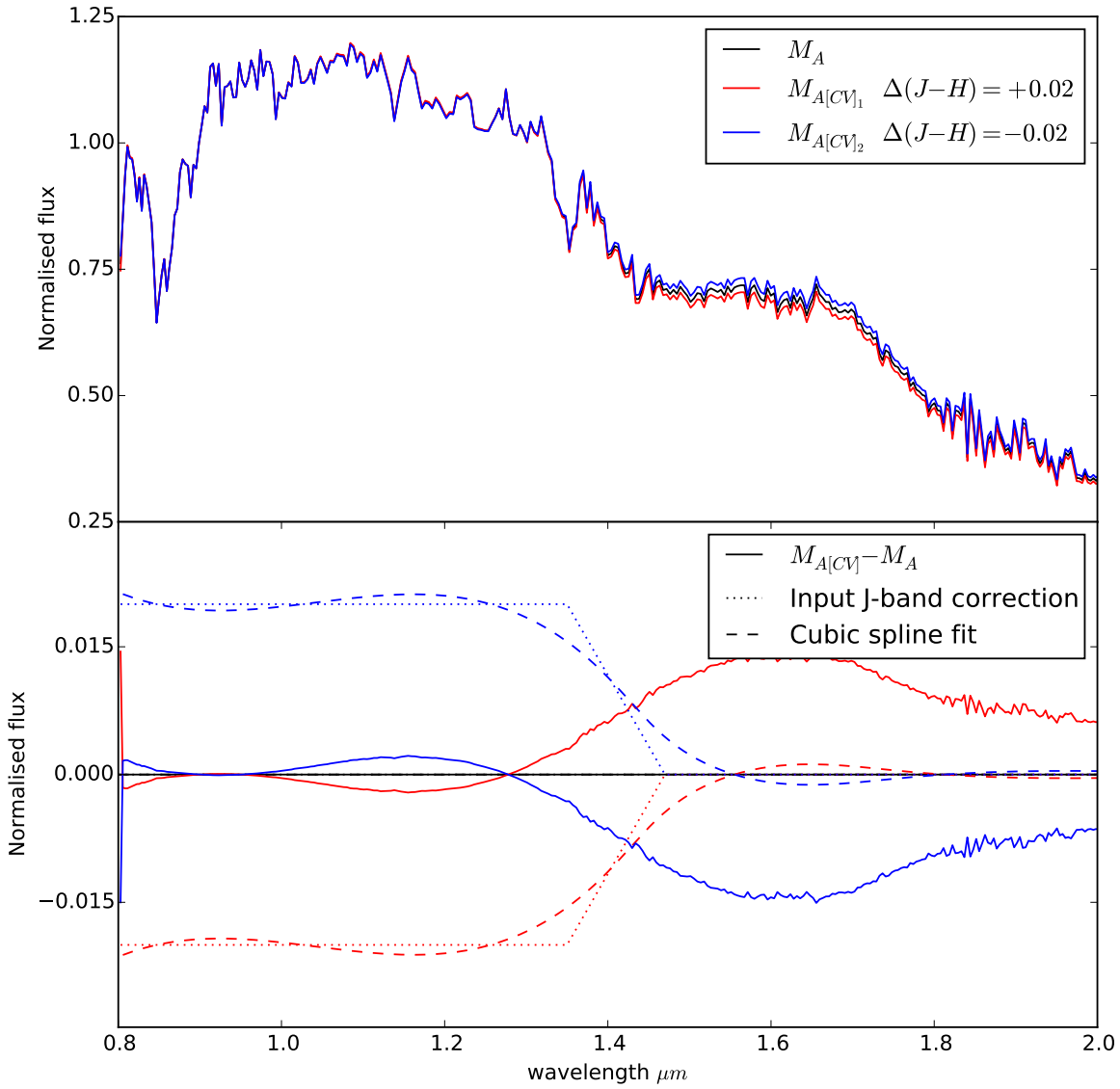


Figure. 4.13: Spectra from the SpeX Prism Spectral Libraries were modified in the J-band to simulate colour-similar spectra(top panel). Colour-variants are denoted by a $CV$ subscript (i.e. $M_{A[CV]}$ ). Spectral subtractions of the colour-variants from the original spectrum ($M_{A-A[CV]}$ ) can be seen in the lower panel (solid line) with the initial modification (dotted line) and the cubic spline fit used as the multiplicative scale factor applied to the spectrum. The original spectrum used here ($M_A$ ) is an M3.5 M dwarf (2MASS J14113696+2112471; Kirkpatrick et al., 2010).

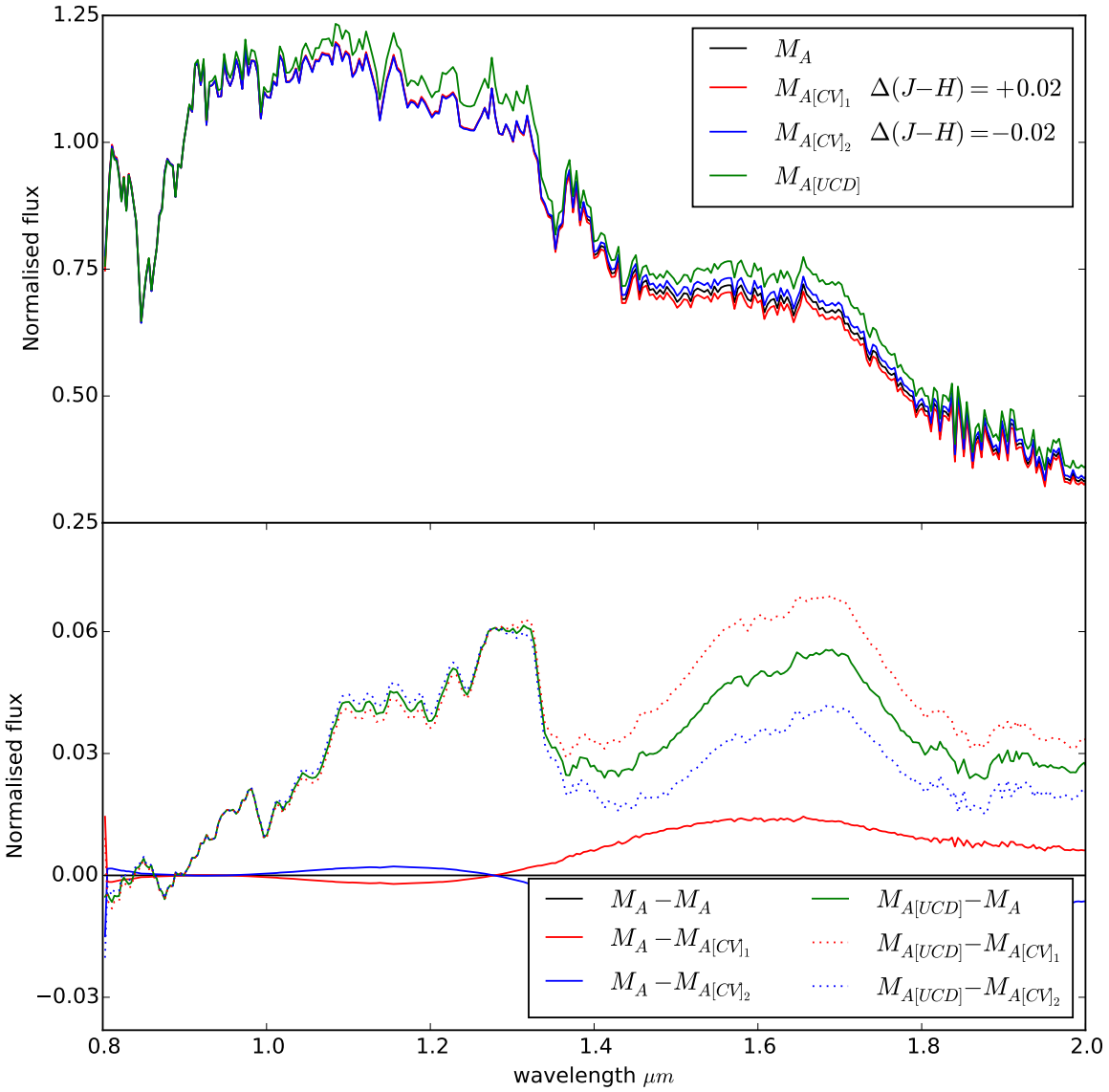


Figure. 4.14: I added a UCD to $M_A$ (i.e. $M_A$ +UCD= $M_{A[UCD]}$ ) and subtracted a colour-variant ($M_{A[CV]}$ ) to give a synthetic version of Figure 4.12 (i.e. $M_{A[UCD]} - M_{A[CV]} = M_{A[UCD]-A[CV]}$ red curve). This was compared to the ideal case (where the M dwarfs are exactly the same $M_{A[UCD]-A}$ , grey curve) and the case where there was no UCD companion present ($M_{A-A[CV]}$ , blue curve).

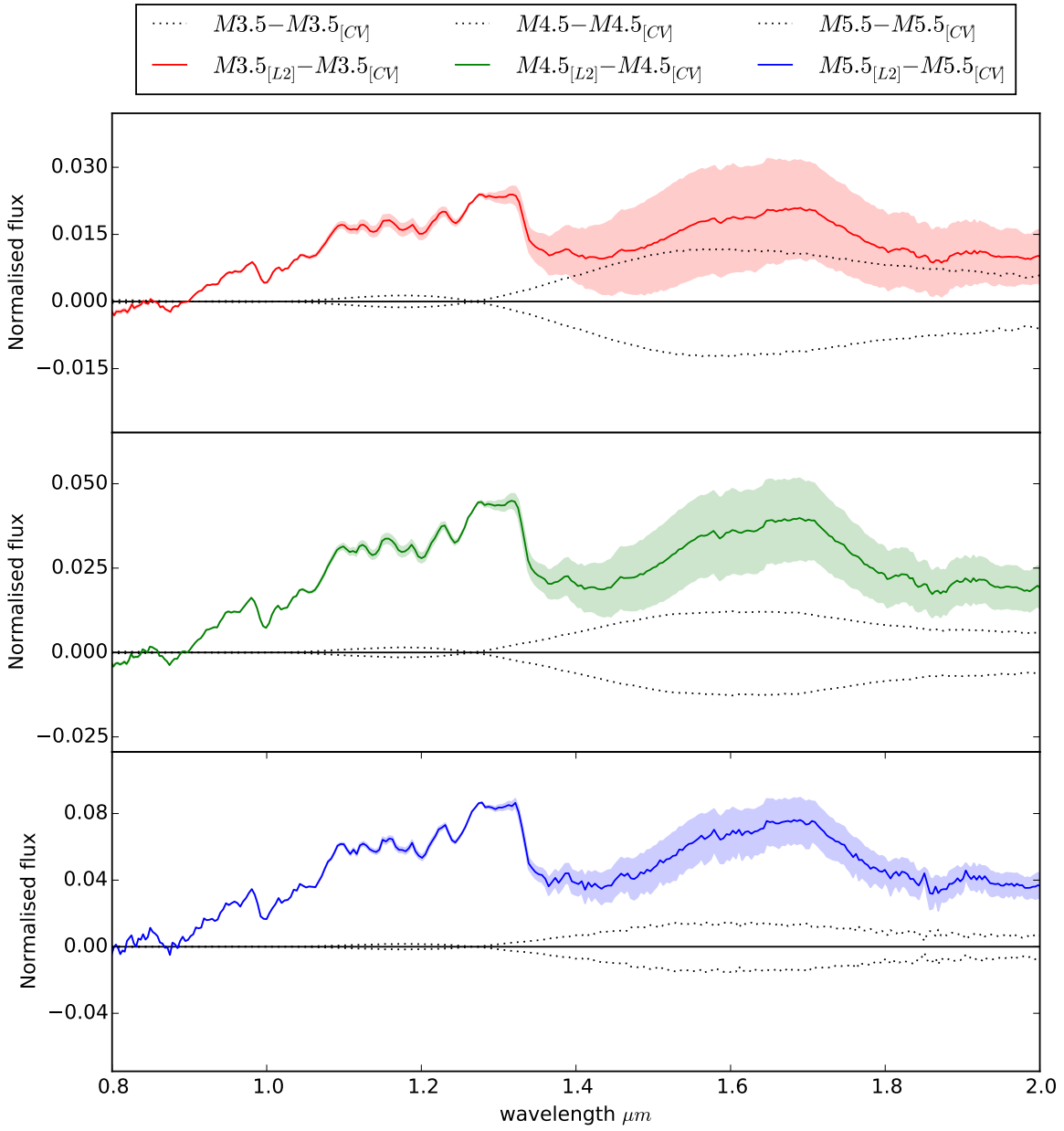


Figure. 4.15: Using my colour-variants enabled me to identify which M dwarf with UCD companions were detectable. The M3.5 is 2MASS J14113696+2112471 (Kirkpatrick et al., 2010), the M4.5 is 2MASS J12471472-0525130 (Kirkpatrick et al., 2010) and the M5.5 is 2MASS J03023398-1028223 (Burgasser et al., 2004). Spectra are from the SpeX Prism Spectral Libraries.

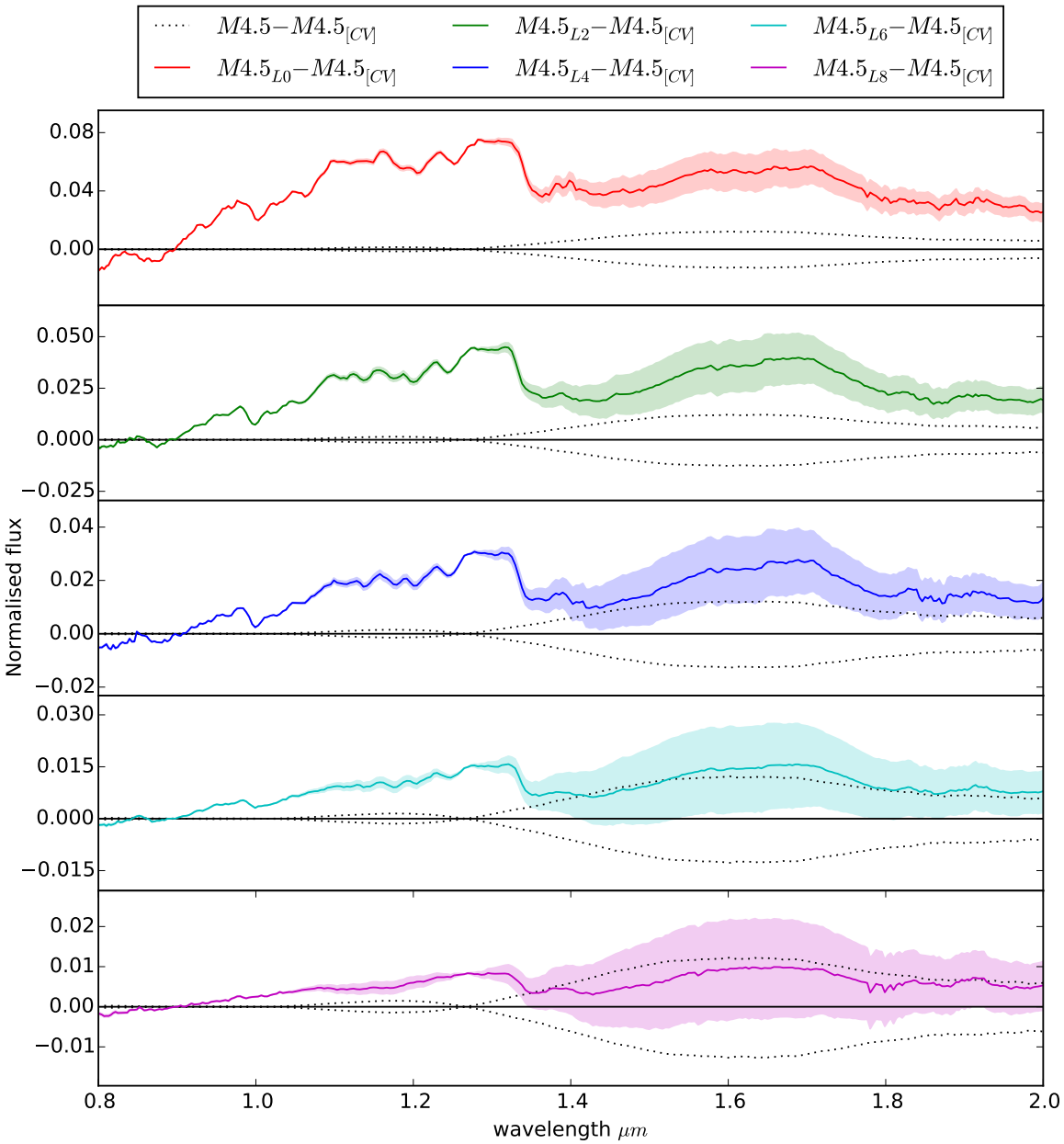


Figure. 4.16: Varying the UCD spectral type enabled me to identify which M dwarf with UCD companions were detectable; the L0 is 2MASS J03454316+2540233 (Burgasser et al., 2006b), the L2 is Kelu-1 (Burgasser, 2007b), the L4 is 2MASS J21580457-1550098 (Kirkpatrick et al., 2010), the L6 is 2MASSI J1010148-040649 (Reid et al., 2006) and the L8 is 2MASSW J1632291+190441 (Burgasser, 2007a) .Spectra are from the SpeX Prism Spectral Libraries.

| Band | $A_0$ | $A_1$ | $B_0$ | $B_1$ | ref |
|---|---|---|---|---|---|
| $H_20 - J$ | 1.140 | 1.165 | 1.260 | 1.285 | 1 |
| $CH_4 - J$ | 1.315 | 1.340 | 1.260 | 1.285 | 1 |
| $H_20 - H$ | 1.480 | 1.520 | 1.560 | 1.600 | 1 |
| $CH_4 - H$ | 1.635 | 1.675 | 1.560 | 1.600 | 1 |
| $H_20 - K$ | 1.975 | 1.995 | 2.080 | 2.100 | 1 |
| $CH_4 - K$ | 2.215 | 2.255 | 2.080 | 2.120 | 1 |
| N1 | 1.260 | 1.285 | 1.480 | 1.520 | 2 |
| N2 | 1.635 | 1.675 | 1.480 | 1.520 | 2 |
| N3 | 1.260 | 1.300 | 1.450 | 1.520 | 2 |
| N4 | 1.260 | 1.300 | 1.010 | 1.050 | 2 |
| N4* | 1.210 | 1.350 | 0.960 | 1.100 | 3 |

Table 4.5: Table of spectral bands used for UCD identification via spectral differences, spectral difference is defined in Equation 4.29. The features these spectral bands relate to can be seen in Figure 4.17. [1] From Burgasser et al. (2010). [2] Custom spectral bands based on those of Burgasser et al. (2010) selected to optimise difference spectra while avoiding known telluric features. [3] After experimentation into minimising the exposure time for observing the band was modified (see Section 4.7).

thus identified spectral bands in which the flux from $M_{A[UCD]-A[CV]}$ was different from $M_{A-A[CV]}$ and due to the presence of a UCD companion. Spectral ratios have been used to identify binaries such as brown dwarf binaries (e.g. Burgasser et al., 2010). However because I was analysing spectral subtractions, with non-detections having little-to-no flux at certain wavelengths (and hence extremely small denominators leading to large indices) I chose to use the difference in scale height between a peak and trough of a UCD's spectral features.

Using my simulated $M_{A[UCD]}$ systems, spectral bands were chosen to sample some of the strong NIR absorption features in L dwarf spectra (that also dictate the flux ratios used to aid spectral typing of L dwarfs; Burgasser et al. 2010). I define a set of spectral difference criteria that are measured using the median flux in a series of bands (see Equation 4.29). My spectral band wavelength ranges are defined in Table 4.5, which also contains the spectral typing bands from Burgasser et al. (2010) for comparison.

$$\text{Spectral difference} = f_{median}(A) - f_{median}(B) \tag{4.29}$$

where $f_{median}(X)$ is the median flux between the wavelengths $X_0$ to $X_1$ (for values see Table 4.5 and see Figure 4.17 for these plotted against UCD spectra).

From these spectral bands $N4$ (1.26 - 1.3 and 1.01 - 1.05 $\mu m$) was selected as giving the best detection results because it shows the most difference between $M_{A[UCD]-A} \pm M_{A[UCD]-A[CV]}$ and $M_{A-A} \pm M_{A-A[CV]}$. This can be seen clearly in Figure 4.18, the $N4$

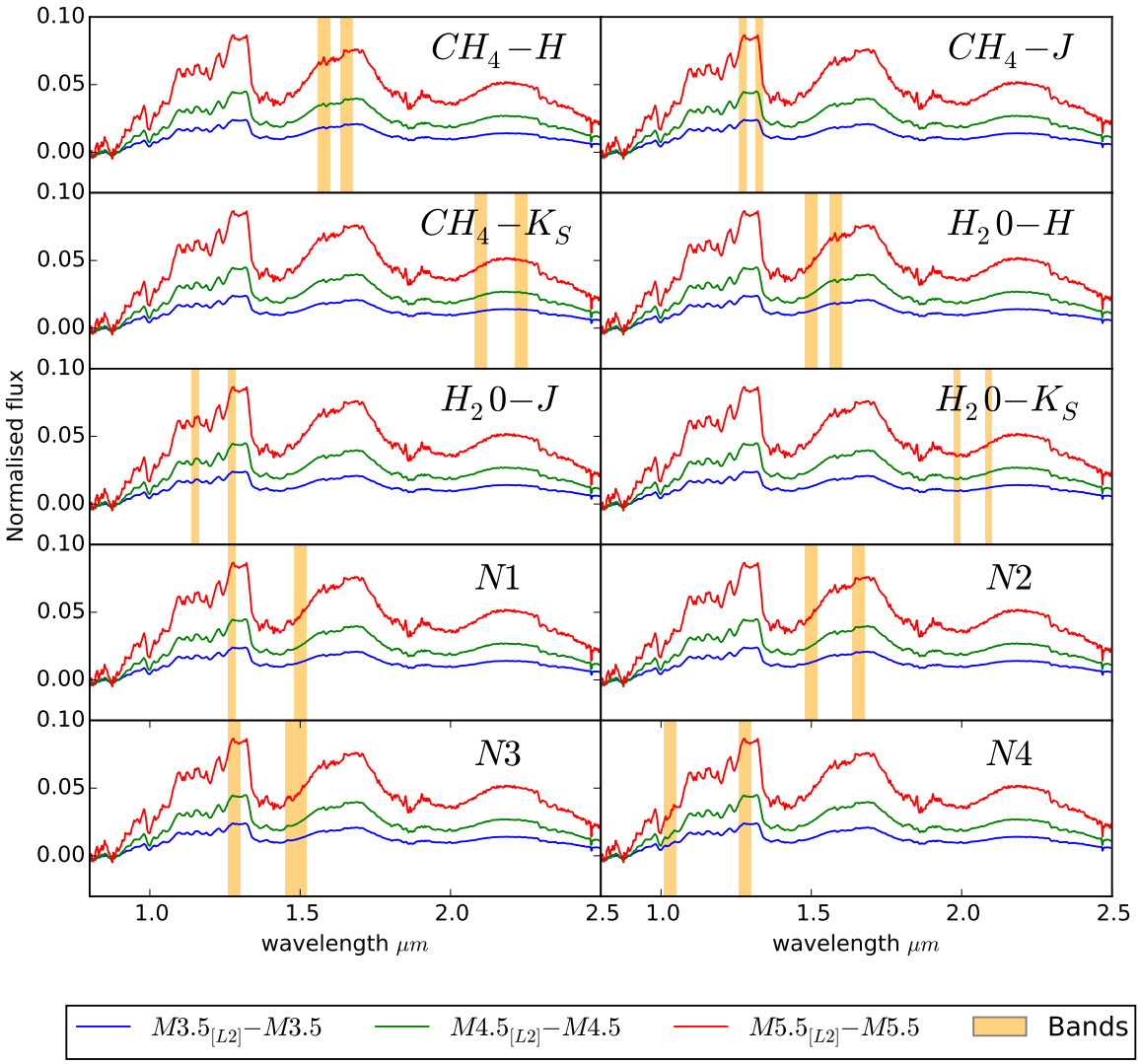


Figure. 4.17: Spectral Bands from Table 4.5. These spectral bands are compared to $M_{A[UCD]-A}$ for various M dwarf spectral types, the M3.5 is 2MASS J14113696+2112471 (Kirkpatrick et al., 2010), the M4.5 is 2MASS J12471472-0525130 (Kirkpatrick et al., 2010) and the M5.5 is 2MASS J03023398-1028223 (Burgasser et al., 2004) and the L2 is Kelu-1 (Burgasser, 2007b).

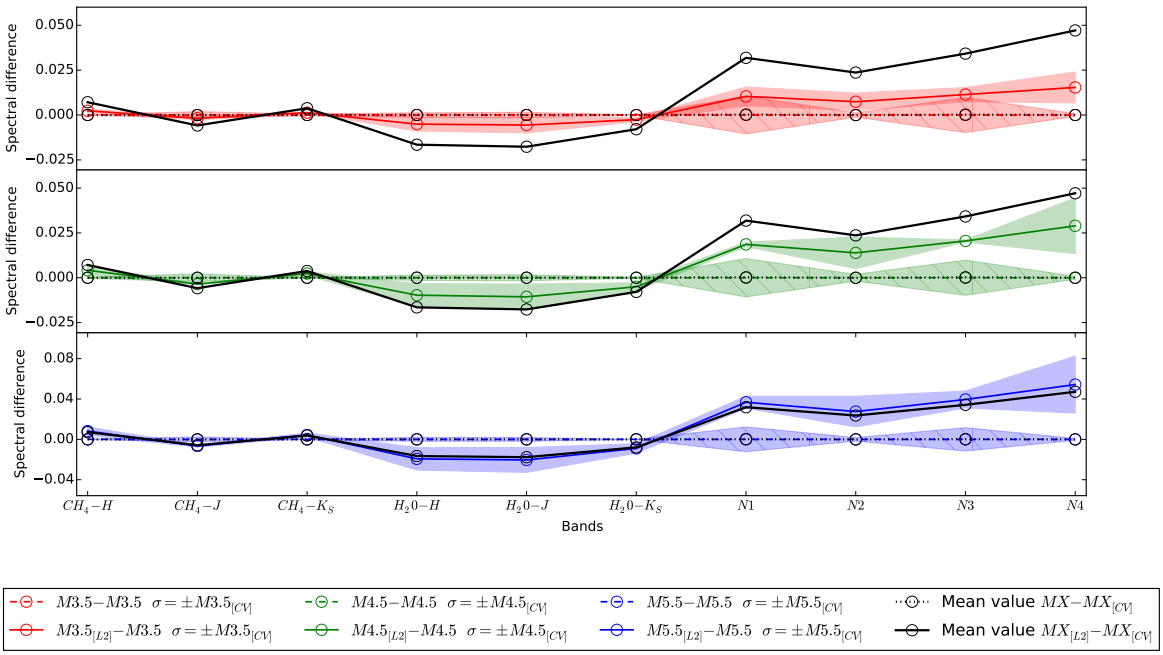


Figure. 4.18: Ideal spectral differences for the spectral bands described in Table 4.5. Solid lines are $M_{A[UCD]-A}$ with filled regions showing the maximum change when subtracting a colour-variant (i.e. $M_{A[UCD]-A[CV]}$ ). Dashed lines show $M_{A-A}$ with hash-filled regions showing the maximum change when subtracting a colour-variant (i.e. $M_{A-A[CV]}$ ). I chose spectral bands $N4$ (1.26 - 1.3 and 1.01 - 1.05 $\mu m$) because it shows the most difference between $M_{A[UCD]-A} \pm M_{A[UCD]-A[CV]}$ and $M_{A-A} \pm M_{A-A[CV]}$ . The M3.5 is 2MASS J14113696+2112471 (Kirkpatrick et al., 2010), the M4.5 is 2MASS J12471472-0525130 (Kirkpatrick et al., 2010) the M5.5 is 2MASS J03023398-1028223 (Burgasser et al., 2004) and the L2 is Kelu-1 (Burgasser, 2007b).

band is much better than the spectral typing bands from Burgasser et al. (2010) and gives the largest spectral difference across the spectral type (with the most difference for a later M dwarf, i.e. M5) thus optimising the detection I can expect from any spectral subtraction.

## 4.6 Likelihood of detection

Using the spectral differences (see Figure 4.19a) I was able to define a spectral difference detection likelihood. This was achieved by assessing how statistically different $M_{A[UCD]-A[CV]}$ was from $M_{A-A[CV]}$ , which was then compared to the ideal case (statistical difference between $M_{A[UCD]-A}$ and $M_{A-A}$ ), see Equation 4.30.

$$Likelihood = \frac{X - Y}{\sigma_{X-Y}} \qquad \sigma_{X-Y} = \sqrt{\Delta X^2 + \Delta Y^2} \tag{4.30}$$

where $X$ is the median of the $M_{A[UCD]-A}$ distribution and $Y$ is median of the $M_{A-A}$

distribution for the ideal case (e.g. the green points and black points respectively in Figure 4.19b), and $A$ is median of the $M_{A[UCD]-A[CV]}$ distribution and $B$ is the median of the $M_{A-A[CV]}$ distribution else-wise (e.g. the red points respectively and the blue points in Figure 4.19b). The $\Delta X$ and $\Delta Y$ are the standard deviations of the distributions of $X$ and $Y$ respectively.

## 4.7 Optimising band selection and observational requirements

As mentioned in Section 4.5 I used a spectral difference (Equation 4.29) to identify M dwarfs with UCD companions. I selected the two spectral bands ($A$ and $B$ from $N4$) which, given an ideal case (i.e. $M_{A[UCD]-A}$ ), gave the best spectral difference compared to the spectral subtraction of my extreme colour-variant (i.e. $M_{A-A[CV]}$ ). An example of this (for the optimal properties of the SpeX Spectra) can been seen in Figure 4.19a. I thus investigated how changing:

1. The SNR
2. The width of each spectral band ($\gamma$, $X_{new,0} = X_{old,0} - \Delta\gamma$, $X_{new,1} = X_{old,1} + \Delta\gamma$)
3. The resolution ($\delta\lambda/\lambda$) of the spectrum
4. The spectral type of the primary ($M3.5 - M5.5$)
5. The spectral type of the secondary ($L0 - L6$)

affected my likelihood results. Using these simulations I constrained the optimum (a $\sim 5\sigma$ detection) and the minimum (a 2-3$\sigma$ detection) requirements needed for observation.

These likelihoods were then plotted against each of the variations (SNR, width, resolution, primary and secondary spectral type). The iterations can be seen in Figure 4.20a-Figure 4.24a for each variation respectively comparing the optimal 3-5$\sigma$ detection.

Parameters were chosen as the minimum required to achieve a $\sim$2-3$\sigma$ detection while giving the shortest possible telescope exposure time (i.e. combination of low SNR and low resolution). My simulations show I require at least a SNR 125 and a $\delta\lambda/\lambda > 20$.

Increasing the SNR can be achieved by reducing the resolution (via binning up the pixels and applying a Gaussian smoothing function) and increasing my bandwidth by a maximum of $\delta\gamma = \pm 0.05\mu m$, corresponding to new spectral bands $N4^* \equiv$ 1.21 - 1.35 and 0.96 - 1.10 $\mu m$. The spectral difference plot for these parameters can be seen in Figure 4.19b and the likelihood plots for these parameters can be seen in Figure 4.20b-Figure 4.24b.

The results for the optimal and minimal cases are presented in Table 4.6

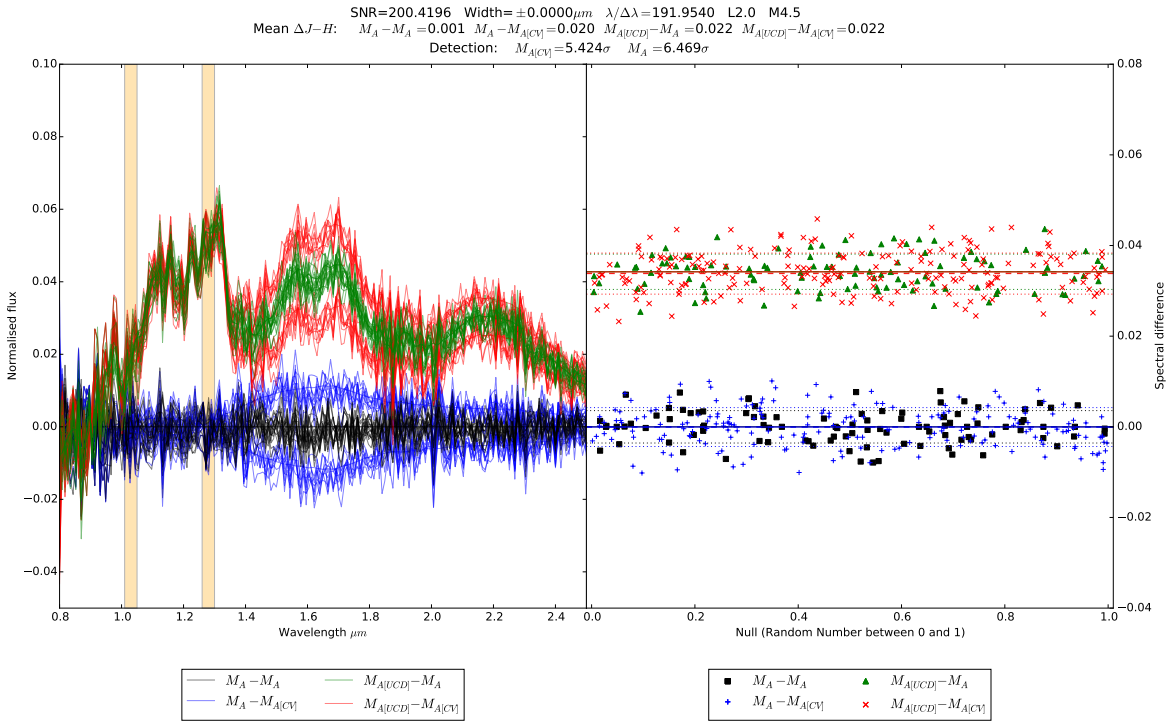


(a)

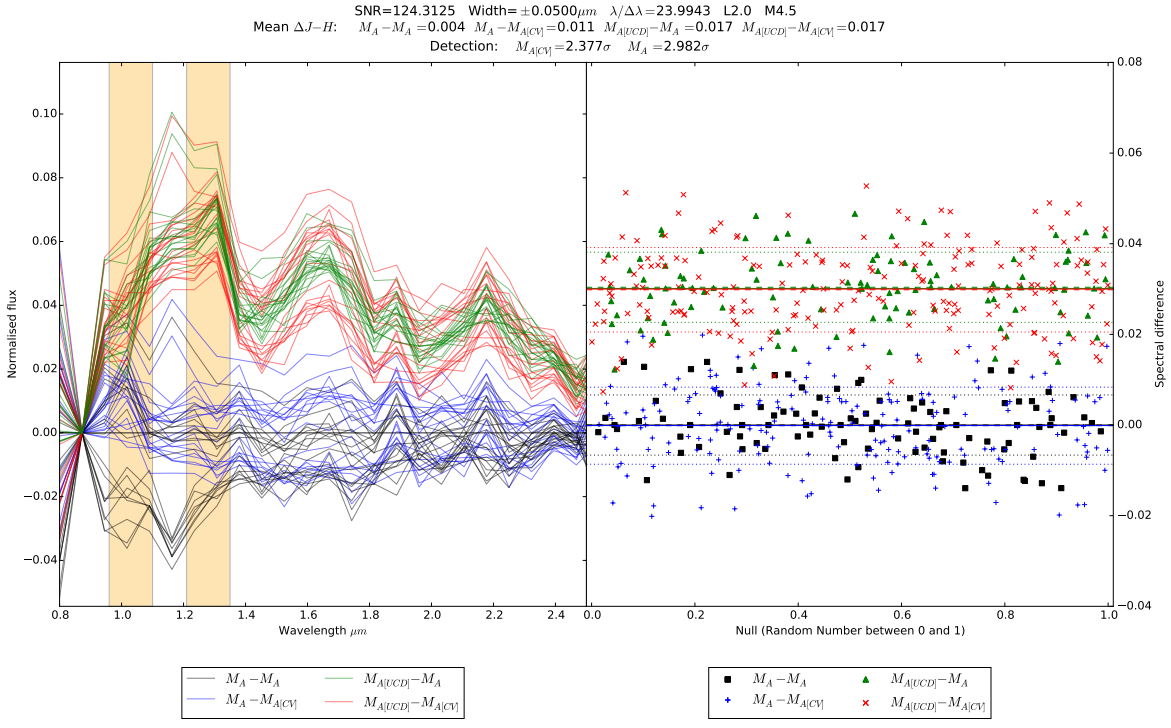


(b)

Figure. 4.19: (a) Spectral difference plot, left panel is the spectral subtractions ($M_{A-A}$, $M_{A[UCD]-A}$, $M_{A-A[CV]}$, and $M_{A[UCD]-A[CV]}$) for various noise-variants and colour-variants. Right panels shows the calculated spectral difference for each distribution (Equation 4.29). The parameters of SNR, width of the spectral band, resolution, L dwarf spectral type and M dwarf spectral type are shown above each figure. Mean colours were calculated for the four distributions and likelihoods were calculated as in Equation 4.30. (b) Parameters were chosen as the minimum required to achieve a $\sim 2\sigma$ detection while giving the shortest possible exposure time (lower SNR).

| Case | SNR | $\delta\gamma$ | $\delta\lambda/\lambda$ | M dwarf | UCD | Ideal detection | Colour-variant detection |
|---|---|---|---|---|---|---|---|
| | $\mu$m | | | | | $\sigma$ | $\sigma$ |
| Optimal | 200 | 0.00 | 200 | M4.5 | L2.0 | 6.47 | 5.42 |
| Minimal | 125 | 0.05 | 25 | M4.5 | L2.0 | 2.98 | 2.38 |

Table 4.6: Results for the likelihood optimal (3-5$\sigma$) observation conditions and the minimal (2-3$\sigma$) observation conditions required. Where $\delta\gamma$ is width added to the $N4$ spectral band and $\delta\lambda/\lambda$ is the spectral resolution.

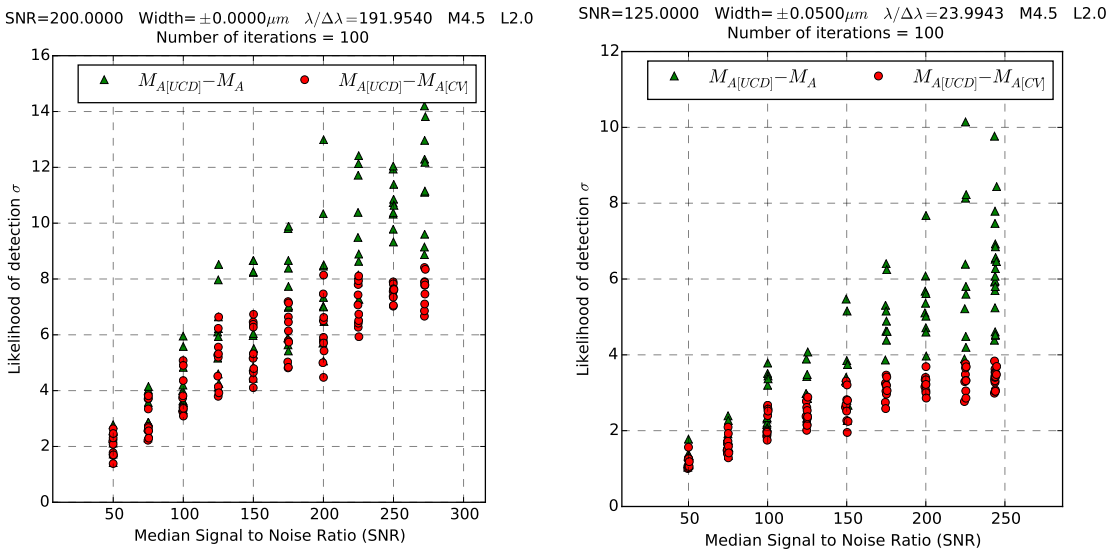


(a) (b)

Figure. 4.20: How likelihood of detection changes across simulated SNR, for (a) ideal case (b) minimal case. Green triangles are the ideal case ($M_{A[UCD]-A}$) and red circles are the simulated colour-variants ($M_{A[UCD]-A[CV]}$). The spectral difference simulation process was repeated multiple times for each set of parameters (SNR, Width, resolution and primary/secondary spectral type) to minimise over-favourable noise and colour-variant situations.

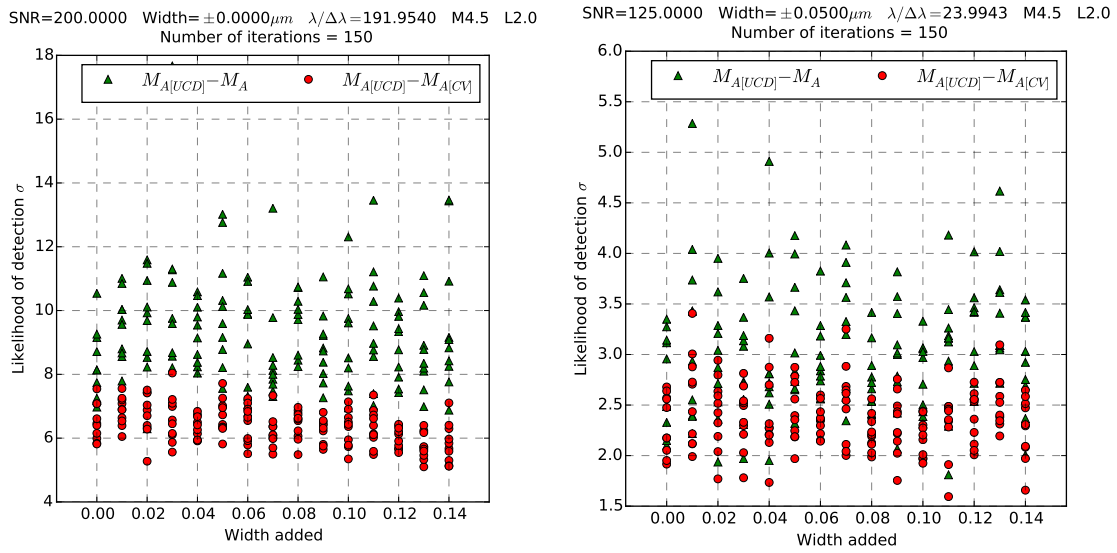


(a) (b)

Figure. 4.21: Same as Figure 4.20, but for likelihood of detection with increasing width.

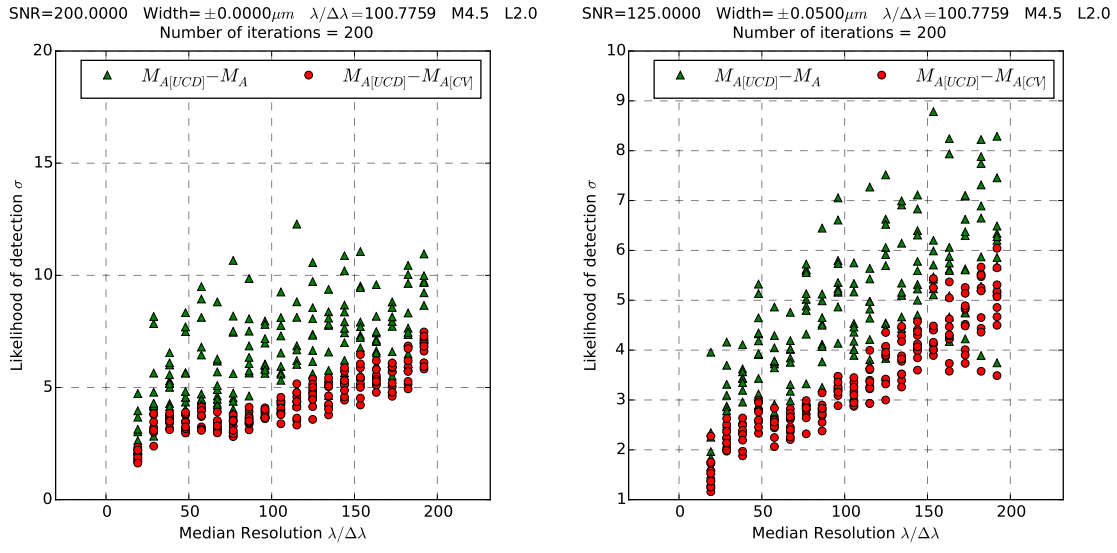


(a) (b)

Figure. 4.22: Same as Figure 4.20, but for likelihood of detection changes across resolution.

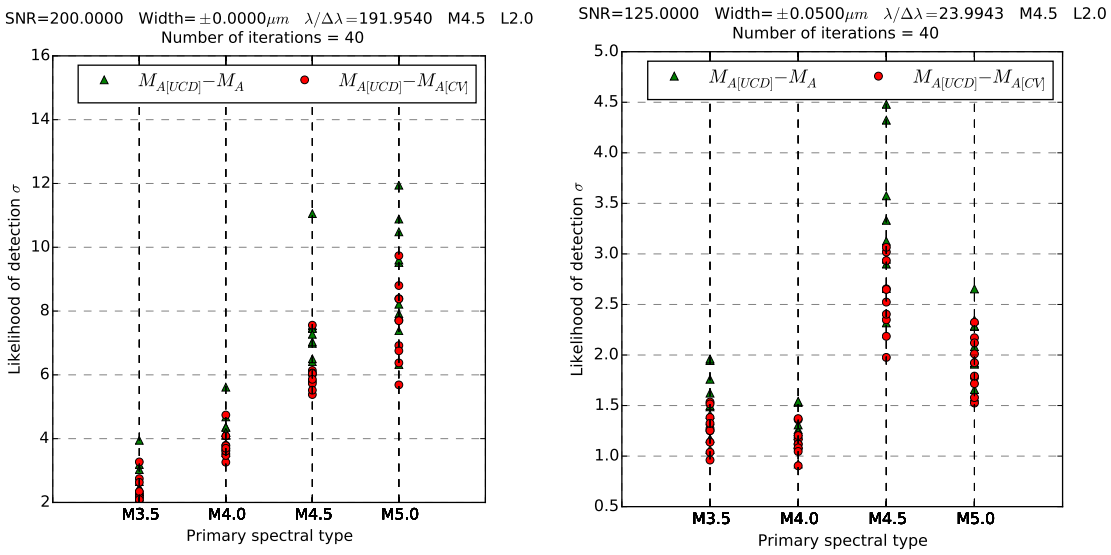


(a) (b)

Figure. 4.23: Same as Figure 4.20, but for likelihood of detection changes with primary spectral type.

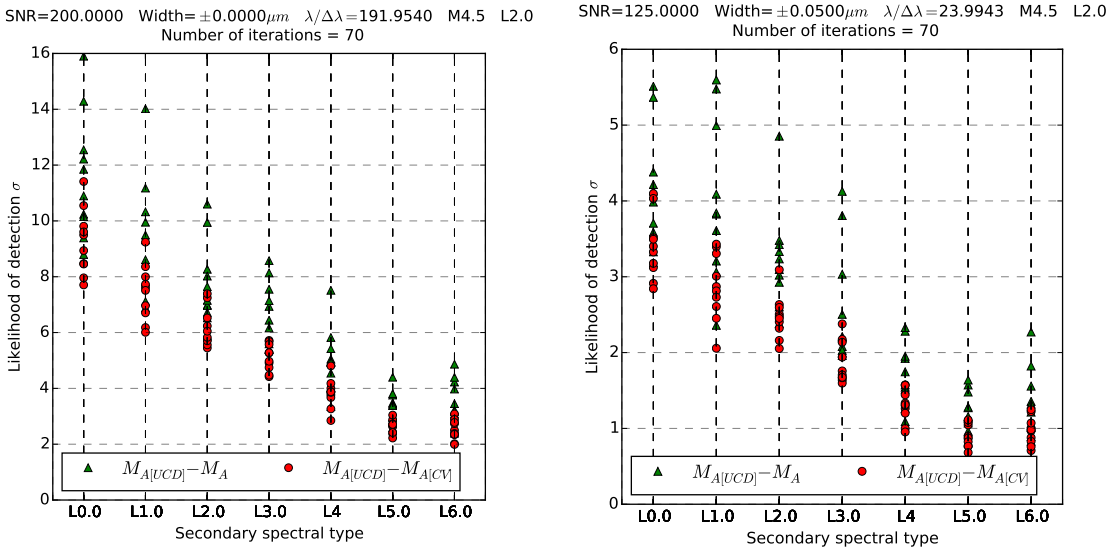


(a) (b)

Figure. 4.24: Same as Figure 4.20, but for likelihood of detection changes with secondary spectral type.

## 4.8 Application to real colour-similar cases

The SpeX Spectral Library contains some colour-similar M dwarf (colour similar defined in Equation 3.8), such that I can apply this process to unmodified spectra (i.e. no UCD or colour-variation added), hereafter I refer to these as 'real' spectra with my test M+UCD candidates identified as $M_A$ and its colour-similar M dwarf identified as $M_B \equiv M_{A[CV]}$. I approached the real spectra in a identical manner to the simulations. First I smoothed the spectra,

$$M_{A[UCD,Smoothed]} = gf(M_{A[UCD]}) \text{ and } M_{A[CV,Smoothed]} = gf(M_{A[CV]}) \tag{4.31}$$

where $gf$ represents a Gaussian smoothing function to a resolution of $\delta\lambda/\lambda \approx 20$.

The noise of each spectra was gauged by the residuals of my real spectrum and its smoothed spectrum (i.e. $Noise = |M_{A[UCD,Smoothed]} - M_{A[UCD]}|$). Creating noise-variants led to the same set of spectra I had for the simulated case ($M_{A-A}$, $M_{A[UCD]-A}$, $M_{A-A[CV]}$, and $M_{A[UCD]-A[CV]}$) but where:

$$M_{A-A} \equiv M_{A[UCD]} \text{ and } M_{A-A[CV]} \equiv M_{A[UCD]-A[CV]} \tag{4.32}$$

I then repeated the spectral difference process. The spectral differences can be seen in Figure 4.25a and shows neither $M_A$ or $M_B$ have a UCD companion (unsurprisingly). This was then repeated for the case where $M_A$ was given an artificially injected UCD companion (Figure 4.25b). From Figure 4.25a and Figure 4.25b it can be seen the colour differences in $M_A$ and $M_{A[CV]}$ lead to a $\sim$0.04 gap between $M_{A-A}$ and $M_{A[UCD]-A}$. However, looking at Figure 4.25 a UCD companion is still clearly seen by another gap in addition to the $\sim$ 0.04 gap. Thus this shows subtracting the colour-similar still achieved a likelihood of detection of $\sim 4\sigma$.

The application to real colour-similar cases has shown that this method can indeed work, if the spectra are colour-similar enough. It also highlights the importance of obtaining more than one colour-similar non-M+UCD candidate, these are needed to define a baseline (that may be non-zero due to the differences in colour). Therefore for any observations I require three of these colour-similar "control" stars in order to confirm a UCD companion around each of my M+UCD candidates.

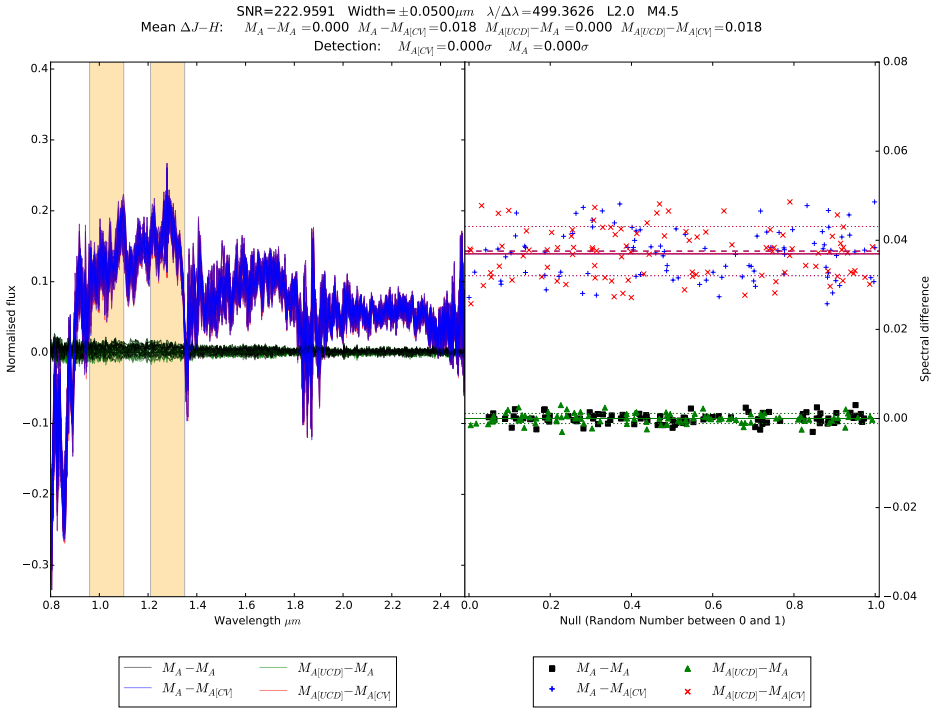


(a)

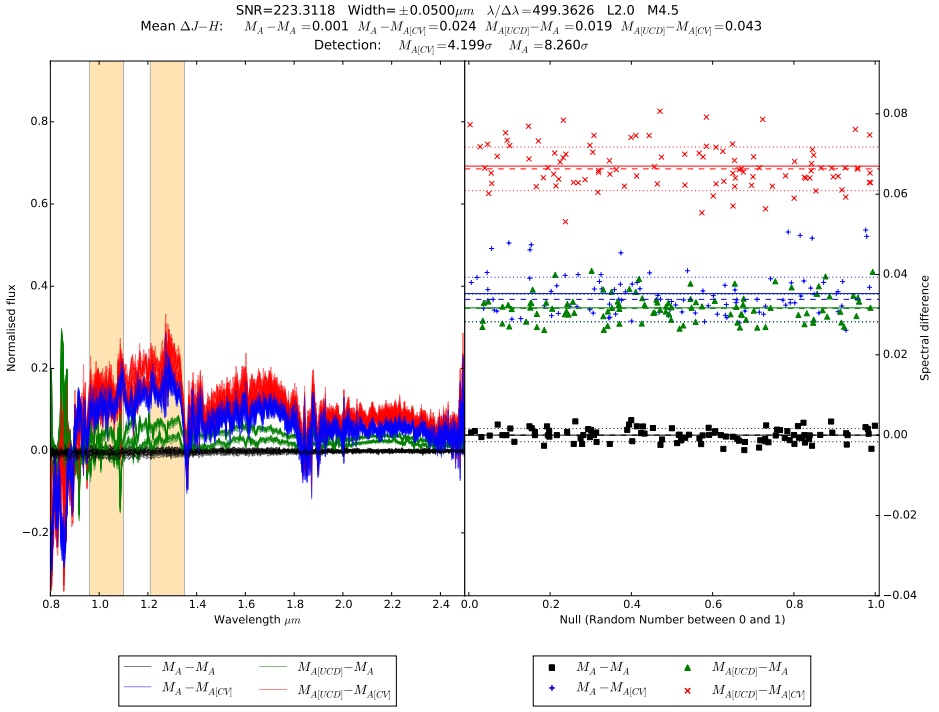


(b)

Figure. 4.25: As Figure 4.19 (a) for SpeX spectra which are colour similar, with no UCD or colour-variation added thus this should return a zero sigma detection. $M_A$ is 2MASS J12471472-0525130, ($spt$ = $M4.5$) and $M_{A[CV]}$ is 2MASS J23343735-1646042, $spt$ = $M3.5$ (b) for SpeX spectra which are colour similar, with no colour-variation added but with a UCD companion added to $M_A$ . The gap between $M_{A-A}$ and $M_{A[UCD]-A}$ is due to colour differences between $M_A$ and $M_{A[CV]}$ , however this does not affect the detection of the UCD companion ($M_{A[UCD,CV]}$ compared to $M_{A-A[CV]}$ ). $M_A$ is 2MASS J12471472-0525130, $spt$ = $M4.5$, and $M_{A[CV]}$ is 2MASS J23343735-1646042, $spt$ = $M3.5$.

## 4.9 Summary of follow-up to the unresolved UCD companions to M dwarfs

To confirm my large number of M+UCD candidates, follow-up was required that used as little observational resources as possible. The first step was to gauge contamination levels (with SIMBAD and LAMOST) of the excess sample and M+UCD candidates (found to be minimal other than a slight contamination from early M dwarfs). I developed a new method to use spectral bands (selected to target spectral features of UCDs) to identify a UCD signature in the residuals of two very similar M dwarfs. The idea was that if I select an M dwarf which was deemed not to have a UCD and deemed similar to a M+UCD candidate the residual should contain some noise (the result of the slight difference between the M dwarfs) and the UCD spectrum (albeit much fainter than either of the M dwarfs). I experimented with difference band selection and developed a procedure to optimise the observational requirements such that a detection was possible with the minimum time needed on a telescope. Using simulations different SNR, resolution, primary and secondary spectral type, and band width of the spectral bands was tested and optimum and minimum constraints were found. This was then tested with real M dwarf and UCD spectra (combined synthetically) and thus verified as a plausible follow-up approach.

# Chapter 5: Further uses for the M dwarf Catalogue

## 5.1 Introduction

In chapters 2, 3 and 4 I have shown that the selection process used to generate my catalogue created a robust (with low levels of contamination) sample of M dwarfs. I have therefore advanced the study of this sample beyond the initial idea to identify unresolved M+UCD binaries. Using spectroscopic data (from LAMOST), light curves (from Kepler 2) and further analysis of the proper motions (included in my catalogue), I have created samples of M dwarfs that should be predominantly; young (Section 5.2), late (Section 5.3), and members of wide multiple systems (Section 5.4 and Section 5.5). Such sub-samples have useful application, which will also be discussed in the following sections.

## 5.2 Finding Young M dwarfs

Young M dwarfs have become a hot topic in astronomy due to their use for studying the formation, evolution and habitability of exoplanets. The age range 10 - 100 $Myr$ coincides with the age when giant planet formation is thought to end and when terrestrial planet formation is active (Mandell, 2007; Ida & Lin, 2008; Shkolnik et al., 2009) . Young M dwarfs are also good candidates for direct imaging as any substellar object will also be young and thus more luminous than at older ages.

As mentioned briefly in Section 4.2.4 young M dwarfs are also more likely to have discs and therefore are extremely interesting for describing disc formation and evolution and their ties to planet formation (e.g. the actively accreting K7 star TW Hydra Henize 1976; Rucinski & Krautter 1983; de la Reza et al. 1989). It is even possible to look for warps and clearings in discs and infer hidden planets (e.g. Facchini et al. 2014).

As mentioned in Section 1.2.3 young M dwarfs are also more active and can be rotating much faster than their older counterparts. I focus on H$\alpha$ and rapid rotation as signatures of youth in the M dwarf population.

### 5.2.1 Using LAMOST spectra to measure pseudo-equivalent widths

After cross-matching with the second internal LAMOST data release I had 10,591 M dwarfs from my full M dwarf candidate catalogue which had LAMOST optical spectra (see Figure 5.1), this enabled me to analyse optical spectral features of my M dwarfs.

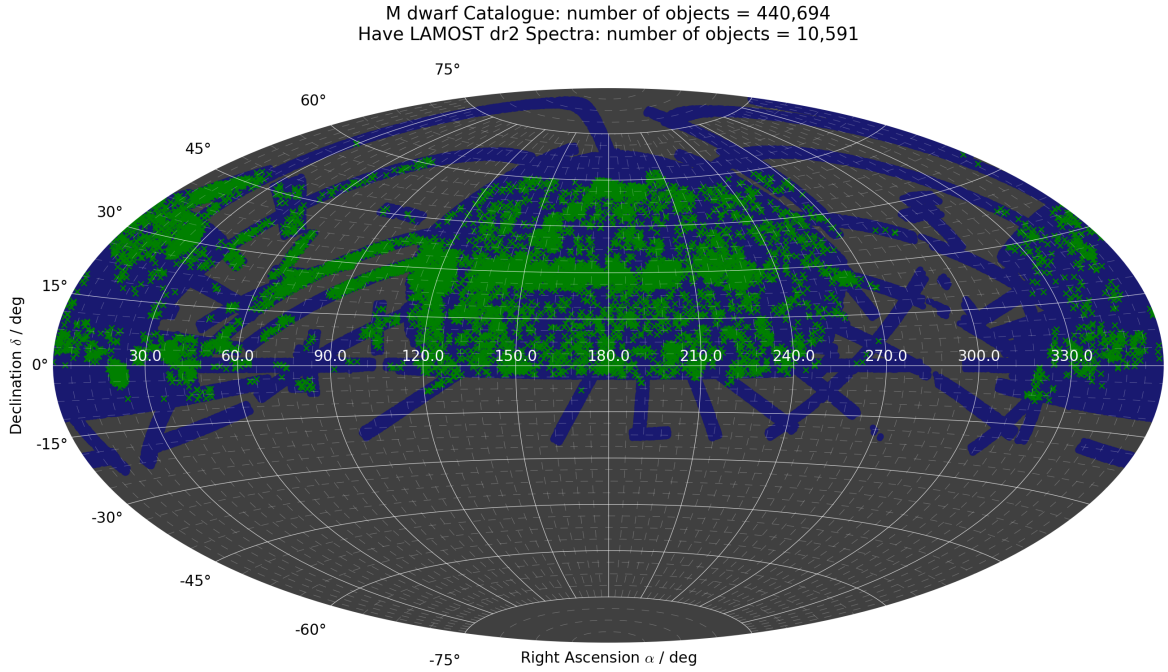


Figure. 5.1: The on sky distribution of my full M dwarf candidate catalogue (blue) and those that cross-match with the second LAMOST spectroscopic catalogue internal data release (green).

Due to the low resolution and SNR of the LAMOST spectra (see Figure 5.2) I decided to use pseudo-equivalent widths[40] (see Figure 5.3, Equation 5.1 and Equation 5.2) to compare the strengths of H$\alpha$ and NaI (H$\alpha$ due to its use as a youth indicator and NaI to make sure the H$\alpha$ detection isn't just from noise).

$$EW = \frac{A}{I} = \int_{\lambda_1}^{\lambda_2} \left( \frac{F_c - F_\lambda}{F_c} \right) d\lambda \tag{5.1}$$

$$EW = h_\lambda \sum_{j=1}^{N} \left[ 1 - \frac{F_j}{F_c} \right] \tag{5.2}$$

where $F_c$ is the relative flux of the continuum, $F_\lambda$ is the relative flux of the spectral line, $F_j$ is the relative flux of pixel j; $\lambda_2$, $\lambda_1$ are the upper and lower limits of the observed line, and $h_\lambda$ is the width of each spectral pixel. I take the definition of the continuum to be a straight line fit to the values of the flux in the continuum bands defined by Terrien et al. (2015) for NaI and Bell et al. (2012) for H$\alpha$ and take $F_j$ between the feature bands (see Table 5.1). By this definition absorption features are positive and emission features (i.e. H$\alpha$ ) will give a negative value. Uncertainties are calculated using the

[40] pseudo-equivalent widths because one uses a fit across the averaged continuum.
[41] Adapted from http://astronomy.swin.edu.au/cosmos/E/Equivalent+Width

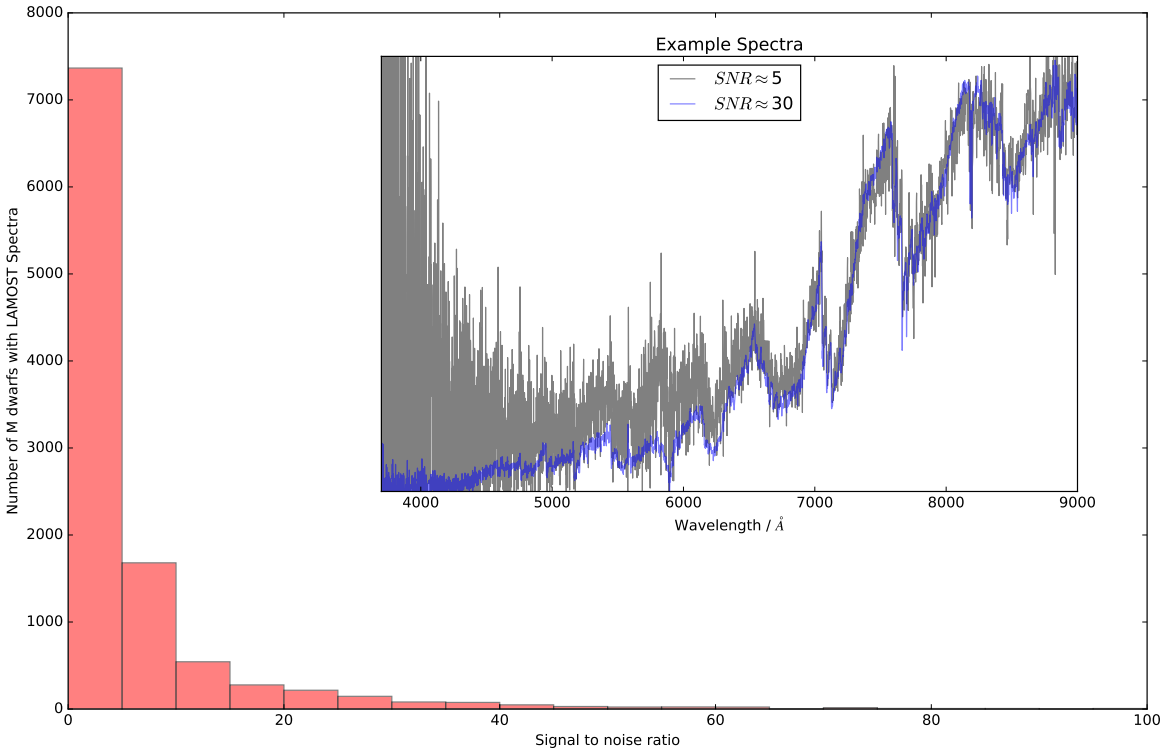


Figure. 5.2: Comparison of LAMOST SNR in the SDSS g band. Inset is an example of a SNR 5 and 30 object for comparison.

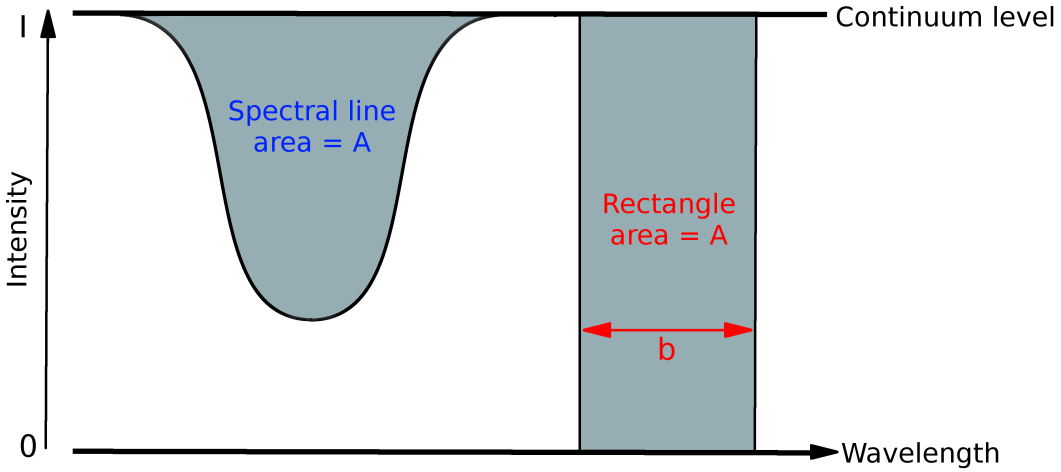


Figure. 5.3: The area, $A$, of a spectral feature below a defined continuum level is equivalent to a rectangle of width $b$ and height $I$ such that $A = I \times b$. Equivalent width is defined as $b$ and the continuum, $F_c$ is at $I$, figure adapted from the web[41].

| line | feature Å | continuum (lower) Å | continuum (upper) Å |
|---|---|---|---|
| NaI | 8175 - 8209 | 8149 - 816.9 | 8224 - 8244 |
| H$\alpha$ | 6555.5 - 6570 | 6498 - 6548 | 6573 - 6623 |

Table 5.1: The continuum and spectral line band definitions by Terrien et al. (2015) for NaI and Bell et al. (2012) for H$\alpha$.

uncertainties from the spectrum $\sigma_j$, uncertainties in the continuum ($\sigma_c$, the standard deviation of the difference in the fit value and the flux values in the continuum) and the uncertainties in the equivalent width ($\sigma_{EW}$) are thus propagated using the standard uncertainty formula.

I then calculated the equivalent width for all my M dwarfs with LAMOST spectra for both H$\alpha$ and NaI. In Figure 5.4 I show a detection of the H$\alpha$ emission feature compared to a non-detection of H$\alpha$ (non-detection defined as one consistent with zero) and in Figure 5.5 I show the detection and non-detection of the NaI absorption feature.

After the process of calculating equivalent widths was completed (possible for 10,454 of the 10,591 LAMOST spectra) I plotted the equivalent width of H$\alpha$ against the equivalent width of NaI. I select all objects which have a detection of both H$\alpha$ and NaI of greater than three times the uncertainties and following the selection of Zapatero Osorio et al. (1998) of young objects having an equivalent width of less than -3 (this is shown for my distribution in Figure 5.6). This left a total of 577 M dwarfs with H$\alpha$ and thus the possibility of youth.

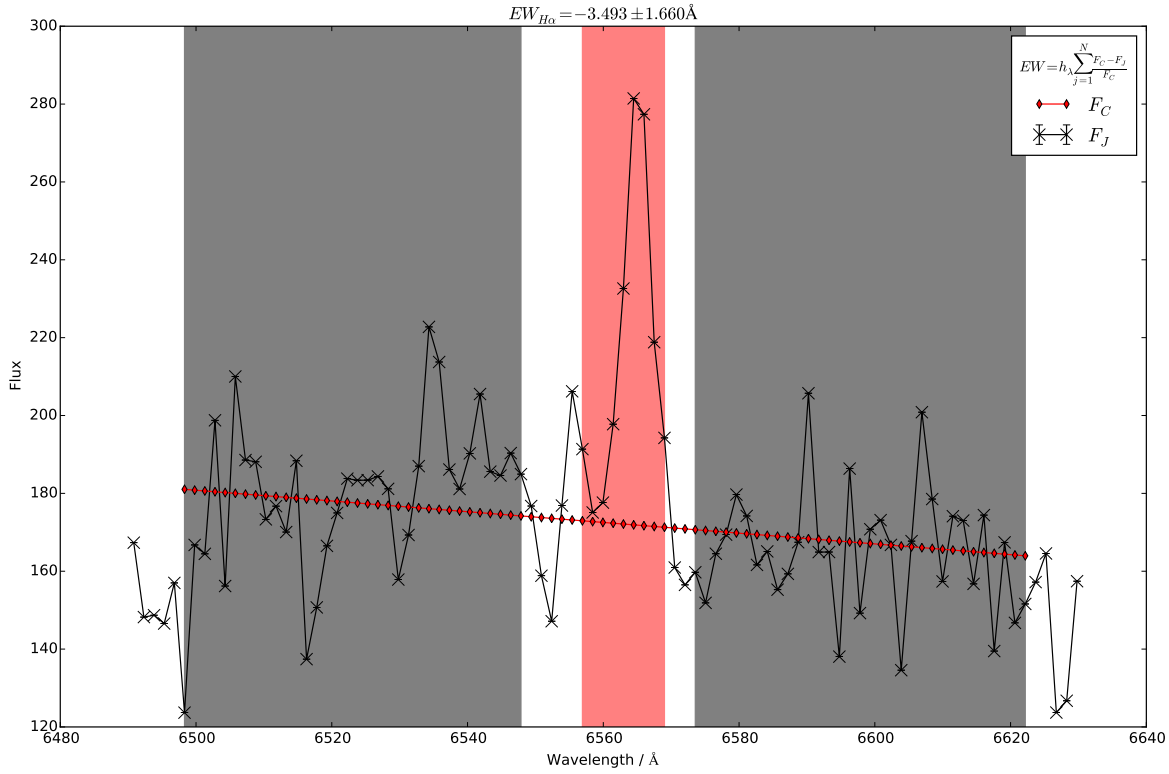


(a)

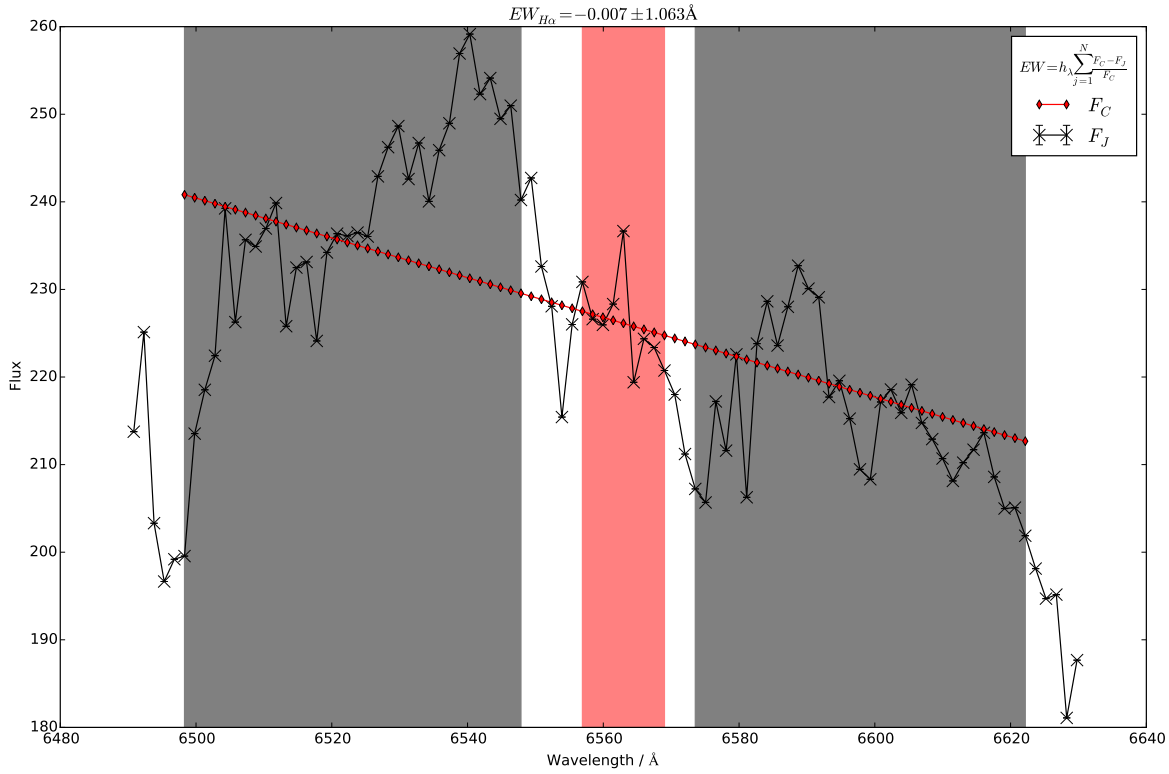


(b)

Figure. 5.4: A comparison between a detection of (a) a H$\alpha$ emission feature and (b) a non-detection of H$\alpha$ for two of my M dwarfs which had LAMOST spectra. The continuum bands are shown in grey and the feature band is shown in red. The linear fit is the continuum fit between the values in the continuum bands.

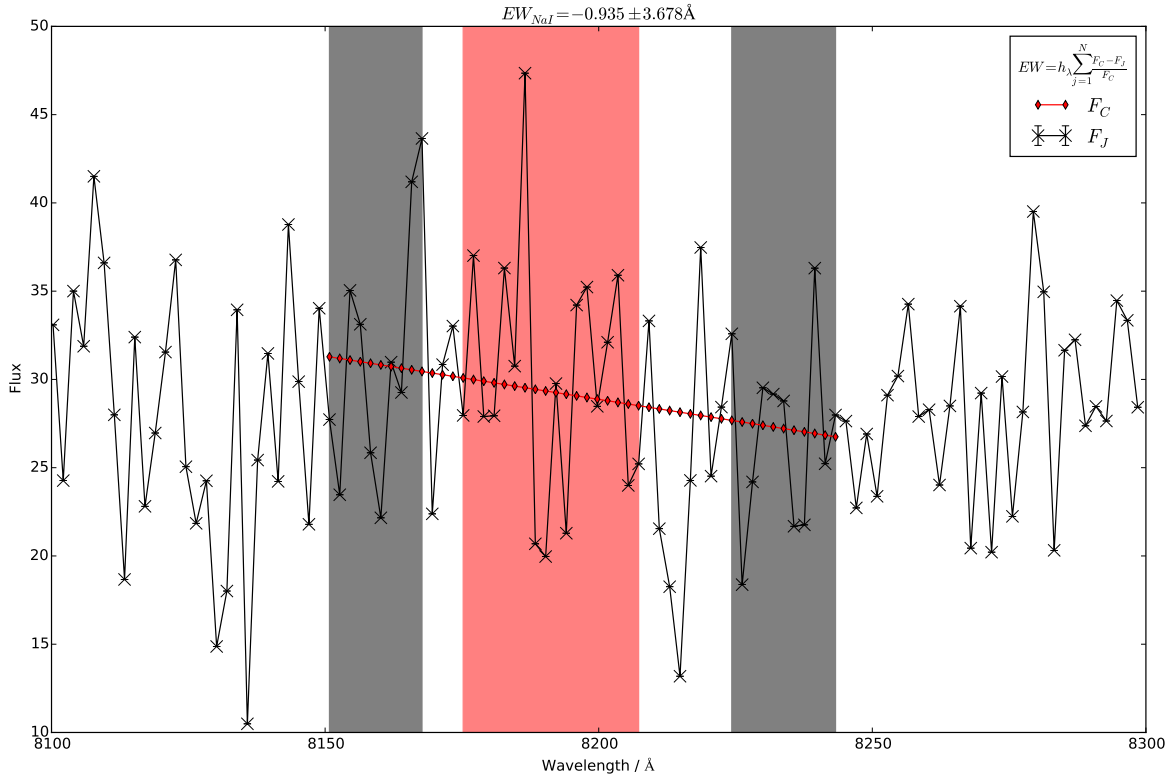


(a)

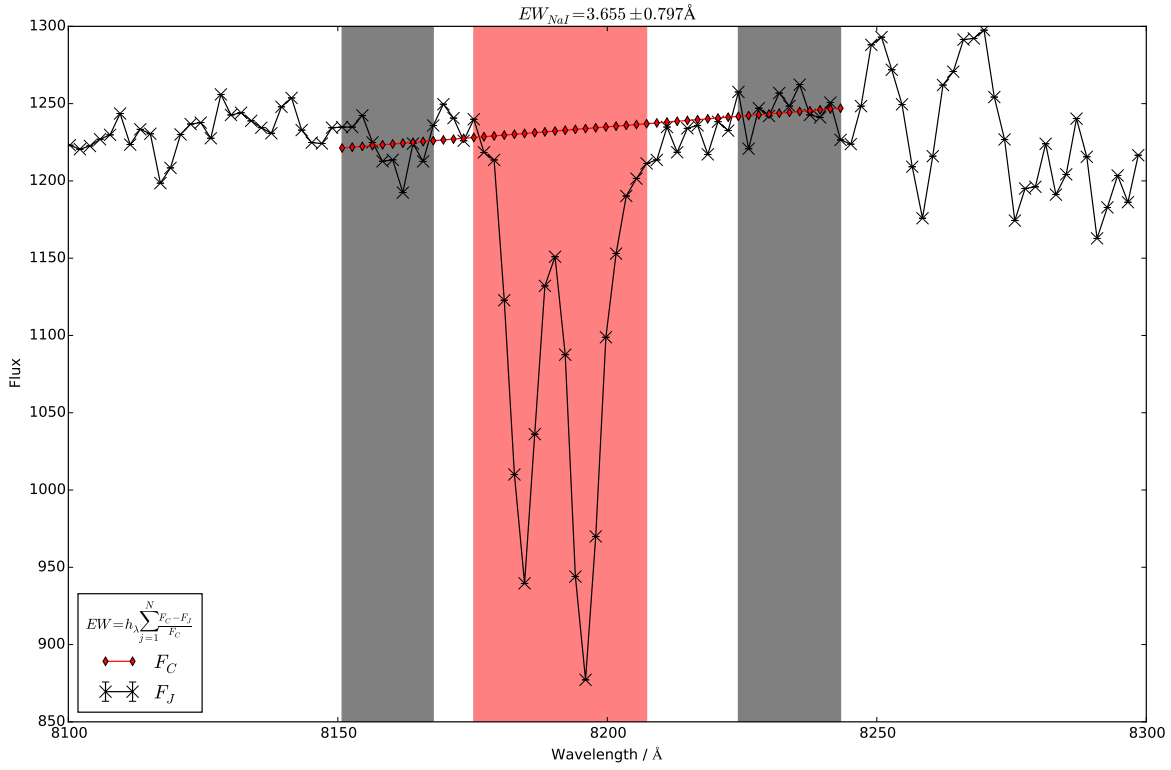


(b)

Figure. 5.5: A comparison between a detection of (a) a NaI absorption feature and (b) a non-detection of NaI for two of my M dwarfs which had LAMOST spectra. The continuum bands are shown in grey and the feature band is shown in red. The linear fit is the continuum fit between the values in the continuum bands.

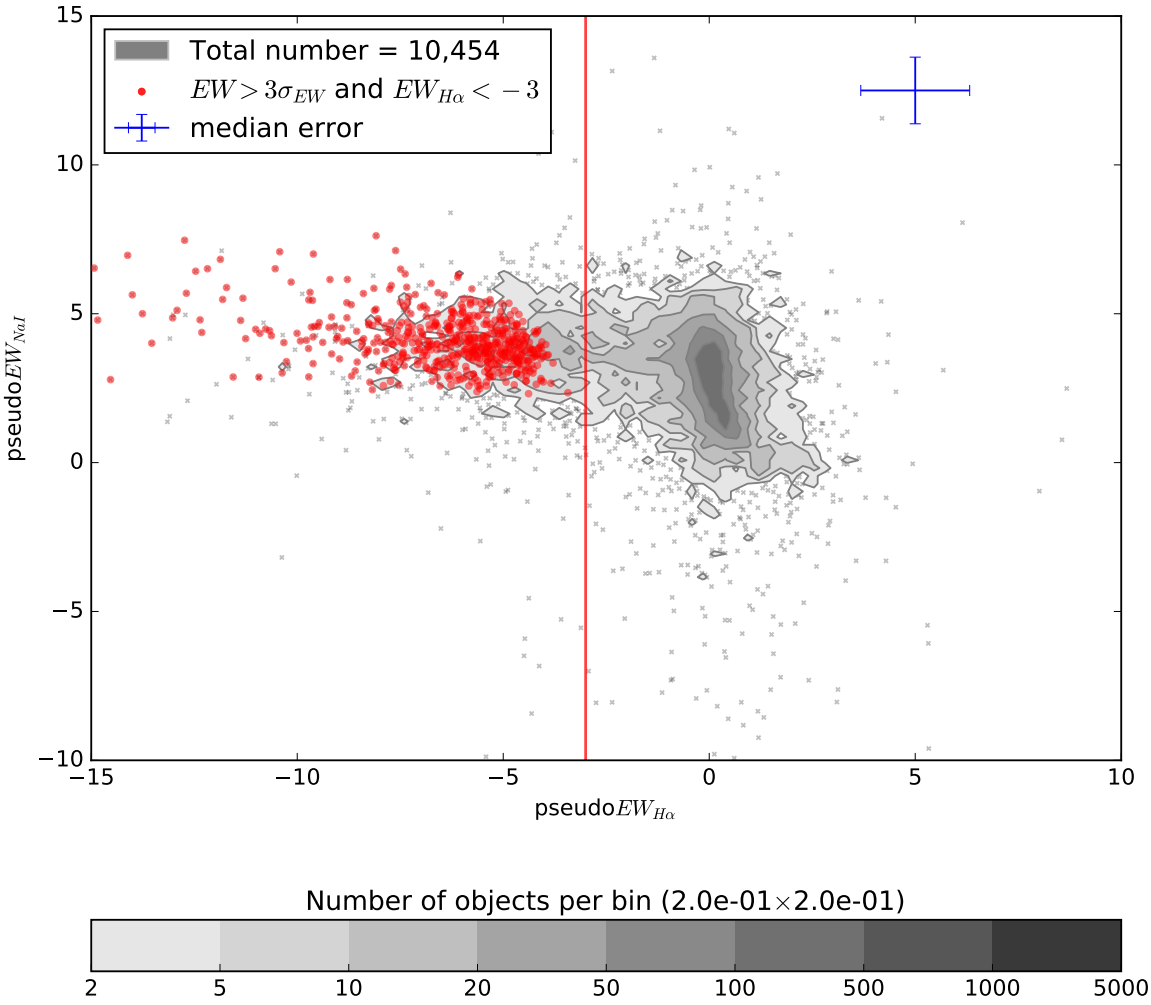


Figure. 5.6: The results of the 10,454 M dwarfs with LAMOST spectra where a equivalent width calculation was possible. Selected are those objects with H$\alpha$ of less than -3 (Zapatero Osorio et al., 1998) and a detection of both H$\alpha$ and NaI of greater than three times the uncertainties.

### 5.2.2 Rotation periods from Kepler 2 light curves

I cross-matched my full M dwarf candidate catalogue with Kepler 2 campaigns 0, 1 and 2 using (Howell et al. 2014, K2C0, K2C1 and K2C2 respectively) using EPIC at MAST[42]. For K2C0, K2C1 and K2C2 I had 44; 1,093 and 12 M dwarfs with light curves respectively. This gave me access to the EPIC identification number and the Kepler magnitude. Using the EPIC identification number I was able to download the processed light curves. Many reductions from the raw data to processed light curves exist and the same is true of methods to determine periodic features in the light curves. Therefore I decided to use two independent processing methods and periodicity finding methods, and to compare the results for similar periodicity signals.

For the first iteration I chose to use the self-flat-field corrected light curves from

[42]Accessed online at https://archive.stsci.edu/k2/

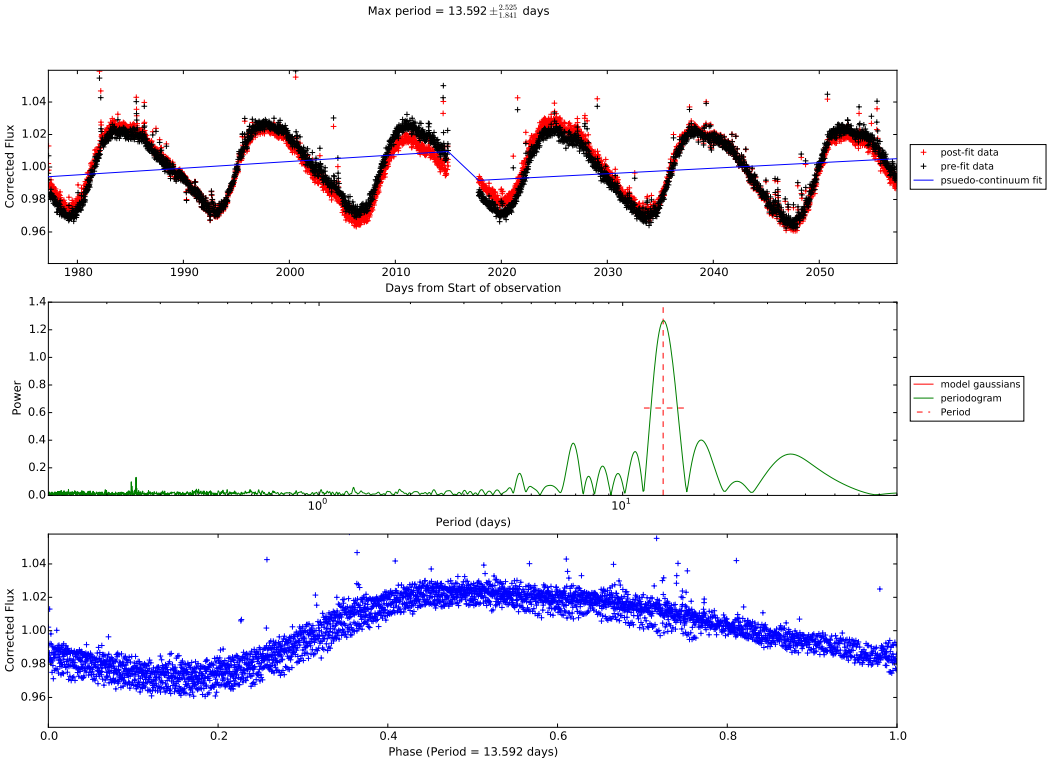


(a)

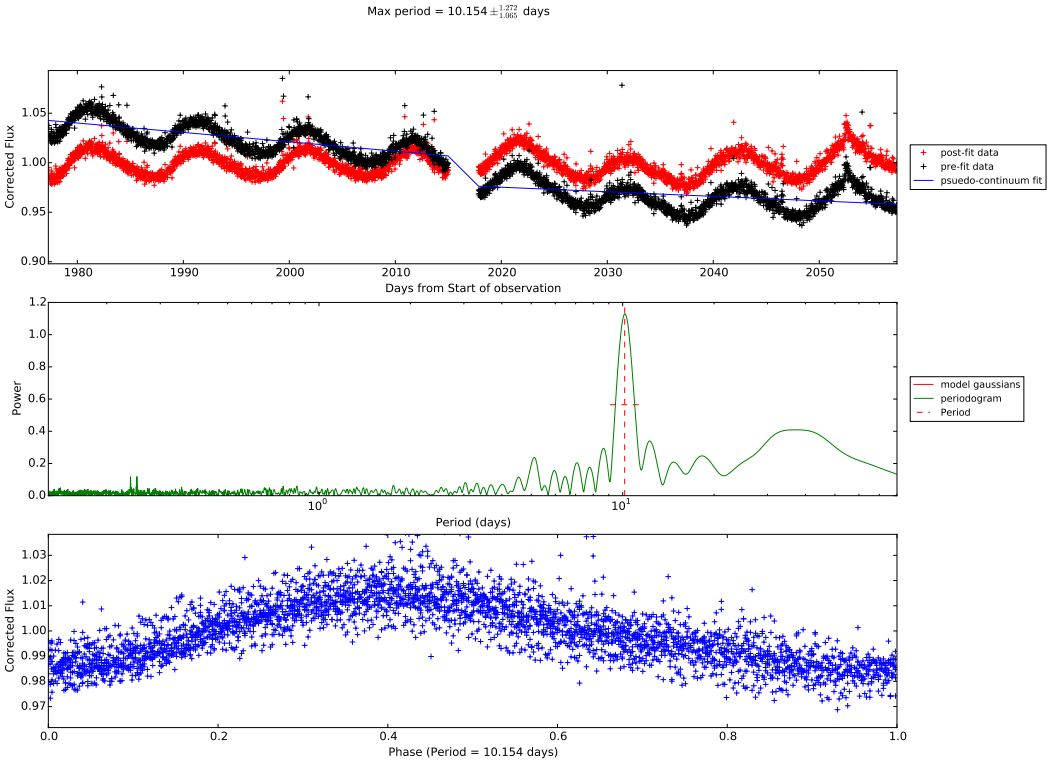


(b)

Figure. 5.7: The Lomb-Scargle periodogram (Lomb, 1976; Scargle, 1982; Townsend, 2010) for (a) WISE J111633.21+052346.1 and (b) WISE J113210.78-020844.7. Top the raw and pseudo-continuum fit light curve, middle the periodogram with selected period indicated, and bottom the phase-folded light curve.

Vanderburg & Johnson (2014)[43]. To these I apply a pseudo-continuum fit in order to remove any gradient found across the data. I used a PYTHON implemented Lomb-Scargle (LS periodogram, Lomb, 1976; Scargle, 1982; Townsend, 2010) subroutine (via SciPy, Jones et al. 2001) to extract the periods and select the most significant period. I estimated the uncertainties by finding the nearest stationary point either side of the selected peak. I plot two examples of the raw and pseudo-continuum fit light curve, periodogram and phase folded light curve in Figure 5.7.

For the second iteration I downloaded the uncorrected aperture photometry from Foreman-Mackey et al. (2015)[44]. I then used a systematics-insensitive periodic signal search by Angus et al. (2016) which uses a set of eigen light curves (from Foreman-Mackey et al. 2015) with a sum of sine and cosine functions over a grid of frequencies (SIP periodogram, Angus et al., 2016). This was done by using the SIP code[45] which produces a conditioned light curve and a periodogram similar to the LS periodogram. I plot two examples of the raw and conditioned light curve, periodogram and phase folded light curve in Figure 5.8 for the same M dwarfs used in Figure 5.7.

I calculated both periods for every M dwarf with a Kepler 2 light curve. Since these two methods are independent I looked for some level of agreement as a sign of genuine and robust periodicities. I thus selected all those where the period agreed to better than 30 per cent (see Figure 5.9). To judge which M dwarfs are young I used the analysis by Newton et al. (2015b). In table 5 Newton et al. (2015b) estimate that period less than 10 days are equivalent to ages $0.7^{+0.5}_{-0.3}$ $Gyr$ and M dwarfs with periods greater than 40 days[46] have an estimated average age of $4.5^{+3.9}_{-2.3}$ $Gyr$ . I thus split these into two samples of M dwarfs, periods <10 days (10 M dwarfs) and periods between 10 and 40 days (334 M dwarfs). These became my candidate young M dwarfs due to their rapid rotation.

[43] Accessed online at https://www.cfa.harvard.edu/~avanderb/k2.html
[44] Accessed online at https://bbq.dfm.io/ketu/
[45] Available at https://github.com/RuthAngus/SIPK2
[46] Newton et al. (2015b) use 70 days but state they find a gap between slow and fast rotators thus can use the 70 day rotation age for all stars rotating slower than around 10 days

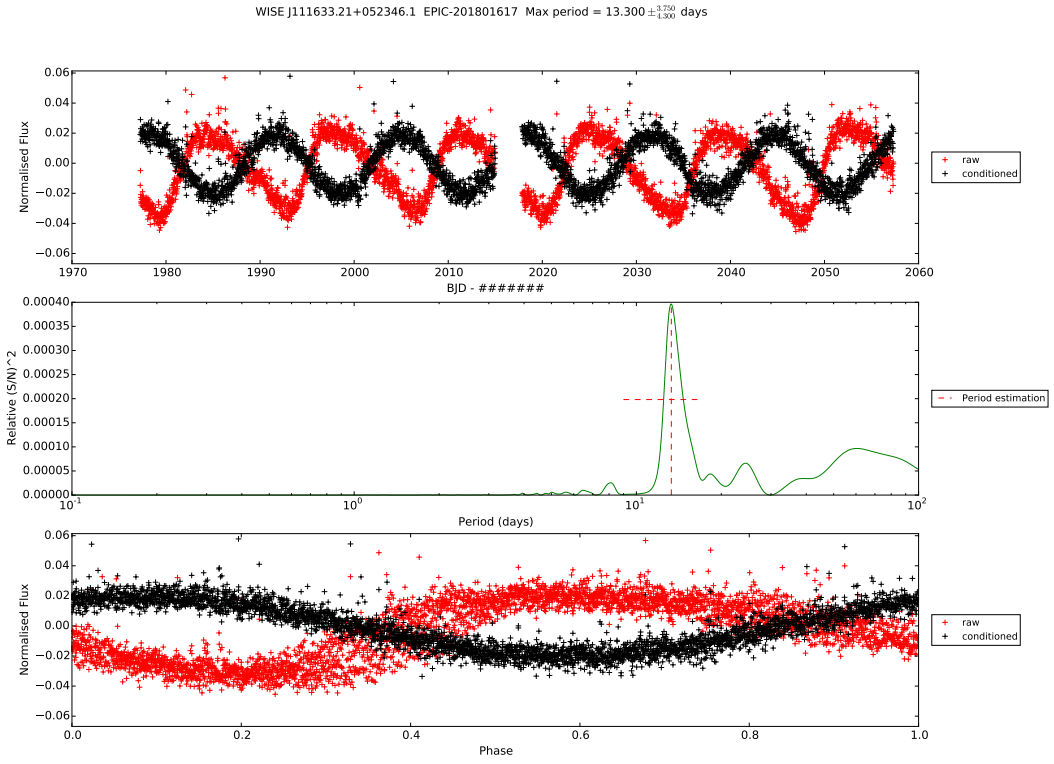


(a)

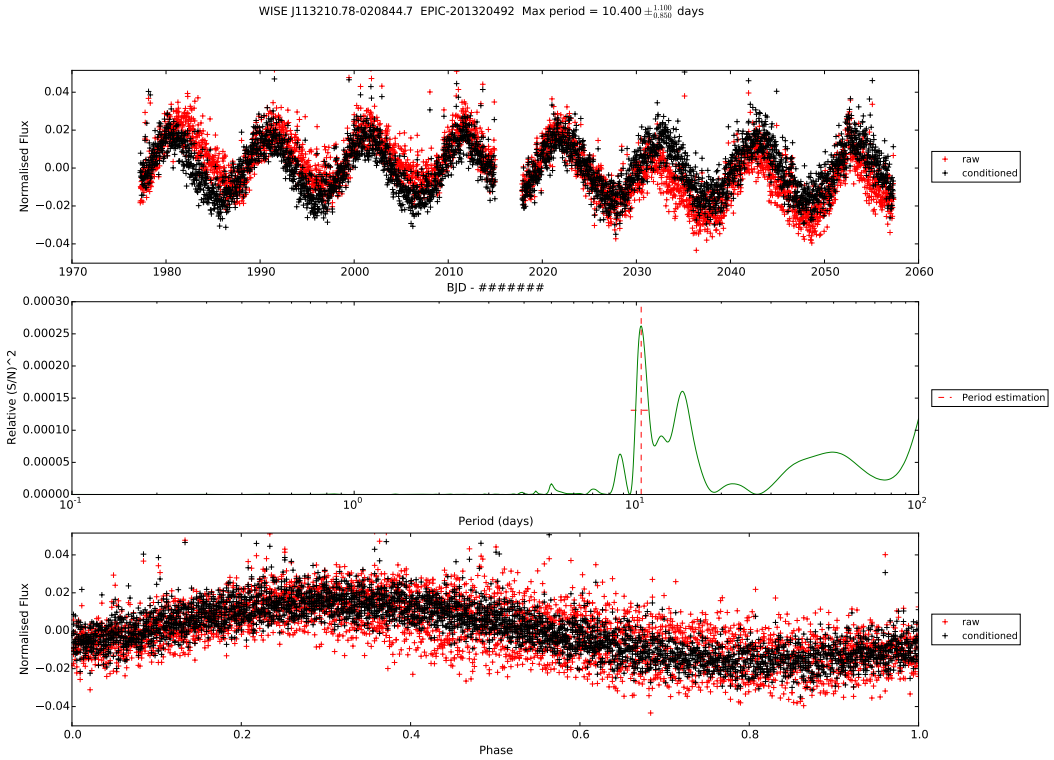


(b)

Figure. 5.8: The SIP periodogram (Angus et al., 2016) for (a) WISE J111633.21+052346.1 and (b) WISE J113210.78-020844.7. Top the raw and conditioned light curve, middle the periodogram with selected period indicated, and bottom the raw and conditioned phase-folded light curve.

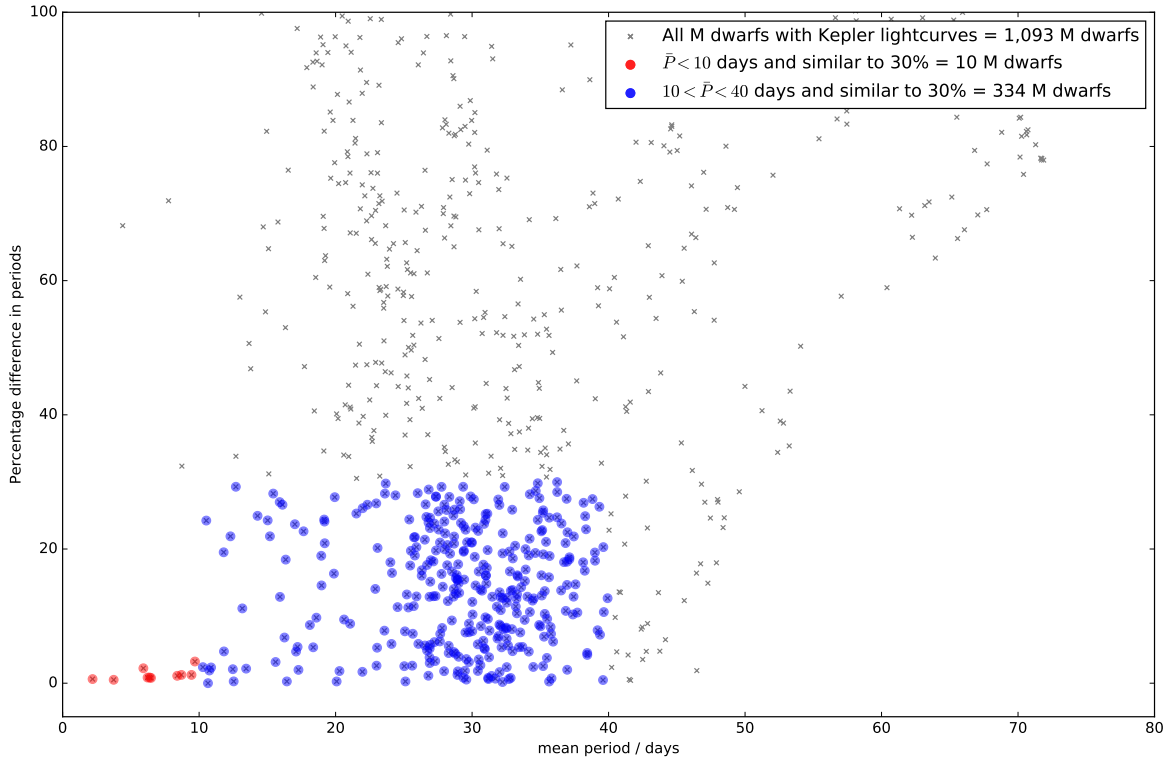


Figure. 5.9: Percentage difference of the LS periodogram and SIP periodogram method against mean period of the two methods. M dwarfs were selected where the periodogram periods agreed to better than 30 per cent and had periods less than 10 days (10 M dwarfs, in red) and periods between 10 and 40 days (344 M dwarfs, in blue).

## 5.3 Finding Late M dwarfs

Late type M dwarfs, defined here as later than M5.5, are also very interesting to the study of exoplanets. They are intrinsically fainter and thus in a photometrically limited sample they will, in general, be nearer than typical earlier M dwarfs in the sample. The fact they are smaller and fainter than early M dwarfs also makes detection of exoplanets relatively easier than for earlier M dwarfs. These systems can be revealed through radial velocity variability (e.g. Charbonneau et al. 2009) and as well as these deeper transits (due to their smaller size) the habitable zone for M dwarfs is closer in, so habitable planets are more likely to be transiting around M dwarfs (compared to FGK stars).

### 5.3.1 Photometric selection of late M dwarfs

To make a photometric selection of my M dwarfs I needed some known M dwarfs to base some new cuts on. I decided to start with the *Gliese Star Catalog and 2MASS cross identifications catalogue* by Stauffer et al. (2010). This is a catalogue of 4,106 2MASS cross-identifications of Gliese objects. I cross-matched this catalogue with SIMBAD for which there were 3,842 matches. This gave me access to the 2MASS photometry, proper motion, any SIMBAD photometry and spectral types (3,403 of the 3,842 SIMBAD matches had spectral types). From this sample I plotted $(J-H)$, $(H-K_S)$ and $(V-J)$ against reduced proper motion (see Section 2.4 and Equation 2.6 for $H_V$, $H_J$, $H_H$ and $H_{K_s}$). Figure 5.10 shows the full Stauffer et al. (2010)-SIMBAD cross-match with the $(V-J)$ cuts for M dwarfs from Section 2.3.3 ($(V-J)>2.7\equiv$ later than K7 from LG11 and my cut $(V-J)>4\equiv$ later than M3). Using the reduced proper motion plots I decided a cut in $H_J$ as a function of $(V-J)$ was suitable for late M dwarfs.

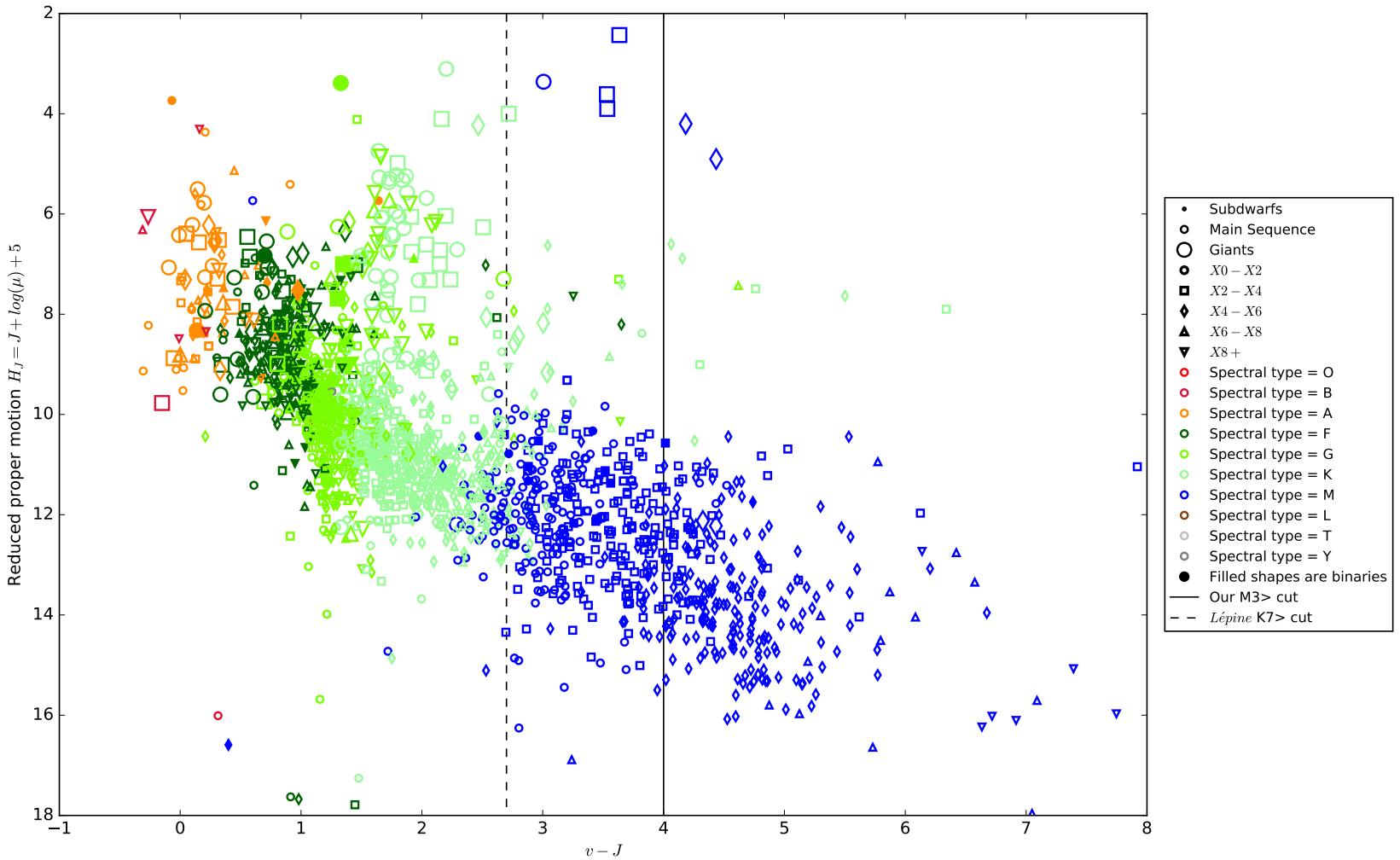


Figure. 5.10: $(V-J)$ against reduced proper motion for the cross-match between catalogues from Stauffer et al. (2010) and SIMBAD. Shown are the $(V-J)$ cuts for M dwarfs from Section 2.3.3 ($(V-J)$ >2.7≡ later than K7 from LG11 and my cut $(V-J)$ >4≡ later than M3). The various sizes denote sub dwarfs, main sequence and giant stars (from small to large respectively), the various shapes represent early to mid to late stars (circles, squares, diamonds to triangles, i.e. X0-X2 could be M0-M2 or A0-A2) and colours represent the spectral types.

To remove bright (earlier than M) contaminants from my test sample I also decided to do a cut in $H_J$. For this I cross-matched the Stauffer et al. (2010)-SIMBAD sample with Hipparcos to get parallaxes (2,381 matches of the 3,403 objects). I complemented this with the M dwarf catalogue from Winters et al. (2015) containing 1,748 southern M dwarf systems of which 582 have high quality parallaxes (and obtain photometric spectral types using $V$ and $J$ with Equation 2.2). I use the Winters et al. (2015) M dwarfs with photometric spectral types greater than M4.5 and M5.5 along with the M dwarfs with SIMBAD spectral types to define my new cuts in reduced proper motion as a function of $(V-J)$ for late M dwarfs (see Figure 5.11, Equation 5.3 and Equation 5.4).

Applying the reduced proper motion cuts to my full M dwarf candidate catalogue I was left with 18,121 M dwarfs later than M4.5 and 5,083 M dwarfs later than M5.5.

$$H_J \geqslant -25(V-J) + 142 \qquad H_J \geqslant 12 \tag{5.3}$$

$$H_J \geqslant -25(V-J) + 152 \qquad H_J \geqslant 13 \tag{5.4}$$

To further constrain the selection of late M dwarfs from my full M dwarf candidate catalogue I decided to use the colour cuts from Table 3 of Covey et al. (2007) ($(g-r)$, $(i-z)$ and $(r-i)$, see Equation 5.5).

$$\begin{aligned} (g-r) &> 1.59 \\ (i-z) &> 0.94 \\ (r-i) &> 1.73 \end{aligned} \tag{5.5}$$

After applying these colour cuts I was left with 9,015 M dwarfs later than M4.5 and 3,013 M dwarfs later than M5.5, the latter of which form my photometrically selected late sample of M dwarfs.

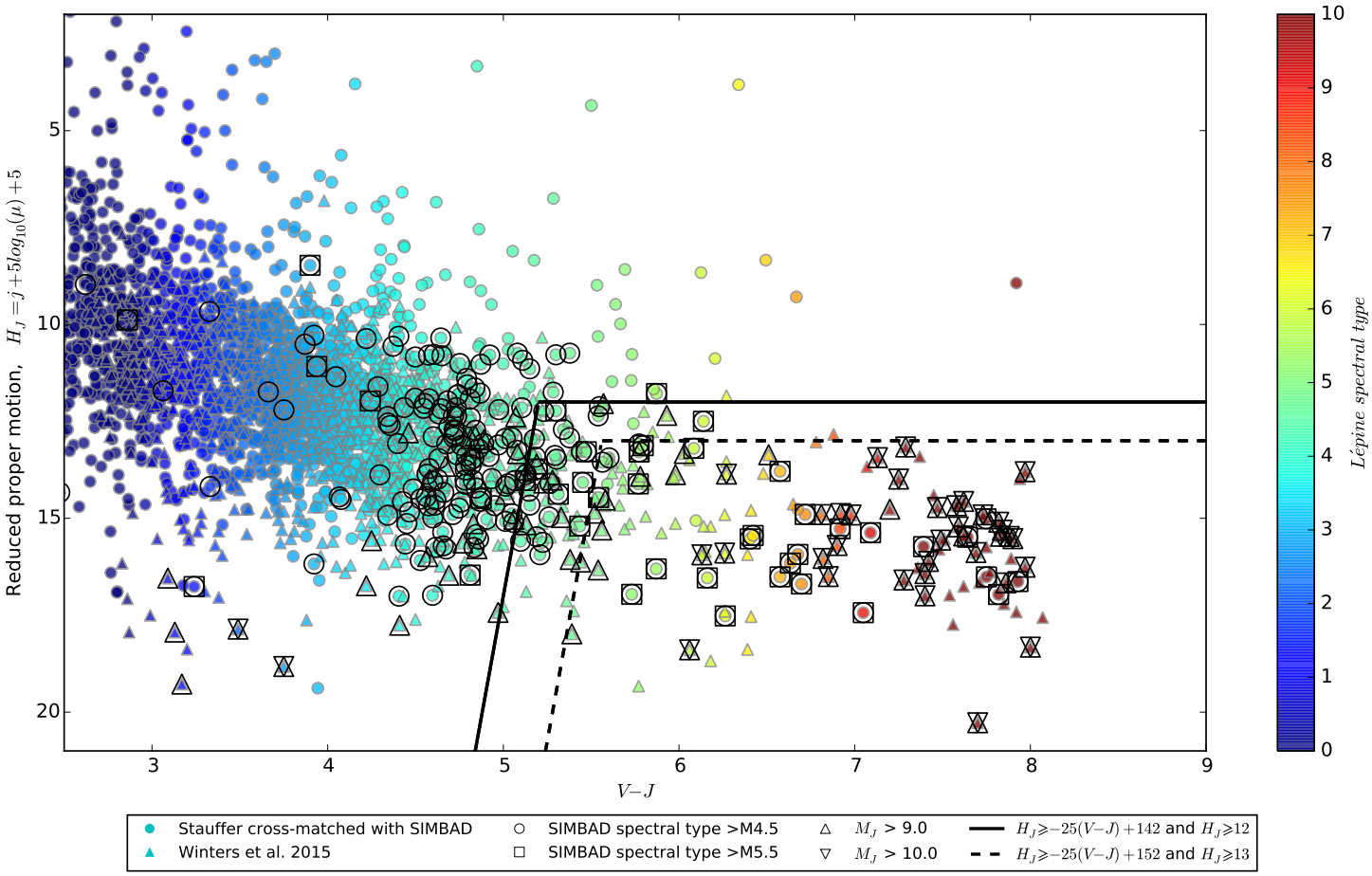


Figure. 5.11: $(V-J)$ against reduced proper motion for the low mass objects in the Stauffer et al. (2010) and Winters et al. (2015) catalogues (circles and triangles respectively). Objects with SIMBAD spectral types are plotted with black open circles and squares. Objects with parallaxes and $M_J$ >9.0 and $M_J$ >10.0 are plotted with black open triangles. Shown are my reduced proper motion cuts for selecting late M dwarfs.

| Spectral index | $\lambda_{num1}$ Å | $\lambda_{num2}$ Å | $\lambda_{den1}$ Å | $\lambda_{den2}$ Å | Reference |
|---|---|---|---|---|---|
| $CaH2$ | 6814 | 6846 | 7042 | 7046 | Reid et al. (1995)[2] |
| $CaH3$ | 6960 | 6990 | 7042 | 7046 | Reid et al. (1995)[2] |
| $PCl$ | 7030 | 7050 | 6525 | 6550 | Martín et al. (1996)[1] |
| $TiO2$ | 7058 | 7061 | 7043 | 7046 | Reid et al. (1995)[1] |
| $TiO5$ | 7126 | 7135 | 7042 | 7046 | Reid et al. (1995)[1,2] |
| $TiO6$ | 7745 | 7765 | 7550 | 7570 | Lépine et al. (2003)[2] |
| $VO1$ | 7430 | 7470 | 7550 | 7570 | Hawley et al. (2002)[2] |
| $VO2$ | 7920 | 7960 | 8130 | 8150 | Lépine et al. (2003)[2] |
| $VO7912$ | 7990 | 8030 | 7900 | 7940 | Martín et al. (1999)[1] |

Table 5.2: The spectral bands used to better constrain the spectral type of my full M dwarf candidate catalogue. Spectral indices are defined as $Index = (\lambda_{num1} - \lambda_{num2}) / (\lambda_{den1} - \lambda_{den2})$. Spectral type to spectral index fitted via [1]Alonso-Floriano et al. (2015) and [2]Lépine et al. (2013) (see Table 5.3).

### 5.3.2 Spectroscopic selection of late M dwarfs

M dwarf spectral types can be measured in a variety of ways, as such I explore the use of different methods to spectral type my M dwarfs and thus select the latest M dwarfs. I compared spectral type measurements from the LAMOST internal second data release (DR2) and the (internal) partial third data release (DR3a1) to spectral indices (used to characterise spectral type) in the literature (see Table 5.2).

I have various spectral types from the internal LAMOST releases:

1. the internal DR2 and DR3a1 spectral types from the LAMOST general catalogue which quote uncertainties of ±1.0 spectral type, using a modified version (Luo et al., 2004) of the HAMMER code (Covey et al., 2014).

2. spectral types from Zhong et al. (2015a) which use a template-fit method to automatically identify and classify M dwarfs from the LAMOST spectra, which quote uncertainties of ±0.5 spectral types.

3. spectral types from Gou (2014) and Lou (2014)'s' work on the LAMOST spectra which quote uncertainties of better than ±0.5 spectral types.

I took the weighted average (Equation 4.28) of these spectral types and these became my new LAMOST spectral types ($SpT_{LAMOST}$).

I used spectral index to spectral type fits from Alonso-Floriano et al. (2015) and Lépine et al. (2013) which use spectral indices from Reid et al. (1995), Martín et al. (1996), Martín et al. (1999), Hawley et al. (2002), and Lépine et al. (2003) (see Table 5.2 and Table 5.3).

By taking the difference between these spectral indices and the LAMOST spectral types (Figure 5.12) I decided the spectral indices are in good agreement with the

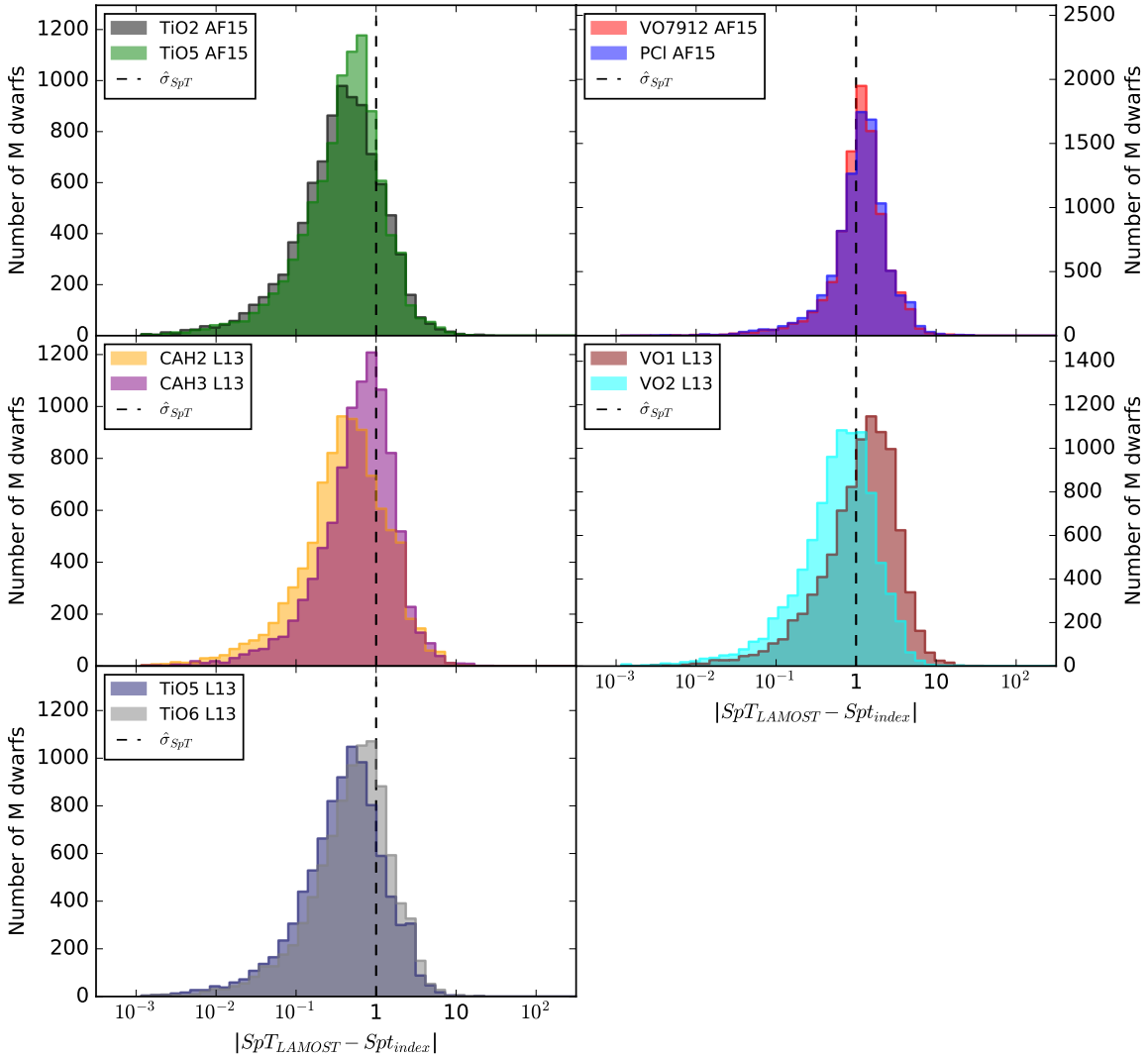


Figure. 5.12: Histograms of the difference in spectral type between the weighted average of the LAMOST spectral types ($SpT_{LAMOST}$) and the individual spectral indices $SpT_{index}$ applied to LAMOST DR2 spectra. Dashed line is the quoted LAMOST uncertainties (±1.0), I use any which have better agreement within ±1 spectral types. Spectral indices define in Table 5.2 and fits from Alonso-Floriano et al. (AF15, 2015) and Lépine et al. (L13 2013) defined in Table 5.3.

| Fit name | $c_0$ | $c_1$ | $c_2$ | $c_3$ |
|---|---|---|---|---|
| AF15 TiO2 | 10.98 | -21.87 | 27.92 | -19.63 |
| AF15 TiO5 | 9.57 | -20.12 | 17.23 | -9.50 |
| AF15 PCl | -49.54 | 97.23 | -58.95 | 12.38 |
| AF15 VO7912 | -520.19 | 1295.56 | -1073.57 | 299.07 |
| L13 CAH2 | 11.50 | -21.71 | 7.99 | 0.00 |
| L13 CAH3 | 18.80 | -21.68 | 0.00 | 0.00 |
| L13 TiO5 | 7.83 | -9.55 | 0.00 | 0.00 |
| L13 TiO6 | 9.92 | -15.68 | 21.23 | -16.65 |
| L13 VO1 | 69.8 | -71.40 | 0.00 | 0.00 |
| L13 VO2 | 9.56 | -12.47 | 22.33 | -19.59 |

Table 5.3: The fits used to convert the spectral indices (see Table 5.2) into spectral type $SpT = \sum_{i=0}^{N=3} c_n x^n$. Spectral type to spectral index fitted via Alonso-Floriano et al. (AF15, 2015) and Lépine et al. (L13 2013).

spectral types from LAMOST. Figure 5.12 also shows that the LAMOST spectral type uncertainties are reasonable estimates. I use the spectral indices where at least ∼70 per cent of the spectral types fall inside the uncertainties of the LAMOST data. This excludes $VO7912$ and $PCl$ from Alonso-Floriano et al. (2015, with only ∼28 and ∼35 per cent inside the uncertainties respectively) and $VO1$ from Lépine et al. (2013, with ∼43 per cent inside the uncertainties) peak to the left of the LAMOST uncertainties. The best agreements are with $TiO2$ and $TiO5$ from Alonso-Floriano et al. (2015, with ∼89 and ∼93 per cent inside the uncertainties) and $CAH2$ from Lépine et al. (2013, with ∼86 per cent inside the uncertainties). I weighted these and combined them with the $SpT_{LAMOST}$ estimates. Using these final weighted average spectral types I then selected all those with spectral type later than M4.5 (703 M dwarfs) and later than M5.5 (257 M dwarfs). These form my spectroscopically selected late sample of M dwarfs.

## 5.4 Identifying common proper motion Tycho-2 FGK Primaries

Although our ability to characterise M dwarfs has improved, in general brighter stars such as FGK stars are far better understood in both stellar properties and characterisation (e.g. due to the complex molecular opacities and uncertainties in convection theory, see Section 1.2). Thus a search for any of my M dwarfs that have physical ties to well understood stars can be used to infer properties of the companion M dwarfs. The Tycho-2 catalogue (Høg et al., 2000) contains position and proper motions to 2.5 million of the brightest stars in the sky, these stars have, in general, been well studied (at least for the Tycho-2 stars lying in the SDSS footprint) and thus would make perfect primary stars for constraining ages, distances, metallicities and compositions of M dwarfs based on the assumption they formed at a similar time, in a similar location from a similar type of material.

### 5.4.1 Obtaining distance estimate for Tycho-2 stars

To search for physically connected systems, I performed a common proper motion cross-match between Tycho-2 and my full M dwarf candidate catalogue. I first had to get a distance constraint for the Tycho-2 stars. To do this I took the Hipparcos catalogue (Perryman & ESA, 1997) which contains 118,218 objects, for which 117,906 have trigonometric parallax and 115,184 have a spectral type entry. Of these 56,176 of the spectral types were machine readable[47]. Hipparcos also gives access to $V$ band magnitudes, $(B-V)$ colour and proper motion information, thus I was able to calculate $M_V$. Using the machine readable spectral types I was able to group these into giant stars, main sequence stars and white dwarfs and thus fit $M_V$ as a function of $(B-V)$ (see Figure 5.13, Equation 5.6, Equation 5.7, and Equation 5.8).

$$M_V\,(\mathrm{G}) = -2.51(B-V) + 3.50 \tag{5.6}$$

$$M_V\,(\mathrm{MS}) = 0.7196(B-V)^3 - 1.7802(B-V)^2 + 6.7241(B-V) + 0.53 \tag{5.7}$$

[47] I extracted a luminosity class, spectral type and spectral subtype from a spectral type string, however many stars could not be automatically identified as giant stars or main sequence stars due to their lack of luminosity class information or due to the complex spectral type given, so these were removed from my sample.

$$M_V\,(\mathrm{WD}) = 14.291(B-V)\,+11.807 \tag{5.8}$$

where G is for giant stars, MS is for main sequence stars and WD is for definewhite dwarfs.

Thus by classifying Tycho-2 stars as giant stars, main sequence stars or white dwarfs I could calculate an estimate of their $M_V$ and thus an estimate of their distance. To classify the Tycho-2 stars I again used the Hipparcos stars as a guide. As Tycho-2 provides proper motion, $(B-V)$ and $V$ band magnitudes, I decided to use cuts in reduced proper motion (see Equation 2.6) to separate giant stars, main sequence stars and white dwarfs (see Figure 5.14, Equation 5.9, Equation 5.10, and Equation 5.11).

$$\begin{aligned} H_V\,(\mathrm{G}) &> 9 \\ H_V\,(\mathrm{G}) &< 14(B-V)\,-5 \end{aligned} \tag{5.9}$$

$$\begin{aligned} H_V\,(\mathrm{MS}) &> \text{ minimum}\,(14(B-V)\,-5, 9) \\ H_V\,(\mathrm{MS}) &< 14(B-V)\,+9 \end{aligned} \tag{5.10}$$

$$H_V\,(\mathrm{WD}) > 14(B-V)\,+9 \tag{5.11}$$

where G is for giant stars, MS is for main sequence stars and WD is for white dwarfs.

Out of the total Tycho-2 catalogue (1,377,525 stars) I classified 353,498 as giant stars, 999,107 as main sequence stars and 25,920 as white dwarfs. I was then able to perform a common proper motion cross-match between Tycho-2 and my full M dwarf candidate catalogue.

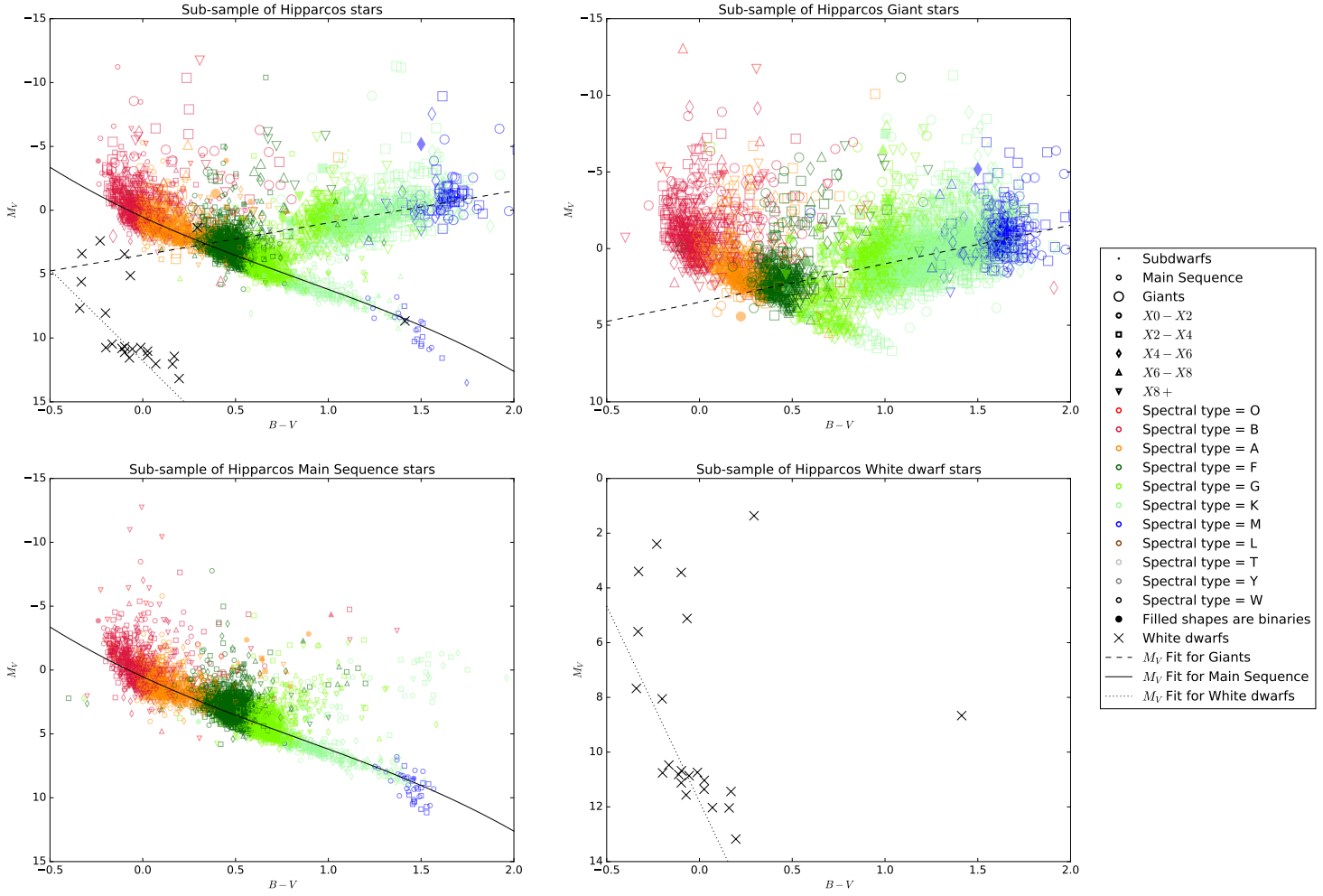


Figure. 5.13: $M_V$ against $(B-V)$. **Top left** a sub sample of 5,000 Hipparcos stars, **top right** a sub sample of 5,000 Hipparcos giant stars, **bottom left** a sub sample of 5,000 Hipparcos main sequence stars, **bottom right** a sub sample of all Hipparcos white dwarfs. Objects classified using the Hipparcos spectral type column. Shown lines are the fits between $M_V$ and $(B-V)$ for giant stars (dashed line), main sequence stars (solid line) and white dwarfs (dotted line). These fits were used to obtain $M_V$ values (and thus a distance estimate) for Tycho-2 stars.

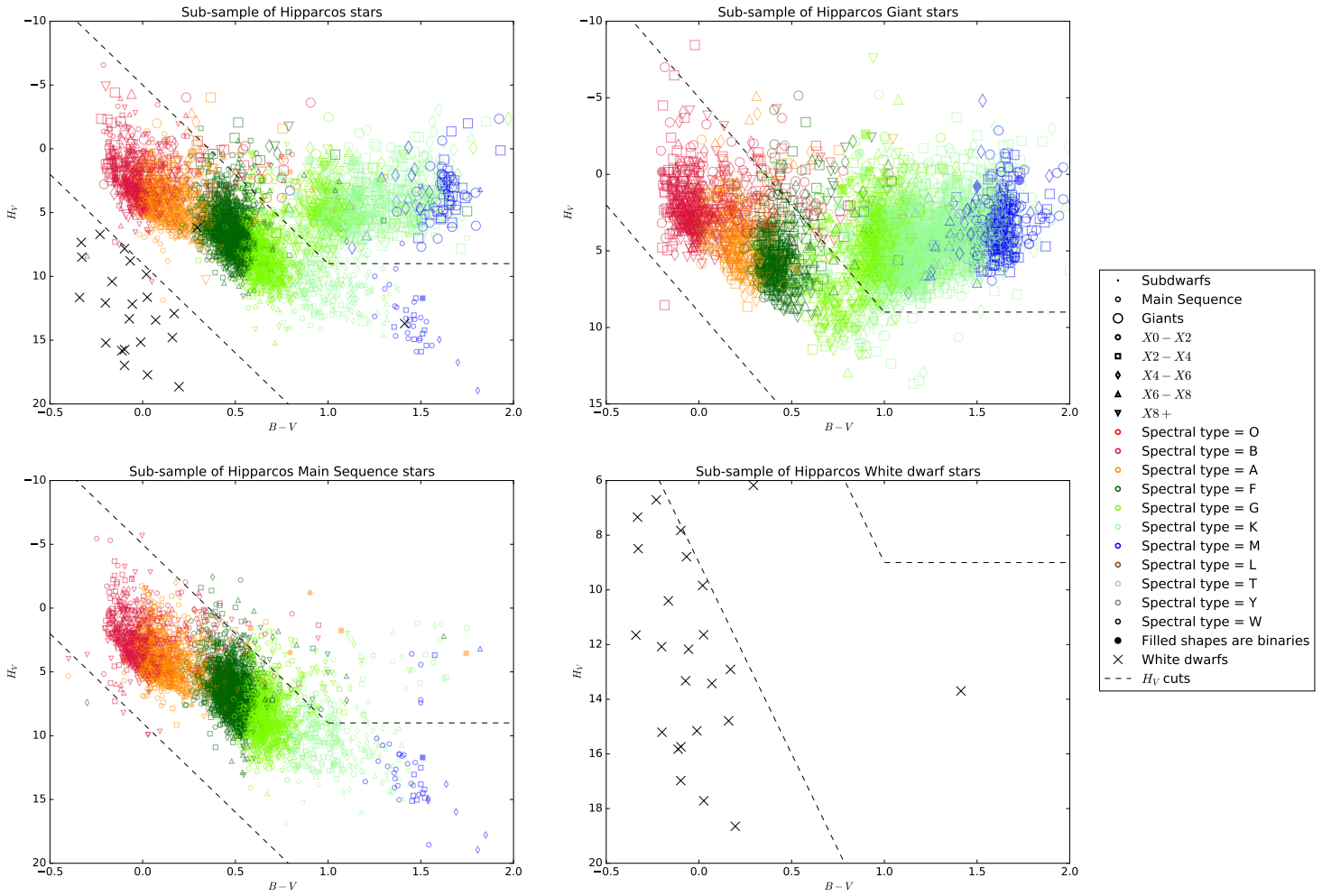


Figure. 5.14: $H_V$ against $(B-V)$. **Top left** a sub sample of 5,000 Hipparcos stars, **top right** a sub sample of 5,000 Hipparcos giant stars, **bottom left** a sub sample of 5,000 Hipparcos main sequence stars, **bottom right** a sub sample of all Hipparcos white dwarfs. Objects classified using the Hipparcos spectral type column. Shown lines are the cuts I defined to separate giant stars, main sequence stars and white dwarfs. These cuts were used to separate giant stars, main sequence stars and white dwarfs in the Tycho-2 catalogue.

### 5.4.2 Common proper motion cross-match

To find stars which are physically bound systems requires them to be at very similar distance (within measurement uncertainties), in the same region of sky (with some separation limitations), and moving with common proper motion (their wide separation leads to very long orbital periods, so there will be no orbital motion observed over time-scales of a few years). I therefore apply a set of cuts based on these conditions to select those objects likely to be physically bound systems.

I define the same location on the sky to be closer than a certain angular separation, $\theta$, (see Equation 5.12 and the numerically better-conditioned form for small distances Equation 5.13 from Sinnott 1984) which given the distance to an object can lead to a physical separation (Equation 5.14). I also require the two objects distances to be within the uncertainties of each others distances (see Equation 5.15). To calculate whether two stars are moving in a similar direction I first apply a uncertainty cut on the total proper motion and then define common proper motion to be where the difference between the two stars proper motion is less than twice the combined uncertainty of the stars difference in proper motion (see Equation 5.16).

$$cos(\theta) = sin(\delta_1)sin(\delta_2) + cos(\delta_1)cos(\delta_2)cos(\alpha_1 - \alpha_2) \tag{5.12}$$

$$sin^2\left(\frac{\theta}{2}\right) = sin^2\left(\frac{\delta_1 - \delta_2}{2}\right) + cos(\delta_1)cos(\delta_2)sin^2\left(\frac{\alpha_1 - \alpha_2}{2}\right) \tag{5.13}$$

$$\left(\frac{r_{1,2}}{AU}\right) = 206{,}264.806 \left(\frac{d_1 + d_2}{pc}\right) sin\left(\frac{\theta}{2}\right) \tag{5.14}$$

$$\begin{aligned} d_2 + \sigma_{d_2} &> d_1 - \sigma_{d_1} \\ d_1 + \sigma_{d_1} &> d_2 - \sigma_{d_2} \end{aligned} \tag{5.15}$$

$$\begin{aligned} \Delta\mu &= \sqrt{(\Delta\mu_\alpha)^2 + (\Delta\mu_\delta)^2} \\ \sigma_{\Delta\mu} &= \frac{1}{\Delta\mu}\sqrt{(\Delta\mu_\alpha)^2(\sigma^2_{\mu_{\alpha_1}} + \sigma^2_{\mu_{\alpha_2}}) + (\Delta\mu_\delta)^2(\sigma^2_{\mu_{\delta_1}} + \sigma^2_{\mu_{\delta_2}})} \end{aligned} \tag{5.16}$$

where $\theta$ is the angular separation, $(\alpha, \delta)$ is the sky location in right ascension and declination of the star, $d$ is the distance to the star, $r$ is the separation between the two stars, ($\mu_\alpha, \mu_\delta$ is the proper motion in right ascension and declination of the star, $\Delta\mu_\alpha = \alpha_1 - \alpha_2$ and $\Delta\mu_\delta = \delta_1 - \delta_2$.

I chose to use a separation of $\theta$=200 arcsec , $\mu > 10\sigma_\mu$ and $\Delta\mu < \sigma_{\Delta\mu}$ (proper motions for my catalogue are from PPMXL, see Section 2.4, proper motions for Tycho-2 are derived from ground-based astrometric catalogues, see Høg et al. 2000). This gave 87 common proper motion pairs between the 440,694 M dwarfs in my full M dwarf candidate catalogue and the 1,377,525 stars in the Tycho-2 catalogue. I judged chance alignments by offsetting my M dwarfs by -2 degrees in galactic longitude and running a similar process (thus simulating a random chance of alignment). This enabled me to work out a probability of chance alignment (see Equation 5.19, Equation 5.18 and Equation 5.19).

$$\eta = \frac{N_{cont}(R_{total})}{\pi R_{total}^2} \tag{5.17}$$

$$N_{cont}(R \pm dR) = \eta\pi \left((R + dR)^2 - (R - dR)^2\right) \tag{5.18}$$

$$P_{cont}(R) = \frac{N_{cand} - N_{cont}(R)}{N_{cand}} \tag{5.19}$$

where $\eta$ is the density of chance alignments in out to the total cross-matching radius $R_{total}$, $N_{cont}$(R) is the number of random chance alignments at a separation $R$, $N_{cand}$ is the number of candidates common proper motion and $P_{cont}(R)$ is the probability of chance alignment.

I then split my 87 candidate common proper motion pairs into four groups; (i) high proper motion bright, (ii) high proper motion faint, (iii) low proper motion bright, and (iv) low proper motion faint, where the definition of high/low proper motion and bright/faint are described in Equation 5.20.

$$\begin{gathered} \text{High } \mu\text{: } \mu \gtrsim 0.1 \text{ arcsec yr}^{-1} \\ \text{Low } \mu\text{: } \mu < 0.1 \text{ arcsec yr}^{-1} \\ \text{bright: } J \lesssim 14 \\ \text{faint: } J > 14 \end{gathered} \tag{5.20}$$

I did the same for my offset sample and found in total I had one high proper motion bright pair, one high proper motion faint pair, both with no offset chance alignments, 32±19 low proper motion bright pairs, and $53^{+56}_{-53}$ low proper motion faint pairs, I then calculated the probabilities for each of these and plot them in Figure 5.15. The results of this can be seen in Table 5.4.

I have identified a small but robust sample of common proper motion pairs consist-

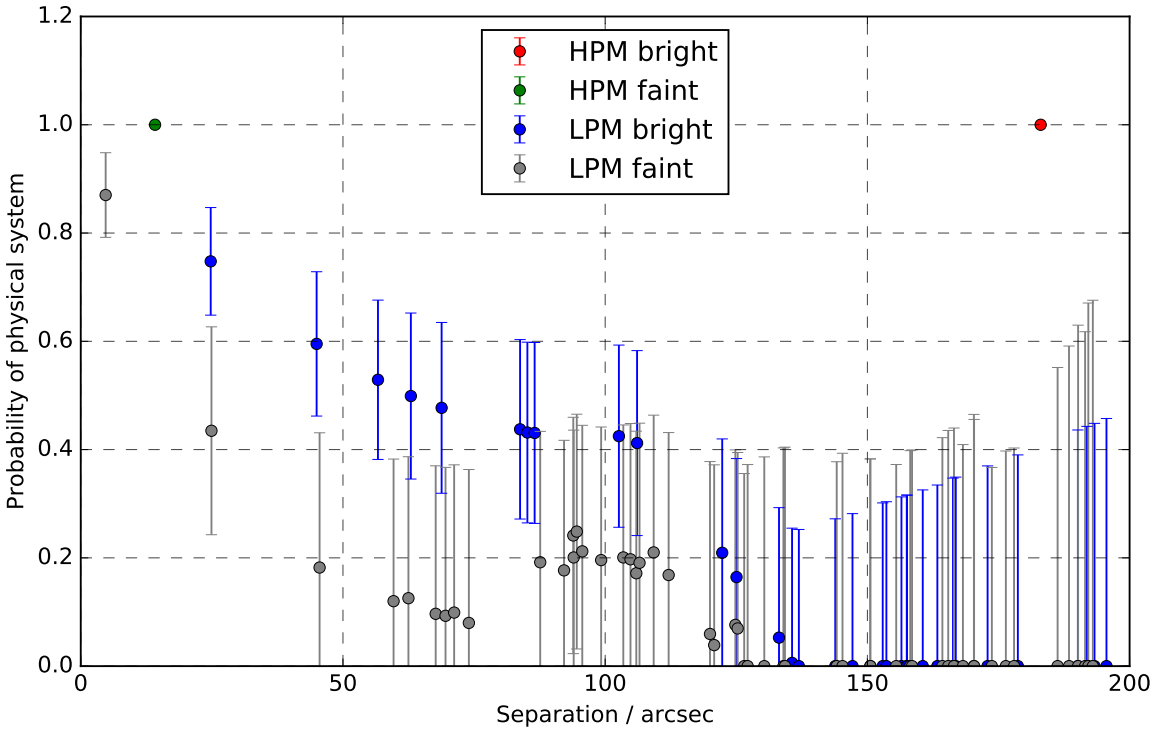


Figure. 5.15: The probability of a Tycho-2+M dwarf common proper motion pair being a physical system was calculated (Equation 5.19) for high proper motion bright stars, high proper motion faint stars, low proper motion bright stars, and low proper motion faint stars (see Equation 5.20).

ing of FGK primaries (from Tycho-2) and widely separated M dwarf companions from my catalogue.

| Group | Number of pairs (no offset) | Number of pairs (offset = 2°) | Probability $> 0.25$ | Probability $> 0.5$ |
|---|---|---|---|---|
| High $\mu$ + bright | 1 | 0 | 1 | 1 |
| Low $\mu$ + faint | 1 | 0 | 1 | 1 |
| High $\mu$ + bright | 32 | 19 | 10 | 3 |
| Low $\mu$ + faint | 58 | 56 | 2 | 1 |
| Total | 87 | 75 | 14 | 5 |

Table 5.4: The results of the cross-match between the Tycho-2 catalogue and my full M dwarf candidate catalogue

| Group | Number of pairs (no offset) | Number of pairs (offset = 2°) | Probability > 0.25 | Probability > 0.5 |
|---|---|---|---|---|
| High $\mu$ + bright | 94 | 10 | 87 | 81 |
| Low $\mu$ + faint | 21 | 9 | 10 | 10 |
| High $\mu$ + bright | 245 | 119 | 99 | 96 |
| Low $\mu$ + faint | 511 | 395 | 55 | 54 |
| Total | 871 | 532 | 251 | 241 |

Table 5.5: The results of the internal cross-match of my full M dwarf candidate catalogue.

## 5.5 Identifying internal common proper motion pairs

As well as having physical connections to brighter stars, some of my M dwarfs may be physically connected to other M dwarfs in my full M dwarf candidate catalogue. I therefore decided to do an internal common proper motion cross-match similar to the match in Section 5.4.2, but instead cross-matching each catalogue member with all other catalogue members. These systems may be interesting for a few reasons, firstly for identifying any higher level hierarchical systems (i.e. and M+M binary where one or both component had an unresolved UCD) or for possible exoplanet detection. Secondly, M dwarfs that are physically connected should share a similar age and thus (taking into account differences in spectral type) should share a common rotation rate. An addition of a close-by exoplanet or substellar companion may lead to a tidal interaction between itself and the host M dwarf, thus leading to a difference in the rotation rates of the two physically connected M dwarfs in the M+M binary. This is an extension of the work in Poppenhaeger & Wolk (2014) where the tidal effects of Hot Jupiters is studied using wide FGK binaries.

I thus used the same method described in Section 5.4.2. I chose to use a separation of $\theta$=600 arcsec , $\mu > 10\sigma_{\mu}$ and $\Delta\mu < \sigma_{\Delta\mu}$. An extra condition was needed to remove self-matches and this was done by changing the separation criteria to not include anything closer than one arcsec . As with the Tycho-2 match I also offset by -2 degrees to gauge contamination from chance alignments and work out a probability of being a physical system using the same definitions for high/low proper motion and bright/faint common proper motion pairs as in Equation 5.20. In results of this can be seen in Table 5.5, the histograms compared to contamination can be seen in Figure 5.16 and the probabilities in Figure 5.17. I identify a robust sample of wide (high proper motion and bright) binaries out to separations of ∼200 arcsec (as evident from Figure 5.16). Figure 5.17 shows that the systems around ∼200 arcsec separation are statistically robust (for the HPM bright case).However, for fainter and/or lower proper motion I have many more multiple systems at closer separation (for a low probability of chance alignment).

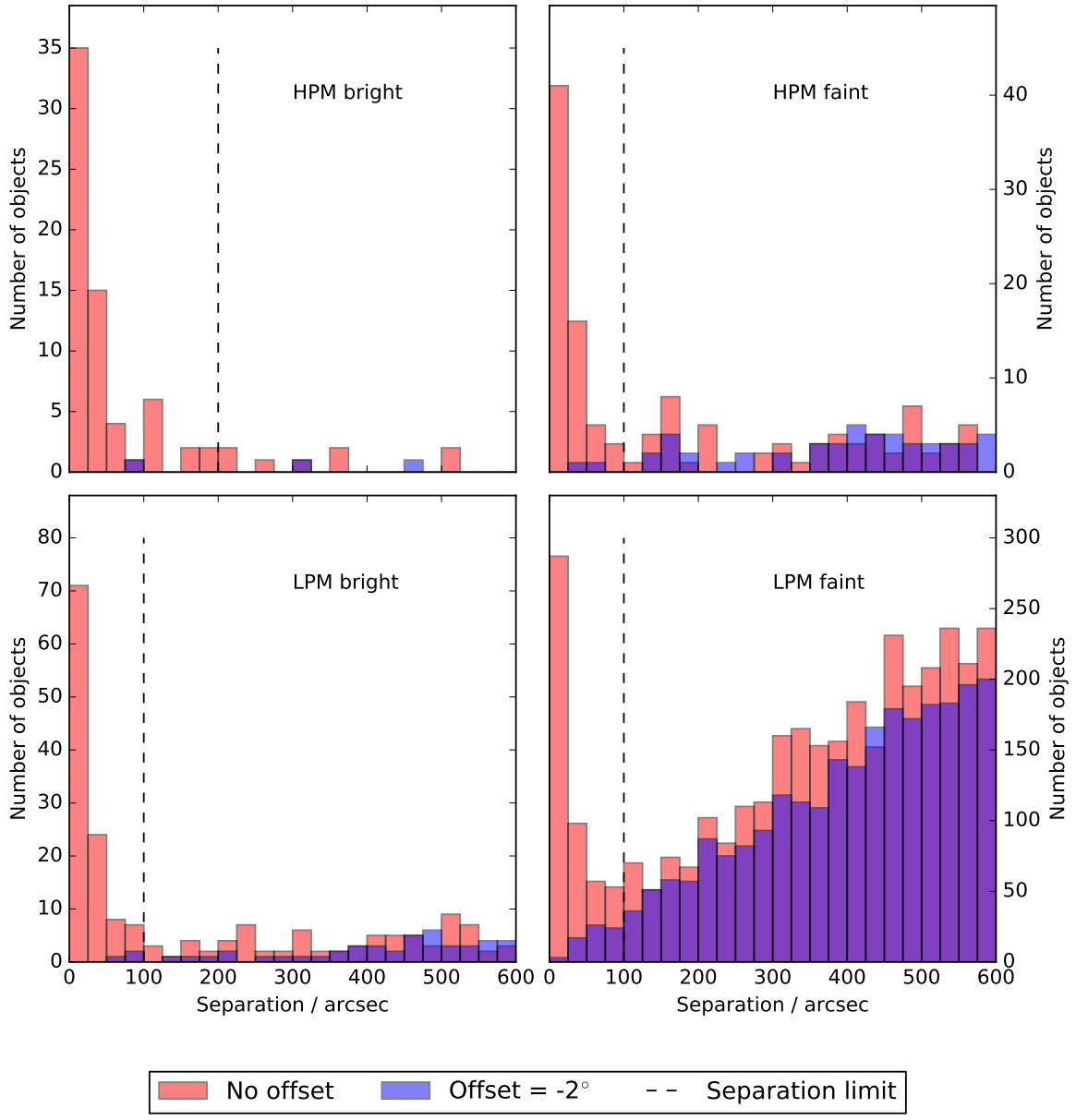


Figure. 5.16: Histograms of the separations of the M+M binaries found for each group (red) over plotted on each is the distributions of chance alignments offset by 2° (blue). Approximate separation limits are indicated with the dashed black lines.

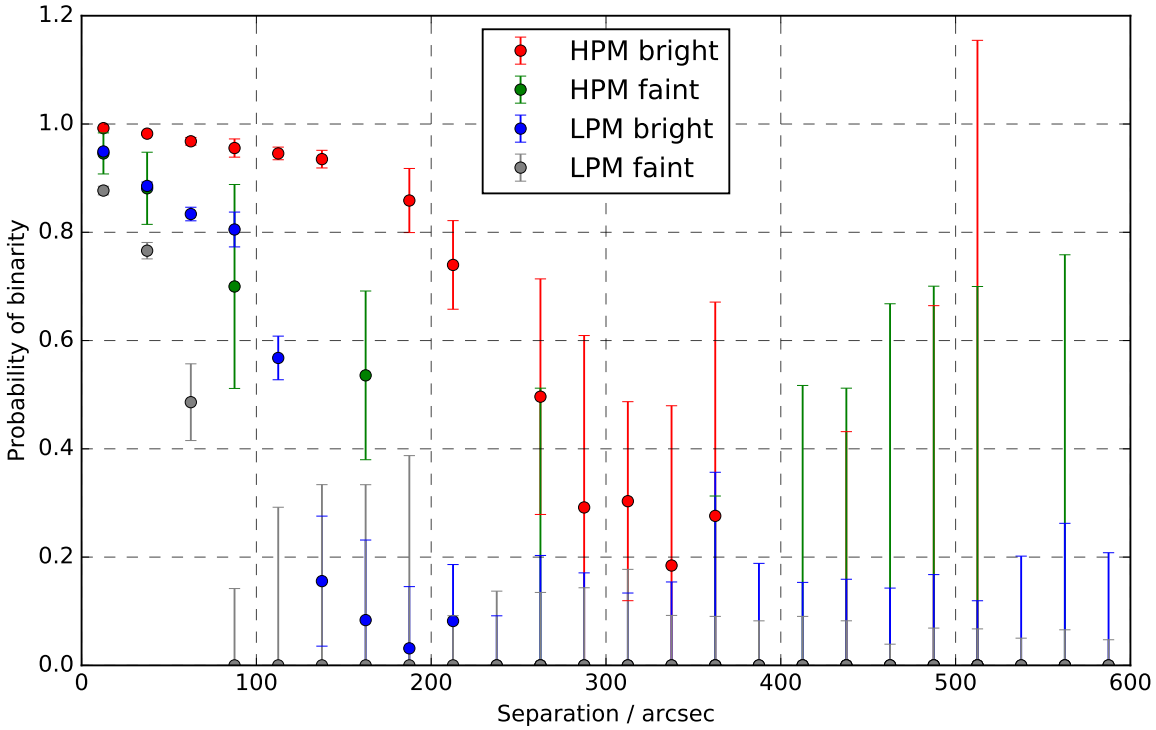


Figure. 5.17: The probability of a M+M dwarf common proper motion pair being a physical system was calculated (Equation 5.19) for high proper motion bright stars, high proper motion faint stars, low proper motion bright stars, and low proper motion faint stars (see Equation 5.20). Unlike Figure 5.15 I have binned up the data into bins of 25 arcsec for clarity (giving the value of the weighted average of each bin).

## 5.6 Summary of further uses for the M dwarf catalogue

As well as serving as a seed catalogue for finding UCD companions to M dwarfs my full M dwarf candidate catalogue of 440,694 M dwarfs can be used to search for other rare and useful M dwarfs.

I searched for young M dwarfs (which are good candidates for exoplanet studies and for direct imaging of companions). This was approached in two ways, the first by measuring pseudo-equivalent widths in a sample of 10,591 of my M dwarfs that had LAMOST spectra (for which 557 M dwarfs had a significant H$\alpha$ detection and thus deemed as young M dwarf candidates). The second approach used a sub sample of my M dwarfs which had Kepler 2 light curves (1,149 in total) and as such could measure possible rotation periods. Ten M dwarfs were selected with possible periods under 10 days and 334 were selected with periods between 10 and 40 days.

Another use for the full M dwarf candidate catalogue was in finding late M dwarfs this was done by two methods. The first used a photometric selection process with cuts in $(V - J)$, reduced proper motion and $(g - r)$, $(i - z)$ and $(r - i)$ which selected 9,015 M dwarfs later than M4.5 and 3,013 M dwarfs later than M5.5. Using the 10,591 LAMOST spectra for a sub sample of my M dwarfs I also selected those M dwarfs with spectral types later than M4.5 (703 M dwarfs) and later than M5.5 (257 M dwarfs), using a weighted average of spectral types supplied from LAMOST in addition to spectral types calculated from a set of spectral indices.

The final use of my full M dwarf candidate catalogue explored was identifying common proper motion pairs, with pairs from internal cross-matches (binary M dwarf systems) and from an external cross-match with Tycho-2 FGK binaries. For the Tycho-2 FGK binaries I found one high proper motion bright pair, one high proper motion faint pair, 32$\pm$19 low proper motion bright pairs, and $53^{+56}_{-53}$ low proper motion faint pairs. For the internal M+M dwarf binaries I found 241 binaries with more than a 50 per cent chance of being true binary systems.

# Chapter 6: Future Work and Conclusions

## 6.1 Observation and continued follow-up

### 6.1.1 Confirmation of the M+UCD candidates

Through my collaboration with the LAMOST project I am obtaining more optical spectra for my M dwarf catalogue and excess sample. The LAMOST team have accepted my proposal to give high priority to my brightest M dwarf candidates, as well as this the third internal data release is now complete (September 2014 - May 2015) bringing the total number of available spectra up to 5,755,126 (see Figure 6.1). This addition will continue to add to the number of my M dwarfs which have optical spectra and thus continue to complement my analysis using the LAMOST spectra (i.e. verifying the spectral types of M dwarfs, Section 4.3, and in the process of identifying candidate young, Section 5.2, and late M dwarfs, Section 5.3).

I was also awarded 40 hours on *The United Kingdom InfraRed Telescope*(UKIRT)[48] and 36 hours on *The InfraRed Telescope Facility*(IRTF) using SpeX in March 2016 (however these data are still in the process of being reduced, Cook et al. 2016b). The data from both UKIRT and the IRTF are being taken in order to use my spectral difference approach (described in Section 4.4 to Section 4.8) to confirm the M+UCD candidates as true M+UCD systems. The candidates with spectroscopic evidence for unresolved UCD companions will be targeted for AO observations (e.g. LBT, VLT and Gemini), and RV measurements to confirm companions over a range of separations.

### 6.1.2 Detectable transits with TESS

TESS will be launched by NASA in 2017 and will observe 200,000 bright main sequence stars. However as well as this TESS will return full frame images with effective exposure times of ∼30 minutes (Ricker et al., 2014). Using Figure 6.2, the transit depth $(R_2/R_1)^2$, and the conversion from Jordi et al. (2006, presented in Equation 6.1)[49] to convert SDSS $i$ magnitude into $I_C$, I was able to estimate the SNR my M+UCD candidates would have given certain combinations of $R_1$ and $R_2$ (where $R_1$ is the mass of the M dwarf and $R_2$ is the mass of the UCD, taken from Section 1.2 and Section 1.1 respectively).

[48] Unfortunately due to bad weather only 5 hours were observable, and of these none of the spectra were usable

[49] Accessed online at https://www.sdss3.org/dr8/algorithms/sdssUBVRITransform.php

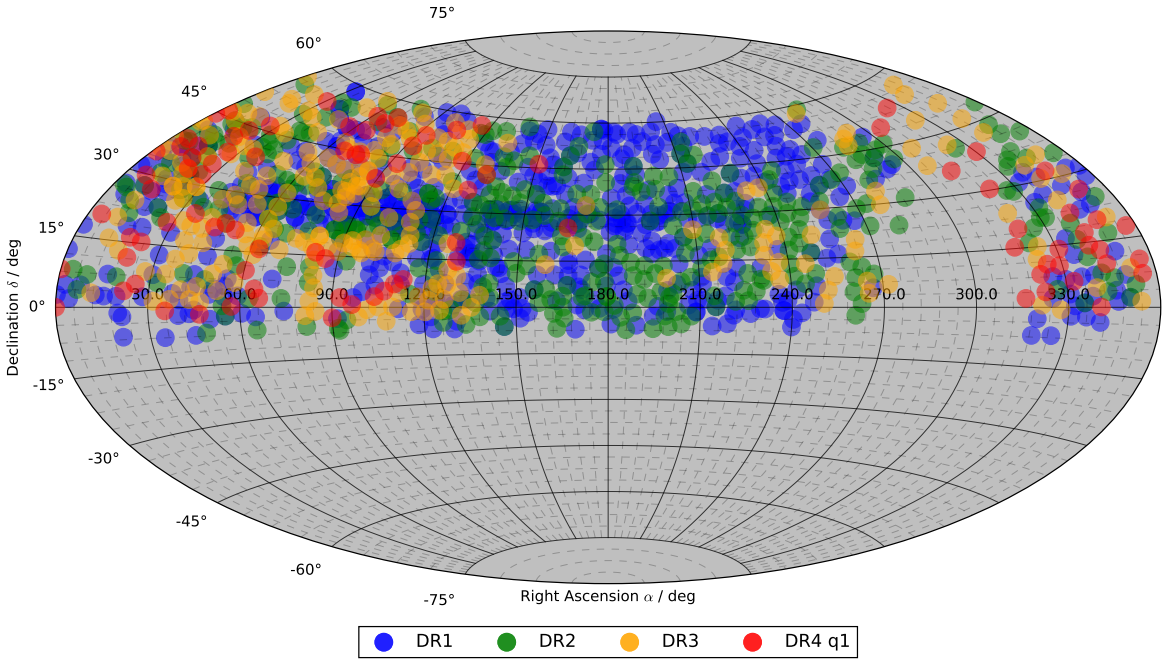


Figure. 6.1: The coverage of all internal data releases of LAMOST (first through fourth, as of March 2016).

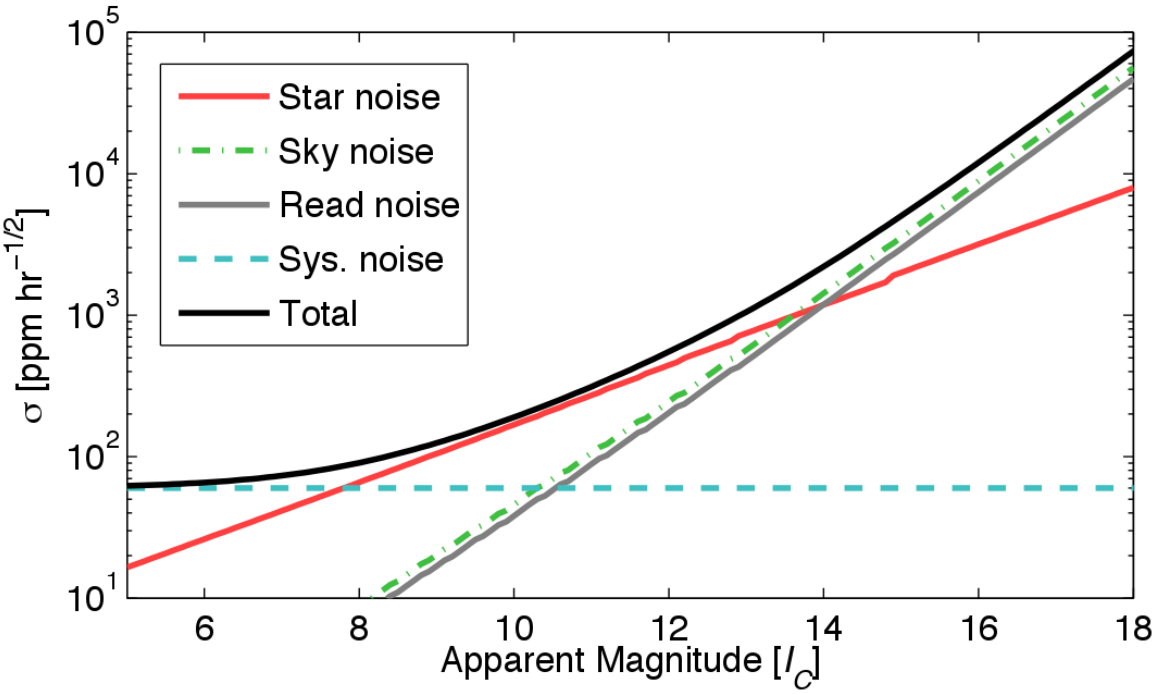


Figure. 6.2: Figure from Ricker et al. (Figure 8, 2014) . Expected one sigma photometric precision from TESS as a function of $I_C$ magnitude. This can be used along with the transit depth $((R_2/R_2)^2$to estimate SNR of a UCD transit around an M dwarf. $R_1$ is the mass of the M dwarf and $R_2$ is the mass of the UCD, taken from Section 1.2 and Section 1.1 respectively.

| $R_1$ $M_\odot$ | $R_2$ $M_{Jup}$ | No. SNR>25 | $R_2$ $M_{Jup}$ | No. SNR>25 | $R_2$ $M_{Jup}$ | No. SNR>25 |
|---|---|---|---|---|---|---|
| 0.2 | 0.75 | 36 | 1.0 | 172 | 1.25 | 558 |
| 0.26 | 0.75 | 6 | 1.0 | 42 | 1.25 | 145 |
| 0.39 | 0.75 | 0 | 1.0 | 2 | 1.25 | 13 |

Table 6.1: Table showing the various number of my M+UCD candidates where the SNR for TESS is greater than 25 assuming that $R_1$ and $R_2$ is the same for every M dwarf.

$$I_C = (-0.386 \pm 0.004)(i - z) - (0.397 \pm 0.001) + i \tag{6.1}$$

Figure 6.3 shows the estimated signal and SNR expected for TESS light curve photometry, and how this applies to my sample of candidate M+UCD unresolved multiple multiple systems. Hence given that a SNR of ∼25 should be detectable, TESS has a very real probability of being able to detect any of my M+UCD candidates that may be transiting (see Table 6.1).

### 6.1.3 Defining a colour similar grid

Currently my process of finding colour excess relies on defining a colour sub-volume centred on each of the M dwarfs in my excess sample (see Section 3.4.2 and specifically Equation 3.8). Using my excess sample I could define a grid (in $(g - r)$, $(g - i)$ and $(r - i)$) such that any M dwarf with $g$, $r$, and $i$ could be used to work out colour excess. This would open my analysis up to a vast number of other M dwarfs for which colour excess (in $(J - W2)$) could be gauged.

One would have to be rather careful about choosing the M dwarfs to use in this analysis. Any reddening would need to be corrected for and spectroscopically selected M dwarfs would make for better targets. For example LAMOST has currently spectroscopically identified nearly 300,000 M dwarfs (DR1, DR2 and DR3), West et al. (2011, via SDSS) has over 70,000 M dwarfs (although fainter many could still be tested for colour excess), the MoVeRS catalogue (Theissen et al., 2016, although again many of these are fainter there are over 3,000,000 M dwarfs available), and new catalogues such as PANSTARSS (Kaiser et al., 2002, which will provide optical bands very similar to SDSS) will provide a host of new M dwarfs to probe for colour excess. The more M+UCD candidates I find the more stringent cuts I can apply and the more chance there is of finding even rarer systems such as UCD transiting M dwarfs (i.e. Section 6.1.2).

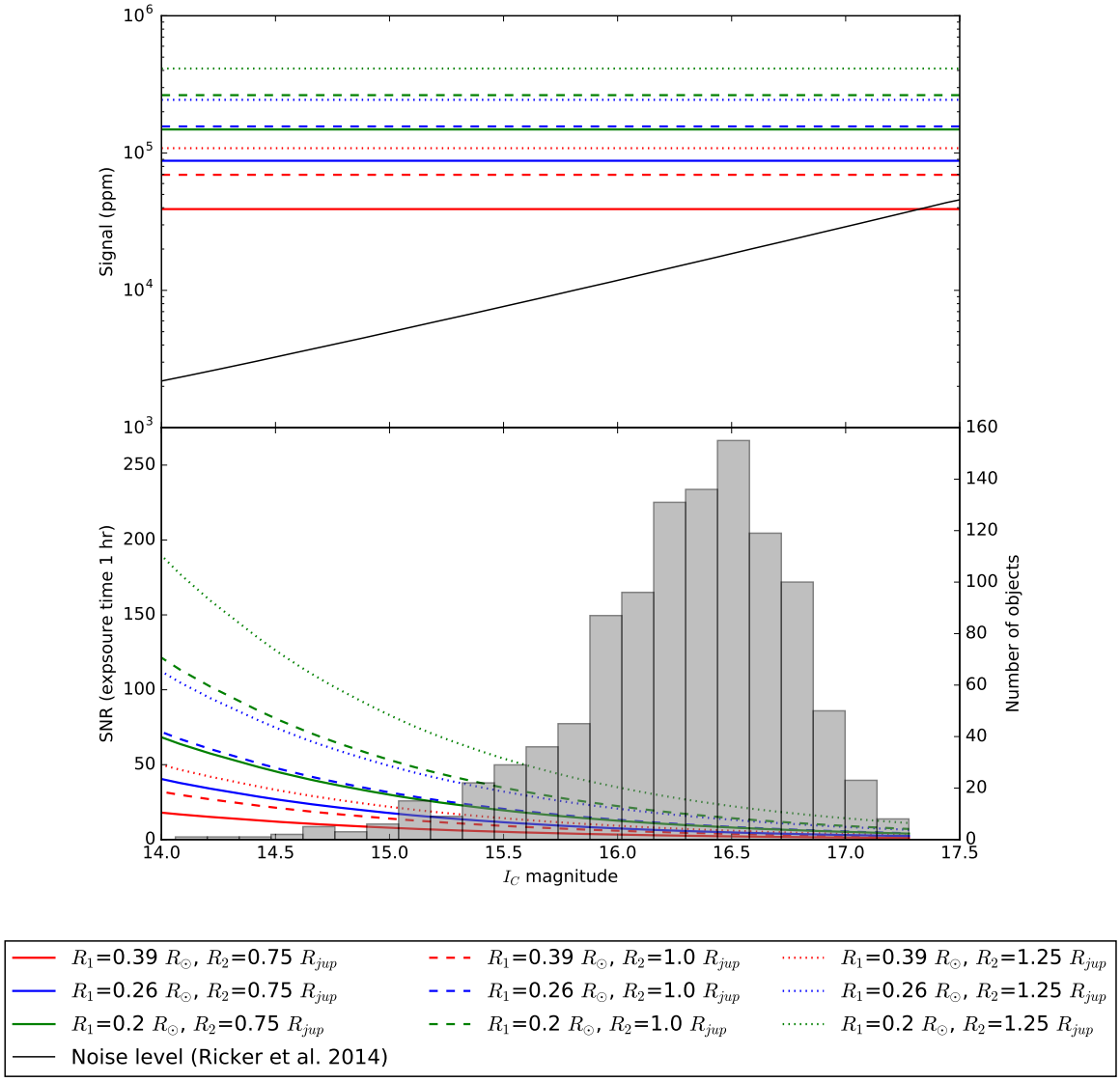


Figure. 6.3: The estimated SNR obtainable from TESS for my M+UCD candidates. A SNR of 25 should be detectable by TESS therefore if any of my M+UCD candidates have a transiting UCD, TESS should be able to detect them.

### 6.1.4 Confirmation of Young and Late M dwarfs

I also wish to confirm the signatures of youth from my young M dwarf sample (see Section 5.2). One way to confirm youth is to measure certain spectral indices from molecular bands across the spectral region (e.g. TiO: 5,847-6,058$\mathring{A}$; 6,080-6,390$\mathring{A}$; 6,510-6,852; 7,053-7,270; 7,650-7,850; 8,206-8,569; 8,859-8,950$\mathring{A}$, VO: 7,350-7,550; 7,850-7,950; 8,500-8,650 $\mathring{A}$, CaH: 6750-7050 $\mathring{A}$, $H_2O-K2$: 2,235-2,255 $\mathring{A}$ as in Manara et al. 2013) to better confirm spectral types. One can also use NaI ($\lambda = 8,183; 8,195; 11,396\mathring{A}$), KI ($\lambda = 7,665; 7,699; 11,692; 11,778; 12,437; 12,529\mathring{A}$), FeH ($\lambda = 9,980; 1,200\mathring{A}$) CaH ($\lambda = 6,960 - 6,990; 6,972.5 - 6,977.5$) to measure surface gravity (e.g. Shkolnik et al. 2009, Allers & Liu 2013).

In addition the use of grids of template spectra (from the literature and models, e.g. Katz et al. 1998, Shkolnik et al. 2011, Manara et al. 2013, Stelzer et al. 2013) could be used to measure $T_{eff}$, $log\, g$, metallicity and/or $vsin(i)$. These properties could then be used to confirm youth and are also invaluable for any exoplanet follow-up.

I could also cross-match my M dwarfs with X-Ray and UV data in order to look for emission associated with youth. Using the *Rosat All-Sky Survey Bright Source Catalogue* (Voges et al., 1999) and *Rosat All-Sky Survey Faint Source Catalogue* (Voges et al., 2000) one could look for young M dwarfs working out $L_X/L_{bol}$ and comparing it to known young M dwarfs. A similar approach could be done with the UV data from *Galaxy Evolution Explorer* (GALEX, Martin et al. 2005) all-sky imaging survey ($FUV$ = 1,350 - 1,750$\mathring{A}$, $NUV$ = 1,750 - 2,750 $\mathring{A}$), again comparing to known young M dwarfs. As well as this another possibility exists in analysing my full M dwarf candidate catalogue with BANYANII (Gagné et al., 2014; Malo et al., 2013), an initial investigation into the membership has revealed at least 108 of my M dwarfs may belong to one or more kinematic moving groups (82 may belong to $\beta$ Pictoris, 49 may belong to AB Doradus, 17 may belong to Tucana Horologium, 20 may belong to Columba and 6 may belong to Argus[50]).

With the Kepler 2 campaigns (see Figure 6.4) continuing there is also the opportunity to observe light curves for more of my M dwarfs[51]. In total campaigns 1, 5, 8, and 12 overlap more than 75 per cent with the SDSS fields, campaigns 0, 2, 3, 4, 6, and 10 have at least some overlap with the SDSS fields, thus future data mining and proposals (other than the current cross-matches with campaigns 0, 1 and 2) should lead to many more of my M dwarfs having light curves, and thus being able to search for young M dwarf candidates.

The photometrically selected late M dwarfs will need spectra to confirm their spectral types, similarly to the way I spectroscopically select late M dwarfs. A growing

[50]Note that this was a preliminary investigation, and many of the best fit moving groups have shared probability of matching a certain group and that some of these objects are only a good match and would fail this test if I had a more reliable distance constraint.

[51]Data accessed from http://keplerscience.arc.nasa.gov/k2-fields.html

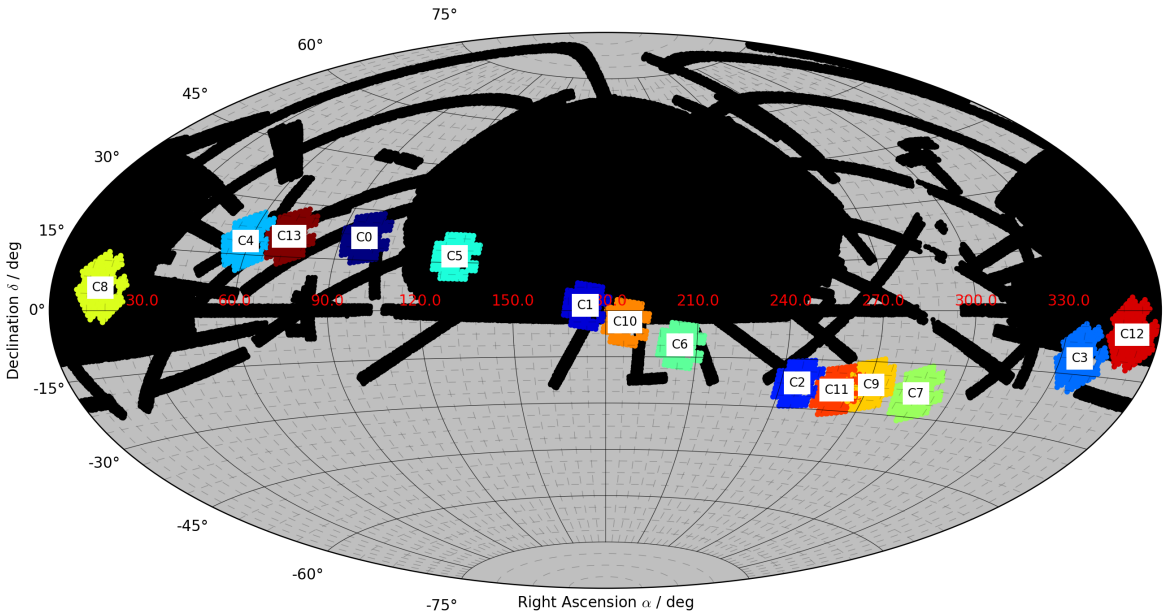


Figure. 6.4: Figure showing the current and planned coverage of the Kepler K2 mission[51]. Campaign 8 ran from January to March 2016, Campaign 9, 10, and 11 will start in April, July and September 2016.

sample of late M dwarfs join the ranks of interesting targets for RV planet hunting using red-optical and/or NIR spectrographs.

### 6.1.5 Confirmation of wide companions

The next step with the wide companions (i.e. Section 5.4 and Section 5.5) would be to verify the distances to the primary and companion. This is because the weakest constraint on the common proper motion criteria is the distance.

Gaia (see Section 6.3) will provide these distances later this year for all the Tycho-2 stars and for all my M dwarfs a few years later. The other follow-up would be to confirm the spectral types of the primary and companion stars and thus start to characterise both the primary and companion. I am currently observing the brightest primaries with the *High Efficiency and Resolution Mercator Echelle Spectrograph* (HERMES) on the 1.2 m Mercator telescope (Raskin et al., 2011, Roque de los Muchachos Observatory on La Palma, Canary Islands, Spain), and spectra will enable better distance constraints (compared to the current photometric distances) thus verifying the nature of these common proper motion pairs, through, in particular, metallicity measurements of the primaries.

## 6.2 Model fitting the LAMOST spectra

As mentioned in Section 4.3 and Section 5.2.1 through the internal LAMOST data releases 10,591 of my M dwarfs have optical spectra. With the addition of the DR3 and DR4 releases this number could double. In Section 3.3.1 I used a Bayesian approach to fit a model (a polynomial fit) to photometric data (using EMCEE[52] and the fitting routine used by Foreman-Mackey et al. 2013 and Hogg et al. 2010). This method could also be used to characterise the stellar properties of my M dwarfs with LAMOST spectra. Using model spectra (CIFIST2011_2015, BT-Settl models Baraffe et al., 2015) I can analyse both the LAMOST data and a spectral energy distribution (SED) created from the eight photometric points I have ($g$, $r$, $i$, $J$, $H$, $K_S$, $W1$, $W2$). By using a grid in temperature, surface gravity, metallicity, limb-darkening, rotation velocity I can fit sections of the LAMOST spectrum to their statistically optimal values. Using the photometry, additional constraints on distance (without needing a parallax measurement) and radius would be possible (through scaling the SED and LAMOST spectra to the same distance as the models, natively defined at the stellar surface of the object). There are several ways one could achieve these fits, I could independently fit the spectrum and the SED leading to two sets of parameters and thus compare them, or combine the Bayesian probabilities to find a combined best fit solution. One should be wary of using the LAMOST spectra (as mentioned in Section 1.4.4) as they should only be considered useful between 6,000 and 8,000 $\mathring{A}$ and initial experimentation has shown that splitting the spectrum into small chunks and combining the best fit probabilities may be better than fitting models to a single spectrum (this may be due to the nature of the LAMOST spectra with regards to the fitting of the continuum, wavelength calibration and flux calibration in the pipeline process).

Figure 6.5 shows my initial experimentation fitting BT-Settl models to M dwarfs with LAMOST spectra. The BT-Settl models currently in use are only for solar metallicity hence in these preliminary fits I only fit for temperature, surface gravity and rotational velocity. The initial fits have varying success fitting extremely well in some places (i.e. around 7,000 $\mathring{A}$) and poorly in others (i.e. 6,500 $\mathring{A}$ and 7,500 $\mathring{A}$). This could be due to the lack of metallicity variation or due to the normalisation I impose to do these initial fits (or a combination of both), this is my basis for future experimentation into splitting up and fitting smaller bands of spectral features and combining the probabilities to find the best fitting BT-Settl model. Extending my fit to use models that vary in metallicity would also make the fit better.

[52] pure-PYTHON implementation of Goodman & Weare (2010) affine invariant MCMC ensemble sampler

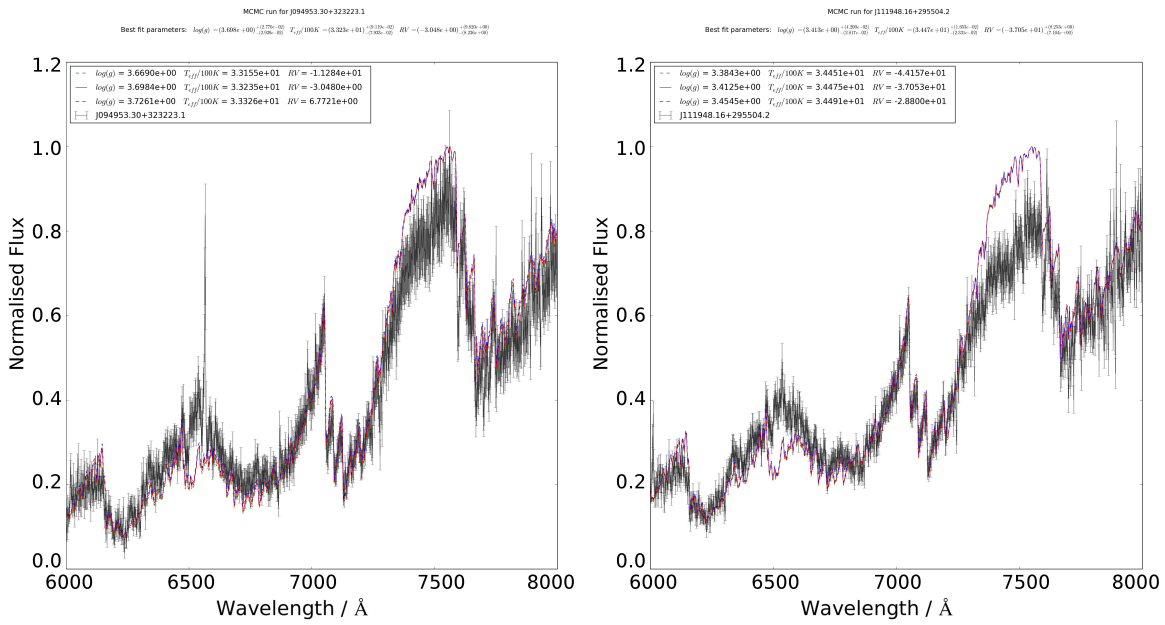


(a) (b)

Figure. 6.5: Initial experimentation fitting BT-Settl models to M dwarfs with LAMOST spectra. The BT-Settl models currently in use are only for solar metallicity hence in these preliminary fits I only fit for temperature, surface gravity and rotational velocity. The initial fits have varying success fitting extremely well in some places (i.e. around 7,000 $\mathring{A}$) and poorly in others (i.e. 6,500 $\mathring{A}$ and 7,500 $\mathring{A}$.

## 6.3 Upcoming surveys and missions

There are some important new and future surveys and missions that will greatly benefit this research. The GPI on Gemini South (Macintosh et al. 2006) and NIRISS on the JWST (Gardner et al. 2006) will allow high contrast imaging and as such could lead to direct detection and possible measurement of orbital parameters. MEarth (Charbonneau et al., 2008), TESS(Ricker et al., 2014) PLATO 2(Rauer et al., 2014) as well as NIR ground-based surveys such as the HPF(Mahadevan et al., 2010), CARMENES (Quirrenbach et al., 2010), SPIRou (Artigau et al., 2014), IRD (Kotani et al., 2014) iLocator (Crepp et al., 2014) will also be very beneficial to following up these rare objects. SPIRou, for example, should allow me to measure mass constraints for my companions. SPIRou could also be used to measure magnetic activity amongst my young M dwarf sample. New transit programs (i.e. TESS, LSST) will allow me to identify transits and measure transit timing variations amongst my M+UCD candidates.

### 6.3.1 Extension to the Southern Hemisphere

My current catalogue covers the northern Sloan sky, and I would like to expand to the south using a full southern sky survey such as *SkyMapper Southern Sky Survey* (Keller

et al., 2007). The Southern Sky Survey is expected to reach depths of 21.7 in $g$ and $r$, and 20.7 in $i$ and is currently nearly eight per cent complete[53]. This will give my catalogue all-sky coverage (with the Southern Sky Survey used in the place of SDSS), and should double the number of excess M dwarfs through the implementation of my method on additional M dwarfs, and allow a more optimal use of telescope facilities in the southern hemisphere.

### 6.3.2 Gaia parallaxes

Gaia is a billion pixel space-based telescope and was launched in December 2013 (Eyer et al., 2013). It is currently accurately measuring positions, parallaxes and proper motions as well as obtaining information on double and multiple systems, photometry, variability and planetary systems (McCaughrean, 2012). It should be able to detect 26 million sources for V<15 magnitudes, 250 million sources for V<18 magnitudes, and an estimated billion sources at the magnitude limit of V∼20 magnitudes (McCaughrean, 2012; Perryman et al., 1997). This puts the effective distance limit of Gaia at 1 Mpc with an accuracy of up to 7 $\mu$arcsec for a V at 10 magnitudes, 12-25 $\mu$arcsec a V at 15 magnitudes, and 100-300 $\mu$arcsec for a V at ∼20 magnitudes (McCaughrean, 2012). The first data release is set for mid 2016 and will provide parallaxes and accurate positions for all Tycho-2 stars. With intermediate catalogues releases following this, every source in my M dwarf catalogue should have accurate positions, distances and proper motions.

As discussed by Sarro et al. (2013) the numbers of UCDs and M dwarfs one should expect to find is shown in Figure 6.6. Although the number of UCDs is low, any UCD as companions to brighter stars (including M dwarfs) will have a primary star with accurate positions, distances and proper motions and thus can be inferred for their companions.

New moving groups will also be found by Gaia (i.e. exploiting Bayesian analysis such as those used by Malo et al. 2013, Gagné et al. 2014) and possible astrometry and RV for confirming my companions.

[53]Information from http://rsaa.anu.edu.au/research/projects/skymapper-southern-sky-survey

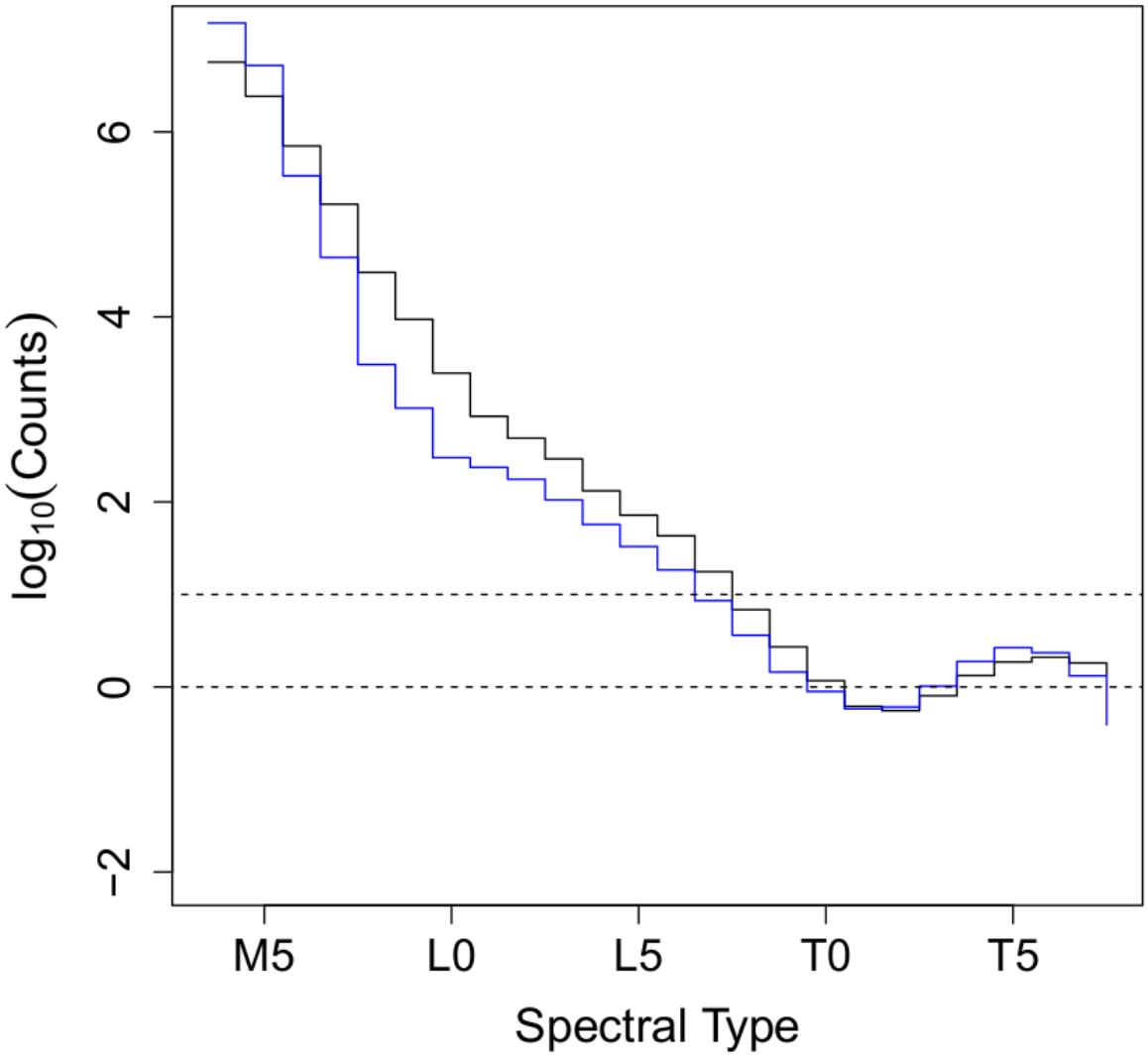


Figure. 6.6: Figure from Sarro et al. (2013) showing the predicted number of counts per spectral type bin for Gaia, the black line represents the data from Caballero et al. (2008), where a spectral type and an I-band relationship is used. The blue line represents the data from the BT-Settl model (Allard et al., 2012). Dashed lines indicate 1 and 10 detection counts. For further details see Sarro et al. (2013).

## 6.4 Conclusions

In conclusion, I have used the cross-match between WISE, 2MASS and SDSS to identify a large sample of M dwarfs (full M dwarf candidate catalogue of 440,694 M dwarfs). I have identified a subset of these M dwarfs which are of sufficiently high quality to look for colour excess, through a strict set of quality control and photometric cuts (the excess sample of 36,898 M dwarfs). From the colour excess sample I selected those objects which show sufficient colour excess in $(J - W2)$ (through the use of improvement contours) to be possible unresolved M+UCD systems. These form my 1,082 M+UCD candidates.

I considered the different types of possible contamination in my sample and thus showed that I should not be finding any M+UCD candidates that are just chance alignments between other M dwarfs, UCDs or giant stars. Some contamination will come from the primary stars being non M dwarfs or early M dwarfs. Through my use of the LAMOST spectra I believe this contamination should be minimal. However, the most common type of contamination is likely to come from chance alignments with red galaxies, in the worst case scenario around ∼100 of my M+UCD candidates, and a best case scenario around ∼35 may be chance alignments with sufficiently red galaxies within the 6 arcsec WISE PSF, this still means that over 90 per cent of my M dwarfs should not be chance aligned with galaxies. I discuss possible follow-up in the form of a set of low resolution spectral differences between my M+UCD candidates and non-M+UCD candidate (control stars). Currently I am in the process of observing some of my M+UCD candidates (and control stars) with SpeX on the IRTF (Cook et al., 2016b), and plan follow-on AO and RV measurements for the most interesting M+UCD candidates.

I also use my full M dwarf candidate catalogue to select other rare objects. I select young and late M dwarf candidates, candidates for possible exoplanet searches. Using common proper motion I also select wide Tycho-2 companions and select M+M binaries from my full M dwarf candidate catalogue.

The products of this thesis (the catalogues and sub-samples presented above) are summarised in Table 6.2.

| Description of Sample | Number of objects | Section |
|---|---|---|
| Full M dwarf candidate catalogue | 440 694 | Section 2.6 |
| Excess sample | 36 898 | Section 3.2.4 |
| M+UCD candidates | 1 082 | Section 3.5.3 |
| M dwarfs with LAMOST spectra (dr1 or dr2) | 10 591 | Section 4.3 |
| M+UCD candidates with LAMOST spectra | 47 | Section 4.3 |
| M+UCD candidates with LAMOST spectra and consistent spectral types | 38 | Section 4.3 |
| M+UCD candidates observed[54] with SpeX | 43 | Section 4.3 |
| M dwarfs with $EWH\alpha <$ -3 and $EW > 3\sigma_{EW}$ | 577 | Section 5.2.1 |
| M dwarfs with K2C0 light curves | 44 | Section 5.2.2 |
| M dwarfs with K2C1 light curves | 1093 | Section 5.2.2 |
| M dwarfs with K2C2 light curves | 12 | Section 5.2.2 |
| M dwarfs with similar Kepler 2 rotation periods | 379 | Section 5.2.2 |
| M dwarfs with similar Kepler 2 rotation periods and $< 10 days$ | 10 | Section 5.2.2 |
| Late M dwarfs (photometrically selected) | 3 013 | Section 5.3.1 |
| Late M dwarfs (spectroscopically selected) | 257 | Section 5.3.2 |
| Tycho-2 common proper motion pairs | 87 | Section 5.4 |
| Tycho-2 common proper motion pairs (P>0.25) | 14 | Section 5.4 |
| M+M common proper motion pairs | 871 | Section 5.4.2 |
| M+M common proper motion (P>0.25) | 251 | Section 5.4.2 |

Table 6.2: Summary of my M dwarf samples produced in this work.

## 6.5 Science acknowledgements

NJC acknowledges support from the UK's Science and Technology Facilities Council [grant number ST/K502029/1], and has benefited from IPERCOOL, grant number 247593 within the Marie Curie 7th European Community Framework Programme. MG acknowledges support from Joined Committee ESO and Government of Chile 2014 and Fondecyt Regular No. 1120601. Support for MG and RGK is provided by the Ministry for the Economy, Development, and Tourisms Programa Inicativa Cientifica Milenio through grant IC 12009, awarded to The Millennium Institute of Astrophysics (MAS) and acknowledgement to CONICYT REDES No. 140042 project. R.G.K. is supported by Fondecyt Regular No. 1130140.

This thesis made use of NASA's Astrophysics Data System. This thesis made use of the NASA/IPAC Infrared Science Archive, which is operated by the Jet Propulsion Laboratory, California Institute of Technology, under contract with the National Aeronautics and Space Administration. Some/all of the data presented in this thesis were obtained from the Mikulski Archive for Space Telescopes (MAST). STScI is operated by the Association of Universities for Research in Astronomy, Inc., under NASA contract NAS5-26555. Support for MAST for non-HST data is provided by the NASA Office of Space Science via grant NNX13AC07G and by other grants and contracts. This thesis made use of the SIMBAD database, operated at CDS, Strasbourg, France. This thesis has benefitted from the SpeX Prism Spectral Libraries, maintained by Adam Burgasser at http://pono.ucsd.edu/~adam/browndwarfs/spexprism. This thesis made use of the VizieR catalogue access tool, CDS, Strasbourg, France. This thesis made use of WebPlotDigitizer (http://arohatgi.info/WebPlotDigitizer/) by Ankit Rohatgi. This thesis made use of the X-shooter Spectral Library Chen et al. (2014) at http://xsl.u-strasbg.fr/.

This thesis made use of Aladin, an interactive software sky atlas (Bonnarel et al., 2000) This thesis made use of APLpy, an open-source plotting package for Python hosted at http://aplpy.github.com. This thesis made use of Astropy, a community-developed core Python package for Astronomy (Astropy Collaboration et al., 2013). This thesis made use of the IPython package (Pérez & Granger, 2007). This thesis made use of matplotlib, a Python library for publication quality graphics (Hunter, 2007). This thesis made use of SciPy (Jones et al., 2001). This thesis made use of TOPCAT, an interactive graphical viewer and editor for tabular data (Taylor, 2005).

This thesis makes use of data products from the Two Micron All Sky Survey(Skrutskie et al., 2006), which is a joint project of the University of Massachusetts and the Infrared Processing and Analysis Center/California Institute of Technology, funded by the National Aeronautics and Space Administration and the National Science Foundation. The Digitized Sky Surveys were produced at the Space Telescope Science

Institute under U.S. Government grant NAG W-2166. The images of these surveys are based on photographic data obtained using the Oschin Schmidt Telescope on Palomar Mountain and the UK Schmidt Telescope. The plates were processed into the present compressed digital form with the permission of these institutions. The National Geographic Society - Palomar Observatory Sky Atlas (POSS-I) was made by the California Institute of Technology with grants from the National Geographic Society. The Second Palomar Observatory Sky Survey (POSS-II) was made by the California Institute of Technology with funds from the National Science Foundation, the National Geographic Society, the Sloan Foundation, the Samuel Oschin Foundation, and the Eastman Kodak Corporation. The Oschin Schmidt Telescope is operated by the California Institute of Technology and Palomar Observatory. The UK Schmidt Telescope was operated by the Royal Observatory Edinburgh, with funding from the UK Science and Engineering Research Council (later the UK Particle Physics and Astronomy Research Council), until 1988 June, and thereafter by the Anglo-Australian Observatory. The blue plates of the southern Sky Atlas and its Equatorial Extension (together known as the SERC-J), as well as the Equatorial Red (ER), and the Second Epoch [red] Survey (SES) were all taken with the UK Schmidt. All data are subject to the copyright given in the copyright summary. Copyright information specific to individual plates is provided in the downloaded FITS headers. Supplemental funding for sky-survey work at the ST ScI is provided by the European Southern Observatory. This thesis is based in part on services provided by the GAVO Data Center and the data products from the PPMXL database of Roeser et al. (2010). Funding for the SDSS and SDSS-II(York et al., 2000) has been provided by the Alfred P. Sloan Foundation, the Participating Institutions, the National Science Foundation, the U.S. Department of Energy, the National Aeronautics and Space Administration, the Japanese Monbukagakusho, the Max Planck Society, and the Higher Education Funding Council for England. The SDSS Web Site is http://www.sdss.org/. The SDSS is managed by the Astrophysical Research Consortium for the Participating Institutions. The Participating Institutions are the American Museum of Natural History, Astrophysical Institute Potsdam, University of Basel, University of Cambridge, Case Western Reserve University, University of Chicago, Drexel University, Fermilab, the Institute for Advanced Study, the Japan Participation Group, Johns Hopkins University, the Joint Institute for Nuclear Astrophysics, the Kavli Institute for Particle Astrophysics and Cosmology, the Korean Scientist Group, the Chinese Academy of Sciences (LAMOST), Los Alamos National Laboratory, the Max-Planck-Institute for Astronomy (MPIA), the Max-Planck-Institute for Astrophysics (MPA), New Mexico State University, Ohio State University, University of Pittsburgh, University of Portsmouth, Princeton University, the United States Naval Observatory, and the University of Washington. Funding for SDSS-III(Ahn et al., 2012) has been provided by the Alfred P. Sloan Foundation,

the Participating Institutions, the National Science Foundation, and the U.S. Department of Energy Office of Science. The SDSS-III web site is http://www.sdss3.org/. SDSS-III is managed by the Astrophysical Research Consortium for the Participating Institutions of the SDSS-III Collaboration including the University of Arizona, the Brazilian Participation Group, Brookhaven National Laboratory, University of Cambridge, Carnegie Mellon University, University of Florida, the French Participation Group, the German Participation Group, Harvard University, the Instituto de Astrofisica de Canarias, the Michigan State/Notre Dame/JINA Participation Group, Johns Hopkins University, Lawrence Berkeley National Laboratory, Max Planck Institute for Astrophysics, Max Planck Institute for Extraterrestrial Physics, New Mexico State University, New York University, Ohio State University, Pennsylvania State University, University of Portsmouth, Princeton University, the Spanish Participation Group, University of Tokyo, University of Utah, Vanderbilt University, University of Virginia, University of Washington, and Yale University. This thesis has made use of the USNO Image and Catalogue Archive operated by the United States Naval Observatory, Flagstaff Station (http://www.nofs.navy.mil/data/fchpix/) from Monet (1998). This thesis makes use of data products from the Wide-field Infrared Survey Explorer(Wright et al., 2010), which is a joint project of the University of California, Los Angeles, and the Jet Propulsion Laboratory/California Institute of Technology, funded by the National Aeronautics and Space Administration.

This thesis includes data collected by the Kepler mission. Funding for the Kepler mission is provided by the NASA Science Mission directorate. This thesis makes use of the Guoshoujing Telescope (the Large Sky Area Multi-Object Fiber Spectroscopic Telescope LAMOST, Cui et al. 2012) and is a National Major Scientific Project built by the Chinese Academy of Sciences. Funding for the project has been provided by the National Development and Reform Commission. LAMOST is operated and managed by the National Astronomical Observatories, Chinese Academy of Sciences.

# References


Aberasturi, M., Burgasser, A. J., Mora, A., Solano, E., Martín, E. L., Reid, I. N., & Looper, D. 2014, AJ, 148, 129 [ADS]

Abt, H. A. & Levy, S. G. 1976, ApJS, 30, 273 [ADS]

Adams, F. C., Hollenbach, D., Laughlin, G., & Gorti, U. 2004, ApJ, 611, 360 [ADS]

Agol, E., Steffen, J., Sari, R., & Clarkson, W. 2005, MNRAS, 359, 567 [ADS]

Ahn, C. P., Alexandroff, R., Allende Prieto, C., Anderson, S. F., Anderton, T., Andrews, B. H., Aubourg, É., Bailey, S., Balbinot, E., Barnes, R., & et al. 2012, ApJS, 203, 21 [ADS]

Alibert, Y., Mordasini, C., Benz, W., & Winisdoerffer, C. 2005, A&A, 434, 343 [ADS]

Allard, F., Hauschildt, P. H., Alexander, D. R., & Starrfield, S. 1997, ARA&A, 35, 137 [ADS]

Allard, F., Homeier, D., & Freytag, B. 2012, Royal Society of London Philosophical Transactions Series A, 370, 2765 [ADS]

Allers, K. N., Jaffe, D. T., Luhman, K. L., Liu, M. C., Wilson, J. C., Skrutskie, M. F., Nelson, M., Peterson, D. E., Smith, J. D., & Cushing, M. C. 2007, ApJ, 657, 511 [ADS]

Allers, K. N. & Liu, M. C. 2013, ApJ, 772, 79 [ADS]

Alonso-Floriano, F. J., Morales, J. C., Caballero, J. A., Montes, D., Klutsch, A., Mundt, R., Cortés-Contreras, M., Ribas, I., Reiners, A., Amado, P. J., Quirrenbach, A., & Jeffers, S. V. 2015, A&A, 577, A128 [ADS]

Anderson, D. R., Collier Cameron, A., Hellier, C., Lendl, M., Maxted, P. F. L., Pollacco, D., Queloz, D., Smalley, B., Smith, A. M. S., Todd, I., Triaud, A. H. M. J., West, R. G., Barros, S. C. C., Enoch, B., Gillon, M., Lister, T. A., Pepe, F., Ségransan, D., Street, R. A., & Udry, S. 2011, ApJ, 726, L19 [ADS]

Angus, R., Foreman-Mackey, D., & Johnson, J. A. 2016, ApJ, 818, 109 [ADS]

Artigau, É., Kouach, D., Donati, J.-F., Doyon, R., Delfosse, X., Baratchart, S., Lacombe, M., Moutou, C., Rabou, P., Parès, L. P., Micheau, Y., Thibault, S., Reshetov, V. A., Dubois, B., Hernandez, O., Vallée, P., Wang, S.-Y., Dolon, F., Pepe, F. A., Bouchy, F., Striebig, N., Hénault, F., Loop, D., Saddlemyer, L., Barrick, G., Vermeulen, T., Dupieux, M., Hébrard, G., Boisse, I., Martioli, E., Alencar, S. H. P., do Nascimento, J.-D., & Figueira, P. 2014, in Proc. SPIE, Vol. 9147, Ground-based and Airborne Instrumentation for Astronomy V, 914715 [ADS]

Assafin, M., Andrei, A. H., Martins, R. V., da Silva Neto, D. N., Camargo, J. I. B., Teixeira, R., & Benevides-Soares, P. 2001, ApJ, 552, 380 [ADS]

Astropy Collaboration, Robitaille, T. P., Tollerud, E. J., Greenfield, P., Droettboom, M., Bray, E., Aldcroft, T., Davis, M., Ginsburg, A., Price-Whelan, A. M., Kerzendorf, W. E., Conley, A., Crighton, N., Barbary, K., Muna, D., Ferguson, H., Grollier, F., Parikh, M. M., Nair, P. H., Unther, H. M., Deil, C., Woillez, J., Conseil, S., Kramer, R., Turner, J. E. H., Singer, L., Fox, R., Weaver, B. A., Zabalza, V., Edwards, Z. I., Azalee Bostroem, K., Burke, D. J., Casey, A. R., Crawford, S. M., Dencheva, N., Ely, J., Jenness, T., Labrie, K., Lim, P. L., Pierfederici, F., Pontzen, A., Ptak, A., Refsdal, B., Servillat, M., & Streicher, O. 2013, A&A, 558, A33 [ADS]

Baraffe, I., Chabrier, G., Allard, F., & Hauschildt, P. H. 2002, A&A, 382, 563 [ADS]

Baraffe, I., Chabrier, G., Barman, T. S., Allard, F., & Hauschildt, P. H. 2003, A&A, 402, 701 [ADS]

Baraffe, I., Homeier, D., Allard, F., & Chabrier, G. 2015, A&A, 577, A42 [ADS]

Bardalez Gagliuffi, D. C., Burgasser, A. J., & Gelino, C. R. 2013, Mem. Soc. Astron. Italiana, 84, 1041 [ADS]

Bardalez Gagliuffi, D. C., Burgasser, A. J., Gelino, C. R., Melis, C., & Blake, C. 2015, in Cambridge Workshop on Cool Stars, Stellar Systems, and the Sun, Vol. 18, 18th Cambridge Workshop on Cool Stars, Stellar Systems, and the Sun, 575–582 [ADS]

Basri, G. 1998, in Astronomical Society of the Pacific Conference Series, Vol. 134, Brown Dwarfs and Extrasolar Planets, 394 [ADS]

Basri, G., Mohanty, S., Allard, F., Hauschildt, P. H., Delfosse, X., Martín, E. L., Forveille, T., & Goldman, B. 2000, ApJ, 538, 363 [ADS]

Bate, M. R. 2000, MNRAS, 314, 33 [ADS]

Batten, A. H. 1973, Binary and multiple systems of stars [ADS]

Beckwith, S. V. W., Sargent, A. I., Chini, R. S., & Guesten, R. 1990, AJ, 99, 924 [ADS]

Bell, K. J., Hilton, E. J., Davenport, J. R. A., Hawley, S. L., West, A. A., & Rogel, A. B. 2012, PASP, 124, 14 [ADS]

Bergfors, C., Brandner, W., Bonnefoy, M., Schlieder, J., Janson, M., Henning, T., & Chauvin, G. 2016, MNRAS, 456, 2576 [ADS]

Bergfors, C., Brandner, W., Janson, M., Daemgen, S., Geissler, K., Henning, T., Hippler, S., Hormuth, F., Joergens, V., & Köhler, R. 2010, A&A, 520, A54 [ADS]

Berta-Thompson, Z. 2014, in Habitable Worlds Across Time and Space, proceedings of a conference held April 28-May 1 2014 at the Space Telescope Science Institute, id.6, 6 [ADS]

Biller, B. A., Close, L. M., Masciadri, E., Nielsen, E., Lenzen, R., Brandner, W., McCarthy, D., Hartung, M., Kellner, S., Mamajek, E., Henning, T., Miller, D., Kenworthy, M., & Kulesa, C. 2007, ApJS, 173, 143 [ADS]

Blanton, M. R. & Roweis, S. 2007, AJ, 133, 734 [ADS]

Bochanski, J. J., Hawley, S. L., Covey, K. R., West, A. A., Reid, I. N., Golimowski, D. A., & Ivezić, Ž. 2010, AJ, 139, 2679 [ADS]

—. 2012, AJ, 143, 152 [ADS]

Boeshaar, P. C. 1976, PhD thesis, Ohio State University, Columbus. [ADS]

Boeshaar, P. C. & Tyson, J. A. 1985, AJ, 90, 817 [ADS]

Bonfils, X., Delfosse, X., Udry, S., Santos, N. C., Forveille, T., & Ségransan, D. 2005, A&A, 442, 635 [ADS]

Bonnarel, F., Fernique, P., Bienaymé, O., Egret, D., Genova, F., Louys, M., Ochsenbein, F., Wenger, M., & Bartlett, J. G. 2000, A&AS, 143, 33 [ADS]

Bonnell, I. A., Larson, R. B., & Zinnecker, H. 2007, Protostars and Planets V, 149 [ADS]

Bonomo, A. S., Sozzetti, A., Santerne, A., Deleuil, M., Almenara, J.-M., Bruno, G., Díaz, R. F., Hébrard, G., & Moutou, C. 2015, A&A, 575, A85 [ADS]

Bopp, B. W. & Schmitz, M. 1978, PASP, 90, 531 [ADS]

Boss, A. P. 1997, Science, 276, 1836 [ADS]

—. 2002, ApJ, 576, 462 [ADS]

Bouchy, F., Bonomo, A. S., Santerne, A., Moutou, C., Deleuil, M., Díaz, R. F., Eggenberger, A., Ehrenreich, D., Gry, C., Guillot, T., Havel, M., Hébrard, G., & Udry, S. 2011a, A&A, 533, A83 [ADS]

Bouchy, F., Deleuil, M., Guillot, T., Aigrain, S., Carone, L., Cochran, W. D., Almenara, J. M., Alonso, R., Auvergne, M., Baglin, A., Barge, P., Bonomo, A. S., Bordé, P., Csizmadia, S., de Bondt, K., Deeg, H. J., Díaz, R. F., Dvorak, R., Endl, M., Erikson, A., Ferraz-Mello, S., Fridlund, M., Gandolfi, D., Gazzano, J. C., Gibson, N., Gillon, M., Guenther, E., Hatzes, A., Havel, M., Hébrard, G., Jorda, L., Léger, A., Lovis, C., Llebaria, A., Lammer, H., MacQueen, P. J., Mazeh, T., Moutou, C., Ofir, A., Ollivier, M., Parviainen, H., Pätzold, M., Queloz, D., Rauer, H., Rouan, D., Santerne, A., Schneider, J., Tingley, B., & Wuchterl, G. 2011b, A&A, 525, A68 [ADS]

Bouy, H., Brandner, W., Martín, E. L., Delfosse, X., Allard, F., & Basri, G. 2003, AJ, 126, 1526 [ADS]

Bouy, H., Duchêne, G., Köhler, R., Brandner, W., Bouvier, J., Martín, E. L., Ghez, A., Delfosse, X., Forveille, T., Allard, F., Baraffe, I., Basri, G., Close, L., & McCabe, C. E. 2004, A&A, 423, 341 [ADS]

Bowler, B. P., Liu, M. C., Shkolnik, E. L., & Tamura, M. 2015, ApJS, 216, 7 [ADS]

Boyajian, T. S., von Braun, K., van Belle, G., McAlister, H. A., ten Brummelaar, T. A., Kane, S. R., Muirhead, P. S., Jones, J., White, R., Schaefer, G., Ciardi, D., Henry, T., López-Morales, M., Ridgway, S., Gies, D., Jao, W.-C., Rojas-Ayala, B., Parks, J. R., Sturmann, L., Sturmann, J., Turner, N. H., Farrington, C., Goldfinger, P. J., & Berger, D. H. 2012, ApJ, 757, 112 [ADS]

Boylan-Kolchin, M., Springel, V., White, S. D. M., Jenkins, A., & Lemson, G. 2009, MNRAS, 398, 1150 [ADS]

Brandner, W., Zinnecker, H., Alcalá, J. M., Allard, F., Covino, E., Frink, S., Köhler, R., Kunkel, M., Moneti, A., & Schweitzer, A. 2000, AJ, 120, 950 [ADS]

Brandt, T. D., McElwain, M. W., Turner, E. L., Mede, K., Spiegel, D. S., Kuzuhara, M., Schlieder, J. E., Wisniewski, J. P., Abe, L., Biller, B., Brandner, W., Carson, J., Currie, T., Egner, S., Feldt, M., Golota, T., Goto, M., Grady, C. A., Guyon, O., Hashimoto, J., Hayano, Y., Hayashi, M., Hayashi, S., Henning, T., Hodapp, K. W., Inutsuka, S., Ishii, M., Iye, M., Janson, M., Kandori, R., Knapp, G. R., Kudo, T., Kusakabe, N., Kwon, J., Matsuo, T., Miyama, S., Morino, J.-I., Moro-Martín, A., Nishimura, T., Pyo, T.-S., Serabyn, E., Suto, H., Suzuki, R., Takami, M., Takato, N., Terada, H., Thalmann, C., Tomono, D., Watanabe, M., Yamada, T., Takami, H., Usuda, T., & Tamura, M. 2014, ApJ, 794, 159 [ADS]

Browning, M. K., Basri, G., Marcy, G. W., West, A. A., & Zhang, J. 2010, AJ, 139, 504 [ADS]

Burgasser, A. J. 2007a, ApJ, 659, 655 [ADS]

—. 2007b, ApJ, 658, 617 [ADS]

Burgasser, A. J. 2011, in Astronomical Society of the Pacific Conference Series, Vol. 450, Astronomical Society of the Pacific Conference Series, 113 [ADS]

Burgasser, A. J., Cruz, K. L., Cushing, M., Gelino, C. R., Looper, D. L., Faherty, J. K., Kirkpatrick, J. D., & Reid, I. N. 2010, ApJ, 710, 1142 [ADS]

Burgasser, A. J., Geballe, T. R., Leggett, S. K., Kirkpatrick, J. D., & Golimowski, D. A. 2006a, ApJ, 637, 1067 [ADS]

Burgasser, A. J., Kirkpatrick, J. D., Brown, M. E., Reid, I. N., Gizis, J. E., Dahn, C. C., Monet, D. G., Beichman, C. A., Liebert, J., Cutri, R. M., & Skrutskie, M. F. 1999, ApJ, 522, L65 [ADS]

Burgasser, A. J., Kirkpatrick, J. D., Cruz, K. L., Reid, I. N., Leggett, S. K., Liebert, J., Burrows, A., & Brown, M. E. 2006b, ApJS, 166, 585 [ADS]

Burgasser, A. J., Kirkpatrick, J. D., Reid, I. N., Brown, M. E., Miskey, C. L., & Gizis, J. E. 2003, ApJ, 586, 512 [ADS]

Burgasser, A. J., Liu, M. C., Ireland, M. J., Cruz, K. L., & Dupuy, T. J. 2008, ApJ, 681, 579 [ADS]

Burgasser, A. J., McElwain, M. W., Kirkpatrick, J. D., Cruz, K. L., Tinney, C. G., & Reid, I. N. 2004, AJ, 127, 2856 [ADS]

Burgasser, A. J., Reid, I. N., Siegler, N., Close, L., Allen, P., Lowrance, P., & Gizis, J. 2007, Protostars and Planets V, 427 [ADS]

Burningham, B., Cardoso, C. V., Smith, L., Leggett, S. K., Smart, R. L., Mann, A. W., Dhital, S., Lucas, P. W., Tinney, C. G., Pinfield, D. J., Zhang, Z., Morley, C., Saumon, D., Aller, K., Littlefair, S. P., Homeier, D., Lodieu, N., Deacon, N., Marley, M. S., van Spaandonk, L., Baker, D., Allard, F., Andrei, A. H., Canty, J., Clarke, J., Day-Jones, A. C., Dupuy, T., Fortney, J. J., Gomes, J., Ishii, M., Jones, H. R. A., Liu, M., Magazzú, A., Marocco, F., Murray, D. N., Rojas-Ayala, B., & Tamura, M. 2013, MNRAS, 433, 457 [ADS]

Burningham, B., Leggett, S. K., Homeier, D., Saumon, D., Lucas, P. W., Pinfield, D. J., Tinney, C. G., Allard, F., Marley, M. S., Jones, H. R. A., Murray, D. N., Ishii, M., Day-Jones, A., Gomes, J., & Zhang, Z. H. 2011, MNRAS, 414, 3590 [ADS]

Burningham, B., Leggett, S. K., Lucas, P. W., Pinfield, D. J., Smart, R. L., Day-Jones, A. C., Jones, H. R. A., Murray, D., Nickson, E., Tamura, M., Zhang, Z., Lodieu, N., Tinney, C. G., & Zapatero Osorio, M. R. 2010, MNRAS, 404, 1952 [ADS]

Burningham, B., Pinfield, D. J., Leggett, S. K., Tamura, M., Lucas, P. W., Homeier, D., Day-Jones, A., Jones, H. R. A., Clarke, J. R. A., Ishii, M., Kuzuhara, M., Lodieu, N., Zapatero Osorio, M. R., Venemans, B. P., Mortlock, D. J., Barrado Y Navascués, D., Martin, E. L., & Magazzù, A. 2008, MNRAS, 391, 320 [ADS]

Burningham, B., Pinfield, D. J., Leggett, S. K., Tinney, C. G., Liu, M. C., Homeier, D., West, A. A., Day-Jones, A., Huelamo, N., Dupuy, T. J., Zhang, Z., Murray, D. N., Lodieu, N., Barrado Y Navascués, D., Folkes, S., Galvez-Ortiz, M. C., Jones, H. R. A., Lucas, P. W., Calderon, M. M., & Tamura, M. 2009, MNRAS, 395, 1237 [ADS]

Burrows, A., Heng, K., & Nampaisarn, T. 2011, ApJ, 736, 47 [ADS]

Burrows, A., Hubbard, W. B., Lunine, J. I., & Liebert, J. 2001, Reviews of Modern Physics, 73, 719 [ADS]

Burrows, A., Marley, M., Hubbard, W. B., Lunine, J. I., Guillot, T., Saumon, D., Freedman, R., Sudarsky, D., & Sharp, C. 1997, ApJ, 491, 856 [ADS]

Butler, R. P., Vogt, S. S., Marcy, G. W., Fischer, D. A., Wright, J. T., Henry, G. W., Laughlin, G., & Lissauer, J. J. 2004, ApJ, 617, 580 [ADS]

Caballero, J. A., Béjar, V. J. S., Rebolo, R., Eislöffel, J., Zapatero Osorio, M. R., Mundt, R., Barrado Y Navascués, D., Bihain, G., Bailer-Jones, C. A. L., Forveille, T., & Martín, E. L. 2007, A&A, 470, 903 [ADS]

Caballero, J. A., Burgasser, A. J., & Klement, R. 2008, A&A, 488, 181 [ADS]

Caballero, J. A., Genebriera, J., Miret, F. X., Tobal, T., & Cairol, J. 2012, The Observatory, 132, 252 [ADS]

Calvet, N., Hartmann, L., & Strom, S. E. 2000, Protostars and Planets IV, 377 [ADS]

Cardelli, J. A., Clayton, G. C., & Mathis, J. S. 1989, ApJ, 345, 245 [ADS]

Carter, J. A., Yee, J. C., Eastman, J., Gaudi, B. S., & Winn, J. N. 2008, ApJ, 689, 499 [ADS]

Chabrier, G. & Baraffe, I. 2000, ARA&A, 38, 337 [ADS]

Chabrier, G., Gallardo, J., & Baraffe, I. 2007, A&A, 472, L17 [ADS]

Chabrier, G., Johansen, A., Janson, M., & Rafikov, R. 2014, ArXiv e-prints [ADS]

Charbonneau, D., Berta, Z. K., Irwin, J., Burke, C. J., Nutzman, P., Buchhave, L. A., Lovis, C., Bonfils, X., Latham, D. W., Udry, S., Murray-Clay, R. A., Holman, M. J., Falco, E. E., Winn, J. N., Queloz, D., Pepe, F., Mayor, M., Delfosse, X., & Forveille, T. 2009, Nature, 462, 891 [ADS]

Charbonneau, D., Irwin, J., Nutzman, P., & Falco, E. E. 2008, in Bulletin of the American Astronomical Society, Vol. 40, American Astronomical Society Meeting Abstracts #212, 242 [ADS]

Charbonneau, P. & MacGregor, K. B. 1997, ApJ, 486, 502 [ADS]

Chauvin, G., Lagrange, A.-M., Dumas, C., Zuckerman, B., Mouillet, D., Song, I., Beuzit, J.-L., & Lowrance, P. 2004, A&A, 425, L29 [ADS]

—. 2005a, A&A, 438, L25 [ADS]

Chauvin, G., Lagrange, A.-M., Lacombe, F., Dumas, C., Mouillet, D., Zuckerman, B., Gendron, E., Song, I., Beuzit, J.-L., Lowrance, P., & Fusco, T. 2005b, A&A, 430, 1027 [ADS]

Cheetham, A. C., Kraus, A. L., Ireland, M. J., Cieza, L., Rizzuto, A. C., & Tuthill, P. G. 2015, ApJ, 813, 83 [ADS]

Chen, Y.-P., Trager, S. C., Peletier, R. F., Lançon, A., Vazdekis, A., Prugniel, P., Silva, D. R., & Gonneau, A. 2014, A&A, 565, A117 [ADS]

Chiu, K., Fan, X., Leggett, S. K., Golimowski, D. A., Zheng, W., Geballe, T. R., Schneider, D. P., & Brinkmann, J. 2006, AJ, 131, 2722 [ADS]

Choi, M., Tatematsu, K., & Kang, M. 2010, ApJ, 723, L34 [ADS]

Choquet, É., Perrin, M. D., Chen, C. H., Soummer, R., Pueyo, L., Hagan, J. B., Gofas-Salas, E., Rajan, A., Golimowski, D. A., Hines, D. C., Schneider, G., Mazoyer, J., Augereau, J.-C., Debes, J., Stark, C. C., Wolff, S., N'Diaye, M., & Hsiao, K. 2016, ApJ, 817, L2 [ADS]

Close, L. M., Siegler, N., Freed, M., & Biller, B. 2003, ApJ, 587, 407 [ADS]

Close, L. M., Zuckerman, B., Song, I., Barman, T., Marois, C., Rice, E. L., Siegler, N., Macintosh, B., Becklin, E. E., Campbell, R., Lyke, J. E., Conrad, A., & Le Mignant, D. 2007, ApJ, 660, 1492 [ADS]

Cook, N. J., Pinfield, D. J., Marocco, F., Burningham, B., Jones, H. R. A., Frith, J., Zhong, J., Luo, A. L., Qi, Z. X., Lucas, P. W., Gromadzki, M., Day-Jones, A. C., Kurtev, R. G., Guo, Y. X., Wang, Y. F., Bai, Y., Yi, Z. P., & Smart, R. L. 2016a, MNRAS, 457, 2192 [ADS]

Cook, N. J., Pinfield, D. J., Marocco, F., Burningham, B., Jones, H. R. A., Frith, J., Zhong, J., Luo, A. L., Qi, Z. X., Lucas, P. W., Gromadzki, M., Kurtev, R. G., Guo, Y. X., Wang, Y. F., Bai, Y., Yi, Z. P., & Smart, R. L. 2016b, MNRAS, 000, 0000

Covey, K. R., Hawley, S. L., Bochanski, J. J., West, A. A., Reid, I. N., Golimowski, D. A., Davenport, J. R. A., Henry, T., Uomoto, A., & Holtzman, J. A. 2008, AJ, 136, 1778 [ADS]

Covey, K. R., Ivezić, Ž., Schlegel, D., Finkbeiner, D., Padmanabhan, N., Lupton, R. H., Agüeros, M. A., Bochanski, J. J., Hawley, S. L., West, A. A., Seth, A., Kimball, A., Gogarten, S. M., Claire, M., Haggard, D., Kaib, N., Schneider, D. P., & Sesar, B. 2007, AJ, 134, 2398 [ADS]

Covey, K. R., West, A. A., Bochanski, J. J., & Hawley, S. L. 2014, The Hammer: An IDL Spectral Typing Suite, Astrophysics Source Code Library [ADS]

Crepp, J. R., Bechter, A., Bechter, E., Berg, M., Carroll, J., Collins, K., Corpuz, T., Ketterer, R., Kielb, E., Stoddard, R., Eisner, J. A., Gaudi, B. S., Hinz, P., Kratter, K. M., Macela, G., Quirrenbach, A., Skrutskie, M. F., Sozzetti, A., Woodward, C. E., & Zhao, B. 2014, in American Astronomical Society Meeting Abstracts, Vol. 223, American Astronomical Society Meeting Abstracts #223, 348.20 [ADS]

Cruz, K. L., Kirkpatrick, J. D., & Burgasser, A. J. 2009, AJ, 137, 3345 [ADS]

Cruz, K. L., Reid, I. N., Kirkpatrick, J. D., Burgasser, A. J., Liebert, J., Solomon, A. R., Schmidt, S. J., Allen, P. R., Hawley, S. L., & Covey, K. R. 2007, AJ, 133, 439 [ADS]

Cruz, K. L., Reid, I. N., Liebert, J., Kirkpatrick, J. D., & Lowrance, P. J. 2003, AJ, 126, 2421 [ADS]

Csizmadia, S., Hatzes, A., Gandolfi, D., Deleuil, M., Bouchy, F., Fridlund, M., Szabados, L., Parviainen, H., Cabrera, J., Aigrain, S., Alonso, R., Almenara, J.-M., Baglin, A., Bordé, P., Bonomo, A. S., Deeg, H. J., Díaz, R. F., Erikson, A., Ferraz-Mello, S., Tadeu dos Santos, M., Guenther, E. W., Guillot, T., Grziwa, S., Hébrard, G., Klagyivik, P., Ollivier, M., Pätzold, M., Rauer, H., Rouan, D., Santerne, A., Schneider, J., Mazeh, T., Wuchterl, G., Carpano, S., & Ofir, A. 2015, A&A, 584, A13 [ADS]

Cui, X.-Q., Zhao, Y.-H., Chu, Y.-Q., Li, G.-P., Li, Q., Zhang, L.-P., Su, H.-J., Yao, Z.-Q., Wang, Y.-N., Xing, X.-Z., Li, X.-N., Zhu, Y.-T., Wang, G., Gu, B.-Z., Luo, A.-L., Xu, X.-Q., Zhang, Z.-C., Liu, G.-R., Zhang, H.-T., Yang, D.-H., Cao, S.-Y., Chen, H.-Y., Chen, J.-J., Chen, K.-X., Chen, Y., Chu, J.-R., Feng, L., Gong, X.-F., Hou, Y.-H., Hu, H.-Z., Hu, N.-S., Hu, Z.-W., Jia, L., Jiang, F.-H., Jiang, X., Jiang, Z.-B., Jin, G., Li, A.-H., Li, Y., Li, Y.-P., Liu, G.-Q., Liu, Z.-G., Lu, W.-Z., Mao, Y.-D., Men, L., Qi, Y.-J., Qi, Z.-X., Shi, H.-M., Tang, Z.-H., Tao, Q.-S., Wang, D.-Q., Wang, D., Wang, G.-M., Wang, H., Wang, J.-N., Wang, J., Wang, J.-L., Wang, J.-P., Wang, L., Wang, S.-Q., Wang, Y., Wang, Y.-F., Xu, L.-Z., Xu, Y., Yang, S.-H., Yu, Y., Yuan, H., Yuan, X.-Y., Zhai, C., Zhang, J., Zhang, Y.-X., Zhang, Y., Zhao, M., Zhou, F., Zhou, G.-H., Zhu, J., & Zou, S.-C. 2012, Research in Astronomy and Astrophysics, 12, 1197 [ADS]

Cumming, A., Butler, R. P., Marcy, G. W., Vogt, S. S., Wright, J. T., & Fischer, D. A. 2008, PASP, 120, 531 [ADS]

Cushing, M. C., Kirkpatrick, J. D., Gelino, C. R., Griffith, R. L., Skrutskie, M. F., Mainzer, A., Marsh, K. A., Beichman, C. A., Burgasser, A. J., Prato, L. A., Simcoe, R. A., Marley, M. S., Saumon, D., Freedman, R. S., Eisenhardt, P. R., & Wright, E. L. 2011, ApJ, 743, 50 [ADS]

Cushing, M. C., Roellig, T. L., Marley, M. S., Saumon, D., Leggett, S. K., Kirkpatrick, J. D., Wilson, J. C., Sloan, G. C., Mainzer, A. K., Van Cleve, J. E., & Houck, J. R. 2006, ApJ, 648, 614 [ADS]

Daemgen, S., Bonavita, M., Jayawardhana, R., Lafreniere, D., & Janson, M. 2014, ArXiv e-prints [ADS]

Day-Jones, A. C., Marocco, F., Pinfield, D. J., Zhang, Z. H., Burningham, B., Deacon, N., Ruiz, M. T., Gallardo, J., Jones, H. R. A., Lucas, P. W. L., Jenkins, J. S., Gomes, J., Folkes, S. L., & Clarke, J. R. A. 2013, MNRAS, 430, 1171 [ADS]

de Bruijne, J. H. J. 2012, Ap&SS, 341, 31 [ADS]

de la Reza, R., Torres, C. A. O., Quast, G., Castilho, B. V., & Vieira, G. L. 1989, ApJ, 343, L61 [ADS]

Deacon, N. R., Schlieder, J. E., Olofsson, J., Johnston, K. G., & Henning, T. 2013, MNRAS, 434, 1117 [ADS]

Deleuil, M., Deeg, H. J., Alonso, R., Bouchy, F., Rouan, D., Auvergne, M., Baglin, A., Aigrain, S., Almenara, J. M., Barbieri, M., Barge, P., Bruntt, H., Bordé, P., Collier Cameron, A., Csizmadia, S., de La Reza, R., Dvorak, R., Erikson, A., Fridlund, M., Gandolfi, D., Gillon, M., Guenther, E., Guillot, T., Hatzes, A., Hébrard, G., Jorda, L., Lammer, H., Léger, A., Llebaria, A., Loeillet, B., Mayor, M., Mazeh, T., Moutou, C., Ollivier, M., Pätzold, M., Pont, F., Queloz, D., Rauer, H., Schneider, J., Shporer, A., Wuchterl, G., & Zucker, S. 2008, A&A, 491, 889 [ADS]

Delfosse, X., Beuzit, J.-L., Marchal, L., Bonfils, X., Perrier, C., Ségransan, D., Udry, S., Mayor, M., & Forveille, T. 2004, in Astronomical Society of the Pacific Conference Series, Vol. 318, Spectroscopically and Spatially Resolving the Components of the Close Binary Stars, 166–174 [ADS]

Delfosse, X., Tinney, C. G., Forveille, T., Epchtein, N., Bertin, E., Borsenberger, J., Copet, E., de Batz, B., Fouque, P., Kimeswenger, S., Le Bertre, T., Lacombe, F., Rouan, D., & Tiphene, D. 1997, A&A, 327, L25 [ADS]

Delorme, P., Delfosse, X., Albert, L., Artigau, E., Forveille, T., Reylé, C., Allard, F., Homeier, D., Robin, A. C., Willott, C. J., Liu, M. C., & Dupuy, T. J. 2008, A&A, 482, 961 [ADS]

Delorme, P., Gagné, J., Malo, L., Reylé, C., Artigau, E., Albert, L., Forveille, T., Delfosse, X., Allard, F., & Homeier, D. 2012, A&A, 548, A26 [ADS]

Díaz, R. F., Damiani, C., Deleuil, M., Almenara, J. M., Moutou, C., Barros, S. C. C., Bonomo, A. S., Bouchy, F., Bruno, G., Hébrard, G., Montagnier, G., & Santerne, A. 2013, A&A, 551, L9 [ADS]

Díaz, R. F., Montagnier, G., Leconte, J., Bonomo, A. S., Deleuil, M., Almenara, J. M., Barros, S. C. C., Bouchy, F., Bruno, G., Damiani, C., Hébrard, G., Moutou, C., & Santerne, A. 2014, A&A, 572, A109 [ADS]

Donati, J.-F., Forveille, T., Collier Cameron, A., Barnes, J. R., Delfosse, X., Jardine, M. M., & Valenti, J. A. 2006, Science, 311, 633 [ADS]

Dressing, C. D. & Charbonneau, D. 2013, ApJ, 767, 95 [ADS]

Duchêne, G. & Kraus, A. 2013, ARA&A, 51, 269 [ADS]

Dupuy, T. J. & Liu, M. C. 2012, ApJS, 201, 19 [ADS]

Dupuy, T. J., Liu, M. C., Bowler, B. P., Cushing, M. C., Helling, C., Witte, S., & Hauschildt, P. 2010, ApJ, 721, 1725 [ADS]

Dupuy, T. J., Liu, M. C., & Ireland, M. J. 2011, in European Physical Journal Web of Conferences, Vol. 16, European Physical Journal Web of Conferences, 4004 [ADS]

Duquennoy, A. & Mayor, M. 1991, A&A, 248, 485 [ADS]

Dutrey, A., Guilloteau, S., Duvert, G., Prato, L., Simon, M., Schuster, K., & Menard, F. 1996, A&A, 309, 493 [ADS]

Eiroa, C., Marshall, J. P., Mora, A., Montesinos, B., Absil, O., Augereau, J. C., Bayo, A., Bryden, G., Danchi, W., del Burgo, C., Ertel, S., Fridlund, M., Heras, A. M., Krivov, A. V., Launhardt, R., Liseau, R., Löhne, T., Maldonado, J., Pilbratt, G. L., Roberge, A., Rodmann, J., Sanz-Forcada, J., Solano, E., Stapelfeldt, K., Thébault, P., Wolf, S., Ardila, D., Arévalo, M., Beichmann, C., Faramaz, V., González-García, B. M., Gutiérrez, R., Lebreton, J., Martínez-Arnáiz, R., Meeus, G., Montes, D., Olofsson, G., Su, K. Y. L., White, G. J., Barrado, D., Fukagawa, M., Grün, E., Kamp, I., Lorente, R., Morbidelli, A., Müller, S., Mutschke, H., Nakagawa, T., Ribas, I., & Walker, H. 2013, A&A, 555, A11 [ADS]

Emerson, J. P. & Sutherland, W. 2002, in Society of Photo-Optical Instrumentation Engineers (SPIE) Conference Series, Vol. 4836, Survey and Other Telescope Technologies and Discoveries, 35–42 [ADS]

Esplin, T. L., Luhman, K. L., & Mamajek, E. E. 2014, ApJ, 784, 126 [ADS]

Eyer, L., Holl, B., Pourbaix, D., Mowlavi, N., Siopis, C., Barblan, F., Evans, D. W., & North, P. 2013, ArXiv e-prints [ADS]

Facchini, S., Ricci, L., & Lodato, G. 2014, MNRAS, 442, 3700 [ADS]

Faherty, J. K. 2014, Mem. Soc. Astron. Italiana, 85, 725 [ADS]

Faherty, J. K., Burgasser, A. J., Bochanski, J. J., Looper, D. L., West, A. A., & van der Bliek, N. S. 2011, AJ, 141, 71 [ADS]

Faherty, J. K., Burgasser, A. J., West, A. A., Bochanski, J. J., Cruz, K. L., Shara, M. M., & Walter, F. M. 2010, AJ, 139, 176 [ADS]

Fischer, D. A. & Marcy, G. W. 1992, ApJ, 396, 178 [ADS]

Fitzpatrick, E. L. 1999, PASP, 111, 63 [ADS]

Foreman-Mackey, D., Hogg, D. W., Lang, D., & Goodman, J. 2013, PASP, 125, 306 [ADS]

Foreman-Mackey, D., Montet, B. T., Hogg, D. W., Morton, T. D., Wang, D., & Schölkopf, B. 2015, ApJ, 806, 215 [ADS]

Fortney, J. J., Marley, M. S., & Barnes, J. W. 2007, ApJ, 659, 1661 [ADS]

Frith, J. & Pinfield, D. 2013, in European Physical Journal Web of Conferences, Vol. 47, European Physical Journal Web of Conferences, 15002 [ADS]

Gagné, J., Lafrenière, D., Doyon, R., Malo, L., & Artigau, É. 2014, ApJ, 783, 121 [ADS]

Gaidos, E., Mann, A. W., Lépine, S., Buccino, A., James, D., Ansdell, M., Petrucci, R., Mauas, P., & Hilton, E. J. 2014, MNRAS, 443, 2561 [ADS]

Giampapa, M. S. & Liebert, J. 1986, ApJ, 305, 784 [ADS]

Gizis, J. E. 1997, AJ, 113, 806 [ADS]

Gizis, J. E., Kirkpatrick, J. D., Burgasser, A., Reid, I. N., Monet, D. G., Liebert, J., & Wilson, J. C. 2001, ApJ, 551, L163 [ADS]

Gizis, J. E., Monet, D. G., Reid, I. N., Kirkpatrick, J. D., Liebert, J., & Williams, R. J. 2000, AJ, 120, 1085 [ADS]

Gliese, W. & Jahreiß, H. 1991, Preliminary Version of the Third Catalogue of Nearby Stars, Tech. rep. [ADS]

Gomes, J. I., Pinfield, D. J., Marocco, F., Day-Jones, A. C., Burningham, B., Zhang, Z. H., Jones, H. R. A., Spaandonk, L. v., & Weights, D. 2013, MNRAS, 431, 2745 [ADS]

Goodman, J. & Weare, J. 2010, Communications in Applied Mathematics and Computational Science

Gorlova, N. I., Meyer, M. R., Rieke, G. H., & Liebert, J. 2003, ApJ, 593, 1074 [ADS]

Gou, Y. X. 2014, private communication

Grether, D. & Lineweaver, C. H. 2006, ApJ, 640, 1051 [ADS]

Group, C. A. 1999, Adaptive Optics on the 200-inch Hale Telescope at the Palomar Observatory

Guenther, E. W., Paulson, D. B., Cochran, W. D., Patience, J., Hatzes, A. P., & Macintosh, B. 2005, A&A, 442, 1031 [ADS]

Guo, Q., White, S., Boylan-Kolchin, M., De Lucia, G., Kauffmann, G., Lemson, G., Li, C., Springel, V., & Weinmann, S. 2011, MNRAS, 413, 101 [ADS]

Hatzes, A. P. & Rauer, H. 2015, ApJ, 810, L25 [ADS]

Hawley, S. L., Covey, K. R., Knapp, G. R., Golimowski, D. A., Fan, X., Anderson, S. F., Gunn, J. E., Harris, H. C., Ivezić, Ž., Long, G. M., Lupton, R. H., McGehee, P. M., Narayanan, V., Peng, E., Schlegel, D., Schneider, D. P., Spahn, E. Y., Strauss, M. A., Szkody, P., Tsvetanov, Z., Walkowicz, L. M., Brinkmann, J., Harvanek, M., Hennessy, G. S., Kleinman, S. J., Krzesinski, J., Long, D., Neilsen, E. H., Newman, P. R., Nitta, A., Snedden, S. A., & York, D. G. 2002, AJ, 123, 3409 [ADS]

Hayashi, C. & Nakano, T. 1963, Progress of Theoretical Physics, 30, 460 [ADS]

Henize, K. G. 1976, ApJS, 30, 491 [ADS]

Hennebelle, P. & Chabrier, G. 2008, ApJ, 684, 395 [ADS]

Henriques, B. M. B., White, S. D. M., Lemson, G., Thomas, P. A., Guo, Q., Marleau, G.-D., & Overzier, R. A. 2012, MNRAS, 421, 2904 [ADS]

Henry, T. J. & Kirkpatrick, J. D. 1990, ApJ, 354, L29 [ADS]

Hinkley, S. 2012, in IAU Symposium, Vol. 282, IAU Symposium, 181–188 [ADS]

Hinz, J. L., McCarthy, Jr., D. W., Simons, D. A., Henry, T. J., Kirkpatrick, J. D., & McGuire, P. C. 2002, AJ, 123, 2027 [ADS]

Høg, E., Fabricius, C., Makarov, V. V., Urban, S., Corbin, T., Wycoff, G., Bastian, U., Schwekendiek, P., & Wicenec, A. 2000, A&A, 355, L27 [ADS]

Hogg, D. W., Bovy, J., & Lang, D. 2010, ArXiv e-prints [ADS]

Howard, A. W., Marcy, G. W., Johnson, J. A., Fischer, D. A., Wright, J. T., Isaacson, H., Valenti, J. A., Anderson, J., Lin, D. N. C., & Ida, S. 2010, Science, 330, 653 [ADS]

Howell, S. B., Sobeck, C., Haas, M., Still, M., Barclay, T., Mullally, F., Troeltzsch, J., Aigrain, S., Bryson, S. T., Caldwell, D., Chaplin, W. J., Cochran, W. D., Huber, D., Marcy, G. W., Miglio, A., Najita, J. R., Smith, M., Twicken, J. D., & Fortney, J. J. 2014, PASP, 126, 398 [ADS]

Hunter, J. D. 2007, Computing In Science & Engineering, 9, 90

Ida, S. & Lin, D. N. C. 2004, ApJ, 616, 567 [ADS]

—. 2005, ApJ, 626, 1045 [ADS]

—. 2008, ApJ, 673, 487 [ADS]

Jahreiß, H., Scholz, R., Meusinger, H., & Lehmann, I. 2001, A&A, 370, 967 [ADS]

Janson, M., Bergfors, C., Brandner, W., Kudryavtseva, N., Hormuth, F., Hippler, S., & Henning, T. 2014, ApJ, 789, 102 [ADS]

Janson, M., Hormuth, F., Bergfors, C., Brandner, W., Hippler, S., Daemgen, S., Kudryavtseva, N., Schmalzl, E., Schnupp, C., & Henning, T. 2012, ApJ, 754, 44 [ADS]

Jarrett, T. H., Cohen, M., Masci, F., Wright, E., Stern, D., Benford, D., Blain, A., Carey, S., Cutri, R. M., Eisenhardt, P., Lonsdale, C., Mainzer, A., Marsh, K., Padgett, D., Petty, S., Ressler, M., Skrutskie, M., Stanford, S., Surace, J., Tsai, C. W., Wheelock, S., & Yan, D. L. 2011, ApJ, 735, 112 [ADS]

Jiang, Y.-F. & Tremaine, S. 2010, MNRAS, 401, 977 [ADS]

Joergens, V. 2008, A&A, 492, 545 [ADS]

Johnson, H. L., Mitchell, R. I., & Iriarte, B. 1962, ApJ, 136, 75 [ADS]

Johnson, J. A., Aller, K. M., Howard, A. W., & Crepp, J. R. 2010, PASP, 122, 905 [ADS]

Johnson, J. A. & Apps, K. 2009, ApJ, 699, 933 [ADS]

Johnson, J. A., Apps, K., Gazak, J. Z., Crepp, J. R., Crossfield, I. J., Howard, A. W., Marcy, G. W., Morton, T. D., Chubak, C., & Isaacson, H. 2011, ApJ, 730, 79 [ADS]

Johnson, J. A., Gazak, J. Z., Apps, K., Muirhead, P. S., Crepp, J. R., Crossfield, I. J. M., Boyajian, T., von Braun, K., Rojas-Ayala, B., Howard, A. W., Covey, K. R., Schlawin, E., Hamren, K., Morton, T. D., Marcy, G. W., & Lloyd, J. P. 2012, AJ, 143, 111 [ADS]

Jones, E., Oliphant, T., Peterson, P., & Others. 2001, SciPy: Open source scientific tools for Python

Jones, M. I., Jenkins, J. S., Rojo, P., Melo, C. H. F., & Bluhm, P. 2015, A&A, 573, A3 [ADS]

Jordi, C. 2009, gAIA-C5-TN-UB-CJ-041 Accessed online at http://www.rssd.esa.int/llink/livelink/open/2760608

Jordi, K., Grebel, E. K., & Ammon, K. 2006, A&A, 460, 339 [ADS]

Kaiser, N., Aussel, H., Burke, B. E., Boesgaard, H., Chambers, K., Chun, M. R., Heasley, J. N., Hodapp, K.-W., Hunt, B., Jedicke, R., Jewitt, D., Kudritzki, R., Luppino, G. A., Maberry, M., Magnier, E., Monet, D. G., Onaka, P. M., Pickles, A. J., Rhoads, P. H. H., Simon, T., Szalay, A., Szapudi, I., Tholen, D. J., Tonry, J. L., Waterson, M., & Wick, J. 2002, in Proc. SPIE, Vol. 4836, Survey and Other Telescope Technologies and Discoveries, 154–164 [ADS]

Kaltenegger, L. & Traub, W. A. 2009, ApJ, 698, 519 [ADS]

Katz, D., Soubiran, C., Cayrel, R., Adda, M., & Cautain, R. 1998, A&A, 338, 151 [ADS]

Keenan, P. C. & McNeil, R. C. 1976, An atlas of spectra of the cooler stars: Types G,K,M,S, and C. Part 1: Introduction and tables [ADS]

—. 1989, ApJS, 71, 245 [ADS]

Keller, S. C., Schmidt, B. P., Bessell, M. S., Conroy, P. G., Francis, P., Granlund, A., Kowald, E., Oates, A. P., Martin-Jones, T., Preston, T., Tisserand, P., Vaccarella, A., & Waterson, M. F. 2007, PASA, 24, 1 [ADS]

Kent, S. M., Mink, D., Fazio, G., Koch, D., Melnick, G., Tardiff, A., & Maxson, C. 1992, ApJS, 78, 403 [ADS]

Kirkpatrick, J. D. 1991, in BAAS, Vol. 23, Bulletin of the American Astronomical Society, 1396 [ADS]

Kirkpatrick, J. D., Cushing, M. C., Gelino, C. R., Griffith, R. L., Skrutskie, M. F., Marsh, K. A., Wright, E. L., Mainzer, A., Eisenhardt, P. R., McLean, I. S., Thompson, M. A., Bauer, J. M., Benford, D. J., Bridge, C. R., Lake, S. E., Petty, S. M., Stanford, S. A., Tsai, C.-W., Bailey, V., Beichman, C. A., Bloom, J. S., Bochanski, J. J., Burgasser, A. J., Capak, P. L., Cruz, K. L., Hinz, P. M., Kartaltepe, J. S., Knox, R. P., Manohar, S., Masters, D., Morales-Calderón, M., Prato, L. A., Rodigas, T. J., Salvato, M., Schurr, S. D., Scoville, N. Z., Simcoe, R. A., Stapelfeldt, K. R., Stern, D., Stock, N. D., & Vacca, W. D. 2011, ApJS, 197, 19 [ADS]

Kirkpatrick, J. D., Gelino, C. R., Cushing, M. C., Mace, G. N., Griffith, R. L., Skrutskie, M. F., Marsh, K. A., Wright, E. L., Eisenhardt, P. R., McLean, I. S., Mainzer, A. K., Burgasser, A. J., Tinney, C. G., Parker, S., & Salter, G. 2012, ApJ, 753, 156 [ADS]

Kirkpatrick, J. D., Henry, T. J., & McCarthy, Jr., D. W. 1991, ApJS, 77, 417 [ADS]

Kirkpatrick, J. D., Looper, D. L., Burgasser, A. J., Schurr, S. D., Cutri, R. M., Cushing, M. C., Cruz, K. L., Sweet, A. C., Knapp, G. R., Barman, T. S., Bochanski, J. J., Roellig, T. L., McLean, I. S., McGovern, M. R., & Rice, E. L. 2010, ApJS, 190, 100 [ADS]

Kirkpatrick, J. D., Reid, I. N., Liebert, J., Cutri, R. M., Nelson, B., Beichman, C. A., Dahn, C. C., Monet, D. G., Gizis, J. E., & Skrutskie, M. F. 1999, ApJ, 519, 802 [ADS]

Konopacky, Q. M., Ghez, A. M., Barman, T. S., Rice, E. L., Bailey, III, J. I., White, R. J., McLean, I. S., & Duchêne, G. 2010, ApJ, 711, 1087 [ADS]

Kotani, T., Tamura, M., Suto, H., Nishikawa, J., Sato, B., Aoki, W., Usuda, T., Kurokawa, T., Kashiwagi, K., Nishiyama, S., Ikeda, Y., Hall, D. B., Hodapp, K. W., Hashimoto, J., Morino, J.-I., Okuyama, Y., Tanaka, Y., Suzuki, S., Inoue, S., Kwon, J., Suenaga, T., Oh, D., Baba, H., Narita, N., Kokubo, E., Hayano, Y., Izumiura, H., Kambe, E., Kudo, T., Kusakabe, N., Ikoma, M., Hori, Y., Omiya, M., Genda, H., Fukui, A., Fujii, Y., Guyon, O., Harakawa, H., Hayashi, M., Hidai, M., Hirano, T., Kuzuhara, M., Machida, M., Matsuo, T., Nagata, T., Onuki, H., Ogihara, M., Takami, H., Takato, N., Takahashi, Y. H., Tachinami, C., Terada, H., Kawahara, H., & Yamamuro, T. 2014, in Proc. SPIE, Vol. 9147, Ground-based and Airborne Instrumentation for Astronomy V, 914714 [ADS]

Kouwenhoven, M. B. N., Brown, A. G. A., Portegies Zwart, S. F., & Kaper, L. 2007, A&A, 474, 77 [ADS]

Kraus, A. L., Ireland, M. J., Martinache, F., & Hillenbrand, L. A. 2011, ApJ, 731, 8 [ADS]

Kraus, A. L., Ireland, M. J., Martinache, F., & Lloyd, J. P. 2008, ApJ, 679, 762 [ADS]

Kroupa, P. & Bouvier, J. 2003, MNRAS, 346, 369 [ADS]

Kumar, S. S. 1963, ApJ, 137, 1121 [ADS]

Kunde, V. G., Flasar, F. M., Jennings, D. E., Bézard, B., Strobel, D. F., Conrath, B. J., Nixon, C. A., Bjoraker, G. L., Romani, P. N., Achterberg, R. K., Simon-Miller, A. A., Irwin, P., Brasunas, J. C., Pearl, J. C., Smith, M. D., Orton, G. S., Gierasch, P. J., Spilker, L. J., Carlson, R. C., Mamoutkine, A. A., Calcutt, S. B., Read, P. L., Taylor, F. W., Fouchet, T., Parrish, P., Barucci, A., Courtin, R., Coustenis, A., Gautier, D., Lellouch, E., Marten, A., Prangé, R., Biraud, Y., Ferrari, C., Owen, T. C., Abbas, M. M., Samuelson, R. E., Raulin, F., Ade, P., Césarsky, C. J., Grossman, K. U., & Coradini, A. 2004, Science, 305, 1582 [ADS]

Lafrenière, D., Jayawardhana, R., Brandeker, A., Ahmic, M., & van Kerkwijk, M. H. 2008, ApJ, 683, 844 [ADS]

Larson, R. B. 2003, in Astronomical Society of the Pacific Conference Series, Vol. 287, Galactic Star Formation Across the Stellar Mass Spectrum, 65–80 [ADS]

Lawrence, A., Warren, S. J., Almaini, O., Edge, A. C., Hambly, N. C., Jameson, R. F., Lucas, P., Casali, M., Adamson, A., Dye, S., Emerson, J. P., Foucaud, S., Hewett, P., Hirst, P., Hodgkin, S. T., Irwin, M. J., Lodieu, N., McMahon, R. G., Simpson, C., Smail, I., Mortlock, D., & Folger, M. 2007, MNRAS, 379, 1599 [ADS]

—. 2013, VizieR Online Data Catalog, 2319 [ADS]

Leggett, S. K., Burningham, B., Saumon, D., Marley, M. S., Warren, S. J., Smart, R. L., Jones, H. R. A., Lucas, P. W., Pinfield, D. J., & Tamura, M. 2010, ApJ, 710, 1627 [ADS]

Leggett, S. K., Cushing, M. C., Saumon, D., Marley, M. S., Roellig, T. L., Warren, S. J., Burningham, B., Jones, H. R. A., Kirkpatrick, J. D., Lodieu, N., Lucas, P. W., Mainzer, A. K., Martín, E. L., McCaughrean, M. J., Pinfield, D. J., Sloan, G. C., Smart, R. L., Tamura, M., & Van Cleve, J. 2009, ApJ, 695, 1517 [ADS]

Lépine, J. R. D. & Leroy, P. 2000, MNRAS, 313, 263 [ADS]

Lépine, S. 2005, AJ, 130, 1680 [ADS]

Lépine, S. & Gaidos, E. 2011, AJ, 142, 138 [ADS]

Lépine, S., Hilton, E. J., Mann, A. W., Wilde, M., Rojas-Ayala, B., Cruz, K. L., & Gaidos, E. 2013, AJ, 145, 102 [ADS]

Lépine, S., Rich, R. M., & Shara, M. M. 2003, AJ, 125, 1598 [ADS]

Lépine, S., Shara, M. M., & Rich, R. M. 2002, AJ, 124, 1190 [ADS]

Lestrade, J.-F., Wyatt, M. C., Bertoldi, F., Menten, K. M., & Labaigt, G. 2009, A&A, 506, 1455 [ADS]

Lissauer, J. J., Levison, H. F., & Duncan, M. J. 1998, in Bulletin of the American Astronomical Society, Vol. 30, AAS/Division of Dynamical Astronomy Meeting #30, 1142 [ADS]

Liu, M. C., Delorme, P., Dupuy, T. J., Bowler, B. P., Albert, L., Artigau, E., Reylé, C., Forveille, T., & Delfosse, X. 2011, ApJ, 740, 108 [ADS]

Lodieu, N., Dobbie, P. D., & Hambly, N. C. 2011, A&A, 527, A24 [ADS]

Lohr, M. E., Norton, A. J., Gillen, E., Busuttil, R., Kolb, U. C., Aigrain, S., McQuillan, A., Hodgkin, S. T., & González, E. 2015, A&A, 578, A103 [ADS]

Lomb, N. R. 1976, Ap&SS, 39, 447 [ADS]

Lou, A. L. 2014, private communication

Lowrance, P. J., Becklin, E. E., Schneider, G., Kirkpatrick, J. D., Weinberger, A. J., Zuckerman, B., Dumas, C., Beuzit, J.-L., Plait, P., Malumuth, E., Heap, S., Terrile, R. J., & Hines, D. C. 2005, AJ, 130, 1845 [ADS]

Lucas, P. W., Roche, P. F., Allard, F., & Hauschildt, P. H. 2001, MNRAS, 326, 695 [ADS]

Lucas, P. W., Tinney, C. G., Burningham, B., Leggett, S. K., Pinfield, D. J., Smart, R., Jones, H. R. A., Marocco, F., Barber, R. J., Yurchenko, S. N., Tennyson, J., Ishii, M., Tamura, M., Day-Jones, A. C., Adamson, A., Allard, F., & Homeier, D. 2010, MNRAS, 408, L56 [ADS]

Lucas, P. W., Weights, D. J., Roche, P. F., & Riddick, F. C. 2006, MNRAS, 373, L60 [ADS]

Luhman, K. L. 2012, ARA&A, 50, 65 [ADS]

—. 2014, ApJ, 786, L18 [ADS]

Luhman, K. L. & Mamajek, E. E. 2012, ApJ, 758, 31 [ADS]

Luhman, K. L., McLeod, K. K., & Goldenson, N. 2005, ApJ, 623, 1141 [ADS]

Luhman, K. L. & Muench, A. A. 2008, ApJ, 684, 654 [ADS]

Luhman, K. L., Peterson, D. E., & Megeath, S. T. 2004, ApJ, 617, 565 [ADS]

Luo, A.-L., Zhang, H.-T., Zhao, Y.-H., Zhao, G., Cui, X.-Q., Li, G.-P., Chu, Y.-Q., Shi, J.-R., Wang, G., Zhang, J.-N., Bai, Z.-R., Chen, X.-Y., Wang, F.-F., Guo, Y.-X., Chen, J.-J., Du, B., Kong, X., Lei, Y.-J., Li, Y.-B., Song, Y.-H., Wu, Y., Zhang, Y.-X., Zhou, X.-L., Zuo, F., Du, P., He, L., Hou, W., Dong, Y.-Q., Li, J., Li, G.-W., Li, S., Song, J., Tian, Y., Wang, M.-X., Wu, K.-F., Yang, H.-Q., Yuan, H.-L., Cao, S.-Y., Chen, H.-Y., Chen, K.-X., Chen, Y., Chu, J.-R., Feng, L., Gong, X.-F., Gu, B.-Z., Hou, Y.-H., Huo, Z.-Y., Hu, H.-Z., Hu, N.-S., Hu, Z.-W., Jia, L., Jiang, F.-H., Jiang, X., Jiang, Z.-B., Jin, G., Li, A.-H., Li, Q., Li, X.-N., Li, Y., Li, Y.-P., Liu, G.-R., Liu, G.-Q., Liu, Z.-G., Lu, Q.-S., Lu, W.-Z., Luo, Y., Mao, Y.-D., Men, L., Ni, J.-J., Qi, Y.-J., Qi, Z.-X., Shi, H.-M., Su, D.-Q., Sun, S.-W., Su, H.-J., Tang, Z.-H., Tao, Q.-S., Tu, L.-P., Wang, D.-Q., Wang, D., Wang, G.-M., Wang, H., Wang, J.-N., Wang, J., Wang, J.-L., Wang, J.-P., Wang, L., Wang, S.-G., Wang, S.-Q., Wang, Y.-N., Wang, Y., Wang, Y.-F., Wei, M.-Z., Xue, X.-X., Xing, X.-Z., Xu, L.-Z., Xu, X.-Q., Xu, Y., Yang, D.-H., Yang, S.-H., Yao, Z.-Q., Yu, Y., Yuan, H., Zhai, C., Zhang, E.-P., Zhang, J., Zhang, L.-P., Zhang, W., Zhang, Y., Zhang, Z.-C., Zhao,

M., Zhou, F., Zhu, Y.-T., Zhu, J., & Zou, S.-C. 2012, Research in Astronomy and Astrophysics, 12, 1243 [ADS]

Luo, A.-L., Zhang, Y.-X., Zhang, J.-N., & Zhao, Y.-H. 2004, in Society of Photo-Optical Instrumentation Engineers (SPIE) Conference Series, Vol. 5493, Optimizing Scientific Return for Astronomy through Information Technologies, 178–185 [ADS]

Ma, B. & Ge, J. 2014, MNRAS, 439, 2781 [ADS]

Magazzu, A., Martin, E. L., & Rebolo, R. 1993, ApJ, 404, L17 [ADS]

Mahadevan, S., Ramsey, L., Redman, S., Zonak, S., Wright, J., Wolszczan, A., Endl, M., & Zhao, B. 2010, in Astronomical Society of the Pacific Conference Series, Vol. 430, Pathways Towards Habitable Planets, 272 [ADS]

Maire, A.-L., Boccaletti, A., Rameau, J., Chauvin, G., Lagrange, A.-M., Bonnefoy, M., Desidera, S., Sylvestre, M., Baudoz, P., Galicher, R., & Mouillet, D. 2014, A&A, 566, A126 [ADS]

Malo, L., Doyon, R., Lafrenière, D., Artigau, É., Gagné, J., Baron, F., & Riedel, A. 2013, ApJ, 762, 88 [ADS]

Mamajek, E. E. 2005, ApJ, 634, 1385 [ADS]

Manara, C. F., Testi, L., Rigliaco, E., Alcalá, J. M., Natta, A., Stelzer, B., Biazzo, K., Covino, E., Covino, S., Cupani, G., D'Elia, V., & Randich, S. 2013, A&A, 551, A107 [ADS]

Mandell, A. M. 2007, PhD thesis, The Pennsylvania State University [ADS]

Manjavacas, E., Goldman, B., Alcalá, J. M., Zapatero-Osorio, M. R., Béjar, V. J. S., Homeier, D., Bonnefoy, M., Smart, R. L., Henning, T., & Allard, F. 2016, MNRAS, 455, 1341 [ADS]

Mann, A. W., Brewer, J. M., Gaidos, E., Lépine, S., & Hilton, E. J. 2013a, AJ, 145, 52 [ADS]

Mann, A. W., Gaidos, E., & Ansdell, M. 2013b, ApJ, 779, 188 [ADS]

Mann, A. W., Gaidos, E., Kraus, A., & Hilton, E. J. 2013c, ApJ, 770, 43 [ADS]

Mann, A. W., Gaidos, E., Lépine, S., & Hilton, E. J. 2012, ApJ, 753, 90 [ADS]

Marcy, G. W. & Butler, R. P. 2000, PASP, 112, 137 [ADS]

Marocco, F., Jones, H. R. A., Day-Jones, A. C., Pinfield, D. J., Lucas, P. W., Burningham, B., Zhang, Z. H., Smart, R. L., Gomes, J. I., & Smith, L. 2015, MNRAS, 449, 3651 [ADS]

Marsh, K. A., Kirkpatrick, J. D., & Plavchan, P. 2010, ApJ, 709, L158 [ADS]

Martin, D. C., Fanson, J., Schiminovich, D., Morrissey, P., Friedman, P. G., Barlow, T. A., Conrow, T., Grange, R., Jelinsky, P. N., Milliard, B., Siegmund, O. H. W., Bianchi, L., Byun, Y.-I., Donas, J., Forster, K., Heckman, T. M., Lee, Y.-W., Madore, B. F., Malina, R. F., Neff, S. G., Rich, R. M., Small, T., Surber, F., Szalay, A. S., Welsh, B., & Wyder, T. K. 2005, ApJ, 619, L1 [ADS]

Martín, E. L., Basri, G., Delfosse, X., & Forveille, T. 1997, A&A, 327, L29 [ADS]

Martín, E. L., Delfosse, X., Basri, G., Goldman, B., Forveille, T., & Zapatero Osorio, M. R. 1999, AJ, 118, 2466 [ADS]

Martín, E. L., Rebolo, R., & Zapatero-Osorio, M. R. 1996, ApJ, 469, 706 [ADS]

Masciadri, E., Mundt, R., Henning, T., Alvarez, C., & Barrado y Navascués, D. 2005, ApJ, 625, 1004 [ADS]

Massa, D. & Savage, B. 1989, in IAU Symposium, Vol. 135, Interstellar Dust, 3 [ADS]

Matzner, C. D. & Levin, Y. 2005, ApJ, 628, 817 [ADS]

Mayor, M. & Queloz, D. 1995, Nature, 378, 355 [ADS]

McCarthy, C. & Zuckerman, B. 2004, AJ, 127, 2871 [ADS]

McCarthy, Jr., D. W., Henry, T. J., Fleming, T. A., Saffer, R. A., Liebert, J., & Christou, J. C. 1988, ApJ, 333, 943 [ADS]

McCaughrean, M. 2012, ESAs Report to the 39th COSPAR Meeting (ESTEC, PO Box 299, 2200 AG Noordwijk, the Netherlands: ESA Communications)

McGovern, M. R., Kirkpatrick, J. D., McLean, I. S., Burgasser, A. J., Prato, L., & Lowrance, P. J. 2004, ApJ, 600, 1020 [ADS]

McQuillan, A., Mazeh, T., & Aigrain, S. 2014, ApJS, 211, 24 [ADS]

Mestel, L. 1968, MNRAS, 138, 359 [ADS]

Metchev, S. A. & Hillenbrand, L. A. 2009, ApJS, 181, 62 [ADS]

Monet, D. 1998, USNO-A2.0 [ADS]

Montet, B. T., Bowler, B. P., Shkolnik, E. L., Deck, K. M., Wang, J., Horch, E. P., Liu, M. C., Hillenbrand, L. A., Kraus, A. L., & Charbonneau, D. 2015, ApJ, 813, L11 [ADS]

Moutou, C., Bonomo, A. S., Bruno, G., Montagnier, G., Bouchy, F., Almenara, J. M., Barros, S. C. C., Deleuil, M., Díaz, R. F., Hébrard, G., & Santerne, A. 2013, A&A, 558, L6 [ADS]

Muirhead, P. S., Becker, J., Feiden, G. A., Rojas-Ayala, B., Vanderburg, A., Price, E. M., Thorp, R., Law, N. M., Riddle, R., Baranec, C., Hamren, K., Schlawin, E., Covey, K. R., Johnson, J. A., & Lloyd, J. P. 2014, ApJS, 213, 5 [ADS]

Muirhead, P. S., Hamren, K., Schlawin, E., Rojas-Ayala, B., Covey, K. R., & Lloyd, J. P. 2012, ApJ, 750, L37 [ADS]

Murillo, N. M., Lai, S.-P., Bruderer, S., Harsono, D., & van Dishoeck, E. F. 2013, A&A, 560, A103 [ADS]

Mužić, K., Radigan, J., Jayawardhana, R., Ivanov, V. D., Faherty, J. K., Kurtev, R. G., Núñez, A., Boffin, H. M. J., Hainaut, O., Cruz, K., Jones, D., Metchev, S., Tyndall, A., & Borissova, J. 2012, AJ, 144, 180 [ADS]

Naab, T., Johansson, P. H., & Ostriker, J. P. 2009, ApJ, 699, L178 [ADS]

Nakajima, T., Oppenheimer, B. R., Kulkarni, S. R., Golimowski, D. A., Matthews, K., & Durrance, S. T. 1995, Nature, 378, 463 [ADS]

Nassau, J. J. & van Albada, G. B. 1949, ApJ, 109, 391 [ADS]

Neuhäuser, R. & Guenther, E. W. 2004, A&A, 420, 647 [ADS]

Neuhäuser, R., Guenther, E. W., Alves, J., Huélamo, N., Ott, T., & Eckart, A. 2003, Astronomische Nachrichten, 324, 535 [ADS]

Newton, E. R., Charbonneau, D., Irwin, J., Berta-Thompson, Z. K., Rojas-Ayala, B., Covey, K., & Lloyd, J. P. 2014, AJ, 147, 20 [ADS]

Newton, E. R., Charbonneau, D., Irwin, J., & Mann, A. W. 2015a, ApJ, 800, 85 [ADS]

Newton, E. R., Irwin, J., Charbonneau, D., Berta-Thompson, Z. K., Dittmann, J. A., & West, A. A. 2015b, ArXiv e-prints [ADS]

Nidever, D. L., Marcy, G. W., Butler, R. P., Fischer, D. A., & Vogt, S. S. 2002, ApJS, 141, 503 [ADS]

Oppenheimer, B. R. 2014, in Astrophysics and Space Science Library, Vol. 401, Astrophysics and Space Science Library, 81 [ADS]

Oppenheimer, B. R., Golimowski, D. A., Kulkarni, S. R., Matthews, K., Nakajima, T., Creech-Eakman, M., & Durrance, S. T. 2001, AJ, 121, 2189 [ADS]

Ossendrijver, M. 2003, A&A Rev., 11, 287 [ADS]

Padmanabhan, N., Schlegel, D. J., Finkbeiner, D. P., Barentine, J. C., Blanton, M. R., Brewington, H. J., Gunn, J. E., Harvanek, M., Hogg, D. W., Ivezić, Ž., Johnston, D., Kent, S. M., Kleinman, S. J., Knapp, G. R., Krzesinski, J., Long, D., Neilsen, Jr., E. H., Nitta, A., Loomis, C., Lupton, R. H., Roweis, S., Snedden, S. A., Strauss, M. A., & Tucker, D. L. 2008, ApJ, 674, 1217 [ADS]

Padoan, P. & Nordlund, Å. 2004, ApJ, 617, 559 [ADS]

Parker, E. N. 1993, ApJ, 408, 707 [ADS]

Parker, R. J. & Reggiani, M. M. 2013, MNRAS, 432, 2378 [ADS]

Pérez, F. & Granger, B. E. 2007, Computing in Science and Engineering, 9, 21

Perryman, M. A. C. & ESA, eds. 1997, ESA Special Publication, Vol. 1200, The HIPPARCOS and TYCHO catalogues. Astrometric and photometric star catalogues derived from the ESA HIPPARCOS Space Astrometry Mission [ADS]

Perryman, M. A. C., Lindegren, L., & Turon, C. 1997, in ESA Special Publication, Vol. 402, Hipparcos - Venice '97, 743–748 [ADS]

Peter, D., Feldt, M., Henning, T., & Hormuth, F. 2012, A&A, 538, A74 [ADS]

Phan-Bao, N., Bessell, M. S., Martín, E. L., Simon, G., Borsenberger, J., Tata, R., Guibert, J., Crifo, F., Forveille, T., Delfosse, X., Lim, J., & de Batz, B. 2008, MNRAS, 383, 831 [ADS]

Phan-Bao, N., Crifo, F., Delfosse, X., Forveille, T., Guibert, J., Borsenberger, J., Epchtein, N., Fouqué, P., Simon, G., & Vetois, J. 2003, A&A, 401, 959 [ADS]

Pinfield, D., Gomes, J., & Day-Jones, A. 2013, in European Physical Journal Web of Conferences, Vol. 47, European Physical Journal Web of Conferences, 6004 [ADS]

Pinfield, D. J., Dobbie, P. D., Jameson, R. F., Steele, I. A., Jones, H. R. A., & Katsiyannis, A. C. 2003, MNRAS, 342, 1241 [ADS]

Pinfield, D. J., Gomes, J., Day-Jones, A. C., Leggett, S. K., Gromadzki, M., Burningham, B., Ruiz, M. T., Kurtev, R., Cattermole, T., Cardoso, C., Lodieu, N., Faherty, J., Littlefair, S., Smart, R., Irwin, M., Clarke, J. R. A., Smith, L., Lucas, P. W., Gálvez-Ortiz, M. C., Jenkins, J. S., Jones, H. R. A., Rebolo, R., Béjar, V. J. S., & Gauza, B. 2014, MNRAS, 437, 1009 [ADS]

Pinfield, D. J., Jones, H. R. A., Lucas, P. W., Kendall, T. R., Folkes, S. L., Day-Jones, A. C., Chappelle, R. J., & Steele, I. A. 2006, MNRAS, 368, 1281 [ADS]

Pinfield, D. J., Jones, H. R. A., & Steele, I. A. 2005, PASP, 117, 173 [ADS]

Plavchan, P., Werner, M. W., Chen, C. H., Stapelfeldt, K. R., Su, K. Y. L., Stauffer, J. R., & Song, I. 2009, ApJ, 698, 1068 [ADS]

Pollack, J. B., Hubickyj, O., Bodenheimer, P., Lissauer, J. J., Podolak, M., & Greenzweig, Y. 1996, icarus, 124, 62 [ADS]

Poppenhaeger, K. & Wolk, S. J. 2014, A&A, 565, L1 [ADS]

Quirrenbach, A., Amado, P. J., Mandel, H., Caballero, J. A., Mundt, R., Ribas, I., Reiners, A., Abril, M., Aceituno, J., Afonso, C., Barrado Y Navascues, D., Bean, J. L., Béjar, V. J. S., Becerril, S., Böhm, A., Cárdenas, M. C., Claret, A., Colomé, J., Costillo, L. P., Dreizler, S., Fernández, M., Francisco, X., Galadí, D., Garrido, R., González Hernández, J. I., Guàrdia, J., Guenther, E. W., Gutiérrez-Soto, F., Joergens, V., Hatzes, A. P., Helmling, J., Henning, T., Herrero, E., Kürster, M., Laun, W., Lenzen, R., Mall, U., Martin, E. L., Martín-Ruiz, S., Mirabet, E., Montes, D., Morales, J. C., Morales Muñoz, R., Moya, A., Naranjo, V., Rabaza, O., Ramón, A., Rebolo, R., Reffert, S., Rodler, F., Rodríguez, E., Rodríguez Trinidad, A., Rohloff, R. R., Sánchez Carrasco, M. A., Schmidt, C., Seifert, W., Setiawan, J., Solano, E., Stahl, O., Storz, C., Suárez, J. C., Thiele, U., Wagner, K., Wiedemann, G., Zapatero Osorio, M. R., Del Burgo, C., Sánchez-Blanco, E., & Xu, W. 2010, in Society of Photo-Optical Instrumentation Engineers (SPIE) Conference Series, Vol. 7735, Society of Photo-Optical Instrumentation Engineers (SPIE) Conference Series [ADS]

Raghavan, D., McAlister, H. A., Henry, T. J., Latham, D. W., Marcy, G. W., Mason, B. D., Gies, D. R., White, R. J., & ten Brummelaar, T. A. 2010, ApJS, 190, 1 [ADS]

Rappaport, S., Swift, J., Levine, A., Joss, M., Sanchis-Ojeda, R., Barclay, T., Still, M., Handler, G., Oláh, K., Muirhead, P. S., Huber, D., & Vida, K. 2014, ApJ, 788, 114 [ADS]

Raskin, G., van Winckel, H., Hensberge, H., Jorissen, A., Lehmann, H., Waelkens, C., Avila, G., de Cuyper, J.-P., Degroote, P., Dubosson, R., Dumortier, L., Frémat, Y., Laux, U., Michaud, B., Morren, J., Perez Padilla, J., Pessemier, W., Prins, S., Smolders, K., van Eck, S., & Winkler, J. 2011, A&A, 526, A69 [ADS]

Rauer, H., Catala, C., Aerts, C., Appourchaux, T., Benz, W., Brandeker, A., Christensen-Dalsgaard, J., Deleuil, M., Gizon, L., Goupil, M.-J., Güdel, M., Janot-Pacheco, E., Mas-Hesse, M., Pagano, I., Piotto, G., Pollacco, D., Santos, Ċ., Smith, A., Suárez, J.-C., Szabó, R., Udry, S., Adibekyan, V., Alibert, Y., Almenara, J.-M., Amaro-Seoane, P., Eiff, M. A.-v., Asplund, M., Antonello, E., Barnes, S., Baudin, F., Belkacem, K., Bergemann, M., Bihain, G., Birch, A. C., Bonfils, X., Boisse, I., Bonomo, A. S., Borsa, F., Brandão, I. M., Brocato, E., Brun, S., Burleigh, M., Burston, R., Cabrera, J., Cassisi, S., Chaplin, W., Charpinet, S., Chiappini, C., Church, R. P., Csizmadia, S., Cunha, M., Damasso, M., Davies, M. B., Deeg, H. J., Díaz, R. F., Dreizler, S., Dreyer, C., Eggenberger, P., Ehrenreich, D., Eigmüller, P., Erikson, A., Farmer, R., Feltzing, S., de Oliveira Fialho, F., Figueira, P., Forveille, T., Fridlund, M., García, R. A., Giommi, P., Giuffrida, G., Godolt, M., Gomes da Silva, J., Granzer, T., Grenfell, J. L., Grotsch-Noels, A., Günther, E., Haswell, C. A., Hatzes, A. P., Hébrard, G., Hekker, S., Helled, R., Heng, K., Jenkins, J. M., Johansen, A., Khodachenko, M. L., Kislyakova, K. G., Kley, W., Kolb, U., Krivova, N., Kupka, F., Lammer, H., Lanza, A. F., Lebreton, Y., Magrin, D., Marcos-Arenal, P., Marrese, P. M., Marques, J. P., Martins, J., Mathis, S., Mathur, S., Messina, S., Miglio, A., Montalban, J., Montalto, M., Monteiro, M. J. P. F. G., Moradi, H., Moravveji, E., Mordasini, C., Morel, T., Mortier, A., Nascimbeni, V., Nelson, R. P., Nielsen, M. B., Noack, L., Norton, A. J., Ofir, A., Oshagh, M., Ouazzani, R.-M., Pápics, P., Parro, V. C., Petit, P., Plez, B., Poretti, E., Quirrenbach, A., Ragazzoni, R., Raimondo, G., Rainer, M., Reese, D. R., Redmer, R., Reffert, S., Rojas-Ayala, B., Roxburgh, I. W., Salmon, S., Santerne, A., Schneider, J., Schou, J., Schuh, S., Schunker, H., Silva-Valio, A., Silvotti, R., Skillen, I., Snellen, I., Sohl, F., Sousa, S. G., Sozzetti, A., Stello, D., Strassmeier, K. G., Švanda, M., Szabó, G. M., Tkachenko, A., Valencia, D., Van Grootel, V., Vauclair, S. D., Ventura, P., Wagner, F. W., Walton, N. A., Weingrill, J., Werner, S. C., Wheatley, P. J., & Zwintz, K. 2014, Experimental Astronomy, 38, 249 [ADS]

Rayner, J. T., Cushing, M. C., & Vacca, W. D. 2009, ApJS, 185, 289 [ADS]

Rebolo, R., Martin, E. L., & Magazzu, A. 1992, ApJ, 389, L83 [ADS]

Reid, I. N. & Cruz, K. L. 2002, AJ, 123, 2806 [ADS]

Reid, I. N., Cruz, K. L., & Allen, P. R. 2007, AJ, 133, 2825 [ADS]

Reid, I. N., Cruz, K. L., Laurie, S. P., Liebert, J., Dahn, C. C., Harris, H. C., Guetter, H. H., Stone, R. C., Canzian, B., Luginbuhl, C. B., Levine, S. E., Monet, A. K. B., & Monet, D. G. 2003, AJ, 125, 354 [ADS]

Reid, I. N. & Gizis, J. E. 1997, AJ, 113, 2246 [ADS]

Reid, I. N., Gizis, J. E., Kirkpatrick, J. D., & Koerner, D. W. 2001, AJ, 121, 489 [ADS]

Reid, I. N. & Hawley, S. L. 2005, New light on dark stars : red dwarfs, low-mass stars, brown dwarfs [ADS]

Reid, I. N., Hawley, S. L., & Gizis, J. E. 1995, AJ, 110, 1838 [ADS]

Reid, I. N., Kirkpatrick, J. D., Gizis, J. E., & Liebert, J. 1999, ApJ, 527, L105 [ADS]

Reid, I. N., Lewitus, E., Burgasser, A. J., & Cruz, K. L. 2006, ApJ, 639, 1114 [ADS]

Reid, I. N. & Mahoney, S. 2000, MNRAS, 316, 827 [ADS]

Reiners, A. 2004, in Proc. the 13th Cool Stars Workshop, ESA Spec. in press

Reiners, A. & Basri, G. 2007, ApJ, 656, 1121 [ADS]

Reipurth, B., Clarke, C. J., Boss, A. P., Goodwin, S. P., Rodríguez, L. F., Stassun, K. G., Tokovinin, A., & Zinnecker, H. 2014, Protostars and Planets VI, 267 [ADS]

Rice, E. L., Faherty, J. K., Cruz, K., Barman, T., Looper, D., Malo, L., Mamajek, E. E., Metchev, S., & Shkolnik, E. L. 2011, in Astronomical Society of the Pacific Conference Series, Vol. 448, 16th Cambridge Workshop on Cool Stars, Stellar Systems, and the Sun, 481 [ADS]

Rice, E. L., Faherty, J. K., & Cruz, K. L. 2010, ApJ, 715, L165 [ADS]

Rice, W. K. M., Armitage, P. J., Bonnell, I. A., Bate, M. R., Jeffers, S. V., & Vine, S. G. 2003, MNRAS, 346, L36 [ADS]

Ricker, G. R., Winn, J. N., Vanderspek, R., Latham, D. W., Bakos, G. Á., Bean, J. L., Berta-Thompson, Z. K., Brown, T. M., Buchhave, L., Butler, N. R., Butler, R. P., Chaplin, W. J., Charbonneau, D., Christensen-Dalsgaard, J., Clampin, M., Deming, D., Doty, J., De Lee, N., Dressing, C., Dunham, E. W., Endl, M., Fressin, F., Ge, J., Henning, T., Holman, M. J., Howard, A. W., Ida, S., Jenkins, J., Jernigan, G., Johnson, J. A., Kaltenegger, L., Kawai, N., Kjeldsen, H., Laughlin, G., Levine, A. M., Lin, D., Lissauer, J. J., MacQueen, P., Marcy, G., McCullough, P. R., Morton, T. D., Narita, N., Paegert, M., Palle, E., Pepe, F., Pepper, J., Quirrenbach, A., Rinehart, S. A., Sasselov, D., Sato, B., Seager, S., Sozzetti, A., Stassun, K. G., Sullivan, P., Szentgyorgyi, A., Torres, G., Udry, S., & Villasenor, J. 2014, in Proc. SPIE, Vol. 9143, Space Telescopes and Instrumentation 2014: Optical, Infrared, and Millimeter Wave, 914320 [ADS]

Riedel, A. R. 2014, Mem. Soc. Astron. Italiana, 85, 710 [ADS]

Roberts, Jr., L. C. & Neyman, C. R. 2002, PASP, 114, 1260 [ADS]

Robertson, P., Endl, M., Cochran, W. D., & Dodson-Robinson, S. E. 2013, ApJ, 764, 3 [ADS]

Robin, A. C., Luri, X., Reylé, C., Isasi, Y., Grux, E., Blanco-Cuaresma, S., Arenou, F., Babusiaux, C., Belcheva, M., Drimmel, R., Jordi, C., Krone-Martins, A., Masana, E., Mauduit, J. C., Mignard, F., Mowlavi, N., Rocca-Volmerange, B., Sartoretti, P., Slezak, E., & Sozzetti, A. 2012, A&A, 543, A100 [ADS]

Roeser, S., Demleitner, M., & Schilbach, E. 2010, AJ, 139, 2440 [ADS]

Rojas-Ayala, B., Covey, K. R., Muirhead, P. S., & Lloyd, J. P. 2012, ApJ, 748, 93 [ADS]

Rucinski, S. M. & Krautter, J. 1983, A&A, 121, 217 [ADS]

Ryden, B. 2003, Introduction to cosmology [ADS]

Sarro, L. M., Berihuete, A., Carrión, C., Barrado, D., Cruz, P., & Isasi, Y. 2013, A&A, 550, A44 [LINK]

Saumon, D., Marley, M. S., Abel, M., Frommhold, L., & Freedman, R. S. 2012, ApJ, 750, 74 [ADS]

Saumon, D., Marley, M. S., Lodders, K., & Freedman, R. S. 2003, in IAU Symposium, Vol. 211, Brown Dwarfs, 345 [ADS]

Scargle, J. D. 1982, ApJ, 263, 835 [ADS]

Schlafly, E. F. & Finkbeiner, D. P. 2011, ApJ, 737, 103 [ADS]

Schlegel, D. J., Finkbeiner, D. P., & Davis, M. 1998, ApJ, 500, 525 [ADS]

Scholz, A., Jayawardhana, R., Muzic, K., Geers, V., Tamura, M., & Tanaka, I. 2012, ApJ, 756, 24 [ADS]

Scholz, R.-D., Irwin, M., Ibata, R., Jahreiß, H., & Malkov, O. Y. 2000, A&A, 353, 958 [ADS]

Schroeder, D. J., Golimowski, D. A., Brukardt, R. A., Burrows, C. J., Caldwell, J. J., Fastie, W. G., Ford, H. C., Hesman, B., Kletskin, I., Krist, J. E., Royle, P., & Zubrowski, R. A. 2000, AJ, 119, 906 [ADS]

Shan, Y., Johnson, J. A., & Morton, T. D. 2015, ApJ, 813, 75 [ADS]

Shatsky, N. & Tokovinin, A. 2002, A&A, 382, 92 [ADS]

Shkolnik, E., Liu, M. C., & Reid, I. N. 2009, ApJ, 699, 649 [ADS]

Shkolnik, E. L., Liu, M. C., Reid, I. N., Dupuy, T., & Weinberger, A. J. 2011, ApJ, 727, 6 [ADS]

Shulyak, D., Sokoloff, D., Kitchatinov, L., & Moss, D. 2015, MNRAS, 449, 3471 [ADS]

Siegler, N., Close, L. M., Cruz, K. L., Martín, E. L., & Reid, I. N. 2005, ApJ, 621, 1023 [ADS]

Sinnott, R. W. 1984, S&T, 68, 158 [ADS]

Siverd, R. J., Beatty, T. G., Pepper, J., Eastman, J. D., Collins, K., Bieryla, A., Latham, D. W., Buchhave, L. A., Jensen, E. L. N., Crepp, J. R., Street, R., Stassun, K. G., Gaudi, B. S., Berlind, P., Calkins, M. L., DePoy, D. L., Esquerdo, G. A., Fulton, B. J., Fűrész, G., Geary, J. C., Gould, A., Hebb, L., Kielkopf, J. F., Marshall, J. L., Pogge, R., Stanek, K. Z., Stefanik, R. P., Szentgyorgyi, A. H., Trueblood, M., Trueblood, P., Stutz, A. M., & van Saders, J. L. 2012, ApJ, 761, 123 [ADS]

Skrutskie, M. F., Cutri, R. M., Stiening, R., Weinberg, M. D., Schneider, S., Carpenter, J. M., Beichman, C., Capps, R., Chester, T., Elias, J., Huchra, J., Liebert, J., Lonsdale, C., Monet, D. G., Price, S., Seitzer, P., Jarrett, T., Kirkpatrick, J. D., Gizis, J. E., Howard, E., Evans, T., Fowler, J., Fullmer, L., Hurt, R., Light, R., Kopan, E. L., Marsh, K. A., McCallon, H. L., Tam, R., Van Dyk, S., & Wheelock, S. 2006, AJ, 131, 1163 [ADS]

Skrzypek, N., Warren, S. J., & Faherty, J. K. 2016, ArXiv e-prints [ADS]

Smart, R. L. 2013, 01, 23

Song, I., Schneider, G., Zuckerman, B., Farihi, J., Becklin, E. E., Bessell, M. S., Lowrance, P., & Macintosh, B. A. 2006, ApJ, 652, 724 [ADS]

Spiegel, D. S., Burrows, A., & Milsom, J. A. 2011, ApJ, 727, 57 [ADS]

Spitzer, L. 1978, Physical processes in the interstellar medium [ADS]

Springel, V., White, S. D. M., Jenkins, A., Frenk, C. S., Yoshida, N., Gao, L., Navarro, J., Thacker, R., Croton, D., Helly, J., Peacock, J. A., Cole, S., Thomas, P., Couchman, H., Evrard, A., Colberg, J., & Pearce, F. 2005, Nature, 435, 629 [ADS]

Stassun, K. G., Mathieu, R. D., & Valenti, J. A. 2006, Nature, 440, 311 [ADS]

Stauffer, J., Tanner, A. M., Bryden, G., Ramirez, S., Berriman, B., Ciardi, D. R., Kane, S. R., Mizusawa, T., Payne, A., Plavchan, P., von Braun, K., Wyatt, P., & Kirkpatrick, J. D. 2010, PASP, 122, 885 [ADS]

Stelzer, B., Frasca, A., Alcalá, J. M., Manara, C. F., Biazzo, K., Covino, E., Rigliaco, E., Testi, L., Covino, S., & D'Elia, V. 2013, A&A, 558, A141 [ADS]

Straižys, V. & Lazauskaitė, R. 2009, Baltic Astronomy, 18, 19 [ADS]

Taylor, M. B. 2005, in Astronomical Society of the Pacific Conference Series, Vol. 347, Astronomical Data Analysis Software and Systems XIV, 29 [ADS]

Terrien, R. C., Mahadevan, S., Bender, C. F., Deshpande, R., & Robertson, P. 2015, ApJ, 802, L10 [ADS]

Theissen, C. A. & West, A. A. 2014, ApJ, 794, 146 [ADS]

Theissen, C. A., West, A. A., & Dhital, S. 2016, AJ, 151, 41 [ADS]

Tinney, C. G. 1993, ApJ, 414, 279 [ADS]

Tobin, J. J., Hartmann, L., Chiang, H.-F., Wilner, D. J., Looney, L. W., Loinard, L., Calvet, N., & D'Alessio, P. 2012, Nature, 492, 83 [ADS]

Todorov, K. O., Luhman, K. L., Konopacky, Q. M., McLeod, K. K., Apai, D., Ghez, A. M., Pascucci, I., & Robberto, M. 2014, ApJ, 788, 40 [ADS]

Tokovinin, A. & Lépine, S. 2012, AJ, 144, 102 [ADS]

Townsend, R. H. D. 2010, ApJS, 191, 247 [ADS]

Tuomi, M., Jones, H. R. A., Barnes, J. R., Anglada-Escudé, G., & Jenkins, J. S. 2014, MNRAS, 441, 1545 [ADS]

Turnshek, D. E. 1985, An Atlas of digital spectra of cool stars [ADS]

van der Plas, G., Menard, F., Ward-Duong, K., Bulger, J., Harvey, P. M., Pinte, C., Patience, J., Hales, A., & Casassus, S. 2016, ArXiv e-prints [ADS]

Vanderburg, A. & Johnson, J. A. 2014, PASP, 126, 948 [ADS]

Voges, W., Aschenbach, B., Boller, T., Bräuninger, H., Briel, U., Burkert, W., Dennerl, K., Englhauser, J., Gruber, R., Haberl, F., Hartner, G., Hasinger, G., Kürster, M., Pfeffermann, E., Pietsch, W., Predehl, P., Rosso, C., Schmitt, J. H. M. M., Trümper, J., & Zimmermann, H. U. 1999, A&A, 349, 389 [ADS]

Voges, W., Aschenbach, B., Boller, T., Brauninger, H., Briel, U., Burkert, W., Dennerl, K., Englhauser, J., Gruber, R., Haberl, F., Hartner, G., Hasinger, G., Pfeffermann, E., Pietsch, W., Predehl, P., Schmitt, J., Trumper, J., & Zimmermann, U. 2000, IAU Circ., 7432 [ADS]

Vogt, N., Mugrauer, M., Neuhäuser, R., Schmidt, T. O. B., Contreras-Quijada, A., & Schmidt, J. G. 2014, ArXiv e-prints [ADS]

Vogt, S. S., Butler, R. P., Marcy, G. W., Fischer, D. A., Pourbaix, D., Apps, K., & Laughlin, G. 2002, ApJ, 568, 352 [ADS]

Walkowicz, L. M. & Hawley, S. L. 2009, AJ, 137, 3297 [ADS]

Weiland, J. L., Arendt, R. G., Berriman, G. B., Dwek, E., Freudenreich, H. T., Hauser, M. G., Kelsall, T., Lisse, C. M., Mitra, M., Moseley, S. H., Odegard, N. P., Silverberg, R. F., Sodroski, T. J., Spiesman, W. J., & Stemwedel, S. W. 1994, ApJ, 425, L81 [ADS]

Weisstein, E. W. 1999, "Spherical Cone." From MathWorld–A Wolfram Web Resource., http://mathworld.wolfram.com/SphericalCone.html, accessed: 2016-02-09

Wenger, M., Ochsenbein, F., Egret, D., Dubois, P., Bonnarel, F., Borde, S., Genova, F., Jasniewicz, G., Laloë, S., Lesteven, S., & Monier, R. 2000, A&AS, 143, 9 [ADS]

West, A. A., Morgan, D. P., Bochanski, J. J., Andersen, J. M., Bell, K. J., Kowalski, A. F., Davenport, J. R. A., Hawley, S. L., Schmidt, S. J., Bernat, D., Hilton, E. J., Muirhead, P., Covey, K. R., Rojas-Ayala, B., Schlawin, E., Gooding, M., Schluns, K., Dhital, S., Pineda, J. S., & Jones, D. O. 2011, AJ, 141, 97 [ADS]

West, A. A., Weisenburger, K. L., Irwin, J., Berta-Thompson, Z. K., Charbonneau, D., Dittmann, J., & Pineda, J. S. 2015, ApJ, 812, 3 [ADS]

Whitworth, A., Bate, M. R., Nordlund, Å., Reipurth, B., & Zinnecker, H. 2007, Protostars and Planets V, 459 [ADS]

Wilson, J. C., Kirkpatrick, J. D., Gizis, J. E., Skrutskie, M. F., Monet, D. G., & Houck, J. R. 2001, AJ, 122, 1989 [ADS]

Winters, J. G., Henry, T. J., Lurie, J. C., Hambly, N. C., Jao, W.-C., Bartlett, J. L., Boyd, M. R., Dieterich, S. B., Finch, C. T., Hosey, A. D., Ianna, P. A., Riedel, A. R., Slatten, K. J., & Subasavage, J. P. 2015, AJ, 149, 5 [ADS]

Wright, E. L., Eisenhardt, P. R. M., Mainzer, A. K., Ressler, M. E., Cutri, R. M., Jarrett, T., Kirkpatrick, J. D., Padgett, D., McMillan, R. S., Skrutskie, M., Stanford, S. A., Cohen, M., Walker, R. G., Mather, J. C., Leisawitz, D., Gautier, III, T. N., McLean, I., Benford, D., Lonsdale, C. J., Blain, A., Mendez, B., Irace, W. R., Duval, V., Liu, F., Royer, D., Heinrichsen, I., Howard, J., Shannon, M., Kendall, M., Walsh, A. L., Larsen, M., Cardon, J. G., Schick, S., Schwalm, M., Abid, M., Fabinsky, B., Naes, L., & Tsai, C.-W. 2010, AJ, 140, 1868 [ADS]

Wright, J. T. & Gaudi, B. S. 2013, Exoplanet Detection Methods, 489 [ADS]

York, D. G., Adelman, J., Anderson, Jr., J. E., Anderson, S. F., Annis, J., Bahcall, N. A., Bakken, J. A., Barkhouser, R., Bastian, S., Berman, E., Boroski, W. N., Bracker, S., Briegel, C., Briggs, J. W., Brinkmann, J., Brunner, R., Burles, S., Carey, L., Carr, M. A., Castander, F. J., Chen, B., Colestock, P. L., Connolly, A. J., Crocker, J. H., Csabai, I., Czarapata, P. C., Davis, J. E., Doi, M., Dombeck, T., Eisenstein, D., Ellman, N., Elms, B. R., Evans, M. L., Fan, X., Federwitz, G. R., Fiscelli, L., Friedman, S., Frieman, J. A., Fukugita, M., Gillespie, B., Gunn, J. E., Gurbani, V. K., de Haas, E., Haldeman, M., Harris, F. H., Hayes, J., Heckman, T. M., Hennessy, G. S., Hindsley, R. B., Holm, S., Holmgren, D. J., Huang, C.-h., Hull, C., Husby, D., Ichikawa, S.-I., Ichikawa, T., Ivezić, Ž., Kent, S., Kim, R. S. J., Kinney, E., Klaene, M., Kleinman, A. N., Kleinman, S., Knapp, G. R., Korienek, J., Kron, R. G., Kunszt, P. Z., Lamb, D. Q., Lee, B., Leger, R. F., Limmongkol, S., Lindenmeyer, C., Long, D. C., Loomis, C., Loveday, J., Lucinio, R., Lupton, R. H., MacKinnon, B., Mannery, E. J., Mantsch, P. M., Margon, B., McGehee, P., McKay, T. A., Meiksin, A., Merelli, A., Monet, D. G., Munn, J. A., Narayanan, V. K., Nash, T., Neilsen, E., Neswold, R., Newberg, H. J., Nichol, R. C., Nicinski, T., Nonino, M., Okada, N., Okamura, S., Ostriker, J. P., Owen, R., Pauls, A. G., Peoples, J., Peterson, R. L., Petravick, D., Pier, J. R., Pope, A., Pordes, R., Prosapio, A., Rechenmacher, R., Quinn, T. R., Richards, G. T., Richmond, M. W., Rivetta, C. H., Rockosi, C. M., Ruthmansdorfer, K., Sandford, D., Schlegel, D. J., Schneider, D. P., Sekiguchi, M., Sergey, G., Shimasaku, K., Siegmund, W. A., Smee, S., Smith, J. A., Snedden, S., Stone, R., Stoughton, C., Strauss, M. A., Stubbs, C., SubbaRao, M., Szalay, A. S., Szapudi, I., Szokoly, G. P., Thakar, A. R., Tremonti, C., Tucker, D. L., Uomoto, A., Vanden Berk, D., Vogeley, M. S., Waddell, P., Wang, S.-i., Watanabe, M., Weinberg, D. H., Yanny, B., Yasuda, N., & SDSS Collaboration. 2000, AJ, 120, 1579 [ADS]

Zapatero-Osorio, M. R., Rebolo, R., & Martin, E. L. 1996, in Astronomical Society of the Pacific Conference Series, Vol. 109, Cool Stars, Stellar Systems, and the Sun, 731 [ADS]

Zapatero Osorio, M. R., Rebolo, R., Martin, E. L., Hodgkin, S. T., Jameson, R. F., Cossburn, M. R., Magazzu, A., Basri, G., & Steele, I. A. 1998, in Astronomical Society of the Pacific Conference Series, Vol. 134, Brown Dwarfs and Extrasolar Planets, 51 [ADS]

Zhao, G., Zhao, Y.-H., Chu, Y.-Q., Jing, Y.-P., & Deng, L.-C. 2012, Research in Astronomy and Astrophysics, 12, 723 [ADS]

Zhong, J., Lépine, S., Hou, J., Shen, S., Yuan, H., Huo, Z., Zhang, H., Xiang, M., Zhang, H., & Liu, X. 2015a, AJ, 150, 42 [ADS]

Zhong, J., Lépine, S., Li, J., Chen, L., Hou, J.-L., Yang, M., Li, G.-W., Zhang, Y., & Hou, Y.-H. 2015b, Research in Astronomy and Astrophysics, 15, 1154 [ADS]

Ziegler, C., Law, N. M., Baranec, C., Riddle, R. L., & Fuchs, J. T. 2014, ArXiv e-prints [ADS]

# Glossary

| | |
|---|---|
| 2MASS | The Two (**2**) **M**icron **A**ll **S**ky **S**urvey (implied point source catalogue) is an all-sky near-infrared ($J$, $H$, $K_S$) catalogue of 470 992 970 objects from Skrutskie et al. (2006) |
| BANYAN | **B**ayesian **A**nalysis for **N**earby **Y**oung **A**ssociatio**N**s I and II are bayesian analysis tools designed to determine the membership probability of candidate stars to nearby young kinematic groups (from Malo et al. 2013 and Gagné et al. 2014 respectively). |
| CARMENES | The **C**alar **A**lto high-**R**esolution search for **M** dwarfs with **E**xo-earths with **N**ear-infrared and optical **E**chelle **S**pectrographs is a next-generation instrument under construction for the 3.5 m telescope at the Calar Alto Observatory (Quirrenbach et al., 2010). |
| CS colour | **C**ompanion **S**ensitive Primary Insensitive **colour**s are the colour chosen to be sensitive to changes in primary (M dwarf) spectral type and insensitive to companion (UCD) spectral type when looking at the colour of an unresolved M+UCD system. |
| DSS2 | The **D**igitized **S**ky **S**urvey **2** is a digitized catalogue of images from archival plates. Images of these surveys are based on photographic data obtained using the Oschin Schmidt Telescope on Palomar Mountain and the UK Schmidt Telescope. |
| EPIC | **E**cliptic **P**lane **I**nput **C**atalog is a catalogue of stars located near the ecliptic plane (established for the Kepler K2 mission by NASA). |
| FWHM | The **F**ull **W**idth **H**alf **M**aximum is the width of the independent variable at which the independent variable is half of its maximum value. |

GUMS-10 The **10**th version of the **G**aia **U**niverse **M**odel **S**napshot is a simulation of the expected contents of the Gaia catalogue, and was created using the MareNostrum supercomputer.

HERMES The **H**igh **E**fficiency and **R**esolution **M**ercator **E**chelle **S**pectrograph is a high-resolution fibre-fed spectrograph for the Mercator telescope (Raskin et al., 2011).

HPF The **H**abitable-zone **P**lanet **F**inder is a proposed high resolution NIR spectrograph for the Hobby Eberly telescope to discover low mass exoplanets around M stars (Mahadevan et al., 2010).

IAU The **I**nternational **A**stronomical **U**nion is a collection of professional astronomers, at the PhD level and beyond, active in professional research and education in astronomy (Statutes of the IAU, VII General Assembly, 1948, ss. 1315).

iLocator iLocator is an ultra-precise spectrometer that is being built and will go on the Large Binocular Telescope at Mount Graham, Arizona, U.S. (Crepp et al., 2014).

IRD The **I**nfra**r**ed **D**oppler instrument is the near-infrared high-precision radial velocity instrument for the Subaru 8.2-m telescope, located at the summit of Mauna Key, Hawai'i, U.S. (Kotani et al., 2014).

IRTF The **I**nfra**R**ed **T**elescope **F**acility is a 3.0 meter telescope, optimised for infrared observations, located at the summit of Mauna Kea, Hawai'i, U.S.

K2C0 **K**epler **2** **C**ampaign **0** is the preliminary data release for the re-purposed Kepler satellite.

K2C1 **K**epler **2** **C**ampaign **1** is the first full data release for the re-purposed Kepler satellite.

K2C2 **K**epler **2** **C**ampaign **2** is the second full data release for the re-purposed Kepler satellite.

LAMOST The **L**arge Sky **A**rea **M**ulti-**O**bject Fibre **S**pectroscopic **T**elescope (also known as the Guo Shoujing Telescope) is a multi-object fibre telescope, located at the Xinglong Station, Hebei Province, China (Cui et al., 2012).

| | |
|---|---|
| MAST | The **M**ikulski **A**rchive for **S**pace **T**elescopes provides a variety of astronomical data archives with the primary focus on scientifically related data sets in the optical, ultraviolet, and near-infrared parts of the spectrum. |
| MCMC | The **M**arkov **C**hain **M**onte **C**arlos methods are a class of algorithms for sampling from a probability distribution. |
| MIR | The **M**id **I**nfrared **R**ed is the wavelength region from $\sim$2$\mu$m to *sim* 20 $\mu$m in the electromagnetic spectrum. |
| MoVeRS | The **M**otion **V**erified **R**ed **S**tars catalogue is a photometric catalog of 8,735,004 proper motion selected low-mass stars (KML-spectral types) within the Sloan Digital Sky Survey (SDSS) footprint (Theissen et al., 2016). |
| NIR | The **N**ear **I**nfrared **R**ed is the wavelength region from $\sim$0.7/0.8 to 2.5$\mu$m in the electromagnetic spectrum. |
| PLATO 2 | The **PLA**netary **T**ransits and **O**scillation of stars mission is a transit survey mission with the goal of detecting and charactering new planets and planetary systemsa round bright stars (Rauer et al., 2014). |
| PPMXL | The **P**ositions and **P**roper **M**otions on the ICRS e**X**tended-**L** catalogue is a catalogue of positions and proper motions on the ICRS, combining USNO-B1.0 and 2MASS (Roeser et al., 2010). |
| PS colour | The **P**rimary **S**ensitive Companion Insensitive **colour**s are the colour chosen to be sensitive to companion (UCD) spectral type and insensitive to changes in primary (M dwarf) spectral type when looking at the colour of an unresolved M+UCD system. |
| PSF | The **P**oint **S**pread **F**unction describes the response of an imaging system to a point source. |
| SDSS | The **S**loan **D**igital **S**ky **S**urvey is a multi-filter imaging and spectroscopic redshift survey using a dedicated 2.5 m optical telescope at Apache Point Observatory, New Mexico, U.S. (York et al., 2000). |
| SED | The **S**pectral **E**nergy **D**istribution is a plot of the brightness or flux density as a function of frequency or wavelength. |

| | |
|---|---|
| SIMBAD | The **S**et of **I**dentifications, **M**easurements, and **B**ibliography for **A**stronomical **D**ata, is an astronomical database providing basic data, cross-identifications, bibliography and measurements for astronomical objects outside the solar system. |
| SNR | The **S**ignal to **N**oise **R**atio, or S/N is a measure of quality of some data compared to its uncertainties. |
| SPIRou | **S**pectro-**P**olarimetre **I**nfra-**R**ouge is a near-IR echelle spectropolarimeter and high-precision velocimeter under construction as a next-generation instrument for the Canada-France-Hawaii-Telescope (Artigau et al., 2014). |
| TESS | The **T**ransiting **E**xoplanet **S**urvey **S**atellite is a space telescope whose primary mission is to survey the brightest stars for transiting exoplanets, currently scheduled for launch in 2017 (Ricker et al., 2014). |
| UKIDSS | The **U**nited **K**ingdom **I**nfrared **D**igital **S**ky **S**urvey is a near-infrared sky survey (the successor to 2MASS) that observed 7 500 square degrees of the northern sky in $J$, $H$ and $K$ (Lawrence et al., 2007). |
| UKIRT | **U**nited **K**ingdom **I**nfrared **T**elescope, is the former U.K. 3.8 m infrared telescope, located at the summit of Mauna Kea, Hawai'i, U.S. |
| USNO-A2.0 | The **U**nited **S**tates **N**aval **O**bservatory Catalogue **A2.0**, is a catalogue of 526 280 881 stars based on a re-reduction of the Precision Measuring Machine scans and USNO-A1.0 catalogue (Monet, 1998). |
| VISTA | The **V**isible and **I**nfrared **S**urvey **T**elescope for **A**stronomy is a 4 m class wide field survey telescope in the southern hemisphere ($Z$, $Y$, $J$, $H$, $K_S$), located at ESO's Cerro Paranal Observatory in Chile (Emerson & Sutherland, 2002) |
| WISE | The **W**ide-Field **I**nfrared **S**urvey **E**xplorer is a space based near-to-mid infrared telescope (3.4, 4.6, 12 and 22 $\mu$m), the all-sky source catalogue contains 563 921 584 objects (Wright et al., 2010). |

# Index

# *Le fin*

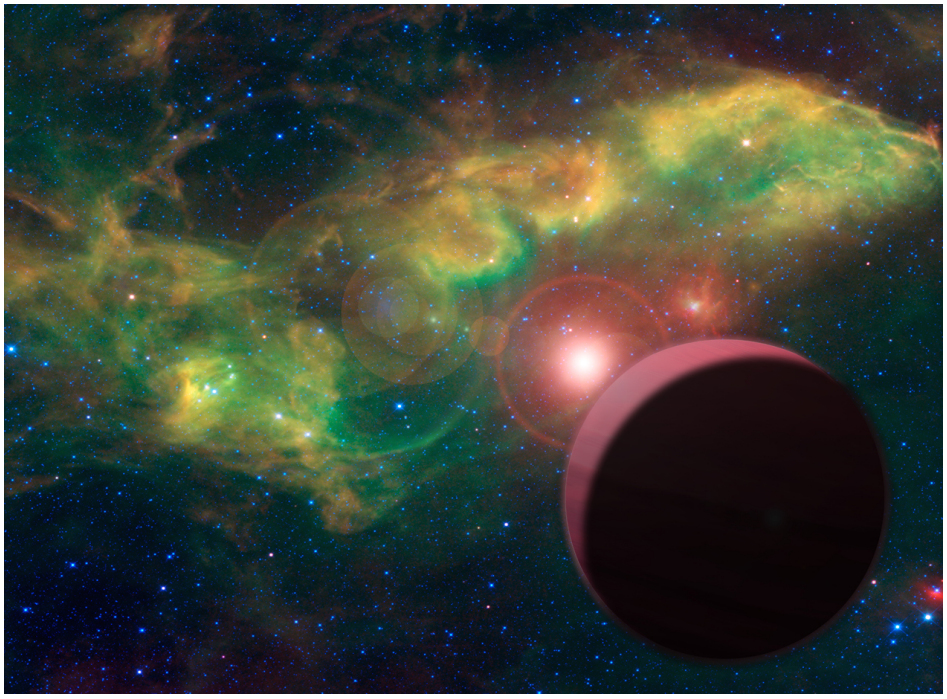

Artistic representation of a M dwarf + UCD system by Neil James Cook with background from WISE 'PIA14881: Jabbah and Associates' NASA/JPL-Caltech/UCLA.